

M

## POLYMER STRUCTURES AND PROPERTIES

TECHNICAL DOCUMENTARY REPORT NO. ML TDR 64-286

September, 1964

AIR FORCE MATERIALS LABORATORY  
RESEARCH AND TECHNOLOGY DIVISION  
AIR FORCE SYSTEMS COMMAND  
WRIGHT-PATTERSON AIR FORCE BASE, OHIO

Project No. 7342, Task No. 734203

**DISTRIBUTION STATEMENT A**

Approved for public release;  
Distribution Unlimited

(Prepared under Contract No. AF 33(657)-10661;

Mellon Institute, Pittsburgh, Pennsylvania;

T. A. Orofino, G. C. Berry, A. Ciferri, E. F. Casassa, J. W. Mickey, Jr.,  
G. L. Bender, T. G. Fox, V. R. Allen, B. D. Coleman, and W. H. Janes, authors)

DEPARTMENT OF DEFENSE  
PLASTICS TECHNOLOGY EVALUATION CENTER  
PICATUNN AVENUE, DOVER, N. J.

DTIC QUALITY INSPECTED

19960605 092

PLASTIC 6390

## NOTICES

When Government drawings, specifications, or other data are used for any purpose other than in connection with a definitely related Government procurement operation, the United States Government thereby incurs no responsibility nor any obligation whatsoever; and the fact that the Government may have formulated, furnished, or in any way supplied the said drawings, specifications, or other data, is not to be regarded by implication or otherwise as in any manner licensing the holder or any other person or corporation, or conveying any rights or permission to manufacture, use, or sell any patented invention that may in any way be related thereto.

Qualified requesters may obtain copies of this report from the Defense Documentation Center (DDC), (formerly ASTIA), Cameron Station, Bldg. 5, 5010 Duke Street, Alexandria, Virginia, 22314.

This report has been released to the Office of Technical Services, U.S. Department of Commerce, Washington 25, D. C., for sale to the general public.

Copies of this report should not be returned to the Research and Technology Division, Wright-Patterson Air Force Base, Ohio, unless return is required by security considerations, contractual obligations, or notice on a specific document.

## FOREWORD

This report was prepared at Mellon Institute under USAF Contract No. AF 33(657)-10661. The contract was initiated under Project No. 7342, "Fundamental Research on Macromolecular Materials and Lubrication Phenomena," Task No. 734203, "Fundamental Principles Determining the Behavior of Macromolecules." The Work was administered under the direction of the Air Force Materials Laboratory, Research and Technology Division. Dr. W. E. Gibbs was the project engineer.

This report covers work done from 1 January 1963 to 31 December 1963.

The investigations described in Part I, "Dilute Solution Studies," were aided by a number of persons in addition to the authors listed. Mr. R. E. Kerwin programmed computer calculations (Sections I, III). Mr. J. W. Mickey, Jr., helped with computations and experimental measurements (Sections I, II). Mr. R. J. Reitz contributed to characterization of solvents (Section II). A cross-linked polystyrene (Section II) was provided by Dr. J. G. Pritchard (now at Hoffman-LaRoche, Inc.). Anionically polymerized linear polystyrenes (Sections II, VII) were prepared by Dr. F. Wenger (now at Celanese Corporation), Mrs. S.-P. S. Yen, and Mr. T. Altares. Dr. B. P. Block of the Pennsalt Corporation provided samples of zinc and chromium coordination polymers (Section IX).

## ABSTRACT

[Theoretical and experimental investigations have been made concerning properties of synthetic polymers in dilute solutions. The dependence of the molecular dimensions of linear polystyrene upon the nature of the solvent and temperature has been studied under "theta" conditions--when the configuration is "unperturbed" by interactions of indirectly connected elements of the chain. A rather comprehensive study has been made of the configurational, hydrodynamic, and thermodynamic behavior (as reflected by the second virial coefficient) of linear polystyrene in decalin over a sufficiently wide temperature range that the solvent character ranges from poor to moderately good. The data are used in assessing the validity of current theories.

The molecular dimensions of branched polymers in dilute solution and the second virial coefficient are the subjects of theoretical treatments: some pertinent experimental data are also presented.

Preliminary dilute solution measurements are reported on two unusual coordination polymers derived from zinc methyl phenyl phosphinate and hydroxyaquo chromium diphenyl phosphinate.]

Two instruments for solution measurements have been constructed and evaluated: a magnetically operated Couette viscometer and a differential refractometer of high precision.

Viscosity data on a variety of polymers, linear and branched, can be correlated empirically by a function of temperature, chain length, concentration of diluent, and the frictional coefficient per chain atom. Introduction into the WLF equation of an energy function derived from estimates of rotational barriers within polymer chains, leads to some success in reducing data on the temperature variation of the friction factor to a common functional dependence.

A "two-state" mechanism is described to explain the stereoblock structures that occasionally result from homogeneous anionic polymerizations. Experimental work in progress has two aims: to furnish more definitive evidence for the two-state mechanism and to provide synthetic methods for poly(methyl methacrylate) of narrow molecular weight distribution and controlled stereoregular structure. In view of conflicting previous evidence, polyvinyl alcohol prepared by hydrolysis of vinyl formate polymers is being studied by nuclear resonance spectroscopy to elucidate the stereostructure.

This technical documentary report has been reviewed and approved.

*William E. Gibbs*

William E. Gibbs  
Chief, Polymer Branch  
Nonmetallic Materials Division  
AF Materials Laboratory



# TABLE OF CONTENTS

## PART I - DILUTE SOLUTION STUDIES

	Page
I. Branched Polymers--Dimensions of Chains with Small Excluded Volume — G. C. Berry and T. A. Orofino . . . . .	1
A. Introduction . . . . .	1
B. Theory . . . . .	2
1. Formulation of the mean square radius . . . . .	3
2. Configuration classes . . . . .	5
C. Computations for Model Structures . . . . .	7
1. Regular star molecules . . . . .	7
2. Regular comb molecules . . . . .	8
3. Numerical results . . . . .	13
4. Discussion . . . . .	19
D. Application to Experiment . . . . .	20
1. Relationship between coil expansion and second virial coefficient . . . . .	20
2. Approximate theories . . . . .	21
II. Temperature Dependence of the Unperturbed Dimensions of Polystyrene — T. A. Orofino and A. Ciferri . . . . .	23
A. Introduction . . . . .	23
B. Experimental . . . . .	24
1. Tension-temperature studies . . . . .	24
2. Intrinsic viscosity studies . . . . .	24
C. Treatment of Data - Review . . . . .	29
1. Tension-temperature studies . . . . .	29
2. Intrinsic viscosity studies . . . . .	29
D. General Treatment for Polymer-solvent Systems . . . . .	30
E. Discussion and Conclusion . . . . .	33

# TABLE OF CONTENTS - continued

## PART I DILUTE SOLUTION STUDIES - continued

	Page
III. The Second Virial Coefficient for Branched Comb Molecules — E. F. Casassa . . . . .	36
A. Introduction . . . . .	36
B. Theory for the Asymmetric Comb . . . . .	38
C. The Symmetric Comb . . . . .	42
D. Discussion of Results . . . . .	45
E. Application to Polymers in Good Solvents . . . . .	50
IV. Dilute Solution Properties of Branched Polymers. Polystyrene Trifunctional Star Molecules — T. A. Orofino and F. Wenger . .	56
V. Dilute Solution Properties of Linear Polystyrene in $\Theta$ -Solvent Media — T. A. Orofino and J. W. Mickey, Jr. . . . .	57
VI. Dilute Solution Properties of Linear Polystyrene in $\Theta$ -Solvent Media. II — T. A. Orofino and J. W. Mickey, Jr. . . . .	58
A. Selection of Polymer-Solvent Systems . . . . .	58
B. Experimental . . . . .	58
C. Discussion . . . . .	64
VII. Thermodynamic and Conformation Properties of Polystyrene in Decalin — G. C. Berry . . . . .	72
A. Introduction . . . . .	72
B. Experimental . . . . .	72
1. Materials . . . . .	72

## TABLE OF CONTENTS - continued

### PART I DILUTE SOLUTION STUDIES - continued

	Page
2. Methods . . . . .	77
C. Results . . . . .	79
D. Discussion . . . . .	85
1. $A_2$ as a function of molecular weight and temperature . . . . .	85
2. Approximate theories for $A_2$ in good solvents . . . . .	88
3. $A_2$ for branched polymers . . . . .	92
4. The mean square radius of gyration . . . . .	93
5. Approximate theories for $s^2$ . . . . .	95
6. A relationship between $A_2$ and $\alpha_2$ . . . . .	100
E. Conclusions . . . . .	105
 VIII. Intrinsic Viscosity of Linear Polystyrene in Decalin — G. C. Berry and G. L. Bender . . . . .	 106
A. Introduction . . . . .	106
B. Experimental . . . . .	107
1. Methods . . . . .	107
2. Materials . . . . .	108
C. Results . . . . .	108
D. Discussion . . . . .	108
1. Theta solvent correlation . . . . .	108
2. Good solvent correlations . . . . .	111
E. Conclusions . . . . .	117
 IX. Investigation of Two Novel Inorganic Polymers — G. C. Berry. .118	.118
 X. Construction of a Couette Viscometer for Steady Flow at Low Shear Rate — G. C. Berry and G. L. Bender . . . . .	 120

## TABLE OF CONTENTS - continued

### PART I DILUTE SOLUTION STUDIES - continued

	Page
A. Introduction . . . . .	.120
B. General Description . . . . .	.120
C. The Magnetic Drive . . . . .	.120
D. Mechanical Construction of the Rotor . . . . .	.123
E. Alignment . . . . .	.124
F. Operating Characteristics . . . . .	.125
1. The effects of rotor position . . . . .	.125
2. The effects of temperature . . . . .	.127
3. The average shear rate . . . . .	.127
G. Photoelectric Timer . . . . .	.129
H. Intrinsic Viscosity Measurements . . . . .	.129
 XI. Differential Refractometer — G. C. Berry . . . . .	 .132
A. Introduction . . . . .	.132
B. Instrument Design . . . . .	.132
C. Data Analysis . . . . .	.135
D. Optical Performance . . . . .	.135
E. Instrument Performance . . . . .	.136
 Part I List of References . . . . .	 .138

## TABLE OF CONTENTS - continued

### PART II FLOW IN CONCENTRATED POLYMER SYSTEMS

	Page
I. The Dependence of the Zero Shear Melt Viscosity and the Related Friction Coefficient and Critical Chain Length on Measurable Characteristics of Chain Polymers — T. G Fox and V. R. Allen . . . . .	.142
A. Introduction . . . . .	.142
B. The General Plan . . . . .	.143
C. The Critical Parameters $Z_c$ and $X_c$ . . . . .	.144
D. The Frictional Coefficient Per Chain Atom, $\zeta$ . . . . .	.150
E. Effect of Branching and of Diluent . . . . .	.150
F. The Critical Chain Entanglement Length, $Z_e$ . . . . .	.152
G. An Approximate (Modified W-L-F) Equation Relating $\zeta$ to Measurable Structure-Dependent Parameters . . . . .	.155
H. Discussion . . . . .	.160
Part II List of References . . . . .	.162

### PART III ANIONIC POLYMERIZATION

I. On the Two-State Mechanism for Homogeneous Ionic Polymerization — B. D. Coleman and T. G Fox . . . . .	.165
A. Introduction . . . . .	.165
B. Chemical Hypotheses . . . . .	.165
C. Diastereosequences . . . . .	.167
D. Molecular Weights . . . . .	.170
E. Comparison With Experiment . . . . .	.172

TABLE OF CONTENTS - continued

PART III ANIONIC POLYMERIZATION - continued

	Page
II. Anionic Polymerization of Methyl Methacrylate — W. H. Janes .	.182
III. NMR Spectroscopy of Poly(vinyl Alcohol) — W. H. Janes . . .	.187
Part III List of References . . . . .	.189

# LIST OF FIGURES

Figure		Page
1	A Class III Configuration . . . . .	7
2	Regular Comb Structures . . . . .	9
3	Plots of $a_1$ Versus $p$ for Regular Star Molecules and for Regular Comb Molecules at Various $r$ Values . . . . .	16
4	Plots of $a_1$ Versus $r$ for Various $p$ -Functional Regular Comb Molecules . . . . .	17
5	Plots of $a_1$ Versus $1-g$ for Star Molecules and For Comb Molecules with Various $r$ and $p$ Values . . . . .	18
6	Tension-Temperature Curves at Constant Length for Polystyrene Networks . . . . .	25
7	Plots of $[\eta]$ Versus Temperature for Polystyrene in 1-Chloro- $n$ -decane (CD), 1-Chloro- $n$ -undecane (CUD) and 1-Chloro- $n$ -dodecane (CDD) . . . . .	27
8	Schematic Representation of Interaction of Two Asymmetric Combs	38
9	Diagram for Double-Contact Interaction of Two Symmetrical Combs	43
10	The Coefficient $B$ for Symmetric and Asymmetric Combs for Various Values of $\underline{f}$ . . . . .	49
11	Plots of $B$ versus $\underline{g}$ for Symmetrical Combs . . . . .	52
12	Square-Root Plots of Reduced Reciprocal Scattering Intensity Versus Polymer Concentration $c$ (g/cc) for the System Polystyrene-1-chloro- $n$ -decane at Various Temperatures . . . . .	59
13	Square-Root Plots of Reduced Reciprocal Scattering Intensity Versus Polymer Concentration $c$ (g/cc) for the System Polystyrene-1-chloro- $n$ -dodecane at Various Temperatures . . . . .	60
14	Plots of $\eta_{sp}/c$ and $(\ln \eta_{rel})/c$ Versus $c$ (g/dl) for the System Polystyrene-1-chloro- $n$ -decane at Various Temperatures . . . . .	61
15	Plots of $\eta_{sp}/c$ and $(\ln \eta_{rel})/c$ Versus $c$ (g/dl) for the System Polystyrene-1-chloro- $n$ -dodecane at Various Temperatures . . . . .	62
16	Plots of $\Gamma_2$ Versus Reciprocal Absolute Temperature for Polystyrene in 1-Chloro- $n$ -decane and 1-Chloro- $n$ -dodecane . . .	65
17	Plots of $[\eta]$ Versus $T-\theta$ for Five Polystyrene- $\theta$ -Solvent Systems	66

# LIST OF FIGURES - continued

Figure	Page
18 Fractionation Scheme for the Star-Shaped Branched Polymer . . .	75
19 Representative Sedimentation Velocity Patterns for Some of the Fractions Shown in Fig. 18 . . . . .	76
20 Variation of $\Theta$ with Solvent Composition for Cis-Trans Mixtures of Decalin . . . . .	78
21 Dependence of the Second Virial Coefficient $\Gamma_2$ (cc/g) on Temperature for Samples A-30, A-5, A-16, A-19, A-13, A-3, and A-25 . . . . .	83
22 Dependence of the Expansion Factor $\alpha^2 = \overline{s^2}/\overline{s^2}_\Theta$ on Temperature for Various Samples . . . . .	84
23 Determination of the Parameter $n^2\beta_0/M^2$ . . . . .	87
24 $A_2M^{1/2}$ as a Universal Function of the Thermodynamic Parameter $z$	89
25 $A_2M^{1/2}/\alpha^3$ as a Function of the Thermodynamic Parameter $z/\alpha^3$ . .	91
26 $A_2M^{1/2}/\alpha^3$ as a Function of the Thermodynamic Parameter $z/\alpha^3$ for the Star Branched Polymer . . . . .	94
27 The Expansion Factor as a Function of the Thermodynamic Para- meter $z$ . . . . .	96
28 The Expansion Factor as a Function of the Thermodynamic Variable $z/\alpha^3$ . . . . .	99
29 The Expansion Factor $\alpha^2$ as a Function of the Thermodynamic Variable $z$ for a Star Shaped Polymer . . . . .	101
30 A Semi-Empirical Correlation Between $A_2M^{1/2}$ and $\alpha^2-1$ . . . . .	102
31 A Semi-Empirical Relation Between $A_2M^{1/2}$ and $\alpha^2-1$ for Data from the Literature on Polystyrene in Methanol, Dichloroethane, and Toluene . . . . .	103
32 Dependence of $\alpha_\eta^3 \equiv [\eta]/[\eta]_\Theta$ on Temperature for Various Molecular Weights . . . . .	109
33 Dependence of $\alpha_\eta^3$ on the Thermodynamic Parameter $z$ . . . . .	112
34 A Test of the Semi-Empirical Equations 104 and 105 . . . . .	113
35 Semi-Empirical Correlations Between $\alpha_\eta^3$ and $\alpha^3$ . . . . .	115



# LIST OF FIGURES - continued

Figure	Page
36 Semi-Empirical Correlations Between $\alpha_\eta^3$ and $\alpha^3$ for Data from the Literature on Polymethyl Methacrylate in Several Solvents .	116
37 Two Coordination Polymers . . . . .	118
38 Schematic Diagram of Low Shear Rate Concentric Cylinder Viscometer . . . . .	121
39 Dependence of the Torque Derived from a Rotational Hysteresis Motor on Temperature . . . . .	128
40 A Schematic Drawing of the Photoelectric Timing Circuit for the Co-Axial Cylinder Viscometer . . . . .	130
41 Schematic Drawing of Optical Components of the Differential Refractometer . . . . .	133
42 Schematic Drawing of Differential Refractometer Thermostat . .	134
43 Calibration Constant for Differential Refractometer . . . . .	137
44 Reduced Viscosity Function $3.4 \log Z_w^* - \log \eta^* + \log (\eta/Z)$ Versus $\log Z$ . . . . .	145
45 Reduced Viscosity Function $\log \eta - A/T_n \exp (-\beta/Z_n)$ Versus $\log Z$ . . . . .	146
46 $-\log \zeta$ Versus $(T-T_g)$ . . . . .	151
47 $\log \eta$ 140° Versus the Parameter $\log Z_{vg}^*$ for Linear and Branched Polycaproylamides . . . . .	153
48 Viscosity-Concentration-Molecular Weight Relations for Fractions of Polystyrene in Benzyl Ether . . . . .	154
49 (a) $-\log \zeta$ Versus $\Delta\alpha_f(T-T_g)$ (b) $-\log \zeta - E/2.3RT$ Versus $\Delta\alpha_f(T-T_g)/0.025 + \Delta\alpha_f(T-T_g)$ . .	158
50 Ultracentrifuge Schlieren Patterns for Poly(Methyl Methacrylate) Samples A8 and A9 . . . . .	185
51 NMR Spectra (Methylene Resonances) from Poly(vinyl alcohol) . .	188

# LIST OF TABLES

Table	Page
I Schematic Representation of Structural Components and Associated $\Gamma$ Terms for a Comb Molecule, $p = 2$ . . . . .	11
II Values of $a_1$ and $g$ for Regular Star Molecules . . . . .	14
III Values of $a_1$ and $g$ for Regular Comb Molecules . . . . .	15
IV Tension-Temperature Data for the Polystyrene Network . . . . .	26
V Characterization Data for Polystyrene- $\Theta$ -solvent Systems . . . . .	28
VI Values of $d \ln \overline{r_0^2} / dT$ for Polystyrene-solvent Systems . . . . .	32
VII Coefficient B for Asymmetric Comb . . . . .	46
VIII Coefficient B for Symmetrical Comb . . . . .	47
IX Symmetrical Comb, $g$ . . . . .	51
X Intrinsic Viscosity and Second Virial Coefficient Data for Polystyrene- $\Theta$ -solvent Systems . . . . .	63
XI Summary of Results for Polystyrene- $\Theta$ -Solvent Systems . . . . .	67
XII Values of $r_0^2/M$ for Polystyrene . . . . .	69
XIII Equivalent Chain Parameters for Polystyrene- $\Theta$ -solvent Systems . . . . .	70
XIV Isomeric Decalin Mixtures . . . . .	73
XV Theta Solvent Parameters for Polystyrene in Decalin . . . . .	74
XVI Light Scattering Data for Polystyrene in Decalin . . . . .	80
XVII Intrinsic Viscosity of Linear Polystyrene in Decalin . . . . .	110
XVIII Values of $Z_c$ and of $X_c$ for Various Polymers . . . . .	147
XIX Comparison of Calculated and Observed $Z_c$ and $Z_e$ . . . . .	156
XX Tentative Values of E for Various Polymers . . . . .	159
XXI NMR Data on Poly(methyl methacrylate) Polymerized Anionically in Hydrocarbon Media . . . . .	174
XXII NMR Data on Poly(methyl methacrylate) Polymerized Anionically in Lewis Bases . . . . .	175

# LIST OF TABLES - continued

Table	Page
XXIII Data on Poly(methyl methacrylate) Polymerized Anionically in Mixtures of Toluene with Lewis Bases . . . . .	176
XXIV NMR Data on Poly(methyl methacrylate) Polymerized in Toluene at -30°C with Butyllithium at Two Different Monomer Concentrations . . . . .	177
XXV NMR Data on Poly- $\alpha$ -methylstyrene . . . . .	178
XXVI Anionic Polymerization of Methyl Methacrylate with Triphenylmethyllsodium Initiator . . . . .	184
XXVII Anionic Polymers of Methyl Methacrylate . . . . .	186

## PART I - DILUTE SOLUTION STUDIES

### I. Branched Polymers--Dimensions of Chains with Small Excluded Volume\* — G. C. Berry and T. A. Orofino

In previous reports (ASD-TR 61-22, Parts II and III) preliminary accounts were given of theoretical calculations of the initial effect of segment-segment excluded volume on the dimensions of branched polymer molecules. In the following text, we present a detailed treatment of the complete investigation while bringing the discussion up to date.

#### A. Introduction

In an earlier communication<sup>1</sup> the unperturbed dimensions of selected star- and comb-shaped branched structures were calculated in accordance with the familiar random flight model. It is the purpose here to extend some of these computations to take into account the initial effect of segment excluded volume on molecular size. In terms of observable systems, the model employed is intended to correspond to polymer-solvent mixtures maintained at temperatures somewhat removed from the  $\Theta$ -point of the selected pair.

Specifically, we shall be concerned with evaluation of the coefficient  $a_1$  appearing in the series development for the mean square radius  $\langle s^2 \rangle$  of a polymer chain<sup>2</sup>

$$\langle s^2 \rangle / \langle s_0^2 \rangle \equiv \alpha^2 = 1 + a_1 z + a_2 z^2 + \dots \quad (1)$$

as applied to certain classes of p-functional regular star and regular comb molecules<sup>3</sup>. In the above relationship, suitable for the description of either linear or branched molecules,  $\alpha^2$  denotes the expansion of the mean square radius about its random flight value (subscript zero) and  $z$  is an interaction parameter defined by

$$z = (3/2\pi b^2)^{3/2} n^{1/2} \beta \quad (2)$$

where  $b$  is the length of one freely jointed chain element of (excluded) volume  $\beta$  and  $n$  is the total number of such segments comprising the polymer model considered. Under random flight conditions ( $\Theta$ -solvent media)  $\beta$  is zero. The coefficient  $a_1$  in Eq. (1), particular for each specified, geometrical chain structure, may thus be taken as a measure of the extent to which weak, (net) segment-solvent interactions augment the molecular radius.

\*Part of this work was presented at the 144th Meeting of the American Chemical Society, April 1963, Los Angeles, California

\*\*Manuscript released by the authors August, 1964, for publication as an ML Technical Documentary Report.

The range of experimental conditions over which Eq. (1), expressed only to the term linear in  $z$ , may be expected to provide an adequate description of a given polymer-solvent pair is usually quite restricted. Nevertheless, knowledge of the parameter  $a_1$  is of importance in: (1) providing a relative comparison between chain dimensions of chemically identical polymers of different structure dissolved in common, poor-solvent media; (2) correlations of  $\alpha^2$  with second virial coefficient data, through which a measure of absolute chain dimensions may be obtained and (3) establishing a rigorous basis for certain approximate treatments of coil size.

## B. Theory

In adapting the relationship (1) to branched polymer systems, we have employed a procedure equivalent in most essential details to that followed by Fixman<sup>2</sup> and earlier investigators in applications to the linear molecule. Before proceeding with the mathematical development, however, it may be useful to provide a brief, descriptive supplement to the general theoretical treatment, expressed somewhat more directly in terms of the molecular model assumed.

The usual analogy drawn between the real polymer molecule dissolved in  $\theta$ -solvent media and the familiar random flight chain suggests the obvious extension to good-solvent systems, viz. representation of the polymer by an equivalent chain model in which each constituent segment pervades a certain volume in space. The latter stipulation imposes restrictions upon the conformational behavior of the assumed model, which may be presumed to relate closely to those experienced by the real polymer chain in dilute solution. Random flight statistics suffice for description of the model system, the computations involved amounting to deletion of those contributions to a particular property which violate the restrictions of volume exclusion. Thus, in calculations of the mean square radii, only those conformations, and the associated dimensions, of random flight chains are retained in which all of the specified elements of volume assigned the segments in no way overlap.

The required enumeration, and subsequent subtraction, of forbidden random flight conformations may be conveniently implemented through an appropriate series designation for the probability of the union of  $\binom{n}{2}$  events, each of which denotes an overlap between two particular chain segments. Retention of only the first term of the series accounts for deletion of all possible random flight conformations, considered individually, in which at least one such overlap occurs. This stage of development, with which we shall be solely concerned in the present treatment of branched molecules, is analogous to the "single contact" approximation originally introduced by Zimm<sup>4</sup> in the related treatment of the second virial coefficient.

In accordance with simplifications adopted in the treatment of the model chain, several assumptions concerning the nature of polymer-solvent interactions in real systems are implied: (1) the polymer

molecule can be regarded as comprised of identical, flexible chain elements (statistical segments); (2) the nature of (net) segment-segment interactions is such as to justify representation by a short range potential function; and (3) the various interactions are pairwise additive (assumption of superposition).

1. Formulation of the mean square radius. Consider a random flight chain, of any specified branching geometry, in which the length of each of the  $n$  contiguous chain elements is governed by a gaussian distribution\*. The probability that the  $t$ -th segment vector assumes the value  $\underline{r}_t$  is proportional to  $\exp(-3r_t^2/2b^2)$  where  $b$  is the rms segment length. The random flight probability distribution for the spatial arrangement of a particular linear sequence of elements (numbered serially) from  $i$  to  $j$  may thus be expressed

$$P^0(\underline{r}_{ij}) = \prod_{t=i}^j (3/2\pi b^2)^{3/2} \exp(-3r_t^2/2b^2) \quad (3)$$

to which  $\underline{r}_{ij}$  is the vector displacement of the terminal elements of the sequence.

Equation (3) can be modified through incorporation of an appropriate weighting factor  $f_{k\ell}$ , to provide for exclusion of those conformations in which any two (contact) elements  $k$  and  $\ell$  occupy a common volume in space. Thus,  $f_{k\ell}$  must assume the value zero in any chain conformation in which elements  $k$  and  $\ell$  overlap within a prescribed element of (excluded) volume  $\beta$ , and must be unity otherwise. Following Fixman<sup>2</sup> we set

$$f_{k\ell} = 1 - \delta(\underline{r}_{k\ell})\beta \quad (4)$$

in which  $\delta(\underline{r}_{k\ell})$  is a three dimensional delta function of the vector separation of contact elements  $k$  and  $\ell$ . The procedure cited\*\* leads to the following expression for  $P(\underline{r}_{ij})$ , the analog of Eq. (3) for a chain model with excluded volume

---

\* The assumption of gaussian segments in the chain model is introduced primarily for the purpose of mathematical expediency in the subsequent development. The same result ensues if the chain is considered to be comprised of a large number of fixed-length segments, each capable of random orientation with respect to its neighbors.

\*\* For the present purpose one could adopt alternatively a simpler model in which  $\beta$  is taken to be proportional to a volume element of configurational space within which simultaneous occupancy by two or more segment vectors is excluded. The  $\delta$ -function formulation of Eq. (4), however, embodies the mathematical features essential in any of a number of segment-segment potential functions whose characteristics need not be further specified.

$$\begin{aligned}
P(\underline{r}_{ij}) d\underline{r} &= P^0(\underline{r}_{ij}) \prod_{k > \ell} (1 - \delta(\underline{r}_{k\ell})\beta) d\underline{r} \\
&= P^0(\underline{r}_{ij}) \left[ 1 - \beta \sum_{k > \ell} \delta(\underline{r}_{k\ell}) + O(\beta^2) \right] d\underline{r}
\end{aligned} \tag{5}$$

In the above equation the summations extend over all possible choices of contact pairs.

The mean square separation of chain elements  $i$  and  $j$  is defined through the general relationship

$$\langle r_{ij}^2 \rangle = \frac{\int \dots \int r_{ij}^2 P(\underline{r}_{ij}) d\underline{r}_i \dots d\underline{r}_j}{\int \dots \int P(\underline{r}_{ij}) d\underline{r}_i \dots d\underline{r}_j} \tag{6}$$

Substitution for  $P(\underline{r}_{ij})$  in accordance with Eq. (5), followed by division of the resulting power series, leads to the expression

$$\langle r_{ij}^2 \rangle = \langle r_{ij}^2 \rangle_0 - \beta \sum_{k > \ell} \int \dots \int \left[ r_{ij}^2 - \langle r_{ij}^2 \rangle_0 \right] \delta(\underline{r}_{k\ell}) P^0(\underline{r}_{ij}) d\underline{r}_i \dots d\underline{r}_j + O(\beta^2) \tag{6a}$$

in which the subscript zero on  $\langle r_{ij}^2 \rangle$  denotes the random flight value. The required integrations over spatial coordinates may be carried out in a systematic fashion appropriate for any particular branched structure of interest. The general result may be more elegantly expressed, however, through application of the Wang-Whlenbeck-Fixman Theorem<sup>2</sup>. Through this procedure, Eq. (6a) in a form suitable for any branched structure becomes

$$\langle r_{ij}^2 \rangle = \langle r_{ij}^2 \rangle_0 + (3/2\pi b^2)^{3/2} b^2 \beta \sum_{k > \ell} (C_2^2/C_1^{5/2}) + O(\beta^2) \tag{6b}$$

where  $C_1$  is the number of chain elements in the closed sequence formed by contact between segments  $k$  and  $\ell$ , and,  $C_2$  is the number of elements common to this sequence and to the contiguous set of elements connecting segments  $i$  and  $j$ .

Summation of Eq. (6b) over all segment pairs  $i$  and  $j$  in accordance with the general defining relation for the mean square radius

$$\langle s^2 \rangle = (1/n^2) \sum_{j > i} \sum_i \langle r_{ij}^2 \rangle \quad (7)$$

generates the desired expression for  $\langle s^2 \rangle$  as a power series in the excluded volume  $\beta$ . Formal division of the series by  $\langle s^2 \rangle$  the appropriate value of the unperturbed mean square radius for the particular branched structure considered, provides the alternative series expression for  $\alpha^2$  in terms of the parameter  $z$  given earlier in Eqs. (1) and (2). The single-contact coefficient  $a_1$  appearing in Eq. (1) may be explicitly expressed in terms of the present formalism and becomes

$$a_1 = (6/gn^{7/2}) \sum_{j > i} \sum_i \sum_{k > \ell} \sum_{\ell} (C_2^2/C_1^{5/2}) \quad (8)$$

In this representation, the unperturbed radius of the molecule enters as a function of  $g$ , the ratio of the mean square radius of the random flight branched chain to that for its linear counterpart containing the same total number of segments. The latter is given by the familiar expression,  $nb^2/6$ .

2. Configuration classes. In the sections following, the evaluation of the coefficient  $a_1$  appearing in Eq. (1) and defined by Eq. (8) will be described for star and comb-branched structures. In each case the disposition of the four chain elements  $i, j$  (vector) and  $k, \ell$  (contact) involved in the latter relationship may be conveniently divided into three general classifications. The required summations over the indices appropriate to each class are readily formulated. For long chains, these may be satisfactorily approximated by elementary integrals which are easily evaluated. The structural classifications, together with the results of the integrations, designated by the symbol  $\Gamma$  with subscript, are listed below.

- I Linear chain - the four segments  $i, j, k$  and  $\ell$  are all members of a common linear sequence of chain elements of total length  $x$  elements. Summation over all permissible permutations of the index segments required by Eq. (8) yields

$$\Gamma_I(x) = \iiint (C_2^2/C_1^{5/2}) di dj dk d\ell = (67/315) x^{7/2} \quad (9)$$



a result obtained previously by Fixman<sup>2</sup> in his treatment of the linear molecule.

- II Single trifunctional branch point--the four segments are distributed among three linear sequences, of lengths  $y_1$ ,  $y_2$  and  $y_3$ , which are jointed together at a common point. Each sequence contains at least one of the index segments. All possible dispositions of the index segments consistent with the foregoing definition are to be considered. The appropriate contribution to Eq. (8) is

$$\begin{aligned} \Gamma_{II}(y_1, y_2, y_3) = & (4/45)[h(y_1, y_2, y_3) + h(y_2, y_3, y_1) \\ & + h(y_3, y_1, y_2)] \end{aligned} \quad (10)$$

where

$$\begin{aligned} h(\lambda, \mu, \nu) = & \lambda(\mu + \nu)^{-1/2} [29(\mu^3 + \nu^3) + 72(\mu^2\nu + \mu\nu^2)] \\ & - 29\lambda^{5/2}(\mu + \nu) - 80\lambda^{3/2}\mu\nu \end{aligned} \quad (11)$$

- III Double trifunctional branch points - each of the four index segments is a member of one of four linear sequences which are joined together through a fifth linear sequence, as shown in Fig. 1. Consideration of all permissible arrangements for this class leads to the expression

$$\begin{aligned} \Gamma_{III}(y_1, y_2, x, y_3, y_4) = & (4/3) x^2 [y_2 y_4 q(y_1, y_3) \\ & + y_2 y_3 q(y_1, y_4) + y_1 y_4 q(y_2, y_3) \\ & + y_1 y_3 q(y_2, y_4)] \end{aligned} \quad (12)$$

where the function  $q$  is defined by

$$q(\lambda, \mu) = x^{-1/2} - (\lambda + x)^{-1/2} - (\mu + x)^{-1/2} + (\lambda + \mu + x)^{-1/2} \quad (13)$$

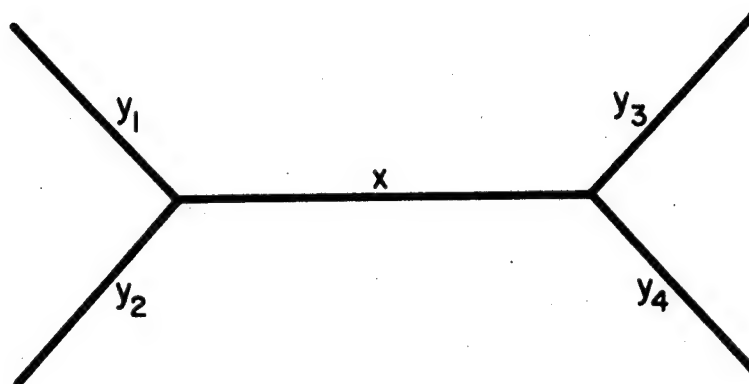


Figure 1 A Class III Configuration

The foregoing analytical expressions\* for the  $\Gamma$  terms, properly combined, suffice (together with  $g$ ) to establish values of  $a_1$  for any branched structure\*\*, and in particular, for those considered in the present treatment. For star molecules the terms  $\Gamma_I$  and  $\Gamma_{II}$  alone need be utilized; for comb molecules, all three are required.

### C. Computations for Model Structures

1. Regular star molecules. The star model considered contains a total of  $n = py$  segments distributed among  $p$  identical, linear branches joined through one end at a common junction.

Resolution of the various contact cases is greatly facilitated by symmetry considerations. Thus, there are a total of  $\binom{p}{2}$  combinations of pairs of branches, each of which contributes a single term of class I in which  $x$  assumes the value  $2y$ . In this enumeration process, however, there occur  $p(p-1)$  identical configurations of class I involving single branches (with  $x$  equal to  $y$ ) of which only  $p$  are required; hence,  $p(p-1) - p = p(p-2)$  must be subtracted. Finally, there are  $\binom{p}{3}$  configurations of class II involving three branches (with  $y_1 = y_2 = y_3 = y$ ). In accordance with Eq. (8),  $a_1$  for these structures thus becomes

\* It may be appreciated from the definitions of the variables  $C_1$  and  $C_2$  appearing in Eq. (8) that a configurational class involving a tetra-functional branch point (each arm of the star shaped structure containing one of the four index segments) makes no contribution in the evaluation of the coefficient  $a_1$ .

\*\* Molecules containing rings or closed loops are specifically excluded. These may be treated through an analogous procedure.

$$a_1 = (6/gp^{7/2}y^{7/2})[(\binom{p}{2}\Gamma_I(2y) - p(p-2)\Gamma_I(y) + \binom{p}{3}\Gamma_{II}(y,y,y)] \quad (14)$$

Insertion of the  $\Gamma$  values given by Eqs. (9) and (10), together with the general expression for  $g$  for regular star molecules<sup>1</sup>

$$g = 3/p - 2/p^2 \quad (15)$$

yields the final result

$$a_1 = 3[p^{1/2}(3p-2)]^{-1}[(p-1)A_1 - 2(p-2)A_2 + 2(p-1)(p-2)A_3] \quad (16)$$

where

$$A_1 = 2^{7/2}A_2 = 2^{7/2}(67/315)$$

$$A_3 = (2/45)(101\sqrt{2} - 138)$$

Note that for  $p$  equal to either one or two (linear molecule), Eq. (16) reduces to the familiar value 134/105.

2. Regular comb molecules. The present calculations for comb-branch molecules have been applied to a convenient structural class which differs slightly from its counterpart of Paper II. As before, the generic molecule consists of a linear backbone to which identical linear side chains of length  $y$  segments are attached at regularly spaced intervals along the main chain. The end branches in this model, however, are symmetrically disposed with respect to the termini of the backbone, as shown in Fig. 2. The regular comb structure is completely specified for the present purposes through assigned values of  $p$ , the number of branches attached, and  $r$ , the ratio of the number of segments in one branch to that in one section of backbone between adjacent branch points. The total number of segments in the molecule may be expressed as  $n = (y/r)(pr + p + 1)$ .

The various single contact configurations involving the index segments  $i, j, k$  and  $l$  must be taken into account in application of Eq. (8) can be systematically enumerated. Again, the symmetry characteristics of the molecule can be exploited, thus greatly simplifying the

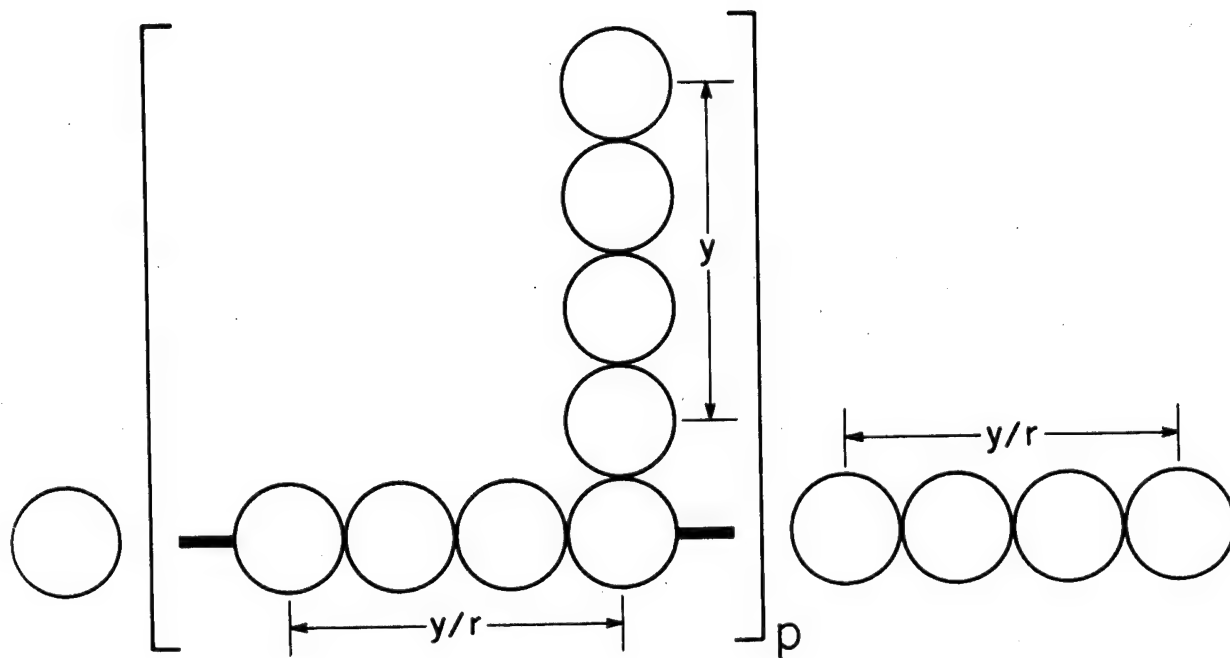


Figure 2 Regular comb structures

subsequent computations. The overall treatment, although much more elaborate, does not differ in principle from that outlined for star structures.

It is convenient to group the various configurations for comb structures according to locations of the index segments which collectively involve:

- 1 - at most one side chain
- 2 - exactly two side chains
- 3 - exactly three side chains
- 4 - exactly four side chains

In cases 1-3 above, the linear backbone of the molecule may or may not also be involved as a designated site for one or more index segments. In terms of the general compartmentalization of molecular sub-units defined earlier (classes I-III), non-zero contributions to Eq. (8) arising from the four groups above may be identified as follows: group 1: class I or II; group 2: class I, II or III; group 3: class II or III; group 4: class III.

Resolution of the various structural components may be illustrated through detailed consideration of the comb molecule containing two branches. The appropriate structural components are depicted in Table I, together with the various contributions to the double sum of Eq. (8) derived therefrom.

The final, general result for the coefficient  $a_1$  of Eq. (1) for regular comb molecules is expressed through the relation

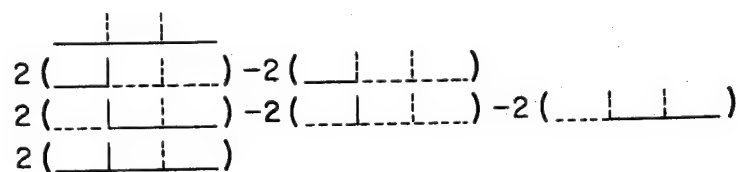
$$a_1 = (6/g)(pr + p + 1)^{-7/2} \sum_{v=1}^4 S_v \quad (17)$$

in which the quantities  $S_v$  are defined by the following equations:

$$S_1 = \Gamma_I(p+1) - p\Gamma_I(r) + \sum_{u=1}^p \left[ 2\Gamma_I(u+r) - 2\Gamma_I(u) + \Gamma_{II}(u, r, p+1-u) \right] \\ + \sum_{u=1}^{p-1} u \left[ \Gamma_I(2r+p-u) - 2\Gamma_I(r+p-u) + \Gamma_I(p-u) \right] \quad (18)$$

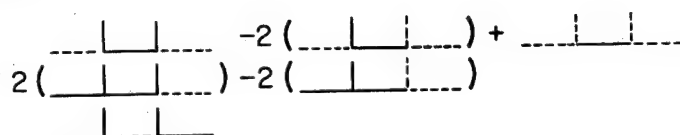
Table I. Schematic representation of structural components (see Fig. 2)  
and associated  $\Gamma$  terms for a comb molecule,  $p = 2$ .

group 1



$$\begin{array}{l}
 \Gamma_I(3y/r) \\
 2\Gamma_I(y/r+y) - 2\Gamma_I(y/r) \\
 2\Gamma_I(2y/r+y) - 2\Gamma_I(y) - 2\Gamma_I(2y/r) \\
 2\Gamma_{II}(y/r, y, 2y/r)
 \end{array}$$

group 2



$$\begin{array}{l}
 \Gamma_I(y/r+2y) - 2\Gamma_I(y/r+y) + \Gamma_I(y/r) \\
 2\Gamma_{II}(y/r, y, y/r+y) - 2\Gamma_{II}(y/r, y, y/r) \\
 \Gamma_{III}(y/r, y, y/r, y, y/r)
 \end{array}$$

group 3, 4

None

$$S_2 = \sum_{u=1}^{p-1} \sum_{v=u+1}^p \left[ 2\Gamma_{II}(u, r, r+v-u) - 2\Gamma_{II}(u, r, v-u) + \Gamma_{III}(u, r, v-u, r, p+1-v) \right] \quad (19)$$

$$S_3 = \sum_{u=1}^{p-2} \sum_{v=u+1}^{p-1} \sum_{w=v+1}^p \left[ \Gamma_{II}(r+v-u, r, r+w-v) - 2\Gamma_{II}(v-u, r, r+w-v) + \Gamma_{II}(v-u, r, w-v) + 2\Gamma_{III}(u, r, v-u, r, r+w-v) - 2\Gamma_{III}(u, r, v-u, r, w-v) \right] \quad (20)$$

$$S_4 = \sum_{t=1}^{p-3} \sum_{u=t+1}^{p-2} \sum_{v=u+1}^{p-1} \sum_{w=v+1}^p \left[ \Gamma_{III}(r+u-t, r, v-u, r, r+w-v) - 2\Gamma_{III}(u-t, r, v-u, r, r+w-v) + \Gamma_{III}(u-t, r, v-u, r, w-v) \right] \quad (21)$$

For these comb structures the parameter  $g$  appearing in Eq. (17) takes the form<sup>\*5</sup>

$$g = [p(r+1) + 1]^{-3} [(p(3p-2)r^3 + p(p+1)(p+2)r^2 + p(2p+1)(p+1)r + (p+1)^3)] \quad (22)$$

\*In terms of  $g$ , the comb-branched molecules of this work differ insignificantly from those at equivalent  $p$  and  $r$  (i.e.,  $py/x$ ) treated in Paper II, provided that  $p$  is greater than about five. In like manner,  $a_1$  values for the two generic structures should be almost identical for all but the simpler members of the series.

Several limiting forms of Eq. (17) and associated quantities are readily ascertainable and serve as a partial check on the accuracy of the general result. For  $p = 0$ , all of the  $S$  terms vanish, except for the first member of Eq. (18). The latter, in accordance with the appropriate, degenerate form of Eq. (17), gives rise to the familiar  $a_1$  value for the linear chain. Similarly, for  $r = 0$  the result for the linear chain is obtained, in this case through identical cancellation of all  $\Gamma_I$  terms except, again, the first member of  $S_1$ . It can also be shown, with a bit more effort, that Eq. (17) yields the correct, general result for regular star molecules (Eq. (16)) upon stipulation that the ratio  $r/p$  be very much greater than unity. Finally, we have compared several additional limiting cases from Eq. (17) with expressions for  $a_1$  derived from independent calculations relevant to certain elementary members of the comb structures.

3. Numerical results. Selected numerical values of the interaction coefficient  $a_1$  computed from Eqs. (16) and (17) for star and comb molecules, respectively, are listed in Tables II and III. Included also are corresponding entries for the branching parameter  $g$  as calculated from Eqs. (15) and (22). Most of the values listed were obtained with the aid of an IBM 704 computer\*, the use of which was indispensable in the protracted calculations of  $a_1$  for comb structures. In all cases, suitable Fortran programs for the necessary operations were devised. Numerical results provided by the computer were checked in a variety of ways in order to insure that proper translation of the required algebraic manipulations into machine instructions had been effected.

The general relation of  $a_1$  to structural characteristics of the branched chains is shown graphically in Figs. 3, 4 and 5 in which the interaction coefficient is plotted versus  $p$ ,  $r$  and  $1-g$ , respectively. Constructions of this kind may also be useful in arriving at approximate, extrapolated values of  $a_1$  in accordance with the suggestions following.

For comb molecules it can be shown that  $a_1$  approaches the asymptotic form

$$\lim_{\substack{r \rightarrow 0 \\ p \rightarrow \infty}} a_1 = (134/105)(1 + r)^{3/2} \quad (23)$$

Thus, in analogy with the linear chain,  $a_1$  for a comb structure characterized by a sufficiently small value of  $r$  approaches a numerical limit which is

---

\*The total array of  $a_1$  values for which machine calculations were carried out consists of the following: star molecules--all integer  $p \leq 50$ ; comb molecules--all combinations of integer  $p$  1 to 10 with  $r$  values 0.01, 0.05, 0.1, 0.2, 0.3, 0.4, 0.5, 0.6, 0.8, 0.9, 1, 2, 3, 5, 7, 10, 15, 2, 5, 1 and 999; all combinations of integer  $p$  11 to 25 with  $r$  values 0.2, 0.5, 1, 2, 5, 10, 20 and 50. Copies of these results are available to interested persons upon request.



Table II

Values of  $a_1$  and  $g$  for Regular Star Molecules

<u>p</u>	<u><math>a_1</math></u>	<u>g</u>
1,2	1.2762	1.0000
3	1.2983	0.7778
4	1.3421 <sup>a</sup>	0.6250
5	1.3940	0.5200
6	1.4488	0.4444
8	1.5594	0.3438
12	1.7702	0.2361
$\rightarrow \infty$	$\rightarrow 0.4298 p^{1/2}$	$\rightarrow 0$

<sup>a</sup> A lower value (1.12) for cruciform star molecules was obtained earlier by Fixman<sup>2</sup>. His apparently erroneous procedure differs from that employed here in the manner in which our Eq. (6b) is applied to specific branched structures.

Table III

Values of  $a_1$  and  $g$  for Regular Comb Molecules

<u>p</u>	<u>r</u>	<u><math>a_1</math></u>	<u>g</u>
1	0.5	1.3144	0.8080
	2	1.3155	0.8125
2	0.5	1.3966	0.7656
	1	1.3858	0.7120
	2	1.3858	0.7201
	5	1.3930	0.8088
3	0.5	1.4574	0.7431
	1	1.4552	0.6676
	2	1.4318	0.6400
	5	1.4060	0.6720
4	0.5	1.5068	0.7289
	1	1.5223	0.6379
	2	1.4922	0.5849
	5	1.4383	0.5776
5	0.5	1.5485	0.7191
	1	1.5865	0.6168
	2	1.5626	0.5459
	5	1.4880	0.5116
10	0.5	1.6893	0.6960
	1	1.8486	0.5659
	5	1.8886	0.3563
	10	1.7745	0.3193
15	0.5	1.7733	0.6871
	1	2.0319	0.5458
	5	2.3916	0.2972
	10	2.2599	0.2474
20	0.5	1.8307	0.6823
	1	2.1668	0.5351
	5	2.9052	0.2661
	10	2.8378	0.2099
	20	2.5709	0.1786
25	0.5	1.8732	0.6793
	1	2.2712	0.5285
	10	3.4644	0.1869
	20	3.1625	0.1532

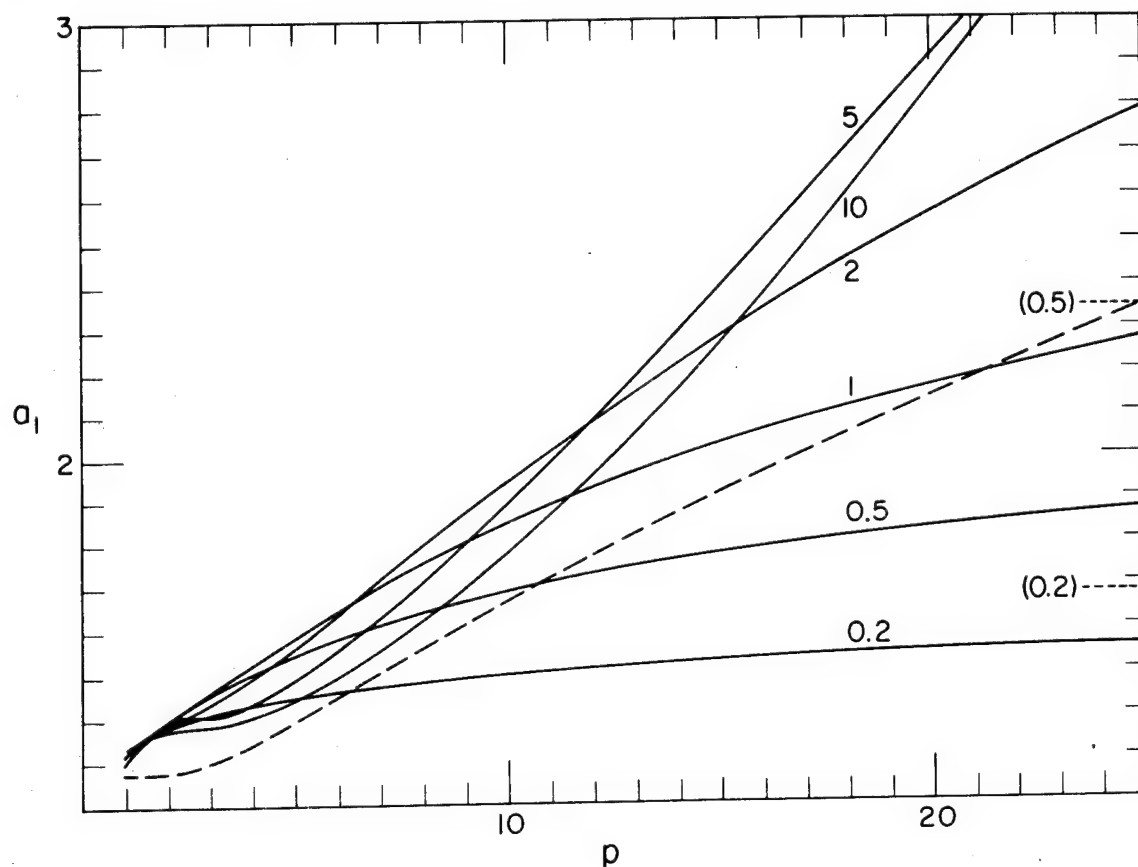


Figure 3 Plots of  $a_1$  versus  $p$  for regular star molecules (dashed curve) and for regular comb molecules at various  $r$  values. Dashed lines denote asymptotic limits of  $a_1$  for comb structures as  $p \rightarrow \infty$  (see text).

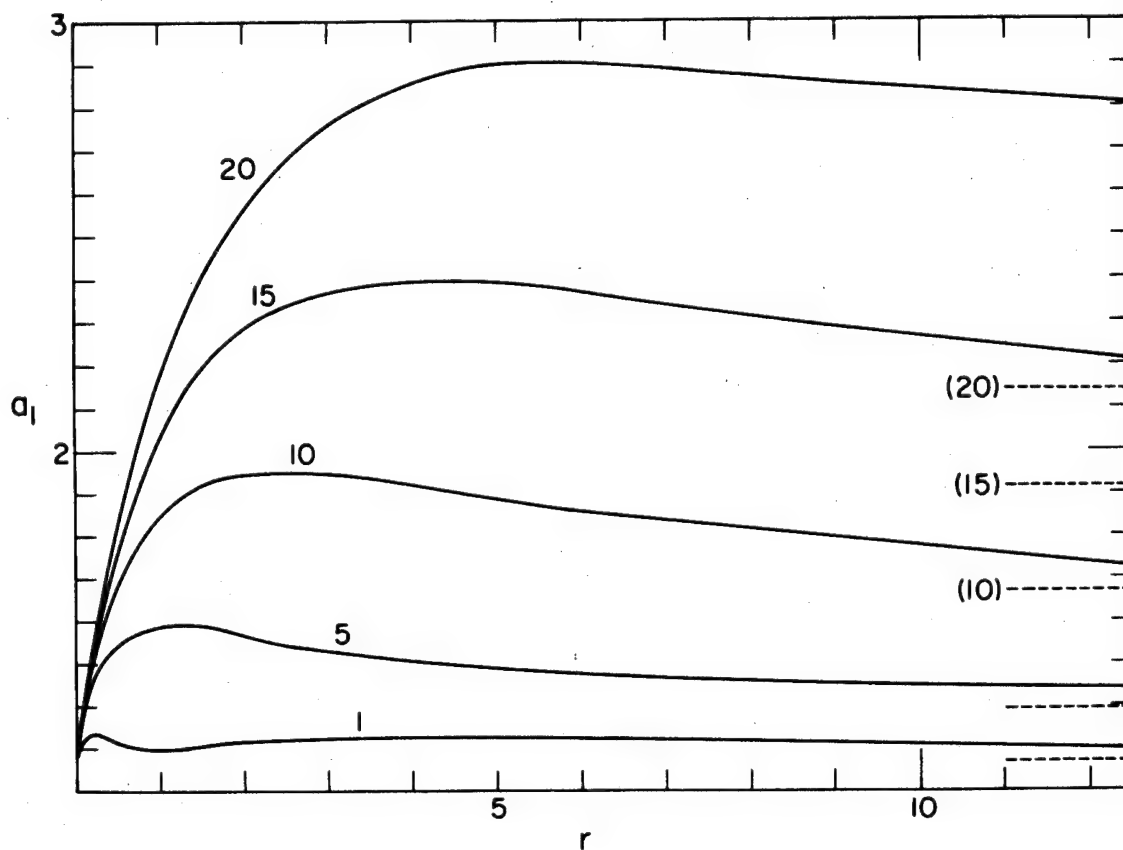


Figure 4 Plots of  $a_1$  versus  $r$  for various  $p$ -functional regular comb molecules. Dashed lines denote asymptotic limits ( $a_1$  for star structures at corresponding  $p$ ).

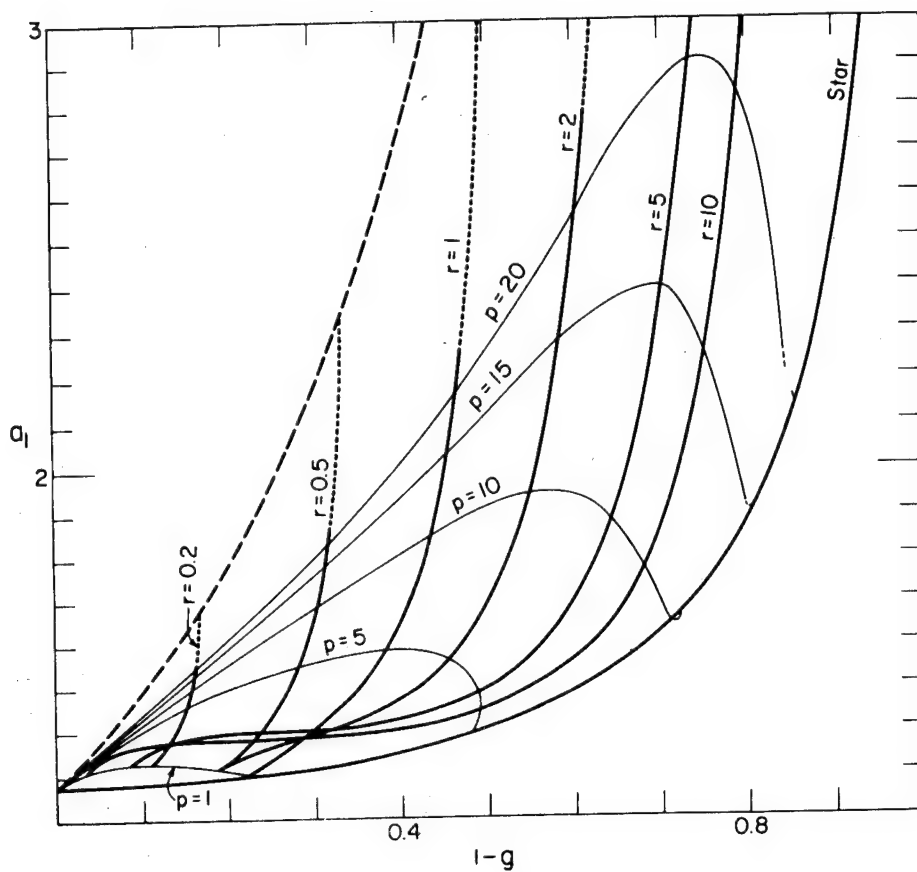


Figure 5 Plots of  $a_1$  versus  $1-g$  for star molecules and for comb molecules with various  $r$  and  $p$  values. Solid portions of the family of curves for the latter denote the range of values computed in this work. The left-hand boundary curve describes a plot of limiting  $a_1$  and  $1-g$  values for  $p \rightarrow \infty$  at fixed  $r$  (see text).

independent of the length ( $\sim p$ ) of the backbone chain. It is apparent from analysis of our tabular data that the foregoing expression approximates  $a_1$  to within a few percent for values of the ratio  $p/r$  greater than about 300. The dashed lines in Fig. 3 represent values of  $a_1$  computed in accordance with Eq. (23) for the  $r$  values denoted. These limits should serve as a useful index in extrapolation of such curves beyond values of  $p$  here considered. An analogous construction, also useful for extrapolation purposes, is employed in Fig. 5; the left-hand boundary curve, a plot of the expression of Eq. (23) versus corresponding, limiting values of  $1-g$  at  $p \rightarrow \infty$  (from Eq. (22)), provides the upper terminus for each member of the  $r$  family of comb curves shown.

The asymptotic behavior of  $a_1$  for comb structures as  $r$  approaches large values at given  $p$  is shown in Fig. 4. The limiting values of  $a_1$  (for star structures, Eq. (16)) are indicated and, again, provide a guide for graphical extrapolation.

4. Discussion. Examination of the preceding results shows that for star structures containing a specified total number  $n$  of segments, the interaction coefficient  $a_1$  increases smoothly with the number of branches attached. This trend might perhaps have been anticipated, in view of the accompanying increase in mean segment density within the domain of the molecular coil. The latter quantity, for the purpose of qualitative discussion, may be considered proportional to  $n/(\langle s_0^2 \rangle)^{3/2}$ , in turn, proportional to  $g^{-3/2}$ ; for star molecules (see Eq. (15)) the mean density thus varies approximately as  $p^{3/2}$ . The dependence of  $a_1$  on chain architecture for comb structures is considerably more complex, but, again, throughout most of the range of  $p$  and  $r$  values, increase of  $a_1$  with mean coil density is indicated. Relative comparisons of  $a_1$  values between the two classes of structures, however, reveal some more interesting results: (1) at a specific value of  $g$  (comparable coil densities) star structures exhibit the lowest value of  $a_1$ . As may be conveniently ascertained through Fig. 5, the maximum value (left-hand boundary curve) is exhibited by a comb molecule containing many branches relatively short in comparison to the length of the backbone. It is noteworthy that the complete (random flight) density profile for such a structure<sup>6</sup> is very similar to that for a linear chain of the same mean square radius; (2) at fixed  $p$ , the maximum value of  $a_1$ , again, is displayed by a comb molecule (Fig. 4)--throughout the range of  $p$  and  $r$  values investigated here, by structures for which the ratio of backbone to branch length is approximately three. In these instances the mean coil densities ( $g^{-3/2}$ ) of the comb molecule are substantially less than those for the star (see Fig. 5).

It is clear from the above observations that excluded volume effects in the relatively tenuous comb structures are generally more pronounced than those exhibited by star molecules. The distinction is undoubtedly attributable to the much greater influence of interactions between elements remotely situated along the molecular chain. Although segment contacts in the relatively compact star structures may occur more frequently (that is, in comparison with the comb molecule, may eliminate a larger fraction of random flight conformations) they are generally less effective in augmenting molecular dimensions.

#### D. Application to Experiment

In the preceding section we have described for two particular classes of branched molecules the detailed computation of the coefficient  $a_1$  appearing in the series expression (1) for the molecular expansion factor. Although a knowledge of the linear term in this series provides a useful, qualitative guide to the effects of chain branching, the resulting, partial expression for  $\alpha^2$  is restricted to a very small range of net polymer-solvent interactions; consequently, it is of limited utility in direct analyses of experimental data. Moreover, the evaluation of  $a_2$  and higher coefficients, for any chain structure, constitutes a progressively formidable undertaking. The results of calculations such as those provided in the present treatment do, however, through various indirect routes, find important application to observable, experimental systems. Some of these are exemplified below.

1. Relationship between coil expansion and second virial coefficient. Perhaps the most significant relationship derivable from Eq. (1) results by combination of this series with the analogous development for the second virial coefficient<sup>4</sup>  $\Gamma_2$

$$\Gamma_2 = \beta(N_0 n^2/2M)(1 + b_1 z + b_2 z^2 + \dots) \quad (24)$$

where  $N_0$  is Avogadro's number,  $M$  is polymer molecular weight,  $b_1$  is a constant and the remaining symbols have the same identity as in Eqs. (1) and (2). A common molecular model is employed in both the treatments of Eq. (1) and Eq. (24). Accordingly, the interaction parameter  $z$  may be eliminated<sup>7</sup> to yield the combined series from

$$\Gamma_2 = (4\pi^{3/2}N_0/a_1)[\langle s_o^2 \rangle^{3/2}/M][(\alpha^2-1) + c_1(\alpha^2-1)^2 + o(\alpha^2-1)^3] \quad (25)$$

where

$$c_1 = (a_1 b_1 - a_2)/a_1^2 \quad (26)$$

The foregoing variant of Eq. (1), in addition to its freedom from somewhat arbitrary chain parameters, affords another advantage in that it appears to describe adequately experimental data over a greater range of polymer-solvent interaction than does either of its component series expressions. According to this relationship, a plot of  $\Gamma_2$  versus  $\alpha^2 - 1$  should define a smooth curve, the limiting tangent to which at  $T = \theta/(\alpha = 1)$  provides a direct measure of absolute coil dimensions. Since it is often possible

to estimate values of  $\alpha^2$  with sufficient precision from ratios of intrinsic viscosities, Eq. (25), with an appropriate value of  $a_1$ , may be employed<sup>8,9</sup> in the assessment of coil dimensions in a system where polymer molecular weight is too low to permit evaluation of  $\langle s^2 \rangle$  by conventional means (e.g., light scattering dissymmetry).

2. Approximate theories. A requirement that one might wish to impose in tests of approximate theories relating  $\alpha$  to polymer-solvent interaction ( $z$ ) over a wide range of the latter, is that in the limit as  $\alpha$  approaches unity the particular expression reduce to the appropriate series expansion Eq. (1).

Recent generalizations<sup>10,11</sup> of Flory's<sup>12</sup> treatment of  $\alpha$  for the linear molecule lead to expressions for branched polymers of the form

$$\alpha^5 - \alpha^3 = CK_b z \quad (27)$$

where  $K_b$  is equal to  $g^{-3/2}$  and  $C$  is a numerical constant. The latter can be assigned the value 134/105 in order that the relationship, when applied to the linear molecule ( $g=1$ ), fit the first order perturbation treatment expressed by Eq. (1). Equivalently, the procedure described equates the product  $CK_b$  with  $a_1$  for the linear case and implies that  $a_1$  for branched structures is adequately approximated by  $(134/105)g^{-3/2}$ . It is interesting to observe that this formulation is, in fact, a valid representation of  $a_1$  for long chain comb molecules containing short branches: combination of the expression for  $a_1$  given in Eq. (23) with the corresponding asymptotic form for  $g$ , derivable from Eq. (22), yields the desired result. The observed coincidence of limiting forms for  $a_1$  in this instance is quite reasonable. As pointed out earlier, the segment density distributions for elongated comb molecules resemble closely\* that for the linear chain--a similarity explicitly assumed in derivations leading to Eq. (27). It is apparent from inspection of Fig. 5, however, that the foregoing designation of  $K_b$ , applied to more compact branched structures, cannot rigorously describe the relationship of  $\alpha$  to  $z$  over a wide range of polymer-solvent interactions which include  $\Theta$  conditions.

An alternative way in which a relation of the form Eq. (27) could be adapted to the representation of  $\alpha$  for branched molecules is through the explicit stipulation that the product  $CK_b$  equal  $a_1$ . In applications to any chain structure, compliance with the first-order perturbation treatment would thus be assured. The suitability of the resulting expression for  $\alpha$  at large values of  $z$ , however, is difficult to assess. In some recent studies this kind of relationship has proved

\* One might in general expect a close similarity in solution properties displayed by an elongated comb molecule containing short branches and a chemically identical, linear molecule of comparable radius, the former approximated by the latter with an augmented excluded volume per chain segment.



useful in the comprehensive description of the solution properties of linear chains<sup>13</sup>, and, somewhat less satisfactorily, in analysis of data on comb molecules<sup>5</sup>.

Finally, in all applications to experimental data that are pertinent to theoretical calculations of the kind presented here, one should bear clearly in mind the marked differences between the model chain and the real polymer immersed in a solvent environment. Parameters characterizing the former can, of course, be unambiguously ascertained through appropriate phenomenological studies on a particular polymer-solvent pair. It cannot be assumed unquestionably, however, that, for example, a series of diverse branched structures of the same chemical composition, dissolved in the same solvent, relate to their respective model chain counterparts by means of the same value for the statistical segment length  $b$  (or volume,  $\beta$ ). There are, in fact, indications from experiment<sup>8</sup> that effects of molecular architecture may extend over linear chain sequences of appreciable length. The foregoing and related difficulties at least are amenable to experimental test and, accordingly, can properly be taken into account in interpretations of experimental data.

## II. Temperature Dependence of the Unperturbed Dimensions of Polystyrene — T. A. Orofino and A. Ciferri\*

### A. Introduction

The average dimensions of a polymer molecule at a given temperature depend upon the thermodynamic and geometric adaptation of the individual segments to the environment provided by other parts of the chain and the external medium in which the molecule is immersed. It is constructive to associate the temperature coefficient of the polymer chain dimensions with the separate<sup>1,2</sup> phenomena: (1) the excluded volume effect, namely, augmentation of coil size, relative to the unperturbed state, arising from interactions between chain elements remote from one another in contiguous sequence along the chain; and (2) the temperature dependent effect of localized segment interactions on the unperturbed chain dimensions. Several procedures have been suggested and utilized in evaluation of the latter effect, which is of great interest in connection with the study of internal bond rotations in polymer chains. Values of the thermal coefficient  $d \ln \bar{r}_0^2 / dT$ , where  $\bar{r}_0^2$  is the mean square separation of the ends of the chain, have thus been obtained for a number of polymers, either directly, through suitable studies on the unperturbed molecule (a) in bulk or (b) in  $\theta$ -solution, or indirectly, from (c) appropriate solution measurements of chain dimensions for which the excluded volume contribution (1) has been separately estimated.

Recent reviews<sup>14,15</sup> of published values for  $d \ln \bar{r}_0^2 / dT$  reveal that although satisfactory agreement between results obtained using methods (a) and (c) has been demonstrated for at least two polymer systems, in general there appear to be significant inconsistencies among the various data which call for a more detailed analysis of the entire problem.

In the present communication, values of  $d \ln \bar{r}_0^2 / dT$  for atactic polystyrene, arrived at through independent studies of the tension-temperature relationship for a cross-linked polymer sample (method (a)), and through  $\theta$ -solvent intrinsic viscosity measurements on the related linear material (method (b)), are reported. To the extent that the undiluted bulk polymer and its constituent linear chains immersed in  $\theta$ -media satisfactorily approximate a common, unperturbed state of the molecule, both sets of measurements may be considered to reflect directly changes in  $\bar{r}_0^2$  with temperature. Recourse to dilute solution theory for independent evaluation of the excluded volume effect, required in method (c), is thus avoided. In addition, an effort has been made to circumvent a fundamental difficulty in method (b) which has not, so far<sup>14</sup>, received adequate consideration. It has been amply demonstrated<sup>9,16-19</sup> that unperturbed dimensions in dilute solution may reflect significant specific solvent effects and, therefore, that  $d \ln \bar{r}_0^2 / dT$  values obtained by comparing coil dimensions of a given polymer in different  $\theta$ -solvents could lead to serious error. The likelihood of this complication has

\*Chemstrand Research Center, Durham, North Carolina

been minimized in the present study through selection of polymer-solvent systems for which the relative influence of specific effects may be presumed quite small.

In addition to the results of the experimental investigations outlined above, some indirect calculations of  $d \ln \bar{r}_0^2 / dT$  from literature data on polystyrene-solvent systems at  $T > \Theta$  are presented and discussed.

## B. Experimental

1. Tension-temperature studies. The polymer network utilized in this work was obtained by high-conversion bulk copolymerization of styrene and divinylbenzene. Soluble material extracted after prolonged swelling in benzene did not exceed 5 percent of the gel. A tension-temperature analysis at six points in the range 120-175°C was carried out with the unswollen polymer according to a technique described in detail elsewhere<sup>20</sup>. The sample was stretched to the desired elongation  $\alpha_e$  at the highest experimental temperature and allowed to relax until the tension  $f$  appeared constant. The temperature was then lowered and constant tension re-established. The procedure was repeated throughout a complete temperature cycle. No hysteresis was observed. Tension-temperature relationships established at three sample elongations are shown in Fig. 6. (Values for  $f$  have not been referred to the initial cross-sectional area of the sample, which was of the order  $15 \times 10^{-3} \text{ cm}^2$ .) Pertinent numerical data are included in Table IV.

2. Intrinsic viscosity studies. Solution viscosities of an anionically polymerized, linear polystyrene sample ( $M_w = 4.06 \times 10^5$ ) in the solvents 1-chloro-n-decane, 1-chloro-n-undecane and 1-chloro-n-dodecane, at four temperatures in the vicinity of each of the respective  $\Theta$ -points, were determined. The data for the chloroundecane system and a description of the experimental technique employed have been presented elsewhere<sup>9</sup>. An analogous investigation was carried out for the other two solvent systems (see Section IV, below).

The  $\Theta$ -temperatures for the polymer-solvent pairs were first estimated from precipitation studies. As described in detail for the chloroundecane system, accurate values of  $\Theta$  were then established through light scattering virial coefficient ( $\Gamma_2$ )-temperature measurements above and below  $\Theta$ , taking as the operational definition of the latter parameter the temperature at which  $\Gamma_2$  vanishes.

In Fig. 7 are plotted the observed intrinsic viscosity values  $[\eta]$  versus temperature for the three-polymer-solvent systems. The trend of  $[\eta]_\Theta$  with  $\Theta$ -temperature is indicated by the dashed line.

Numerical values assigned to  $\Theta$  and  $[\eta]_\Theta$ , together with the Huggins constants  $k'_\Theta$  and characterization data for the solvents, are compiled in Table V.

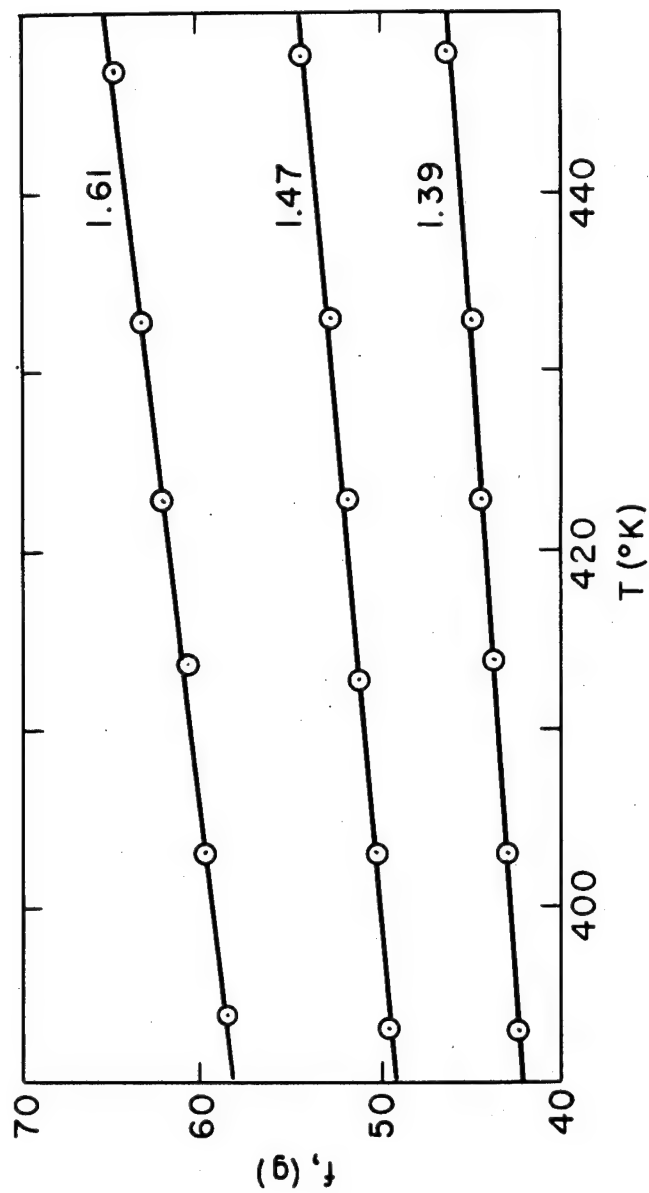


Figure 6 Tension-temperature curves at constant length for polystyrene networks. The elongation ratio  $\alpha_e$  (measured at 170°C) is indicated

Table IV

Tension-Temperature Data for the Polystyrene Network

$\alpha_e$	$10^3 (\partial f / \partial T)_{p,L}$ (from Fig. 1)	$\bar{f}_{150^\circ C}$ (grams)	$-10^3 [\partial \ln(f/T) / \partial T]_{p,L}$	$10^3 \beta / (\alpha_e^3 - 1)$	$10^3 (d \ln \bar{r}_0^2 / dT)$
1.39	70.0	44.1	0.79	0.35	0.44
1.47	88.3	51.8	0.68	0.27	0.41
1.61	120.0	61.6	0.43	0.18	0.25
					mean 0.37

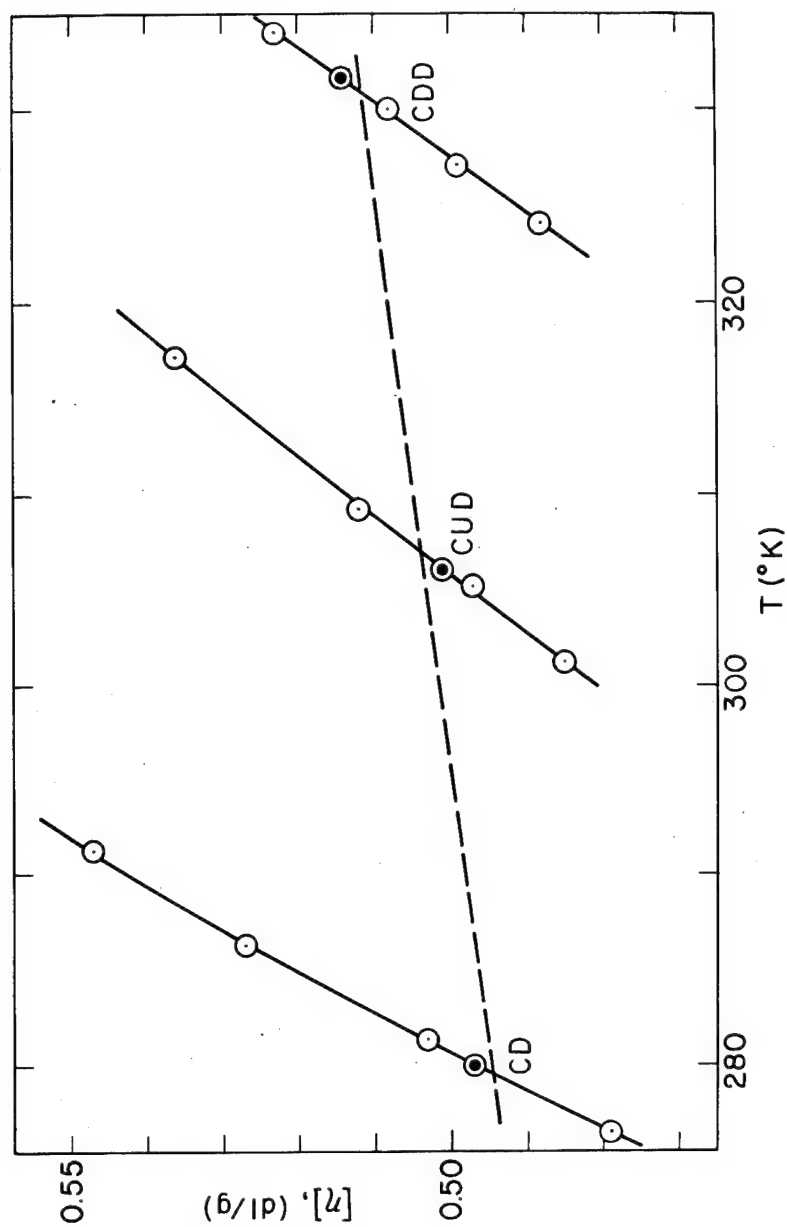


Figure 7 Plots of  $[\eta]$  versus temperature for polystyrene in 1-chloro-n-decane (CD), 1-chloro-n-undecane (CUD) and 1-chloro-n-dodecane (CDD). The filled circles denote interpolated  $[\eta]_{\theta}$  values.

Table V

Characterization Data for Polystyrene- $\theta$ -solvent Systems

Solvent	B.P., °C (observed)	$n_D^{20}$ (observed)	% Purity (Chroma- tography)	Principal Impurity	$\theta$ , °C	$[\eta]_{\theta}^c$ , dl/g	$k'_{\theta}$	$\delta^d$
1-chloro-n-decane	108.5 (18 mm)	1.4374	99.9	---	6.6 <sup>a</sup>	0.497	0.80	8.2
1-chloro-n-undecane	106.2 (7 mm)	1.4406	99.6	(undecyl alcohol)	32.8 <sup>b</sup>	0.501	0.68	8.2
1-chloro-n-dodecane	187.3 (100 mm)	1.4427	99.4	dodecene	58.6 <sup>a</sup>	0.514	0.56	8.2

(a) estimated uncertainty  $\pm 1.5^\circ\text{C}$ (b) estimated uncertainty  $\pm 1^\circ\text{C}$ (c) estimated uncertainty  $\pm 0.01$ 

(d) calculated solubility parameter

### C. Treatment of Data - Results

1. Tension-temperature studies. The variation of the unperturbed end-to-end distance with temperature may be determined from the data and constructions of Fig. 7 in accordance with the relationship<sup>20,21</sup>

$$\begin{aligned} d \ln \bar{r}_0^2 / dT &= 1/T - (1/f) (\partial f / \partial T)_{p,L} - \beta / (\alpha_e^3 - 1) \\ &= - [\partial \ln(f/T) / \partial T]_{p,L} - \beta / (\alpha_e^3 - 1) \end{aligned} \quad (28)$$

where  $\beta$  is the coefficient of cubical expansion for the polymer, taken<sup>22,23</sup> as  $5.85 \times 10^{-4} \text{ deg.}^{-1}$ . Intermediate data necessary for the calculation are compiled in Table IV, together with the final results in the last column. A positive value,  $(0.4 \pm 0.2) \times 10^{-3}$ , is found for the coefficient  $d \ln \bar{r}_0^2 / dT$ . This result may be considered compatible with the small value for  $d \ln \bar{r}_0^2 / dT$  indicated in Tobolsky's earlier study<sup>24</sup> of polystyrene networks.

2. Intrinsic viscosity studies. According to the Flory-Fox theory<sup>25</sup>, the intrinsic viscosity of a linear polymer in a  $\theta$ -solvent is given by the relationship

$$[\eta]_{\theta} = \Phi (\bar{r}_0^2 / M)^{3/2} M^{1/2} \quad (29)$$

where  $M$  is polymer molecular weight and  $\Phi$  is a constant. In general, the unperturbed dimension  $\bar{r}_0^2$  appearing in the above equation must be considered to depend upon both the temperature and the specific nature of the  $\theta$ -medium in which a particular polymer (of given molecular weight) is dissolved. In view of the close structural and chemical similarity of the  $\theta$ -media selected for the present study, the effect of the latter, relative to that operative with any given member of the solvent series, may be presumed small. Accordingly, to a first approximation, observed changes in  $[\eta]_{\theta}$  with environment may be attributed exclusively to concomitant changes in ( $\theta$ ) temperature. With this simplification, an expression for the thermal coefficient of  $\bar{r}_0^2$  is readily obtained through differentiation of Eq. (29). The result is

$$d \ln \bar{r}_0^2 / dT = (2/3) (d \ln [\eta]_{\theta} / d\theta) \simeq (2/3 [\eta]_{\theta}) (d [\eta]_{\theta} / d\theta) \quad (30)$$

The slope of the dashed line in Fig. 7 provides the increment  $d [\eta]_{\theta} / d\theta$ ; we calculate from Eq. (30) the value  $0.44 \times 10^{-3}$  for  $d \ln \bar{r}_0^2 / dT$ , in good agreement with the tension-temperature results. With respect to accountable uncertainties in the experimental data involved, the precision of the former value is estimated at  $\pm 0.2 \times 10^{-3}$ .



Previous studies based upon changes in  $[\eta]_{\theta}$  with temperature in various  $\theta$ -solvents have yielded zero<sup>26</sup>, or negative<sup>17,27</sup> values for  $d \ln \bar{r}_0^2 / dT$ .

#### D. General Treatment for Polymer-solvent Systems

Derivation of the thermal coefficient of  $\bar{r}_0^2$  through analysis of intrinsic viscosity data in non-ideal solvents, otherwise analogous to that outlined above for  $\theta$ -media, entails, in addition, the evaluation of the excluded volume contribution to the  $[\eta]$ -T relationship. It will be of interest to compare the results of such calculations, extracted from pertinent literature data, with the value of  $d \ln \bar{r}_0^2 / dT$  arrived at in the present experimental studies.

Extension<sup>25,28,29</sup> of Eq. (29) to polymer-solvent systems at temperatures  $T > \theta$  leads to the relationship

$$[\eta]_T = \Phi (\bar{r}_0^2 / M)_T^{3/2} M^{1/2} \alpha^p \quad (31)$$

$$2.4 \leq p \leq 3$$

where  $\alpha = (\bar{r}^2 / \bar{r}_0^2)_T^{1/2}$  denotes the expansion of the end-to-end distance relative to its unperturbed value at the same temperature  $T^*$ . Differentiation of Eq. (31) leads to the expression

$$d \ln \bar{r}_0^2 / dT = (2/3) (d \ln [\eta] / dT) - (2/3) (p/\alpha) (d\alpha / dT) \quad (32)$$

According to the above equation,  $d \ln \bar{r}_0^2 / dT$  may be extracted from readily and accurately ascertainable  $[\eta]$ -T data on any polymer-solvent system, provided that  $\alpha$  and  $d\alpha/dT$  can also be established. The contribution of the second term in Eq. (32) is least when the quantity  $T - \theta$  is greatest and, thus, calculations of  $d \ln \bar{r}_0^2 / dT$  are best applied to data on systems which are far above their  $\theta$ -temperatures (very good solvents). Practically, the most suitable systems are those for which  $[\eta]$ -T can be established at ordinary temperatures and for which  $\theta$  is equal to zero (athermal solvents)<sup>30,31,32</sup>.

\* For most purposes the ratio  $[\eta]_T / [\eta]_{\theta}$  provides a sufficiently accurate estimate of  $\alpha^p$ . For cases in which  $T - \theta$  is large, however,  $\alpha$  should more properly be expressed

$$\alpha^p = ([\eta]_T / [\eta]_{\theta}) [1 - (3/2) (T - \theta) (d \ln \bar{r}_0^2 / dT) + O(d \ln \bar{r}_0^2 / dT)]$$

possible specific solvent effects, in instances in which  $[\eta]_T$  and  $[\eta]_{\theta}$  refer to different solvents, being neglected.

According to the interpretation of Stockmayer and Fixman<sup>33</sup> concerning identification of the parameter  $\underline{z}$  appearing in their theories, various current forms for the relationship of  $\alpha$  to temperature may all be expressed by the proportionality

$$F(\alpha) \propto (1 - \theta/T)\sigma(T)/(\overline{r}_0^2)^{3/2} \quad (33)$$

where for present purposes  $\sigma(T)$  is to be considered an arbitrary function of temperature. Combination of Eqs. (32) and (33) leads to the result

$$\begin{aligned} d \ln \overline{r}_0^2 / dT = [2/3(3-3p(d \ln \alpha / d \ln F))][d \ln [\eta] / dT \\ - p(d \ln \alpha / d \ln F)(\theta/T(T-\theta) + d \ln \sigma / dT)] \end{aligned} \quad (34)$$

According to the Flory theory<sup>12,34</sup>,  $F(\alpha) = \alpha^5 - \frac{3}{\alpha}$  and  $\sigma(T) = \overline{v}^2/V_1$ , where  $\overline{v}$  is the partial specific volume of the polymer and  $V_1$  the molar volume of solvent. For this case Eq. (34) assumes the particular form

$$\begin{aligned} d \ln \overline{r}_0^2 / dT = [(3/2)(5\alpha^2 - p\alpha^2 + p - 3)]^{-1} [(5\alpha^2 - 3)(d \ln [\eta] / dT) \\ - p(\alpha^2 - 1)(\theta/T(T-\theta) + d \ln (\overline{v}^2/V_1) / dT)] \end{aligned} \quad (35)$$

According to Fixman's<sup>2,33</sup> theory,  $F(\alpha) = \alpha^3 - 1$  and Eq. (34) becomes<sup>29,\*</sup>

$$\begin{aligned} d \ln \overline{r}_0^2 / dT = [(1/2)(3\alpha^3 - p\alpha^3 + p)]^{-1} [\alpha^3(d \ln [\eta] / dT) \\ - (p/3)(\alpha^3 - 1)(\theta/T(T-\theta) + d \ln \sigma / dT)] \end{aligned} \quad (36)$$

Values of  $d \ln \overline{r}_0^2 / dT$  calculated from viscosity-temperature data for polystyrene in benzene<sup>27</sup>, toluene<sup>27,36</sup> and decalin<sup>6,37</sup> in accordance with each of the Eqs. (35) and (36) are compiled in Table VI. For the first two systems, the values of  $\theta$  and  $\alpha$  utilized are as given by Fox and Flory<sup>27</sup> in their original treatment of these data, extended to include an alternate choice for the exponent  $p$  appearing in Eq. (31). For simplicity, the  $\sigma$  term appearing in Eq. (36) has been identified with the molar volume ratio explicitly provided by the Flory Eq. (35).

\*The analogous expression for  $d \ln \overline{r}_0^2 / dT$  derived according to the Kurata-Stockmayer-Roig<sup>35</sup> theory yields, numerically, very similar results for all values of  $\alpha$ .

Table VI

Values of  $\frac{d \ln \overline{r_0^2}}{dT}$  for Polystyrene-solvent Systems

Solvent	$\Theta, ^\circ K$	$10^{-6} M$	$10^3 (d \ln [\eta] / dT)$	$10^3 (d \ln \sigma / dT)$	$10^3 (d \ln \overline{r_0^2} / dT)$		
					Flory, Eq. (35) p=3	Fixman, Eq. (36) p=2.5	Fixman, Eq. (36) p=2.5
benzene (45°C)	(100) <sup>a</sup>	1.27	-0.93	-0.21	-1.9	-1.6	-4.4
toluene (45°C)	(160) <sup>a</sup>	0.98	-0.23	-0.03	-1.9	-1.6	-4.7
decalin (90°C)	288 <sup>b</sup>	1.16	3.60	-0.07	-0.3	+0.3	-4.2
							-2.1

(a) derived, from  $[\eta]$ -T extrapolation

(b) observed, from  $\Gamma_2$ -T interpolation

The entries in Table VI generally indicate a negative value for  $\ln \bar{r}_0^2/dT$ , in contrast with the small positive value for this parameter found in our experimental studies. The disparity is particularly evident in the case of computations carried out according to the Fixman Eq. (36). Similar calculations applied to polymethylmethacrylate<sup>38</sup> and polyisobutylene<sup>39,40</sup> systems, for which values of  $\Theta$  and the ratio  $[\eta]/[\eta]_0$  are reported\*, likewise yield estimates for  $\ln \bar{r}_0^2/dT$  which are (algebraically) smaller than those either derived through thermoelastic measurements, or indicated by differences in  $[\eta]_0$  in related  $\Theta$ -solvents. In the cases of polyethylene<sup>21,30</sup> and polydimethylsiloxane<sup>20,31,32</sup>, however, for each of which viscosity data in athermal solvents ( $\Theta$  taken equal to zero) have been utilized in the calculation of  $\ln \bar{r}_0^2/dT$  according to Eq. (35), satisfactory agreement with bulk measurements has been found. It is nevertheless noteworthy that even in these instances values of  $\ln \bar{r}_0^2/dT$  arrived at through the former method appear to be slightly smaller (cf. in particular, Ref. 31).

#### E. Discussion and Conclusion

The agreement between results obtained independently from tension-temperature data and from viscosity data in structurally similar  $\Theta$ -solvents demonstrated in the present study is satisfactory. In view of the limited objections which can be raised to the validity of the two methods (cf. introductory section and discussion below), we feel justified in concluding that a small positive value for  $\ln \bar{r}_0^2/dT$ , approximately  $0.4 \times 10^{-3}$ , properly describes the variation of the unperturbed dimensions of atactic polystyrene with temperature. The slight difference between our results and those of Schulz and Baumann<sup>28</sup>, based upon viscometric data in various  $\Theta$ -solvents, could be attributed to the effect of specific solvent perturbations in the latter systems.

Our results pose two basic questions: one concerns the significance of the positive value for  $\ln \bar{r}_0^2/dT$  with regard to the nature of internal bond rotations in the polystyrene chain; the other concerns the apparent disagreement between our results and those obtained from solution data in non  $\Theta$ -solvents. As far as the first problem is concerned, we can merely note that the family of polymers for which positive values of  $\ln \bar{r}_0^2/dT$  are found is increasing, and that no satisfactory general interpretation for this effect exists. For polydimethylsiloxane<sup>41</sup>, a plausible explanation has been advanced based upon the occurrence of Si-O-Si bond angles differing substantially from the normal tetrahedral value. Ptitsyn's theory<sup>42</sup>, on the other hand, predicts zero or negative values of  $\ln \bar{r}_0^2/dT$  for all vinyl

\* For a sample of polyisobutylene<sup>39</sup> ( $M = 1.5 \times 10^6$ ) in heptane ( $\Theta = 0^\circ K$ ); 2,2,3-trimethylbutane (0); 2,4,4-trimethyl-2-pentane (84); and cyclohexane (126), values of  $10^3 (\ln \bar{r}_0^2/dT)$  at  $30^\circ C$  calculated according to Eq. (35) with  $p = 3$  are:  $-1.9^\circ$ ;  $-2.0$ ;  $-1.9$ ; and  $-1.3$ , respectively. Stress-temperature measurements<sup>35</sup> yield the value  $-0.1 \times 10^{-3}$ .

polymers. In particular, this parameter is supposed to equal  $-2.5 \times 10^{-3}$  for isotactic polystyrene and to be zero for the syndiotactic form. Results obtained from early dilute solution work<sup>27</sup> in  $\Theta$ -solvents, which indicate a value of about  $-1.5 \times 10^{-3}$  for  $\ln \bar{r}_0^2/dT$  of atactic polystyrene, were in fact considered<sup>42</sup> to be in agreement with the predictions of the Ptitsyn theory. The later, more extensive studies of Schulz and Baumann<sup>26</sup>, however, now substantiated by our results, cast doubt upon the validity of the early polystyrene work as a suitable index for assessment of  $\ln \bar{r}_0^2/dT$ . Data on stereoregular polymers would, of course, provide a basis for a more significant test of the Ptitsyn theory, specifically developed for tactic polymers. Unfortunately, these data are still scarce and an experimental study of  $\ln \bar{r}_0^2/dT$  for stereoregular polystyrene has not yet been undertaken.

The origin of the disparity between our results for  $\ln \bar{r}_0^2/dT$  and those calculated from the data on interacting polymer-solvent systems ( $T > \Theta$ ) in Table VI could conceivably be attributed to one or more of the following sources: (1) errors in the experimental quantity  $\ln [\eta]/dT$ , (2) inadequacies of current  $\alpha - T$  relationships in satisfactorily assessing the excluded volume contribution to  $[\eta]$ , (3) substantial errors in the values of  $\Theta$  assigned the particular systems investigated, and (4) specific solvent effects. Possibility (1) does not alone provide a sufficient explanation in the important cases of the benzene and toluene entries of Table VI. In each of these systems a change in the sign of  $\ln [\eta]/dT$  would be required in order to effect significant improvement in agreement with our present, experimental value for  $\ln \bar{r}_0^2/dT$ . Errors of this magnitude in the derived  $[\eta] - T$  relationships do not seem likely. In regard to possibility (2) we note, again with reference to either the benzene or toluene system, that according to the general Eq. (32) a negative value for  $d\alpha/dT$  would be required, in conjunction with the observed  $\ln [\eta]/dT$ , in order to yield a positive temperature coefficient of  $\bar{r}_0^2$ . For these systems, relationships of the form of Eq. (33) yield positive values for  $d\alpha/dT$ . Thus, crucial inaccuracies in theory would not appear to stem primarily from, for example, the derived form Eq. (35), but rather would have to be of more fundamental character. In view of this conclusion, other explanations for the observed discrepancies should first be sought.

The possibility (3) of substantial errors in reported  $\Theta$  values, in systems for which this parameter is less than about 200°K, must be seriously considered. Estimates of  $\Theta$  arrived at by extrapolation of data obtained in the vicinity of room temperature could be subject to large, systematic errors. It is not inconceivable, for example, that a value of  $\Theta < 0$  properly characterizes the system polystyrene-benzene, which assignment would lead to a calculated value for  $\ln \bar{r}_0^2/dT$  more compatible with our present experimental findings\*. It is interesting to note in this connection that in instances in which the value of  $\Theta$  may be accepted with more assurance, better agreement between the

\*The results for polyisobutylene systems (see Ref. 39) would be similarly improved through assignment of lower values for  $\Theta$ .

results of calculations from Eq. (32) and those obtained by other methods is found. The entry for the polystyrene-decalin system in Table VI is illustrative. Similarly, the satisfactory agreement reported in studies on polyethylene<sup>21,30</sup> and polydimethylsiloxane<sup>20,31,32</sup> systems, in each of which, low molecular weight homologs of the respective polymers were employed as athermal solvents, may be justified on the basis that the value  $\Theta = 0^\circ\text{K}$  assigned is a valid approximation for these polymer-solvent pairs.

Finally, with reference to item (4) above, one cannot dismiss the possibility that the different values found for  $d\ln \bar{r}_0^2/dT$  pointed out earlier<sup>14</sup> and in this communication indeed reflect, in part, appropriate indications of the thermal coefficient of  $\bar{r}_0^2$  in the various media considered. Comprehensive specification of a particular system may involve even more subtle considerations, *viz.*, the possibility of fundamental changes in the geometry of the polymer chain in some temperature interval<sup>43</sup>. Expressed in another way, this would amount to failure of the convenient analytical form  $d\ln \bar{r}_0^2/dT$  to retain approximate constancy over a wide temperature range. We understand that aspects of this general problem are currently under investigation<sup>44</sup>.

### III. The Second Virial Coefficient for Branched Comb Molecules — Edward F. Casassa

#### A. Introduction

In the previous report (ASD-TR 61-22, Part III) and in a published paper<sup>45</sup>, we explored in some detail the thermodynamic behavior of branched "star" molecules--structures comprising identical linear chains attached at one end to a common junction. Here we generalize the theoretical computation to obtain the second virial coefficient for "regular comb" molecules. In this model we have a backbone chain to which are attached at uniform intervals identical linear chains forming the branches. We let the main chain and the branches be of the same chemical structure, and thus exclude from consideration copolymers formed by grafting chains of a different species to a backbone. In one limit--as the interstices between branches become very short--the comb model evidently reduces the star model previously studied.

As in the case of the stars, the investigation of combs was stimulated by the fact that methods have been developed for synthesizing definitely characterized branched polymers. Regular combs, which are convenient for the theoretical derivation, have not indeed been made; but the similar random combs, with identical branches distributed along the main chain have been prepared<sup>46</sup> and are being studied in dilute solution<sup>6</sup>.

Except for the special branched structure of the polymers, the model we employ is the familiar statistical "string of beads", conventional for many years in the study of configurational and thermodynamic properties of flexible macromolecules. That is, we shall deal with linear sequences of statistical segments, or "beads", connected by universal joints. A segment is characterized by a mean square length  $b_0^2$  and a volume  $\beta$  of mutual exclusion for a segment pair; it is not to be identified with any structural repeating unit in the chain. Our purpose here is the calculation of the second virial coefficient  $A_2$  in the equation of state expressed as a power series in concentration (in units of mass per unit volume). For the osmotic pressure  $\Pi$ , for example we write,

$$\frac{\Pi}{RTc} = \frac{1}{M} + A_2c + \dots \quad (37)$$

According to the general statistical theory of fluids, the virial coefficient is given by<sup>47</sup>

$$A_2 = - \frac{N_0}{2VM^2} \int g_2(1,2) d(1) d(2) \quad (38)$$

$$g_2(1,2) = F_2(1,2) - F_1(1)F_1(2) \quad (39)$$

where  $M$  is the molecular weight,  $N_0$  is Avogadro's number, and  $V$  is the volume of the macroscopic system under consideration. The Macmillan-Mayer distribution functions  $F_1(1)$ ,  $F_1(2)$ , for the single molecules 1 and 2 and  $F_2(1,2)$  for the pair of molecules considered simultaneously are expanded in series, as described by Zimm<sup>4</sup>; and then the integration over the spatial coordinates, symbolized by (1) and (2), of all segments of the two molecules is carried out term-by-term to obtain a series in powers of  $\beta$ :

$$-\int g_2(1,2)d(1)d(2) = \beta V \sum_{k_1, k_2} \left[ 1 - \beta \sum_{m_1, m_2} P(0_{m_1 m_2})_{k_1 k_2} + O(\beta^2) \right] \quad (40)$$

The indices  $k_1$ ,  $k_2$ ,  $m_1$ ,  $m_2$  indicate segment  $k$  on molecule 1, segment  $k$  on molecule 2, and so on. The symbol  $P(0_{m_1 m_2})_{k_1 k_2}$  designates the probability density for an intermolecular contact between segments  $m_1$  and  $m_2$  conditional upon the presence of an initial contact between segments  $k_1$  and  $k_2$ . A contact exists for any configuration of two segments which would place both centers within the small volume  $\beta$ . To this point, we have needed to specify nothing as to the specific structure of the chain: we have assumed only that the mean potentials of average force between segments are pairwise additive and are of short range character in the sense that the interaction can be described adequately by a three-dimensional delta function<sup>34</sup>. Utilizing another property of the model, that the configuration of the unperturbed chain can be described by random flight probabilities, we can introduce these for the  $P(0_{m_1 m_2})_{k_1 k_2}$  and write the virial coefficient in the form

$$A_2 = \frac{N_0 \beta N^2}{2M^2} [1 - Bz + O(z^2)] \quad (41)$$

where  $N$  is the number of segments in the molecule and

$$z = \left( \frac{3}{2\pi b_0^2} \right)^{3/2} \beta N^{1/2}$$

The quantity  $\Gamma_2$  used above is  $A_2 M$ .

Here we shall be concerned only with evaluation of the power series in Eq. (40) through the second term, and thus with the coefficient  $B$  in Eq. (41). This means that only those configurations of a bimolecular cluster that involve no more than two intermolecular contacts need be considered<sup>4</sup>. Since the series converges slowly, the results in this approximation can be practically useful only for rather poor solvent systems near the Flory temperature $\theta$ , where  $A_2$  vanishes. We shall be able



to suggest, though, how the fairly rigorous information obtainable at this limit can be utilized in more speculative approximate theories describing behavior of polymers in good solvents, in which  $A_2$  is large and the higher order contacts indicated by  $O(\beta^2)$  in Eq. (40) cannot be ignored.

### B. Theory for the Asymmetric Comb

Turning now to the problem of calculating  $B$  for the comb, we consider two variants of the model. The simpler one is the "asymmetric comb": we can imagine a sequence of  $p$  identical linear "L-shaped" elements each of  $n$  segments, with the sequence of bases of the L's forming the main chain as illustrated in Fig. 8. One more quantity is needed to specify

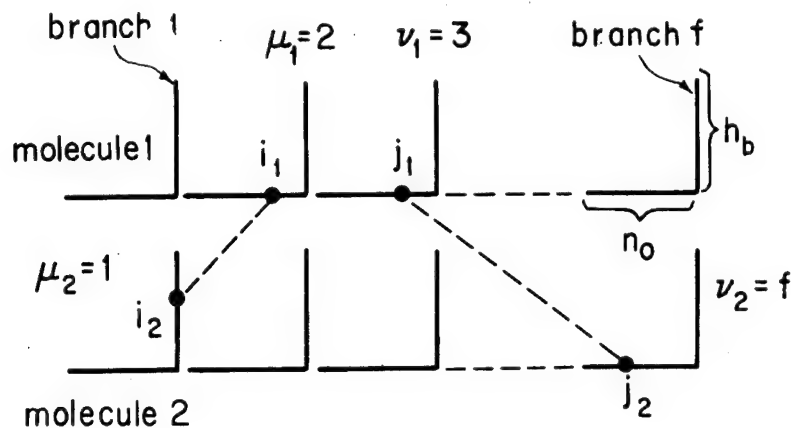


Figure 8 Schematic representation of interaction of two asymmetric combs. The dashed lines indicate contacts between pairs of segments.

the structure completely by fixing the numbers of segments contributed by each L to the backbone and to a branch. A convenient magnitude is

$$\gamma \equiv \frac{n_0}{n} = \frac{n_0}{n_0 + n_b}$$

$n_b$  and  $n_0$  being respectively the numbers of segments in a branch and in a backbone section between two branches. Thus,  $\gamma$  represents the fraction of the molecule in the backbone (if we ignore the anomaly that the branch at one end is actually part of the backbone). In writing some expressions, however, it will be more convenient to use a different ratio

$$r \equiv \frac{n_b}{n_0} = \frac{1-\gamma}{\gamma}$$

For any double contact configuration, the conditional random-flight probabilities that determine the coefficient B are given by

$$P(0_{m_1 m_2})_{k_1 k_2} = \left( \frac{3}{2\pi b_0^2} \right)^{3/2} (X_1 + X_2)^{-3/2} \quad (42)$$

where  $X_1$  and  $X_2$  are the numbers of segments, respectively of molecules 1 and 2 forming the closed loop passing through the four segments,  $m_1$ ,  $m_2$ ,  $k_1$ , and  $k_2$ , which form the contacts. We find it convenient to number segments on each L from 1 to  $n$  so that  $1 \leq i \leq n$ , etc., as indicated in Fig. 1, and then denote the particular L's concerned, by Greek letters  $\mu_1, \mu_2, \nu_1, \nu_2$  (relating to  $i_1, i_2, j_1, j_2$  so that  $1 \leq \mu \leq f$ , etc.) Thus, in counting configurations we shall need to introduce summations explicitly running over the branch numbers. Two cases are distinguished for each molecule of the pair: that is, with the contact segments on one L and

$$X_1 = |j_1 - i_1| \quad \text{and} \quad \nu_1 = \mu_1,$$

and with the segments on different L's

$$X_1 = (\nu_1 - \mu_1 - 1)n_0 + |i_1 - n_0| + j_1 \quad \text{for} \quad \nu_1 > \mu_1$$

Combination of the two classes of contours in double contacts then generates three classes of bimolecular configurations: those with contact segments distributed over 2, 3, or 4 of the L's. (A configuration of the last type is the one illustrated diagrammatically in Fig. 8.)

Since we are interested only in the situation where  $n$  is large, we can without sensible error replace the sums in Eq. (40) in part by integrals. It then becomes useful to introduce reduced variables

$$x = i_1/n; \quad y = i_2/n; \quad u = j_1/n; \quad v = j_2/n$$

each running from zero to one, and the quantities

$$p = v_1 - \mu_1; \quad q = v_2 - \mu_2$$

to write, for example, the contribution from all the configurations with contact segments on four L's:

$$\begin{aligned} & \sum_{v_1} \sum_{v_2} \sum_{\mu_1} \sum_{\mu_2} \sum_{i_1} \sum_{i_2} \sum_{j_1} \sum_{j_2} P(0_{j_1 j_2}^{i_1 i_2}) \\ &= 2n^{5/2} \left( \frac{3}{2\pi b_0^2} \right)^{3/2} \sum_{v_1} \sum_{v_2} \sum_{\mu_1} \sum_{\mu_2} \iiint \left[ (p-1)\gamma + (q-1)\gamma + |x-\gamma| \right. \\ & \quad \left. + |y-\gamma| + u + v \right]^{3/2} dudvdx dy \end{aligned} \quad (43)$$

The factor 2 is introduced on the right hand side to account for the distinguishable additional configurations obtained by interchange of  $\mu$  and  $v$  in either molecule. The integrations are straightforward though maddeningly tedious. Carrying them out and converting the remaining quadruple sum to a double sum by noting that any  $p$  and  $q$  can be realized in  $f-p$  and  $f-q$  ways, we have finally

$$\begin{aligned} \sum \dots \sum P(0_{j_1 j_2}^{i_1 i_2}) &= 2n^{5/2} \left( \frac{3}{2\pi b_0^2} \right)^{3/2} \sum_{p=1}^{f-1} \sum_{q=1}^{f-1} (f-p)(f-q) T(p+q, r) \quad (44) \\ & \text{(all configurations} \\ & \text{with } v_1 \neq \mu_1, v_2 \neq \mu_2) \end{aligned}$$

where  $T(p+q, r)$  is a function of the ratio  $r$ , and of the indices  $p$  and  $q$ , which contains the last two variables only in the combination  $t = p + q$ :

$$\begin{aligned} T(p+q, r) \equiv T(t, r) &= \frac{16}{15} (1+r)^{-5/2} \left[ -4(t-2)^{5/2} + 4(t-1)^{5/2} \right. \\ & \left. - t^{5/2} + 4(t-2+r)^{5/2} + 6(t-1+r) - 8(t+r)^{5/2} + 2(t+1+r)^{5/2} \right] \end{aligned}$$

$$\begin{aligned}
& - (t - 2 + 2r)^{5/2} - 8(t - 1 + 2r)^{5/2} + 4(t + 1 + 2r)^{5/2} - (t + 2 + 2r)^{5/2} \\
& + 2(t - 1 + 3r)^{5/2} + 4(t + 3r)^{5/2} - 2(t + 1 + 3r)^{5/2} - (t + 4r)^{5/2} \Big] \quad (45)
\end{aligned}$$

An additional simplification is possible since one more summation can be performed immediately:

$$\sum_p \sum_q (f - p)(f - q)T(t, r) = \sum_{t=2}^{2t-2} (t - 1) \left\{ t^2 - t \left( f - \frac{t+1}{6} \right) \right\} T(t, r) \quad (46)$$

Contributions from double contacts involving three L's are obtained from a calculation of similar pattern leading to another linear combination of irrational terms

$$\begin{aligned}
& \sum_{v_1} \sum_{\mu_1} \sum_{v_2=\mu_2} \sum_{i_1} \sum_{i_2} \sum_{j_1} \sum_{j_2} P^{(0)}_{j_1 j_2} i_1 i_2 \\
& \quad (v_1 \neq \mu_1) \\
& = 2n^{5/2} \left( \frac{3}{2\pi b^2} \right)^{3/2} \sum_{v_1} \sum_{\mu_1} \sum_{v_2=\mu_2} \iiint \left[ (p - 1) + |x - \gamma| + u + |y - v| \right]^{-3/2} dx dy du dv \\
& \quad (v_1 > \mu_1) \\
& = 2n^{5/2} \left( \frac{3}{2\pi b_0^2} \right)^{3/2} \sum_{p=1}^f f(f - p) S(p, r) \quad (47)
\end{aligned}$$

where

$$\begin{aligned}
S(p, r) &= \frac{16}{3} (1 + r)^{-3/2} \left[ 2(p - 1)^{3/2} - p^{3/2} - (p - 1 + r)^{3/2} - 2(p + r)^{3/2} \right. \\
&\quad \left. + (p + 1 + r)^{3/2} + (p + 2r)^{3/2} \right] \\
&+ \frac{32}{15} (1 + r)^{-5/2} \left[ 2(p - 1)^{5/2} - p^{5/2} - (p - 1 + r)^{5/2} - 4(p + r)^{5/2} \right. \\
&\quad \left. + 2(p + 1 + r)^{5/2} + 2(p + 2r)^{5/2} + 2(p + 1 + 2r)^{5/2} - (p + 2 + 2r)^{5/2} \right. \\
&\quad \left. - (p + 1 + 3r)^{5/2} \right] \quad (48)
\end{aligned}$$

The final contribution to the sum over probabilities in Eq. (40) comes from configurations in which  $v_1 = \mu_1$  and  $v_2 = \mu_2$  simultaneously. This is obviously just the well-known B for interaction of two linear chains of  $\underline{n}$  segments taken  $\underline{f}^2$  times.

$$\sum \cdots \sum P(0_{i_1 i_2}) j_1 j_2 = f^2 B_{lin}$$

(all configurations with  $p, q = 0$ )

$$B_{lin} = 2w_0 = \frac{32}{15}(7 - 4\sqrt{2}) = 2.865$$

(We used the symbol  $w_0$  or  $w_{01}$  in earlier papers on linear chains and branched stars.)

Assembling the above results, we have for the coefficient of the linear term in Eq. (41)

$$B = \frac{2}{f^{5/2}} \left\{ f^2 w_0 + \sum_{p=1}^f f(f-p)S(p,r) + \sum_{p=1}^f \sum_{q=1}^f (f-p)(f-q)T(p+q,r) \right\} \quad (49)$$

For the sake of uniformity with results to be given presently we have written sums as running up to  $p = f$  and  $q = f$  although the added term is obviously zero. Equation (49) represents the final stage we can accomplish analytically. Since we are concerned always with finite, and usually quite small, numbers of branches  $f$ , the remaining sums cannot be converted to integrals; and further recourse must be to numerical calculations.

### C. The Symmetrical Comb

A model more attractive in some ways is provided by what we choose to call the "symmetrical comb" illustrated in Fig. 9. Here we have merely added an extra vertebral section a "tail", of  $n_0$  segments to form a molecule symmetrical about its midpoint. Thus we obviate the artifice of classifying a longer linear sequence at one end as partly a branch.

The results already given can be utilized directly (the numbering of chain segments and branches being unchanged); but some additional terms have to be computed. These involve double-contact probabilities for configurations in which one or more of the participating segments are on the extra backbone element. Since the calculations go much as before they need not be described in detail. Again one has simply to compute the number of segments around the loop formed by two intermolecular contacts and do

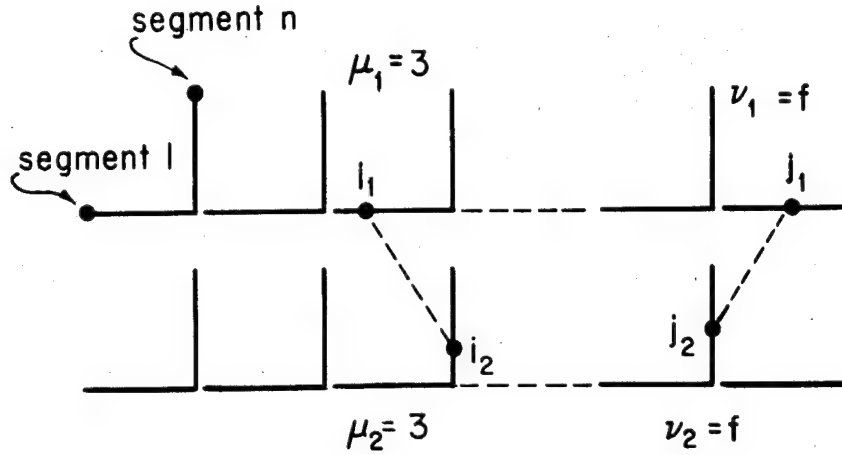


Figure 9 Diagram for double-contact interaction of two symmetrical combs

the necessary summations and integrations over the appropriate ranges. For instance, in configurations (like the one in Fig. 9) with one segment,  $j_1$ , on a tail, the loop length is

$$(f - \mu_1)n_0 + |i_1 - n_0| + j_1 + (\nu_2 - \mu_2 - 1)n_0 + |i_2 - n_0| + j_2$$

with,

$$0 \leq i_1 \leq n; \quad 0 \leq i_2 \leq n; \quad 0 \leq j_1 \leq n_0; \quad 0 \leq j_2 \leq n$$

The final result for B is

$$B_{\text{sym}} = \frac{2}{(f + \gamma)^{5/2}} \left\{ (f^2 + \gamma^2)w_0 + fY \right. \\ \left. + \sum_{p=1}^f [f(f-p)S(p,r) + U(p,r) + fV(p,r) + (f-p)W(p,r)] \right. \\ \left. + \sum_{p=1}^f \sum_{q=1}^f (f-p)(f-q)T(p+q,r) + X(p+q,r) + 2(f-p)Z(p+q,r) \right\} \quad (50)$$

$$Y = \frac{16}{15} \left[ 2 + 5\gamma + 5\gamma^{3/2} + 2\gamma^{5/2} - 2(1 + \gamma)^{5/2} \right] \quad (51)$$

$$\begin{aligned} U(p, r) = & \frac{16}{3} (1 + r)^{-5/2} \left[ 2(p - 1)^{3/2} - 3p^{3/2} + (p + 1)^{3/2} - (p - 1 + r)^{3/2} \right. \\ & \left. + (p + r)^{3/2} \right] + \frac{32}{15} (1 + r)^{-5/2} \left[ 2(p - 1)^{5/2} - 5p^{5/2} \right. \\ & \left. + 4(p + 1)^{5/2} - (p + 2)^{5/2} - (p - 1 + r)^{5/2} + 2(p + r)^{5/2} \right. \\ & \left. - (p + 1 + r)^{5/2} \right] \end{aligned} \quad (52)$$

$$\begin{aligned} V(p, r) = & \frac{16}{3} (1 + r)^{-3/2} \left[ 2(p - 1)^{3/2} - 3p^{3/2} + (p + 1)^{3/2} - (p - 1 + r)^{3/2} \right. \\ & \left. + (p + r)^{3/2} \right] + \frac{32}{15} (1 + r)^{-5/2} \left[ 2(p - 1)^{5/2} - 3p^{5/2} + (p + 1)^{5/2} \right. \\ & \left. - (p - 1 + r)^{5/2} - (p + r)^{5/2} + 3(p + 1 + r)^{5/2} - (p + 2 + r)^{5/2} \right. \\ & \left. + (p + 2r)^{5/2} - (p + 1 + 2r)^{5/2} \right] \end{aligned} \quad (53)$$

$$\begin{aligned} W(p, r) = & \frac{16}{3} (1 + r)^{-5/2} \left[ 2(p - 1)^{3/2} - p^{3/2} - (p - 1 + r)^{3/2} - 2(p + r)^{3/2} \right. \\ & \left. + (p + 1 + r)^{3/2} + (p + 2r)^{3/2} \right] + \frac{32}{15} (1 + r)^{-5/2} \left[ 2(p - 1)^{5/2} \right. \\ & \left. - 3p^{5/2} + (p + 1)^{5/2} - (p - 1 + r)^{5/2} - (p + r)^{5/2} \right. \\ & \left. + 3(p + 1 + r)^{5/2} - (p + 2 + r)^{5/2} + (p + 2r)^{5/2} - (p + 1 + 2r)^{5/2} \right] . \end{aligned} \quad (54)$$

$$\begin{aligned} X(p + q, r) = & \frac{16}{15} (1 + r)^{-5/2} \left[ -4(t - 2)^{5/2} + 12(t - 1)^{5/2} - 13t^{5/2} \right. \\ & \left. + 6(t + 1)^{5/2} - (t + 2)^{5/2} + 4(t - 2 + r)^{5/2} - 10(t - 1 + r)^{5/2} \right. \\ & \left. + 8(t + r)^{5/2} - 2(t + 1 + r)^{5/2} - (t - 2 + 2r)^{5/2} \right. \\ & \left. + 2(t - 1 + 2r)^{5/2} - (t + 2r)^{5/2} \right] \end{aligned} \quad (55)$$

$$\begin{aligned}
Z(p + q, r) = \frac{16}{15} (1 + r)^{-5/2} & \left[ -4(t - 2)^{5/2} + 8(t - 1)^{5/2} - 5t^{5/2} + (t + 1)^{5/2} \right. \\
& + 4(t - 2 + r)^{5/2} - 2(t - 1 + r)^{5/2} - 6(t + r)^{5/2} \\
& + 5(t + 1 + r)^{5/2} - (t + 2 + r)^{5/2} - (t - 2 + 2r)^{5/2} - 3(t - 1 + 2r)^{5/2} \\
& \left. + 6(t + 2r)^{5/2} - 2(t + 1 + 2r)^{5/2} + (t - 1 + 3r)^{5/2} - (t + 3r)^{5/2} \right] \quad (56)
\end{aligned}$$

The new quantities in Eq. (50) arise from various types of configurations as follows:

$\gamma^{5/2} w_0$  for two segments on each tail (interaction of two chains, each with  $n_0$  segments);

Y for two segments on a tail and the other two on one L (interaction of two linear chains of unequal lengths  $n$  and  $n_0$ ).

U for three segments on tails;

V for one segment on a tail and two on a single L of the other chain;

W for two segments on one tail and two segments on different L's of the other chain;

X for one segment on each tail;

Z for segments on three different L's and one tail (as illustrated in Fig. 9).

#### D. Discussion of Results

Determination of any number of values of  $B$  as a function of  $\underline{f}$  and  $\gamma$  (or  $\underline{r}$ ) would be prohibitively time consuming without the aid of a digital computer. Consequently Fortran programs were written for both the asymmetric and symmetric combs, and processed to obtain the results given in Tables VII and VIII. In the machine calculations there was no particular advantage in resolving the double sums over  $p$  and  $q$  into single sums over  $t$  as in Eq. (46). Although the computations were a fairly straightforward matter, one problem perhaps deserves mention. When calculations were first carried out with the IBM 704 computer, it was found that errors were appearing at the third or fourth significant figure at the largest values of  $\underline{f}$  used. It was easily established that the eight significant figures maintained in the machine calculations did not provide adequate precision for evaluating the functions  $S(t, r)$ ,  $T(p, r)$ , etc., which become smaller as the magnitudes of the terms of alternating sign of which they are composed become larger with increasing  $p$  and  $t$ .



Table VII

Coefficient B for Asymmetric Comb

$f \setminus \gamma$	0	0.1	0.2	0.3	0.4	0.5	0.6	0.7	0.8	0.9
1	2.8654	2.8654	2.8654	2.8654	2.8654	2.8654	2.8654	2.8654	2.8654	2.8654
2	2.8654	3.0256	3.1232	3.1858	3.2213	3.2328	3.2213	3.1858	3.1232	3.0256
3	3.2790	3.4489	3.5268	3.5567	3.5517	3.5172	3.4557	3.3668	3.2478	3.0905
4	3.8733	3.9486	3.9569	3.9140	3.8425	3.7475	3.6307	3.4914	3.3263	3.1274
5	4.5858	4.5053	4.3839	4.2467	4.0985	3.9399	3.7697	3.5853	3.3823	3.1518
6	5.3897	5.0680	4.7976	4.5541	4.3256	4.1043	3.8843	3.6600	3.4251	3.1696
7	6.2704	5.6359	5.1947	4.8381	4.5289	4.2474	3.9815	3.7216	3.4593	3.1832
8	7.2189	6.2029	5.5742	5.1010	4.7122	4.3736	4.0654	3.7737	3.4875	3.1941
9	8.2288	6.7652	5.9364	5.3452	4.8788	4.4862	4.1390	3.8186	3.5114	3.2030
10	9.2955	7.3206	6.2821	5.5727	5.0313	4.5877	4.2044	3.8580	3.5320	3.2105
12	11.5854	8.4052	6.9273	5.9850	5.3013	4.7639	4.3161	3.9240	3.5659	3.2226
14	14.0664	0.4508	7.5178	6.3498	5.5343	4.9129	4.4088	3.9778	3.5930	3.2319
16	16.7228	10.4557	8.0605	6.6759	5.7382	5.0411	4.4874	4.0228	3.6153	3.2396
18	19.5425	11.4203	8.5617	6.9701	5.9190	5.1533	4.5554	4.0611	3.6342	3.2462
20	22.5157	12.3460	9.0266	7.2374	6.0810	5.2526	4.6150	4.0942	3.6504	3.2520
22	25.6343	13.2346	9.4596	7.4821	6.2273	5.3415	4.6680	4.1234	3.6645	3.2572
24	28.8914	14.0880	9.8642	7.7072	6.3605	5.4217	4.7157	4.1494	3.6768	3.2617

Table VIII

Coefficient B for Symmetrical Comb

$f \backslash \gamma$	0	0.1	0.2	0.3	0.4	0.5	0.6	0.7	0.8	0.9
1	2.8654	2.9976	3.1235	3.2118	3.2627	3.2790	3.263	3.2179	3.1421	3.0321
2	2.8654	3.2033	3.3980	3.5051	3.5467	3.5362	3.4823	3.3905	3.2628	3.0958
3	3.2790	3.6262	3.7801	3.8334	3.8186	3.7533	3.648	3.5089	3.3379	3.1315
4	3.8733	4.1299	4.1880	4.1554	4.0668	3.9391	3.781	3.5988	3.3915	3.1551
5	4.5858	4.6698	4.5953	4.4599	4.2909	4.1001	3.8928	3.6708	3.4326	3.1723
6	5.3897	5.2258	4.9921	4.7445	4.4934	4.2414	3.9877	3.7304	3.4655	3.1855
7	6.2704	5.7875	5.3746	5.0097	4.6772	4.3666	4.0701	3.7811	3.4928	3.1960
8	7.2189	6.3485	5.7414	5.2590	4.8449	4.4788	4.1426	3.8247	3.5160	3.2047
9	8.2288	6.9053	6.0924	5.4880	4.9986	4.5801	4.207	3.8634	3.5360	3.2121
10	9.2955	7.4555	6.4282	5.7042	5.1402	4.6722	4.2652	3.8976	3.5535	3.2184
12	11.5854	8.5308	7.0569	6.0982	5.3931	4.8340	4.3658	3.9560	3.5830	3.2286
14	14.0664	9.5682	7.6340	6.4488	5.6132	4.9723	4.4505	4.0043	3.6070	3.2368
16	16.7228	10.5658	8.1657	6.7637	5.8072	5.0925	4.523	4.0453	3.6271	3.2437
18	19.5425	11.5239	8.6576	7.0487	5.9801	5.1983	4.586	4.0805	3.6443	3.2496
20	22.5157	12.4438	9.1146	7.3085	6.1356	5.2926	4.6424	4.1113	3.6592	3.2549
22	25.6343	13.3272	9.5408	7.5467	6.2766	5.3773	4.692	4.1385	3.6722	3.2597
24	28.8914	14.1759	9.9396	7.7664	6.4052	5.4540	4.737	4.1629	3.6837	3.2638

For example,  $T(t,0)$  is always zero; but when  $t$  is 50, individual terms attain the order of  $10^5$ . The difficulty persists for finite  $\underline{r}$ , and the large percentage inaccuracy in the computed  $T(t,r)$  is only partially counterbalanced by the fact that the least accurate values are given least weight in the sum over  $t$ . Although double precision programs (retaining sixteen significant figures) are available for the IBM 704, they are relatively time-consuming. By going to another machine, the IBM 7094, which is directly adapted to double precision computations, we were able to do the necessary operations efficiently and with all the accuracy required over the entire range of  $f$  and  $\gamma$  desired. Hence, the values of  $B$  given in the tables are correct to the number of significant figures shown.

In Fig. 10, values of  $B$  for both symmetric and asymmetric combs are plotted as functions of  $\gamma$  for several values of  $f$ . Either model reduces to the linear and star structures studied earlier as special cases: thus, as  $\gamma$  approaches unity,  $B$  approaches the linear limit 2.865; and when  $\gamma$  becomes zero,  $B$  for the corresponding  $f$ -functional regular star is recovered. Since one- and two-branched stars are "pathological" structures representing merely linear chains, the plots for  $f = 1$  and  $f = 2$  must give the linear value for  $\gamma = 0$ ; and, of course, the asymmetric comb with  $f = 1$  is always linear. The symmetrical comb with  $f = 1$  gives a curve nearly symmetrical about a maximum at or very close to  $\gamma = 1/2$ ; and since the model for  $\gamma = 1/2$  represents a triply branched regular star, the value of  $B$  there is equal to the intercept at  $\gamma = 0$  for  $f = 3$ . Both kinds of combs give the same  $B$  at the star limit, but with  $\gamma$  finite the plot for the asymmetric model falls below that for the symmetric one having the same  $f$  and approaches the curve for the symmetric comb with one less branch as both curves approach  $B_{lin}$  at  $\gamma = 1$ .

It is interesting that the maximum appearing in the curves for the symmetric models with  $f = 1$  and  $f = 2$  still persists with  $f = 4$  and  $f = 5$  although it become less marked and shifts progressively to the left. When  $f$  is greater than 5, however, a monotone decrease of  $B$  with increasing  $\gamma$  is established. The same character is seen qualitatively in the plots for the asymmetric model but the maximum is not so prominent. The behavior of  $B$  stands in some contrast to that of the coefficient  $a_1$  of the linear term in the power series in  $\underline{z}$  for the expansion of the mean square radius  $\langle s^2 \rangle$  beyond the random flight value  $\langle s^2 \rangle_0$

$$\frac{\langle s^2 \rangle}{\langle s^2 \rangle_0} = 1 + a_1 z + O(z^2)$$

Berry and Orofino (see Section I, above) found that  $a_1$  for symmetrical combs passes through a maximum as a function of  $\gamma$ . This is, however, more pronounced than that in  $B_{sym}$ , and it does not disappear as  $\underline{f}$  becomes large.

In a qualitative way, the variation of  $B$  for either model with  $\gamma$  and  $\underline{f}$  agrees with intuition. Sufficiently close to the Flory temperature, the first two terms on the righthand side of Eq. (41) will be sufficient

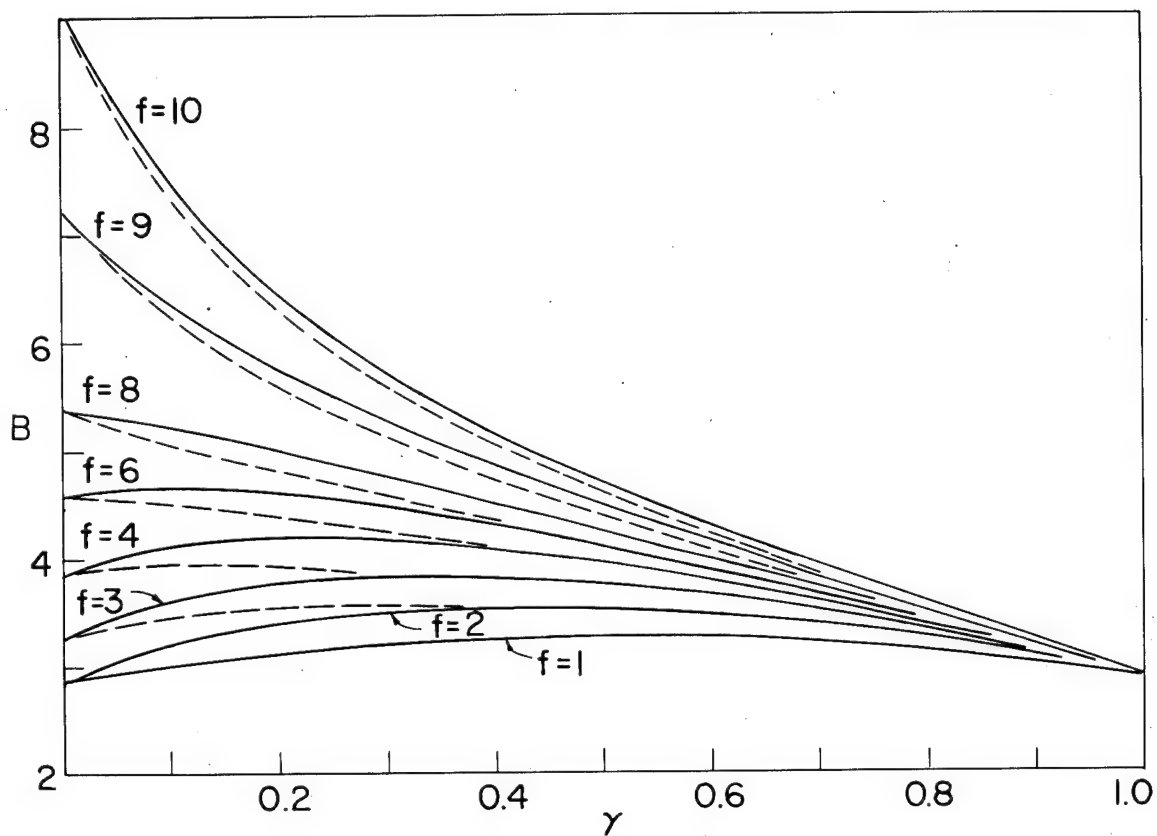


Figure 10 The coefficient  $B$  for symmetric (solid curves) and asymmetric (dashed curves) combs for various values of  $\underline{f}$ . For a given value of  $\underline{f}$ , the two curves join at the left. For  $f = 1$ ,  $B_{\text{asym}}$  is constant and equal to  $B_{\text{lin}}$  for  $f = 2$ , it almost coincides with the solid curve  $B_{\text{sym}}$  for  $f = 1$ .

to determine  $A_2$ . Then, if  $B$  increases while the molecular weight and the structure-independent parameters  $\beta$  and  $b_0$  are held fixed,  $A_2$  becomes smaller. This change is seen to occur as one passes from the extended linear configuration via the comb to the usually more compact star structure, or if one keeps  $\gamma$  fixed and increases  $\underline{f}$ . Since the virial coefficient is a measure of the interaction of two molecules, it would be expected to be smallest for the model that is the least space-filling. Conversely, one might expect the intramolecular excluded volume effect, as evidenced by the increase in  $\langle s^2 \rangle$  beyond the random-flight value, to be greatest for the most compact configuration. This is indeed found to be the case as  $\underline{f}$  increases at fixed  $\gamma$ ; but the effect of varying  $\gamma$ , as already noted, is not as simple.

These observations on the dependence of  $B$  on structure can be put on a more nearly quantitative basis. If the "compactness" of the molecule is the factor determining  $B$ , the most obvious correlation to seek would be one with the ratio  $g$  of the mean square radius of the branched molecule to that of the linear chain of the same mass. For the symmetrical comb this is given by the expression

$$g(f + \gamma)^3 = 3f^2 - 2f + f(f^2 - 6f + 8) + \gamma^2 f(6f - 9) + \gamma^3(6f + 1) \quad (57)$$

which is equivalent to Eq. (22). Values of  $g$  for this model were then computed for each  $f$  and  $\gamma$  represented in Table VIII. The results, recorded in Table IX were used to construct the graphs given in Fig. 11, of  $B_{\text{sym}}$  versus  $\gamma$ .

It is clear from the plots that  $B_{\text{sym}}$  does show the expected marked correlation with  $g$  regardless of  $\underline{f}$  or  $\gamma$ . As  $\gamma$  decreases from unit  $\gamma$ ,  $g$  decreases initially and all the curves of  $B$  versus  $g$  increase from the limit  $B_{\text{lin}}$ . For each curve with  $1 \leq f \leq 5$ ,  $g$  exhibits a minimum (corresponding at least approximately with the maximum in  $B$ ). Then as  $\gamma$  decreases further,  $g$  increases once more as  $B$  falls until  $B_{\text{lin}}$  (for  $f = 1$  and  $f = 2$  or the regular star value (for  $3 \leq f \leq 5$  is reached. The curve for  $f = 1$  in Fig. 11 is actually a loop, but on the scale of the plot this cannot be distinguished from a curve segment retraced to its origin. For  $f > 5$ ,  $B$  increases monotonically with decreasing  $g$  as well as with decreasing  $\gamma$ . With successively larger values of  $f$ , the superposition of the plots appears to improve. As  $\underline{f}$  becomes sufficiently large,  $B_{\text{star}}$  approaches  $0.2201 f^{3/2}$ ; but this limiting behavior is reasonably approximated only at values of  $\underline{f}$  greater than appear in Fig. 9<sup>45</sup>.

#### E. Application to Polymers in Good Solvents

In earlier papers<sup>45,48,49</sup> we have developed an approximate theory for solutions of linear and star polymers in good solvents. The same approach

Table IX

Symmetrical Comb; g

$f \setminus \gamma$	0	0.1	0.2	0.3	0.4	0.5	0.6	0.7	0.8	0.9
1	1	0.9594	0.8889	0.8280	0.7901	0.7778	0.7891	0.8205	0.8683	0.9291
2	1	0.8717	0.7836	0.7308	0.7083	0.7120	0.7378	0.7824	0.8426	0.9159
3	0.7778	0.7045	0.6602	0.6412	0.6446	0.6676	0.7078	0.7630	0.8312	0.9107
4	0.6250	0.5894	0.5750	0.5795	0.6011	0.6379	0.6883	0.7510	0.8247	0.9080
5	0.5200	0.5095	0.5153	0.5359	0.5702	0.6168	0.6747	0.7429	0.8204	0.9064
6	0.4444	0.4514	0.4715	0.5038	0.5474	0.6013	0.6648	0.7370	0.8174	0.9053
7	0.3878	0.4075	0.4383	0.4793	0.5299	0.5893	0.6571	0.7326	0.8152	0.9045
8	0.3438	0.3733	0.4122	0.4600	0.5160	0.5799	0.6511	0.7291	0.8135	0.9039
9	0.3086	0.3458	0.3912	0.4444	0.5049	0.5722	0.6462	0.7262	0.8121	0.9035
10	0.2800	0.3234	0.3740	0.4315	0.4956	0.5659	0.6421	0.7239	0.8110	0.9031
12	0.2361	0.2888	0.3474	0.4116	0.4813	0.5561	0.6358	0.7203	0.8093	0.9026
14	0.2041	0.2635	0.3278	0.3970	0.4707	0.5488	0.6312	0.7177	0.8081	0.9022
16	0.1797	0.2441	0.3128	0.3857	0.4625	0.5432	0.6276	0.7156	0.8071	0.9019
18	0.1605	0.2289	0.3010	0.3768	0.4560	0.5387	0.6248	0.7140	0.8063	0.9017
20	0.1450	0.2165	0.291	0.3695	0.4508	0.5351	0.6225	0.7127	0.8057	0.9015
22	0.1322	0.2063	0.2835	0.3635	0.4464	0.5321	0.6205	0.7116	0.8052	0.9014
24	0.1215	0.1978	0.2768	0.3585	0.4428	0.5296	0.6189	0.7107	0.8048	0.9013

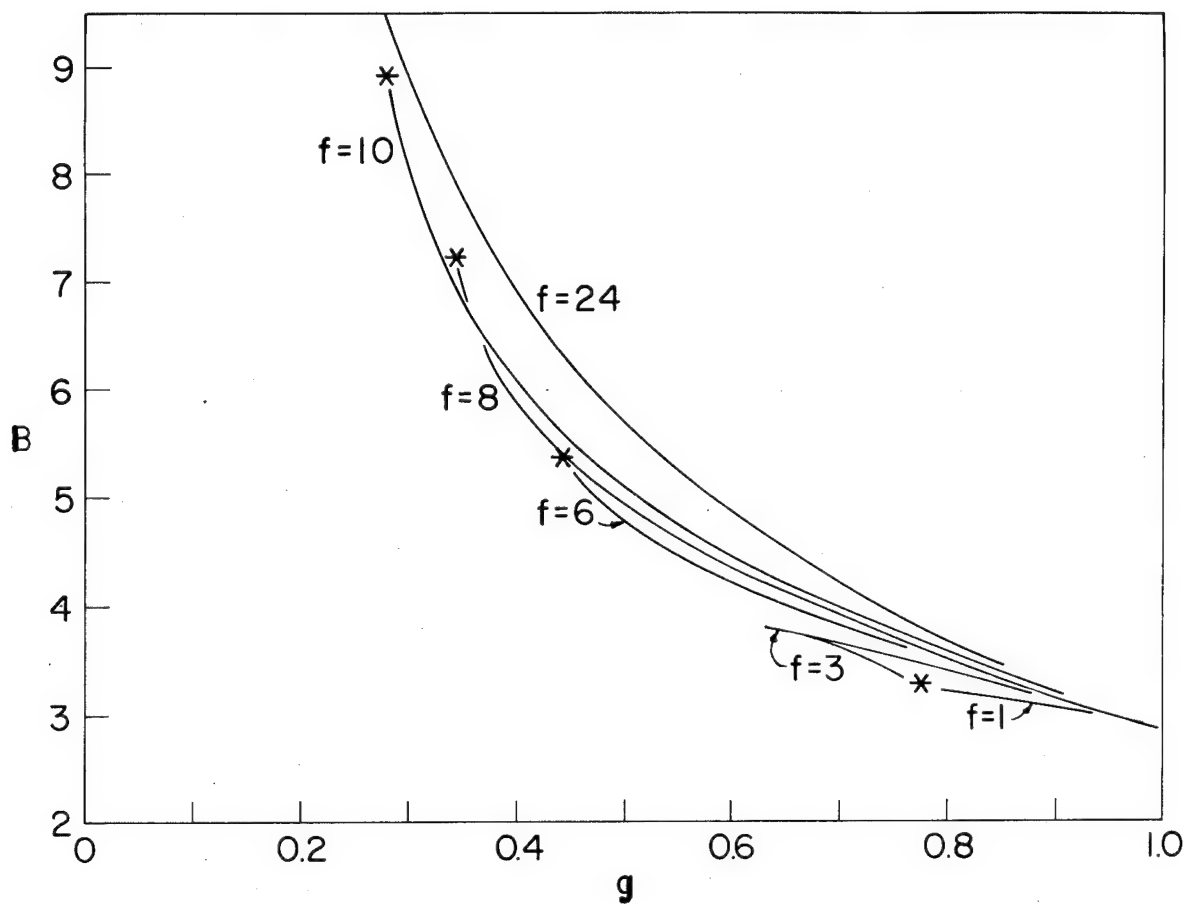


Figure 11 Plots of  $B$  versus  $g$  for symmetrical combs. The curves are for  $\underline{f}$  as indicated. Points for the limiting regular stars are denoted by \*.

can be used in dealing with interaction of combs to obtain a closed expression, which, when expanded in series, reproduces correctly the first two terms of the series in Eq. (41). The simplifications, which therefore introduce approximations in the higher terms of Eq. (41), are of two kinds.

(a) The intramolecular excluded volume effect is assumed to cause a uniform expansion of all molecular dimensions by a scale factor  $\alpha$ ; hence, the distribution functions remain random-flight quantities with the segment length  $b_0$  replaced by a modified length  $\alpha b_0$ . It follows that  $A_2$  can be written as a power series in a variable  $\xi = z/\alpha^3$ . Since  $\alpha^3$  can be expressed as a series  $1 + O(z)$ , this approximation does not affect the coefficient of the linear term in Eq. (41). In a refinement of the theory<sup>49</sup> it has been proposed that the  $\alpha$  involved in the problem of intermolecular interactions should not be that for an isolated molecule but rather an averaged quantity  $\alpha_2$  relating to a bimolecular cluster. Evaluation of  $\alpha_2$  (or of  $\alpha$ , for that matter) in a good solvent is an important problem, but we shall avoid discussing it here by regarding the expansion factor simply as a quantity obtained by independent means.

(b) The probabilities for multiple intermolecular contacts appearing in higher terms of Eq. (40) are approximated by products of independent probabilities for contacts in addition to an initial one; thus,

$$P(O_{m_1 m_2}, O_{n_1 n_2} \dots O_{p_1 p_2})_{k_1 k_2} = P(O_{m_1 m_2})_{k_1 k_2} P(O_{n_1 n_2})_{k_1 k_2} \dots P(O_{p_1 p_2})_{k_1 k_2}$$

With these two approximations, Eq. (38) becomes

$$-\int g_2(1,2) d(1) d(2) = \beta V \sum_{k_1} \sum_{k_2} \varphi(h, \xi) = \frac{\beta V}{N^2} (\xi, f, \gamma) \quad (58)$$

where the functions  $\varphi$  and  $h$  are

$$\varphi(h, \xi) = \frac{1 - e^{-h(k_1, k_2, f, \gamma)\xi}}{h(k_1, k_2, f, \gamma)\xi} \quad (59)$$

and

$$h(k_1, k_2, f, \gamma) = (\beta/\xi) \sum_{m_1} \sum_{m_2} P(O_{m_1 m_2})_{k_1 k_2} \quad (60)$$



The sums (integrations) over  $m_1$  and  $m_2$  can be done immediately and, in fact, have already been evaluated at an intermediate stage in the calculation of  $B$ . The remaining sums over  $k_1$  and  $k_2$ , which accomplish an averaging process over all choices for the "initial" intermolecular contact, are intractable analytically; but the evaluation has been done by numerical integration both for linear chains and regular stars. Numerical results for combs could be obtained in the same way; but since  $B$  is now a function of three variables  $\underline{f}$ ,  $\gamma$ , and  $\zeta$  (two parameters describe a regular star; and only one, a straight chain) the calculations appear somewhat unattractive. Furthermore, the earlier work<sup>48</sup> suggests the additional approximation of replacing the sum of  $\phi(h, \zeta)$  over  $k_1$  and  $k_2$  by  $\phi$  itself evaluated at

$$h_0(f, \gamma) = (\beta/\zeta) \sum_{k_1} \sum_{k_2} \sum_{k_3} \sum_{k_4} P(0_{m_1 m_2})_{k_1 k_2} = 2B \quad (61)$$

With this final simplification, the virial coefficient in any solvent is given by:

$$\frac{2M^2 A_2}{N_0 \beta N^2} \approx F_0(\zeta, f, \gamma) = \frac{1 - \exp(-2B\zeta)}{2B\zeta} \quad (62)$$

Obviously, upon expansion of the exponential, this result duplicates the first two terms of the series in Eq. (41). For a polymer-solvent system of given chemical nature, the virial coefficient will, according to Eq. (62), depend on branch architecture through  $B$  and  $\zeta$ . The primary dependence appears in  $B$ , which, we have shown, may be regarded to a first approximation as a function of  $\underline{g}$ . The molecular weight dependence appears entirely in  $\zeta$  which will also depend on structure through variation of  $\alpha_2$  with  $\gamma$  and  $\underline{f}$ . The results of Berry and Orofino on  $\alpha$  (Section I, preceding) suggest that an approximation giving  $\alpha_2$  as a function of  $\underline{z}$  and  $\underline{g}$  only, would not be very satisfactory. Otherwise,  $F^0$  would depend only on  $\underline{z}$  and  $\underline{g}$ .

Since we have not integrated the function  $\phi$  it is not possible to compare  $F$  with  $F^0$  in detail. However, this has been done numerically for star molecules, and those results<sup>45</sup> serve to show the nature of the approximation. As already mentioned,  $F$  and  $F^0$  have the same first derivative with respect to  $\zeta$  at  $\zeta = 0$ . Thence,  $F^0$  becomes smaller than  $F$  as  $\zeta$  increases. For linear chains, the maximum error is always less than two percent, but it increases as  $f$  becomes larger (for  $f = 9$  the error at large  $\zeta$  is ten percent). We expect that similar behavior obtains for combs with the value of  $F^0/F$  depending rather closely on the value of  $B$ .

In endeavoring to show that  $B$  depends primarily on  $\underline{g}$ , we were motivated by the fact that several approximate theories of the virial coefficient in good solvents result in functions of  $\underline{g}$  and  $\underline{z}$ . Flory and

Krigbaum,<sup>50,51</sup> for example, represented a dissolved polymer molecule as a Gaussian density distribution of chain segments centered about the molecular center of mass and normalized to give the mean square radius of the real molecule. Then, they calculated the second virial coefficient by considering the interpenetration of two such "soft spheres" much as in the standard statistical mechanical derivation of the equation of state of the imperfect gas. This model, and some variants<sup>52,53,54</sup> differing only in the character of the density function, were used in treating straight chains but since the models actually contain no specific structural features dependent on branching, the theories can be applied to chains of any architecture provided merely that the proper radius is used. Thus, for the Flory-Krigbaum theory one can write

$$A_2 = \frac{N_0 \beta N^2}{2M^2} F_{FK}(X) \quad (63)$$

$$X = 3^{3/2} \zeta / g^{3/2}$$

The function  $F_{FK}(X)$  has been given graphically by Flory and Krigbaum. In determining  $X$  they identified  $\alpha_2$  with  $\alpha$ . The symmetry of their model suggests this as the simplest expedient. Logically, a more elaborate treatment would seem to require that interaction of a pair of molecules create an asymmetric deformation of each molecule, but such a refinement would presumably make calculations difficult. Although the work of Berry and Orofino makes us doubt that  $\alpha_2$  can actually be described adequately as a function of  $\underline{z}$  and  $\underline{g}$ , a self-consistent treatment of the Flory-Krigbaum model would necessarily lead to such a functional dependence. Thus, within the framework of the theory  $F_{FK}(X)$  depends entirely on  $\underline{z}$  and  $\underline{g}$ .

Elsewhere<sup>45</sup>, we have given plots of  $F_{FK}(X)$  and of our analogous quantity  $F(\zeta, f, 0)$  for stars of various functionalities  $\underline{f}$ . Qualitatively, the same behavior applies in the case of combs. When  $\zeta$  is zero,  $F_{FK}$  and  $F$  are both unity, but  $F_{FK}$  decreases much less rapidly with increasing  $\zeta$  for any value of  $f$  or  $\gamma$ . Although the absolute values for  $A_2$  as predicted by the two theories may be quite different, the comparison between branched and linear chains is not so marked for physically realistic values of  $\zeta$ . Thus, the ratios  $F(\zeta, f, \gamma)/F(\zeta, 0, 1)$  and  $F_{FK}[X(\zeta, g)]/F_{FK}[X(\zeta, 1)]$  are probably much the same at any given  $\zeta$ ,  $f$ , and  $\gamma$ .

IV. Dilute Solution-Properties of Branched Polymers. Polystyrene Trifunctional Star Molecules — T. A. Orofino and Franz Wenger

An article bearing this title has been published in J. Phys. Chem. 67, 566 (1963). The abstract follows. The work was described in ASD-TR 61-22, Part II.

The results of intrinsic viscosity, second virial coefficient and related thermodynamic measurements on samples of polystyrene trifunctional star molecules are reported. These branched polymers were synthesized by means of a coupling reaction between essentially monodisperse polystyryllithium and 1,2,4-tris(chloromethyl) benzene. The homogeneity of the materials obtained with regard to molecular weight and functionality was established by fractionation, sedimentation, and absolute molecular weight determinations. Intrinsic viscosities and second virial coefficients in both poor and good solvent media were found to be less for these materials than for linear polystyrenes of comparable molecular weights. The Huggins viscosity constant  $k'$  in good solvents was unaffected by branching; in poor solvent media, an augmentation of  $k'$  with branching was noted. The results of these and other dilute solution studies are discussed from the point of view of current theoretical interpretations. An attempt is made to extend them in applicability to more general branched polymer systems.

V. Dilute Solution Properties of Linear Polystyrene in  $\Theta$ -Solvent Media —  
T. A. Orofino and J. W. Mickey, Jr.

An article bearing this title has been published in J. Chem. Phys. 38, 2512 (1963). An abstract follows. This work was discussed in ASD-TR 61-22, Parts II and III.

Dilute solution parameters descriptive of polymer coil size and segment-solvent interaction have been evaluated for each of three polystyrene-solvent systems at various temperatures in the vicinity of the  $\Theta$ -value characteristic of a given pair. The pure solvents selected for these studies were diethyl malonate, cyclohexane and 1-chloro-n-undecane, which with polystyrene display  $\Theta$ -temperatures of 35.9, 34.8 and 32.8°C, respectively, as ascertained from analyses of second virial coefficient-temperature relationships. A single polymer sample of narrow molecular weight distribution was employed in all investigations.

Parameters interpolated for each polystyrene-solvent pair at the  $\Theta$ -temperature of the system are examined from the point of view of the specific influence of the medium on coil characteristics. Differences are observed, for example, among the intrinsic viscosity values. Accurate, relative comparison of such solution properties is facilitated through use of the common polymer sample and intentional selection of pure solvents displaying  $\Theta$ -temperatures in proximity. The complicating effects of variable molecular weight, molecular weight distribution and temperature per se are thus conveniently eliminated.

Intrinsic viscosity and second virial coefficient data obtained for each pair at various temperatures near  $\Theta$  are examined in accordance with the formal functional interdependence predicted by certain theoretical treatments, applicable to weakly interacting systems of the kind here investigated.

VI. Dilute Solution Properties of Linear Polystyrene in  $\Theta$ -Solvent Media.  
II — T. A. Orofino and J. W. Mickey, Jr.

The properties of polystyrene in selected  $\Theta$ -solvents have been investigated as part of a continuing study carried out over the past few years aimed at (a) characterization of polystyrene in weakly interacting media, and (b) elucidation of temperature and solvent effects in  $\Theta$ -systems. Results concerned with an earlier phase of this study have been reported previously (cf. ASD-TR 61-22, Part III). The experimental portion of investigations subsequently undertaken is described below, together with a preliminary analysis of properties observed for the various systems.

A. Selection of Polymer-Solvent Systems

Evaluation of the solution properties of a single polystyrene sample ( $\bar{M}_w = 4.0 \times 10^5$ ) in various  $\Theta$ -media, confined initially to consideration of the solvents cyclohexane, diethylmalonate and 1-chloro-n-undecane, has been extended to include two additional media, 1-chloro-n-decane and 1-chloro-n-dodecane. Data for each of the five systems may be examined individually from the point of view of establishing values for "equivalent chain" or other parameters descriptive of the polymer-solvent pair. In addition, selective grouping of the data provides (1) a set of three diverse systems for which the  $\Theta$ -values are virtually identical (cyclohexane, diethylmalonate and 1-chloro-n-undecane); and (2) a second set of three systems in which the solvent components vary only slightly in structural and chemical characteristics (1-chloro-n-alkanes). It is evident that, to a preliminary, first approximation, analysis of data in accordance with the above groupings provides an immediate means for phenomenological resolution of temperature and specific solvent effects in polystyrene  $\Theta$ -solvent systems.

B. Experimental

Phase studies, light scattering and viscosity measurements, and auxiliary determinations were carried out for the polystyrene-1-chloro-n-decane and dodecane systems in accordance with procedures described earlier (cf. ASD-TR 61-22, Part III). Suitable modifications of equipment and techniques were required, however, in order to contend effectively with the less accessible  $\Theta$ -temperatures of the new systems. As before,  $\Theta$  was ascertained for each polymer-solvent pair from the second virial coefficient ( $\Gamma_2$ ) - temperature relationship, established from light scattering data collected at various temperatures, scattering angles, and polymer concentrations, the operational definition of  $\Theta$  being taken as the temperature at which  $\Gamma_2$  vanishes. Intrinsic viscosity measurements were carried out at several convenient temperatures in the vicinity of  $\Theta$ . The customary plots of reduced reciprocal light scattering intensities and reduced specific viscosities versus polymer concentration are shown in Figs. 12-15. Values of  $\Gamma_2$  and  $[\eta]$  derived therefrom are compiled in Table X. and expressed graphically as functions of

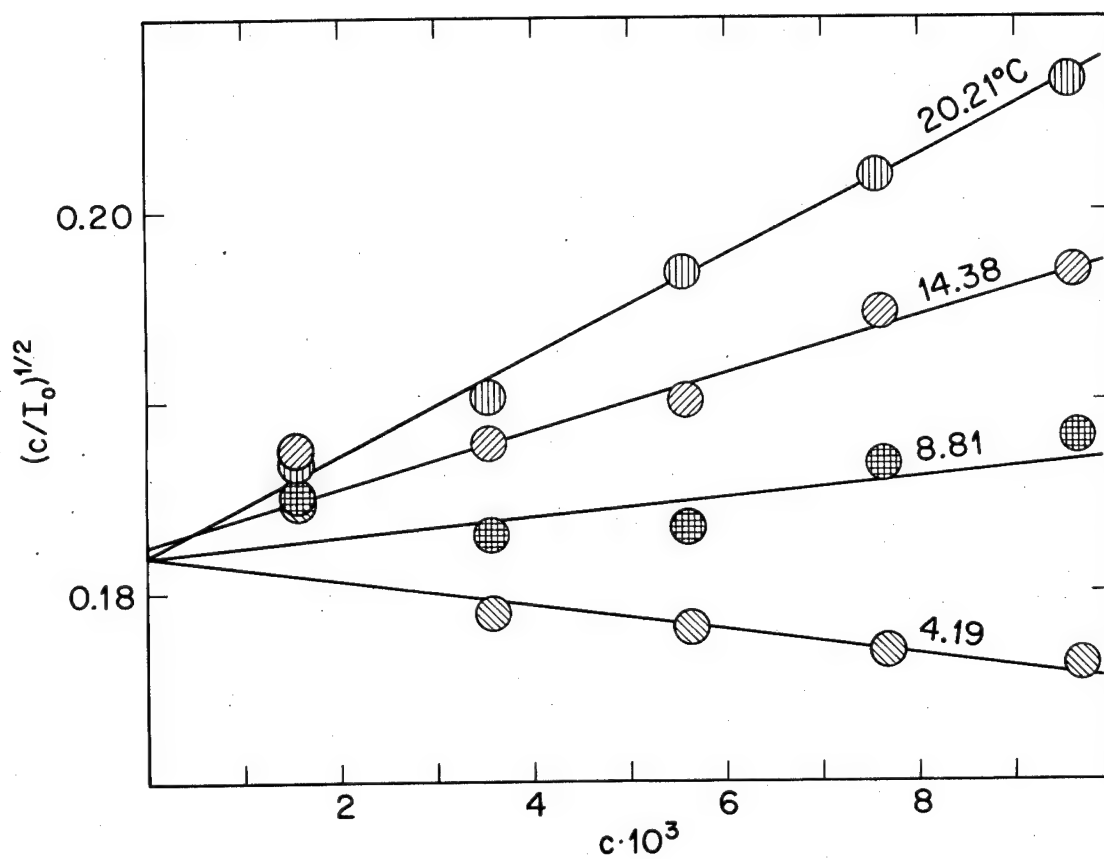


Figure 12 Square-root plots of reduced reciprocal scattering intensity versus polymer concentration  $c$  (g/cc) for the system polystyrene-1-chloro-n-decane at various temperatures.

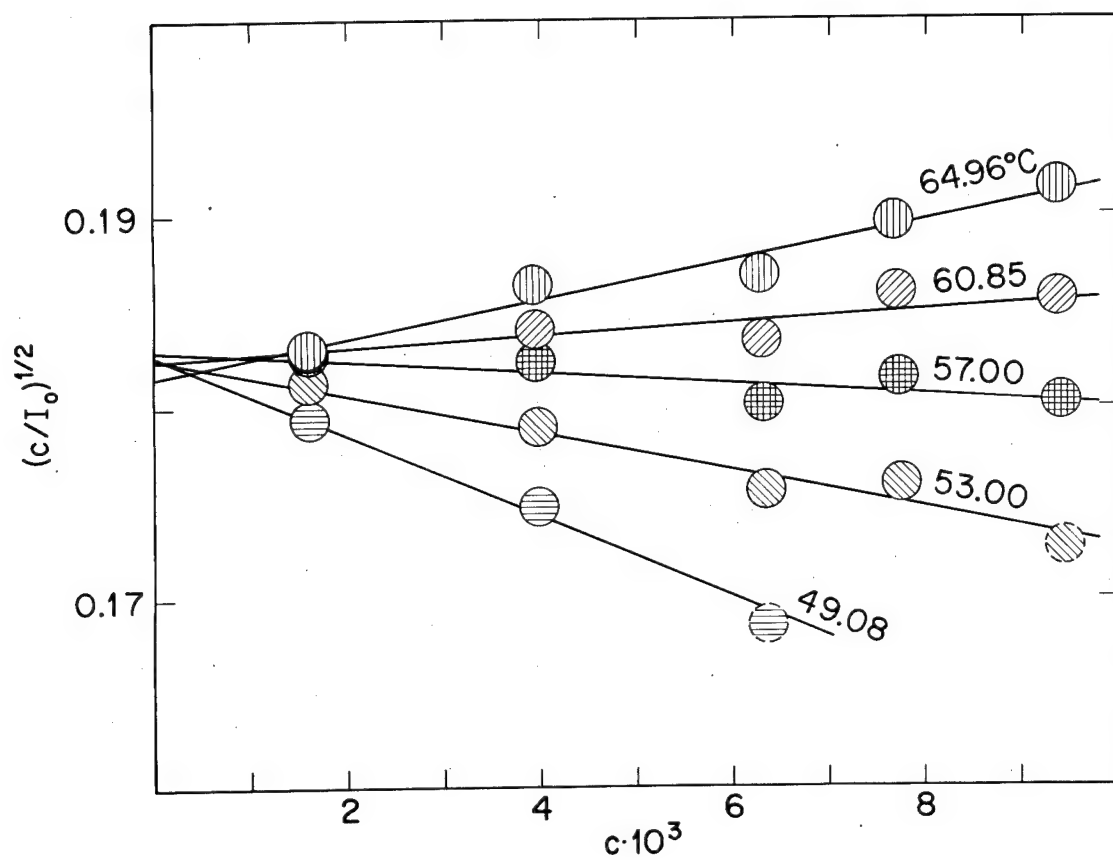


Figure 13 Square-root plots of reduced reciprocal scattering intensity versus polymer concentration  $c$  (g/cc) for the system polystyrene-1-chloro-n-dodecane at various temperatures.

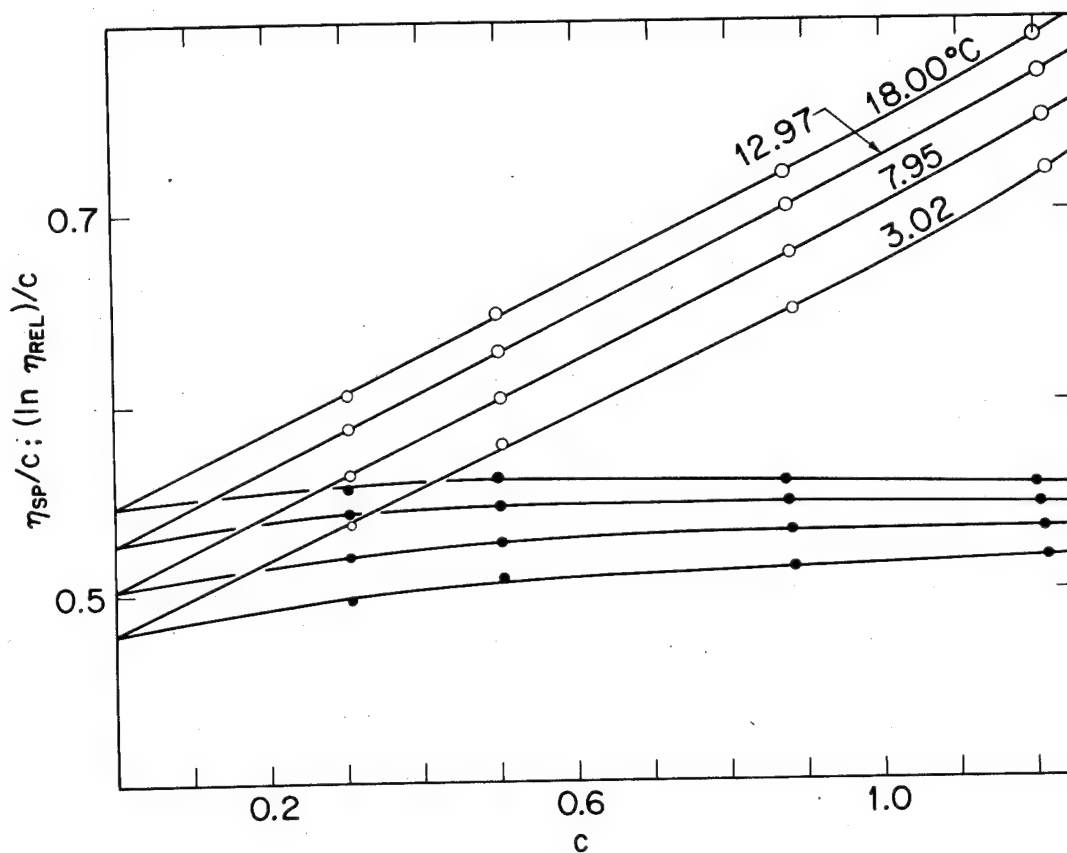


Figure 14 Plots of  $\eta_{sp}/c$  (open circles) and  $(\ln \eta_{rel})/c$  versus  $c$  (g/dl) for the system polystyrene-1-chloro-n-decane at various temperatures.



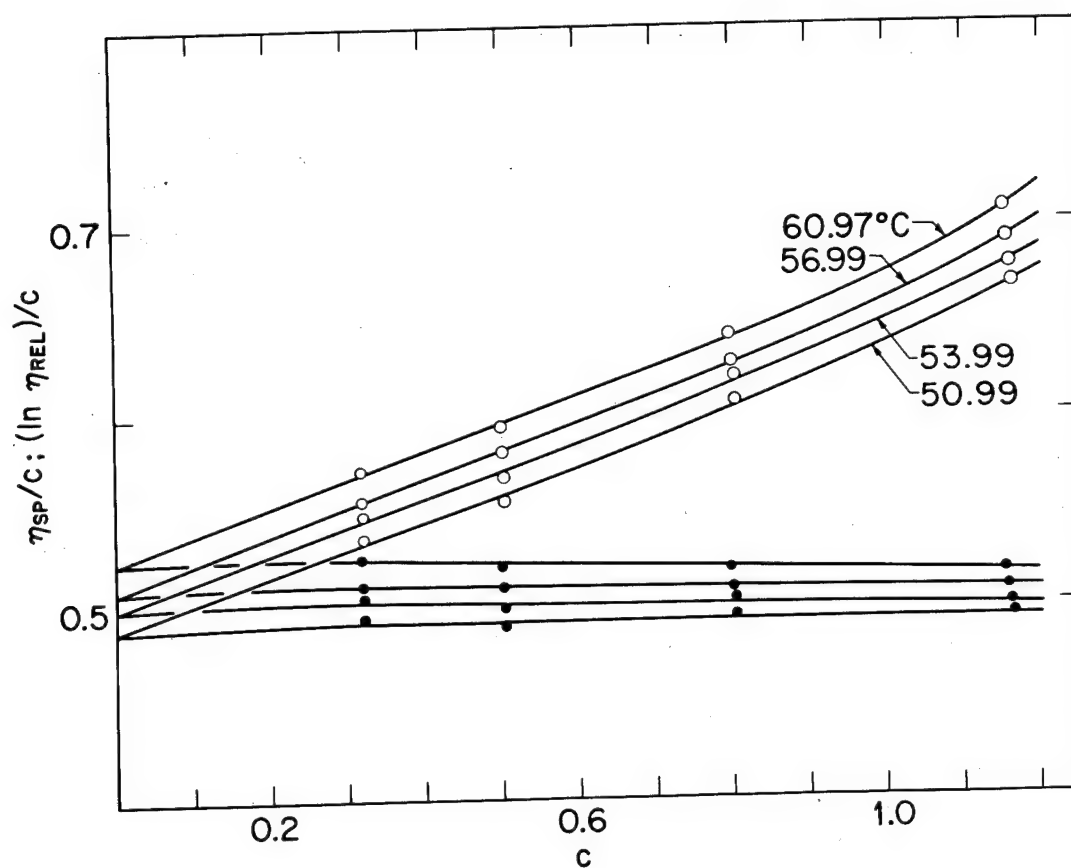


Figure 15 Plots of  $\eta_{sp}/c$  (open circles) and  $(\ln \eta_{rel})/c$  versus  $c$  (g/dl) for the system polystyrene-1-chloro-n-dodecane at various temperatures.

Table X

Intrinsic Viscosity and Second Virial Coefficient Data  
for Polystyrene- $\Theta$ -Solvent Systems

1-chloro-n-decane			1-chloro-n-dodecane		
t°C	$\Gamma_2$	$[\eta]$ , dl/g	t°C	$\Gamma_2$	$[\eta]$ , dl/g
20.21	14.5		64.96	5.6	
18.00		0.547	60.97		0.523
14.38	8.2		60.85	1.8	
12.97		0.527	57.00	-1.6	
8.81	2.9		56.99		0.508
7.95		0.503	53.99		0.499
4.19	-3.6		53.00	-5.4	
3.02		0.479	50.99		0.488
			49.08	-11.5	

temperature in Figs. 16 and 17. ( $[\eta] - T$  relationships for all five solvent systems are shown.) Properties of the polymer-solvent systems at  $\Theta$ , together with physical data for the solvents, are collected in Table XI.

### C. Discussion

Analysis of the foregoing results in accordance with the grouping of polymer-solvent pairs suggested above (A) leads to the following observations: (1)  $\Theta$ -temperatures for the cyclohexane, diethyl malonate, and 1-chloro-n-undecane systems are virtually identical, whereas the corresponding intrinsic viscosity values differ significantly. Specific effects of the solvent, disassociated from concomitant changes in  $\Theta$  usually accompanying alteration in the medium, are thus unambiguously demonstrated to influence dimensions of the polystyrene coil at  $\Theta$ ; (2) to the extent that relative solvent effects in the structurally similar 1-chloro-n-decane, -undecane and -dodecane systems may be presumed negligible, observed changes in  $[\eta]_{\Theta}$  with  $\Theta$ -temperature of the three polymer-solvent pairs indicate a small, positive thermal coefficient of unperturbed chain dimensions for polystyrene. This interpretation is examined in more detail in a separate study (cf. Section II).

The judicious selection and classification of  $\Theta$ -systems considered above provides a useful scheme for the approximate resolution and assessment of temperature and solvent effects. A more sophisticated analysis of general applicability is clearly required, however, if the latter perturbations are to be meaningfully correlated with detailed characteristics of the polymer-solvent pairs. The evaluation of descriptive chain parameters, next considered, provides a basis for some further considerations.

The polystyrene molecule in each medium at temperatures near  $\Theta$  is considered to be representable by an equivalent chain of  $n$  flexible links of length  $b$  and (excluded) volume  $\beta$ . The latter parameter is zero at  $T = \Theta$  and is assumed to be adequately represented at other temperatures through the formulation  $\beta_0(1 - \Theta/T)$ , where  $\beta_0$  may be temperature dependent. Alteration of equivalent chain parameters in a given system, and properties dependent thereon, is assumed to occur solely through the temperature dependence of  $\beta$  and  $b$ . The following set of equations suffices to fix the values of the various chain parameters at  $T = \Theta$  in terms of observable quantities.

$$[\eta] \sim (\overline{r_0^2})^{3/2} \alpha^p; \quad 2.4 \leq p \leq 3 \quad (64)$$

$$\overline{r_0^2} = nb^2 \quad (65)$$

$$\alpha^2 = \overline{r^2}/\overline{r_0^2} = 1 + (4/3)z + O(z^2) \quad (66)$$

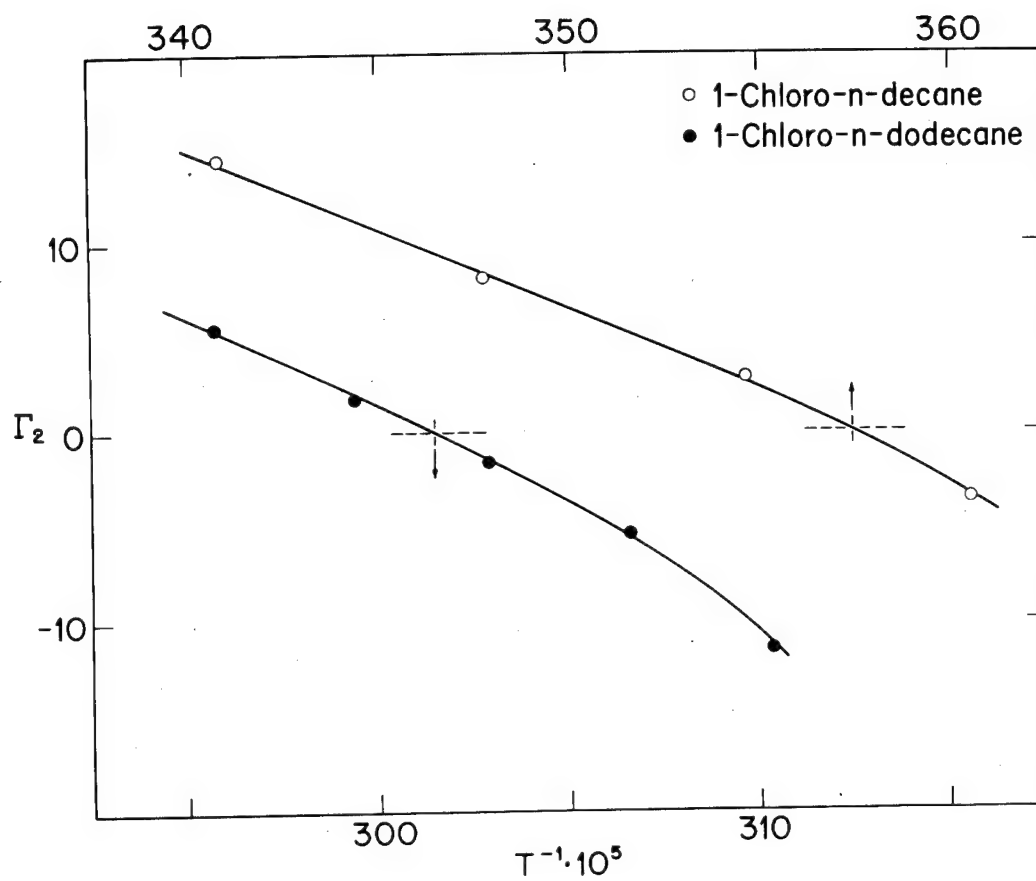


Figure 16 Plots of  $\Gamma_2$  versus reciprocal absolute temperature for polystyrene in 1-chloro-n-decane and 1-chloro-n-dodecane.

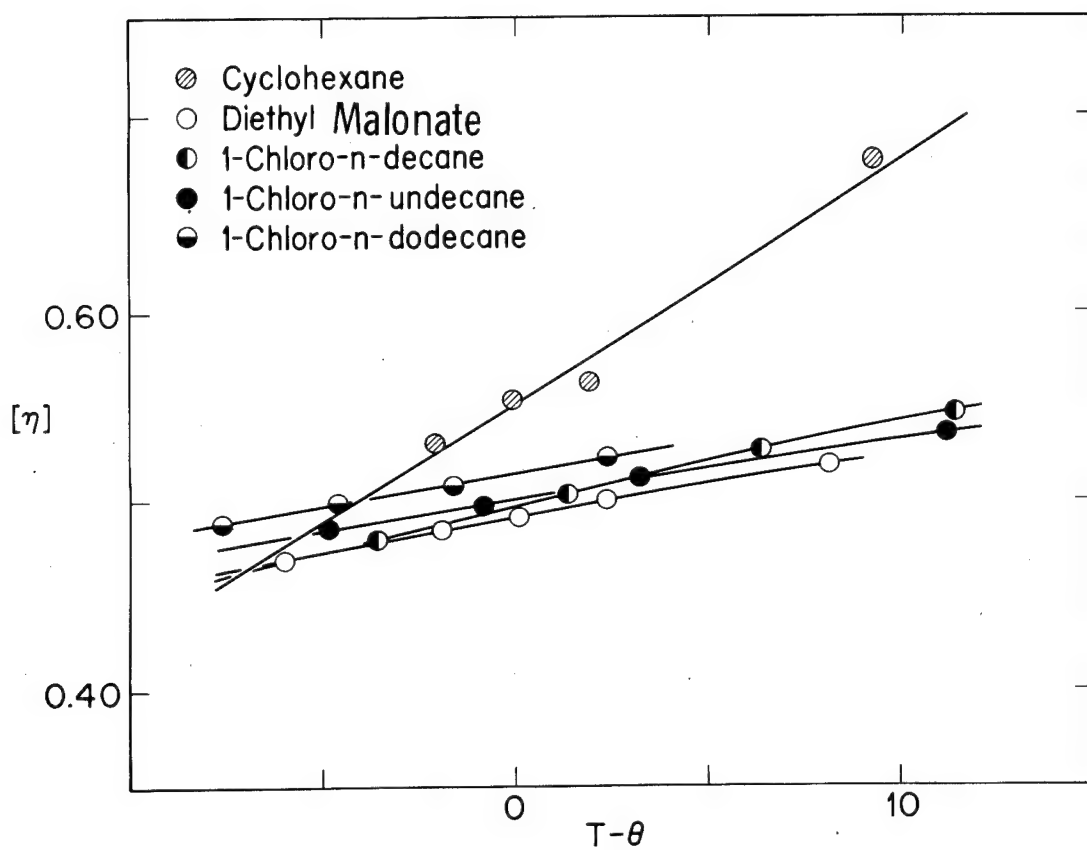
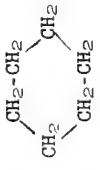
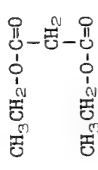
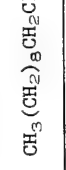
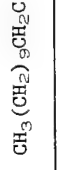
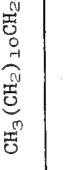


Figure 17 Plots of  $[\eta]$  versus  $T - \theta$  for five polystyrene- $\theta$ -solvent systems.

Table XI

Summary of Results for Polystyrene- $\theta$ -Solvent Systems

Solvent	Structure	$\delta^a$	obs. B.P., °C	obs. $n_D^{20}$	$\rho = a_0 + a_1(t-25) + a_2c$ <sup>b</sup>			Purity (chromato- graphy)	Principal Impurity	$\theta$ (°C)	$[\eta]_\theta$ (dl/g)	$k'_\theta$ <sup>c</sup>	$10^3$ $\left(\frac{d[\eta]}{dT}\right)_\theta$ <sup>d</sup>	$\left(\frac{d^2[\eta]}{dT^2}\right)_\theta$ <sup>e</sup>
					$a_0$ $\rho(25^\circ\text{C})$	$10^3a_1$	$10^3a_2$							
cyclohexane		8.2	80.8 760 mm	1.4257	0.774	-1.1	3.2	99.5	2,4-dimethyl- pentane	34.8	0.552	0.50	12.6	2.87
diethyl- malonate		9.5	97.0 21 mm	1.4137	1.049	-1.1	2.7	(97.9)	ethanol	35.9	0.490	0.60	3.74	0.91
1-chloro-n- decane		8.2	108.5 18 mm	1.4374	0.866	-0.8	1.8	99.9	---	6.6	0.497	0.80	4.87	1.07
1-chloro-n- undecane		8.2	106.2 7 mm	1.4406	0.865	-0.7	2.1	99.6	(n-undecyl- alcohol)	32.8	0.501	0.68	3.37	0.81
1-chloro-n- dodecane		8.2	187.3 100 mm	1.4427	0.864	-0.8	2.6	99.4	dodecene	58.6	0.514	0.56	3.47	0.86

(a) Calculated solubility parameter.

(b) Empirical density relation:  $t$  in °C,  $c$  in g/dl,  $\rho$  in g/cc.(c) Huggins constant at  $\theta$  (interpolated).

(d) These values represent a refined analysis and differ slightly from those quoted (for three systems) in the publication (see Section V).

(e) These values represent slopes extrapolated from the region  $T > \theta$ . They represent a refined analysis of data and differ significantly from those quoted in the publication (see Section V).

(f) See explanatory note in publication cited in Section V.

$$\Gamma_2 = n^2 \beta (N_0/2M)(1 + O(z)) \quad (67)$$

$$z = (3/2\pi)^{3/2} n^2 \beta / (nb^2)^{3/2} \quad (68)$$

$$\beta = \beta_0(T)(1 - \Theta/T) \quad (69)$$

$$\Theta = T(\Gamma_2)|_{\Gamma_2=0} \quad (70)$$

$$L = nb = (2k - 1)d \quad (71)$$

Symbols in the above relationships are defined as follows:  $\overline{r^2}$  is the mean-square separation of polymer chain ends, the subscript zero denoting values at  $T = \Theta$ ;  $\alpha$  is the factor by which chain dimensions are expanded as a consequence of excluded volume effects;  $N_0$  is Avogadro's number;  $M$  is polymer molecular weight;  $L$  is the contour length of the polymer molecule;  $k$  is the number of styrene units in the polymer chain; and  $d$  is the C-C bond distance in the molecule.

The equivalent chain parameter combinations  $nb$ ,  $n^2\beta_0$  and  $nb^2$  may be obtained from experimental data treated in accordance with Eq. (71) and the following Eqs. (72) and (73), respectively.

$$n^2\beta_0 = (2\Theta M/N_0)(d\Gamma_2/dT)_\Theta \quad (72)$$

$$(nb^2)^{3/2} = p[\eta]_\Theta (3/2\pi)^{3/2} (Ma_1/N_0) \left[ \frac{(d\Gamma_2/dT)_\Theta / (d[\eta]/dT)_\Theta}{1 - (3/2)(d \ln \overline{r_0^2}/dT)_\Theta / (d \ln [\eta]/dT)_\Theta} \right] \quad (73)$$

$$a_1 = 4/3$$

The results of calculations from the latter relationship, expressed as the quantity  $\overline{r_0^2}/M$ , are compiled for each polystyrene-solvent system in Table XII. The quantity  $d \ln \overline{r_0^2}/dT$  required has been taken as  $+0.4 \times 10^{-3}$  (see Section II, above); for comparison, calculations have also been carried out for the value zero.

Individual values for the three "equivalent chain" parameters  $n$ ,  $b$ , and  $\beta_0$  are entered in Table XIII.

It is evident from the entries in Table XII that reasonable estimates of polymer chain dimensions may be ascertained through the

Table XII

Values of  $\underline{r}_0^2/M$  for Polystyrene

Solvent	$[\eta]_\Theta$	$10^{16} \overline{r_0^2}/M$		
		$p=3$		$p=2.5$
		$10^3(d \ln \overline{r_0^2}/dT) =$ +0.4      0	$10^3(d \ln \overline{r_0^2}/dT) =$ +0.4      0	
cyclohexane	0.552	0.58	0.57	0.51
diethylmalonate	0.490	0.58	0.55	0.49
1-chloro-n-decane	0.497	0.54	0.52	0.46
1-chloro-n-undecane	0.501	0.59	0.55	0.49
1-chloro-n-dodecane	0.514	0.61	0.58	0.51



Table XIII

Equivalent Chain Parameters for Polystyrene- $\theta$ -Solvent Systems

Solvent	$\theta$ , °K	p = 3			p = 2.5		
		n	$10^8 b$	$10^{21} \beta_0$	n	$10^8 b$	$10^{21} \beta_0$
cyclohexane	308.0	611	19.6	3.20	689	17.4	2.51
diethylmalonate	309.1	608	19.7	1.03	686	17.5	0.81
1-chloro-n-decane	279.8	652	18.4	0.95	736	16.3	0.75
1-chloro-n-undecane	306.0	602	19.9	0.92	680	17.7	0.72
1-chloro-n-dodecane	331.8	579	20.7	1.14	653	18.3	0.90

indirect procedure described. The results for  $\overline{r_0^2}/M$ , particularly if  $p$  is taken less than 3, compare favorably with the generally accepted value, about  $0.50 \pm 0.05 \times 10^{-16}$ . Possibly also significant is the trend of  $\overline{r_0^2}$  with temperature for the chloroalkane solvents, in agreement with the observed trend in  $[\eta]_\theta$  for these three polymer-solvent systems. The relatively large size of the polystyrene coil in cyclohexane, indicated by the corresponding  $[\eta]_\theta$  value, is much less apparent in the magnitude of  $\overline{r_0^2}$  derived, however.

From the point of view of the specific influence of solvents, the most striking results of this study are the large values of  $[\eta]_\theta$ ,  $(d[\eta]/dT)_\theta$ , and  $(d\overline{r_0^2}/dT)_\theta$  displayed by the polystyrene-cyclohexane pair. The relatively large value of  $\beta_0$  (Table XIII) is compatible with augmentation of both molecular size and its temperature coefficient in this system. Thus, in the environment of compact, approximately spherical cyclohexane molecules, the polystyrene chain is prevented from assuming a large number of conformations, involving segment-segment proximity, which would be attainable in a medium comprised of linear solvent molecules. Excluded volume effects are accordingly larger in the former system, in a particular sense, even at  $T = \theta$ . Since all of the remaining four solvents examined here belong to the chain-like category, the unique augmentation of coil size in the cyclohexane system can at least be rationalized. Similarly, the temperature coefficient of size near  $\theta$ , proportional to the excluded volume parameter  $\beta_0$ , should be greatest in those systems in which the polymer chain is already relatively expanded in an attempt to conform to restrictions imposed by the solvent medium.

## VII. Thermodynamic and Conformation Properties of Polystyrene in Decalin — G. C. Berry

### A. Introduction

The study of dilute solution thermodynamic properties of the system polystyrene-decalin described in the previous report (ASD-TR 61-22, Part III) has been continued and extended to include initial investigation of branched structures.

A general discussion of this subject may be found in the report cited above. We will introduce only those relations for which there will be specific need below.

The scattering from a dilute polymer solution, including both inter- and intraparticle interference, may be expressed as

$$\frac{K_{\theta} c}{R_{\theta}} = \frac{1}{MP(u,0)} \left\{ 1 + 2\Gamma_2 P(u,0) \left[ Q(u,c) - (\Gamma_2 P(u,0))^{-1} \frac{2P(u,c)}{2c} \right] c + O(c^2) \right\} \quad (74)$$

Here  $u = (4\pi/\lambda')^2 \overline{s^2} \sin(\theta/2)$ ;  $R_{\theta}$  is the Rayleigh ratio at angle  $\theta$ ;  $K_{\theta}$  is an angle dependent constant for a given system;  $c$  is the concentration (g/ml);  $M$  is the molecular weight;  $\Gamma_2$  is the second virial coefficient;  $\lambda'$  is the wavelength of light in the medium;  $P(u,c)$  is the intramolecular scattering factor at concentration  $c$ , normalized to unity at zero angle--  $P(u,0)$  is usually denoted simply by  $P(u)$  or  $P(\theta)$ --and  $Q(u,c)$  is a scattering factor depending on both inter- and intraparticle interference effects, and also normalized to unity at  $\theta = 0$ . We are concerned primarily with the analysis of the data to yield  $\Gamma_2$ , or  $A_2$ , and the mean square radius of gyration  $\overline{s^2}$ . The former may be obtained from data extrapolated to  $\theta = 0$  while the latter may be derived from data extrapolated to  $c = 0$ .

### B. Experimental

1. Materials. Solvents: The cis, trans, and cis-trans mixtures of decalin were obtained by distillation under partial vacuum after treatment with silica gel. Isomeric compositions were determined by gas-liquid chromatography as given in Table XIV.

Cyclohexane was purified by a procedure similar to that used for the decalin\*.

Linear Polymers: The linear polystyrene samples listed in Table XV were all prepared by anionic polymerization. Samples A-5, A-16 and

\* It was found that reagent grade cyclohexane is often highly fluorescent.

Table XIV

Isomeric Decalin Mixtures

Solvent Code	% cis	% trans
1	51.4	48.4
2	61.7	38.3
3	66.1	33.9
4	>99.9	0

A-30 were fractionated into three parts and the center fraction was used here. In the other cases, the whole polymer was used. The polymers were freeze dried from benzene solution and evacuated at ca.  $10^{-6}$  mm Hg for several days.

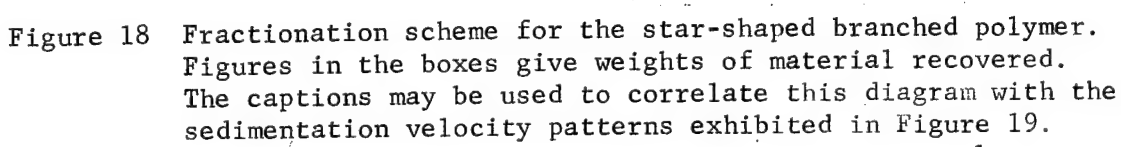
**Branched Polymer:** The tetrafunctional star-shaped branched polymer was prepared by anionic polymerization. Linear polymer of molecular weight M was terminated with 1,2,4,5 tetrachloromethyl benzene by methods discussed fully in the previous report. Unfortunately, the primary reaction does not take place stoichiometrically at these molecular weights; and thus, the polymerization product contains polymers of molecular weight M, 2M, 3M, 4M and small amounts of higher molecular weight material (here, polymers with molecular weight 3M, 4M, etc. are tri-star, tetra-star, etc.). Fractionation proved difficult because of the high molecular weights involved, and because branching tends to increase solubility. Accordingly, multiple refractionations were required to separate the desired tetra-star product. The precipitation fractionation was effected in a benzene-methanol solution. In every case, sufficient methanol was added to reach the cloud point, the solution was heated 3-5°C until clear, and then cooled slowly to a temperature 0.1° to 1° below the initial temperature, depending on the size of the fraction desired. Fractions were recovered from benzene solution by freeze-drying. The fractionation scheme is shown schematically in Fig. 18. Representative sedimentation velocity patterns for some of these samples are given in Fig. 19. Fig. 19a shows superimposed patterns for the bulk polymer and the starting materials used for the branches. Figs. 19b and 19c illustrate the composition of initial fractions still containing some polymer of 2M and 3M in addition to the desired 4M species, but with most of the polymer of weight M removed. Fig. 19d shows the sample after further concentration of the 2M, 3M and 4M products. Figs. 19e and 19f show further fractions in which the 2M peak is almost absent and the 3M peak is diminished, in addition, polymer of molecular weight >4M can now be seen. Figs. 19g, 19h, and 19i show three of the final fractions. Comparison of the sedi-

Table XV

Theta Solvent Parameters for Polystyrene in Decalin

Sample	Solvent <sup>a</sup>	$\Theta^b$	$10^{-6} M_w$	$10^{10} (s^2)_\Theta$	$10^{18} (s^2/M)_\Theta$
<u>Linear Polymers</u>					
A-30	2	15.2°C	4.84	0.455	9.40
A-30	CH	--	4.81	0.464	9.63
A-5	1,2	15.4	1.74	0.132	7.58
A-5	CH	--	1.74	0.121	6.93
A-18	CH	--	1.46	0.0990	6.77
A-17	CH	--	1.32	0.0928	7.03
A-16	2	15.2	1.15	0.0772	6.66
A-16	CH	--	1.16	0.0722	6.23
A-19	4	12.2	0.701	0.0463	6.60
A-19	CH	--	0.689	0.0484	7.04
L-10	CH	--	0.685	0.0463	6.76
A-48	CH	--	0.433	0.0305	7.04
A-13	2	15.0	0.205	0.0158	7.69
A-13	CH	--	0.200	--	--
A-3	4	12.0	0.138	--	--
A-3	CH	--	0.135	--	--
A-25	3	14.2	0.0530	--	--
<u>Tetrafunctional star polymers</u>					
A-48-p4-2	4	12.1	1.90	0.0832	4.37 <sup>c</sup>
A-48-P4-2	CH	--	1.85	0.0802	4.33 <sup>c</sup>

<sup>a</sup>See Table XIV, CH = cyclohexane.<sup>b</sup> $\Theta$  not determined here, but taken as 34.8°C for cyclohexane.<sup>c</sup>Multiply by  $g^{-1}$  to compare with the above:  $g = 0.625$ ;  $10^{18} (s^2/gM) = 6.94$ .



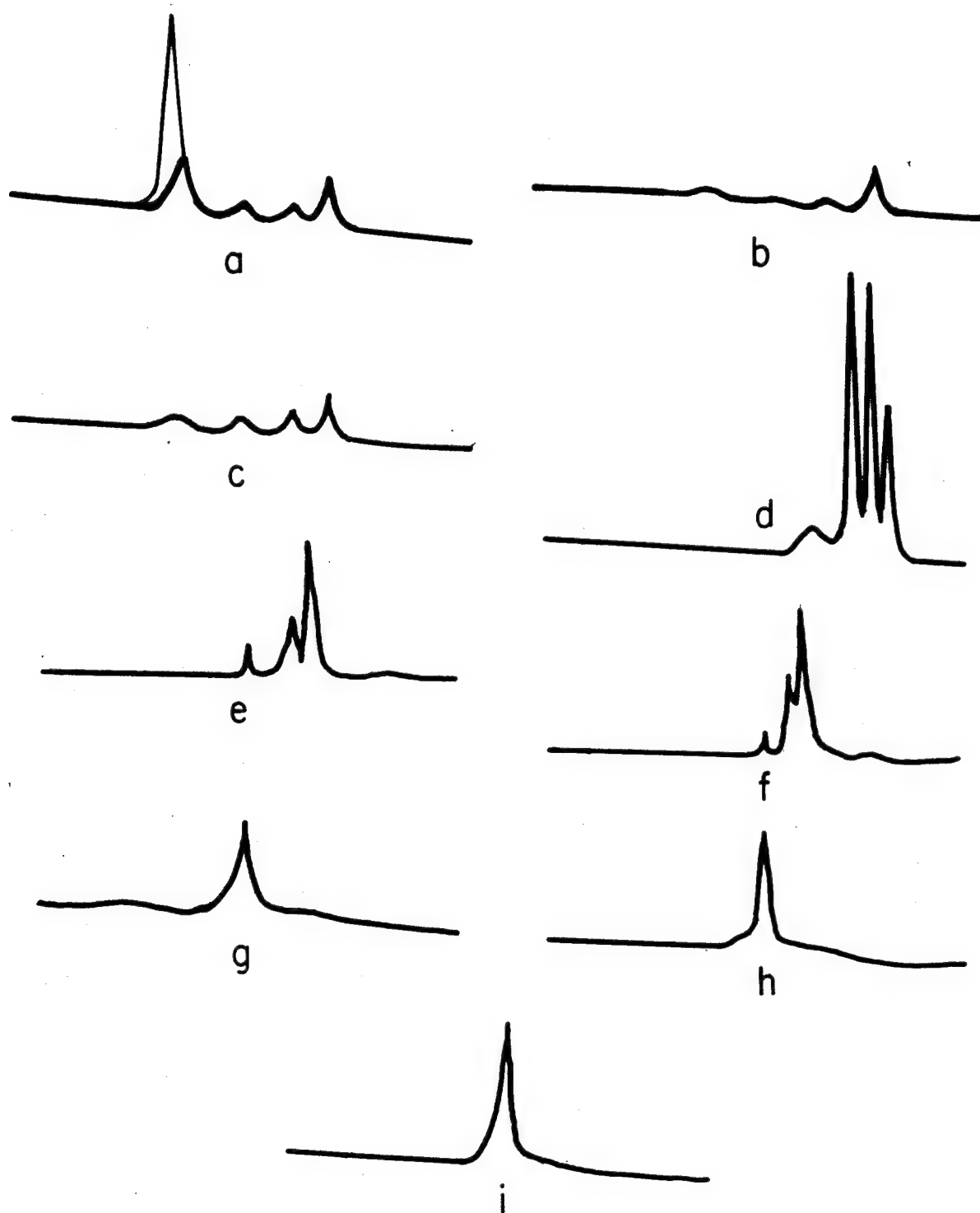


Figure 19 Representative sedimentation velocity patterns for some of the fractions shown in Fig. 18. With reference to Fig. 18, the fractions are: (a) I; (b) II; (c) III; (d) IV; (e) V; (f) VI; (g) A-48-p4-1; (h) A-48-p4-2; (i) A-48-p4-3.

mentation constants for the peaks in the last three figures indicates that they are all the same species. The fraction A-48-P4; 2 studied here is essentially free of material of molecular weight below 4M, but contains small (<1%) amounts of branched polymers of higher functionality.

2. Methods. The experimental procedure used to obtain and analyze the light scattering data is described fully in the previous report. It was shown there that extrapolation of  $\xi \equiv \sqrt{K_\theta c/R_\theta}$  versus  $u$  for data at  $c = 0$  yields a better estimate for  $s^2$  than extrapolation of  $\xi^2$  versus  $u$  as is usually done. Extrapolation of  $\xi$  versus  $c$  for data at  $u = 0$  has long been known to yield better estimates for  $A_2$  and is the technique used here.

The possibility that the isomeric solvent mixture (cis and trans decalin) might affect the analysis of the light scattering data for  $M$ ,  $s^2$  or  $A_2$  through modification<sup>35</sup> of  $K_\theta$  was investigated by determining the scattering from a polystyrene-decalin solution as a function of isomeric composition. Any effect on  $K_\theta$  of varying solvent composition should appear as a variation in apparent  $M$  with solvent composition. The results given in Fig. 20 indicate no such trend. Also included in Fig. 20 is the theta temperature as a function of solvent composition. In no case does  $\theta$  rise to the value 31°C reported by some other investigations<sup>26,56</sup>. The value of 19.8 C at 23% cis reported by Okada, Toyoshima and Fujita<sup>57</sup> is, however, in good agreement with our results.

A calculation of  $P(u)$  for star-shaped branched chains has been carried out to facilitate extrapolation of  $\xi_c = 0$  versus  $u$  to obtain  $(s^2)$ . The results yield

$$P_{br}(u) = \frac{2(p-1)}{p} P_\ell(2u/gp) - \frac{(p-2)}{p} P_\ell(u/gp) \quad (75)$$

for a chain with  $p$  branches where  $g$  is the ratio of the mean square radii of branched and linear chains of molecular weight  $M$  and  $P_\ell$  designates the particle scattering function for a linear chain:

$$P_\ell(x) = \frac{2}{x^2} [x-1 + \exp(-x)] \quad (76)$$

Eq. (75) may be rewritten as

$$P_{br}(u) = \frac{g^2}{u^2} \left\{ \frac{2u}{g} + p(p-3) + p(p-1) \exp\left(-\frac{2u}{gp}\right) - 2p(p-2) \exp\left(-\frac{u}{gp}\right) \right\} \quad (77)$$

which agrees with the special case ( $p=4$ ) obtained by Benoit<sup>58</sup>.

Determinations of polymer concentrations in decalin were checked by infrared absorption, in addition to methods cited in the previous report. The absorption at 698  $\text{cm}^{-1}$  does not strictly obey Beer's law for



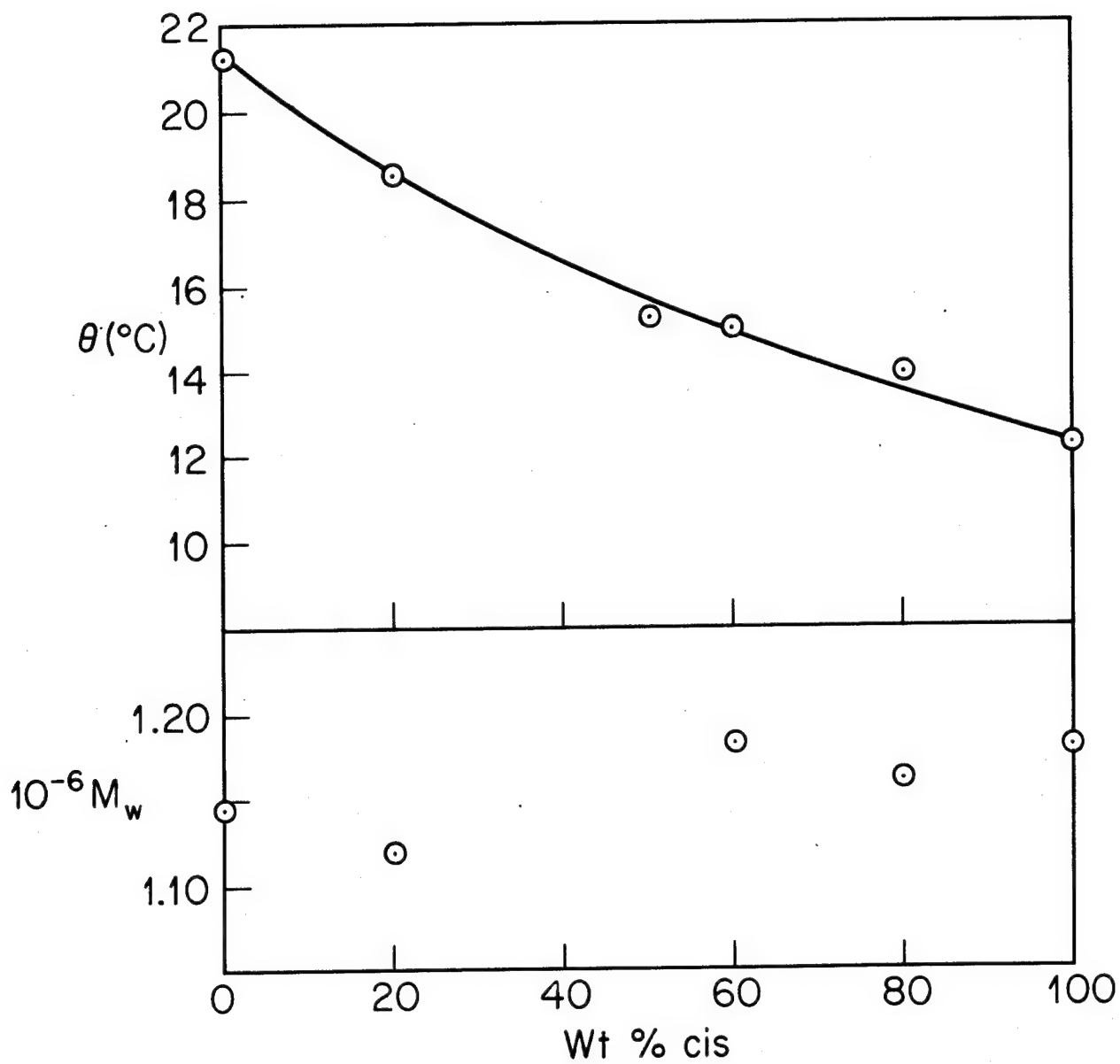


Figure 20 Variation of  $\theta$  with solvent composition for cis-trans mixtures of decalin. Constancy of apparent molecular weight with solvent composition.

low concentrations, but a calibrated curve can be used to determine the concentration from the absorption.

Light scattering measurements have been made for at least five concentrations in every case, over a temperature interval of ca. 100°C, and for angles from 18° to 135°. The principle parameters extracted from the light scattering data are the molecular weight, the second virial coefficient, and the mean square radius of gyration calculated respectively as

$$M = \lim_{c, u=0} \xi^{-2} \equiv \xi_0^{-2}$$

$$\Gamma_2 = MA_2 = \lim_{c, u=0} \frac{\partial \xi}{\partial c}$$

$$\overline{s^2} = \left( \frac{3}{8\pi^2} \right) (\lambda')^2 \lim_{c, u=0} \frac{\partial \xi / \partial u'}{\xi_0}$$

where

$$u' = \sin^2 \left( \frac{\theta}{2} \right)$$

The slight temperature variation in  $K_\theta$  is accounted for by referring all data to molecular weights calculated at 25°C.

Molecular weights in cyclohexane ( $dn/dc = 0.181$ ) are consistently 10% higher than those in decalin ( $dn/dc = 0.131$ ), probably because of errors in one or both of the values used for  $dn/dc$ . Consequently, all molecular weights reported here are referred to measurements in cyclohexane at 34.8°C.

### C. Results

The parameters determined under theta conditions are listed in Table XV. Data as a function of temperature are given in Table XVI and in Figs. 21 and 22. The extrapolations to obtain  $\overline{s^2}$  are most uncertain when  $\overline{s^2}$  becomes so small ( $\overline{s^2} \approx 2 \times 10^{-13} \text{ cm}^2$ ) that the initial slope  $(\partial \xi / \partial u')_{c, u=0}$  cannot be determined accurately or when the shape of  $P^{-1/2}(u)$  is such that initial slope is not accurately determined over the span of angles available (18° to 135°). The latter situation arises for large  $\overline{s^2}$  ( $\overline{s^2} > 4 \times 10^{-11} \text{ cm}^2$ ) or for some branched structures.

The ratio  $10^{18} (\overline{s^2}/M)_\theta$  is taken as 7.0 for all calculations here. The effects of molecular weight heterogeneity are ignored for these nearly homogeneous samples. The principal deviation occurs for the highest molecular weight polymer A-30. It is not yet clear if this

Table XVI

Light Scattering Data for Polystyrene in Decalin(t in °C;  $\Gamma_2$  in ml/g;  $\alpha^2 = \overline{s^2/s_0^2}$ )

Sample: A-30 in decalin 2									
t	14.1	14.6	15.1	15.5	16.0	17.0	18.5	19.9	22.0
$\alpha^2$	0.928	0.990	0.977	1.03 <sub>3</sub>	1.05 <sub>8</sub>	1.157	1.202	1.257	1.276
$\Gamma_2$	-29.7	-21.1	+6.7 <sub>1</sub>	23.0	40.3	61.4 <sub>5</sub>	90.2	109.4	139.9
t	25.0	30.2	35.0	40.0	45.1	49.9	60.7	70.2	80.0
$\alpha^2$	1.368	1.453	1.555	1.696	1.777	1.804	1.922	1.937	1.955
$\Gamma_2$	173.5	204.8	256.9	292.0	322.5	343.6	386.6	425.2	431.4
t	90.2	104.8							
$\alpha^2$	2.02	2.03							
$\Gamma_2$	449.8	459.9							
Sample: A-5 in decalin 1 or decalin 2 (denoted by *)									
t	14.1	14.7	14.7*	15.1*	15.5	15.5*	16.5	16.5*	17.5
$\alpha^2$	0.923	0.985	--	--	1.01 <sub>1</sub>	--	1.07 <sub>2</sub>	--	1.093
$\Gamma_2$	-16.1 <sub>3</sub>	-4.7 <sub>9</sub>	-11.2	-5.4 <sub>4</sub>	+1.7 <sub>7</sub>	1.3 <sub>9</sub>	12.0 <sub>9</sub>	12.0 <sub>0</sub>	23.0

continued

Table XVI (continued)

t	17.5*	19.8	19.9*	24.8	24.8*	34.8	44.5	54.5	70.0
$\alpha^2$	--	1.152	--	1.281	--	1.436	1.525	1.627	1.712
$\Gamma_2$	21.2	47.2	40.0	73.3	72.8	105.3	131.8	159.3	181.2
t	80.0	90.0	98.0						
$\alpha^2$	1.724	1.745	1.81						
$\Gamma_2$	189.4	190.7	201.8						
Sample: A-16 in decalin 2									
t	13.2 <sub>5</sub>	14.0	14.5	15.0	15.5 <sub>5</sub>	16.0	17.4 <sub>5</sub>	20.0	25.0
$\alpha^2$	0.945	0.985	0.985	1.00 <sub>3</sub>	1.01 <sub>3</sub>	1.02 <sub>3</sub>	1.06 <sub>2</sub>	1.076	1.255
$\Gamma_2$	-16.9 <sub>2</sub>	-9.8 <sub>4</sub>	-3.0 <sub>4</sub>	0.00	+5.0 <sub>5</sub>	9.60	19.6 <sub>6</sub>	32.2 <sub>5</sub>	54.7
t	35.0	45.0	55.0	62.2	70.2	77.8	85.1	92.4	99.8
$\alpha^2$	1.420	1.568	1.660	1.670	1.685	1.755	1.785	1.812	1.870
$\Gamma_2$	88.8	107.2	119.8	126.0	137.1	155.4	160.4	169.8	--
Sample: A-19 in decalin 4									
t	10.0	10.7	11.3	12.1	12.7	13.3	14.1	15.3	17.1
$\alpha^2$	--	--	--	1.00	1.02	1.00	1.02	1.06	1.06
$\Gamma_2$	10.9 <sub>6</sub>	-9.9 <sub>3</sub>	-5.5 <sub>4</sub>	-0.71	+2.7 <sub>9</sub>	4.8 <sub>6</sub>	8.7 <sub>5</sub>	13.1 <sub>8</sub>	18.75
t	20.9	26.5	36.9	46.7	56.5	68.0	79.5	93.6	108.5
$\alpha^2$	1.10	1.19	1.34	1.42	1.47	1.58	1.63	1.59	1.66
$\Gamma_2$	30.28	45.4	63.0	75.2	84.1	91.9 <sub>5</sub>	101.2	106.8	115.3

continued

Table XVI (continued)

Sample: A-13 in decalin 2									
t	14.0	14.4	15.0	15.5	16.7	17.2	20.0	30.3	45.0
$\Gamma_2$	-2.31	-0.93	0.00	+1.21	2.41	3.63	7.16	16.74	24.3
t	43.7	61.8 <sub>5</sub>	80.6	111.0					
$\Gamma_2$	28.8	33.1	33.5	33.3					
Sample: A-3 in decalin 4									
t	8.15	9.1	9.9 <sub>5</sub>	10.8	11.6	13.2	15.2	22.5	28.8 <sub>5</sub>
$\Gamma_2$	-4.83	-3.20	-2.07	-1.18	-0.15	+1.43	3.50	9.31	12.71
t	43.7	61.8 <sub>5</sub>	80.6						
$\Gamma_2$	17.60	23.60	25.24						
Sample: A-25 in decalin 3									
t	12.1	13.7	15.0	16.3	18.1	20.0	24.5	35.3	49.9
$\Gamma_2$	-0.80	-0.20	+0.40	0.93 <sub>7</sub>	1.47 <sub>8</sub>	2.42	3.67	6.05	8.04
t	65.8	79.6							
$\Gamma_2$	9.99	11.25							

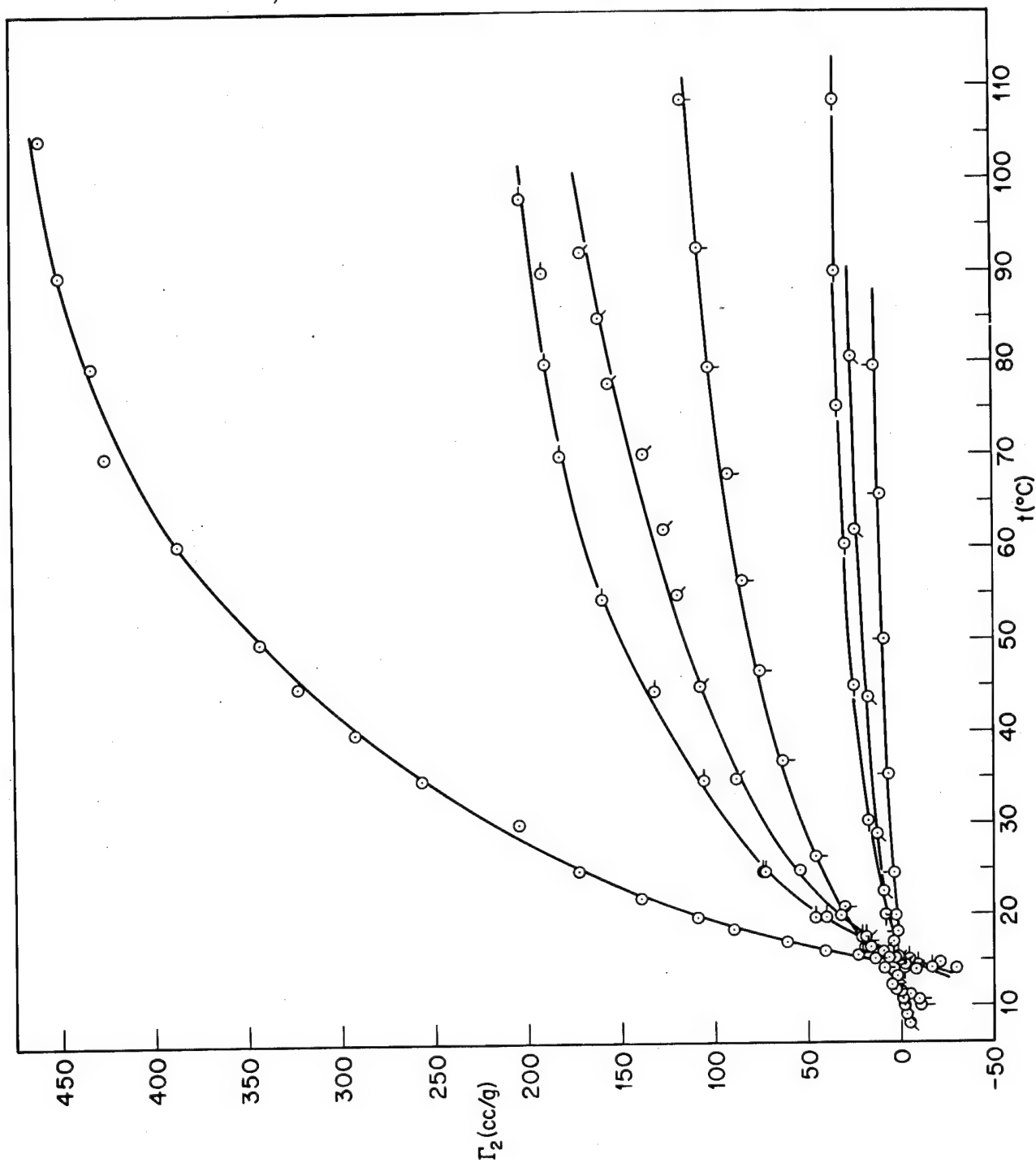


Figure 21 Dependence of the second virial coefficient  $\Gamma_2$  (cc/g) on temperature for samples A-30,  $\emptyset$ ; A-5,  $\phi$ ; A-16, Q; A-19  $\phi$ ; A-13,  $\emptyset$ ; A-3,  $\phi$ ; A-25,  $\phi$ .

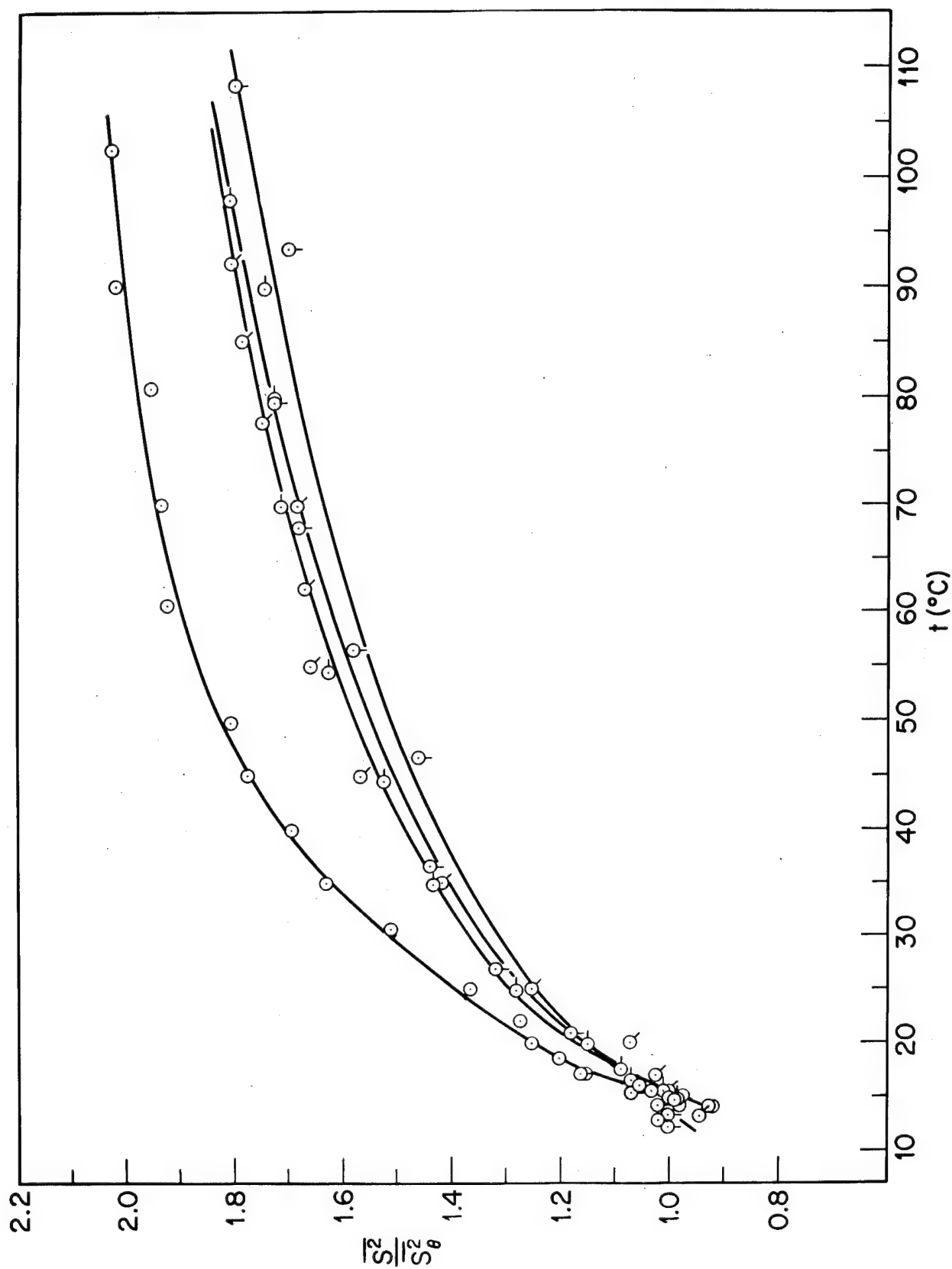


Figure 22 Dependence of the expansion factor  $\alpha^2 = \overline{s^2}/\overline{s^2}_0$  on temperature for various samples. The symbols are defined in Figure 21.

reflects a real variation in  $(\overline{s^2}/M)_0$ , or if a systematic error was made in the extrapolations to obtain  $\overline{s^2}$  for A-30. This would have the most effect on  $\overline{s^2}$ , and less on  $\Gamma_2$  and M.

The term in square brackets in Eq. (75) involving  $Q(u,c)$  and  $\partial P/\partial c$  is principally due to intramolecular interference, although  $Q(u,c)$  also includes some terms due to intermolecular interference in the scattered radiation. The data here suggest that the bracketed term is never far from unity. This being the case, further investigation has not been attempted.

#### D. Discussion

##### 1. $A_2$ as a function of molecular weight and temperature.

The statistical theories for  $\Gamma_2$  and  $\overline{s^2}$  and the relation of the statistical chain parameters to the macroscopic thermodynamic properties were discussed in the previous report. The statistical model consists of an equivalent chain of  $n$  freely rotating segments, each of mean square length  $b_0^2$ . In general,  $n$  is less than the degree of polymerization and  $b_0$  is greater than the distance between adjacent atoms along the chain. It is assumed that multiple interactions between the segments can be represented as additive pairwise and that the solvent can be treated as a continuum whose properties may be accounted for by the use of suitable average interaction potentials. This type of model has been studied at various levels of mathematical rigor and yields the general result.

$$A_2 M^{1/2} = 4N_0 \pi^{3/2} A^3 z F'(z) \quad (78)$$

where

$$z = BA^{-3} M^{1/2}$$

$$B = [1/4 \pi^{3/2}] \left( \frac{n^2 \beta}{2M^2} \right)$$

$$6A^2 = 6(\overline{s^2}/M)_0 = (n/M)b_0^2$$

The temperature dependence of  $A_2$  resides in the excluded volume parameter  $B$  which may be approximated (rigorously in the limit  $z = 0$ ) as

$$B = B_0(1 - \Theta/T) \quad (79)$$

Unfortunately, experimental methods do not yield the parameters  $(n/M)$ ,  $b_0$  or  $\beta_0$ , but only the products  $(n/M)b_0^2$  and  $(n/M)^2\beta_0$  unless further assumptions are made\*. Thus, a direct evaluation of  $\beta$  for

\* For example, the Kuhn approximation that the contour length of the real chain is identical to that of the equivalent chain<sup>59</sup>.



$T \neq \Theta$  does not appear feasible unless a relation such as Eq. (79) is assumed. We here assume that Eq. (79) will hold for  $T \neq \Theta$  and reserve further comment until after the  $\alpha^2$ - $A_2$ - $T$ - $M$  data have been analyzed.

All the parameters in Eq. (78) may be determined experimentally. Thus,  $\Theta$  is the temperature for which  $A_2 = 0$ ;  $N_0(n^2\beta_0/2M^2)$  is the initial slope  $[\partial A_2/\partial(1 - \Theta/T)]_{T=\Theta}$ ;  $A^2$  is the ratio  $(s^2)_0/M$ ; and values of  $A_2$  and  $\alpha^3$  are of course known empirically as functions of temperature and molecular weight. The numerical parameters for polystyrene-decalin used to analyze these data read

$$A_2 M^{1/2} = 0.249 z F'(z)$$

$$z = 0.01023 M^{1/2} (1 - \Theta/T)$$

The values of  $\Theta$  are listed in Table XV;  $10^3 N_0(n^2\beta_0/2M^2) = 2.55$  and  $10^{18} A^2 = 7.0$ . No trend in either  $\Theta$  or  $n^2\beta_0/2M^2$  with molecular weight was detected. The observed value of  $\Theta$  for A-25 may indicate the onset of a decrease of  $\Theta$  with  $M$ , but the deviation is barely outside experimental error for this molecular weight. Fig. 23 shows the plot of  $A_2/F'(z)$  versus  $(1 - \Theta/T)^*$  used to compute  $n^2\beta_0/2M^2$ . The values of the constants entering into the expression for  $z$  (except  $M$ ,  $\Theta$  and  $T$ ) do not affect the test for superposition of the  $A_2$  data as a function of  $z$  since, at this stage, no numerical comparison of theory and data is being made.

An assumption concerning the temperature dependence of  $A^2$  is required in this analysis since in general the unperturbed dimensions will depend on temperature. The extensive investigation of  $A^2(T)$  for polystyrene given above by Orofino and Ciferri, in which data on bulk polymer and on dilute solutions near  $\Theta$  and for  $T > \Theta$  are examined (including data on the temperature dependence of  $[\eta]$  in some polystyrene-decalin given in the next section) suggests that  $dA^2/dT$  is slightly positive, in contrast to the large negative values previously reported. The effect of even a relatively large  $dA^2/dT$  is small and so the small  $dA^2/dT$  is ignored here. The general conclusions reached are unaffected by this neglect\*\*.

\* This initial slope may be determined by first plotting  $A_2$  against  $(1 - \Theta/T)$  to determine an estimate for  $n^2\beta_0/M^2$ . This estimate can then be used to plot  $A_2/F'(z)$  against  $(1 - \Theta/T)$  to obtain an improved estimate for  $n^2\beta_0/M^2$  since this plot will exhibit linearity for larger values of  $(1 - \Theta/T)$ . Any of the relations (Eqs. 81-85, below) may be used here with equivalent results. The first and second estimates for  $n^2\beta_0/M^2$  usually agree satisfactorily.

\*\* Also neglected is a possible temperature dependence of  $n^2\beta_0/M^2$  which results if  $n^2\beta_0/M^2$  is interpreted in terms of lattice theories<sup>34</sup>. This effect is negligibly small for the system polystyrene-decalin, if in fact it should be included.

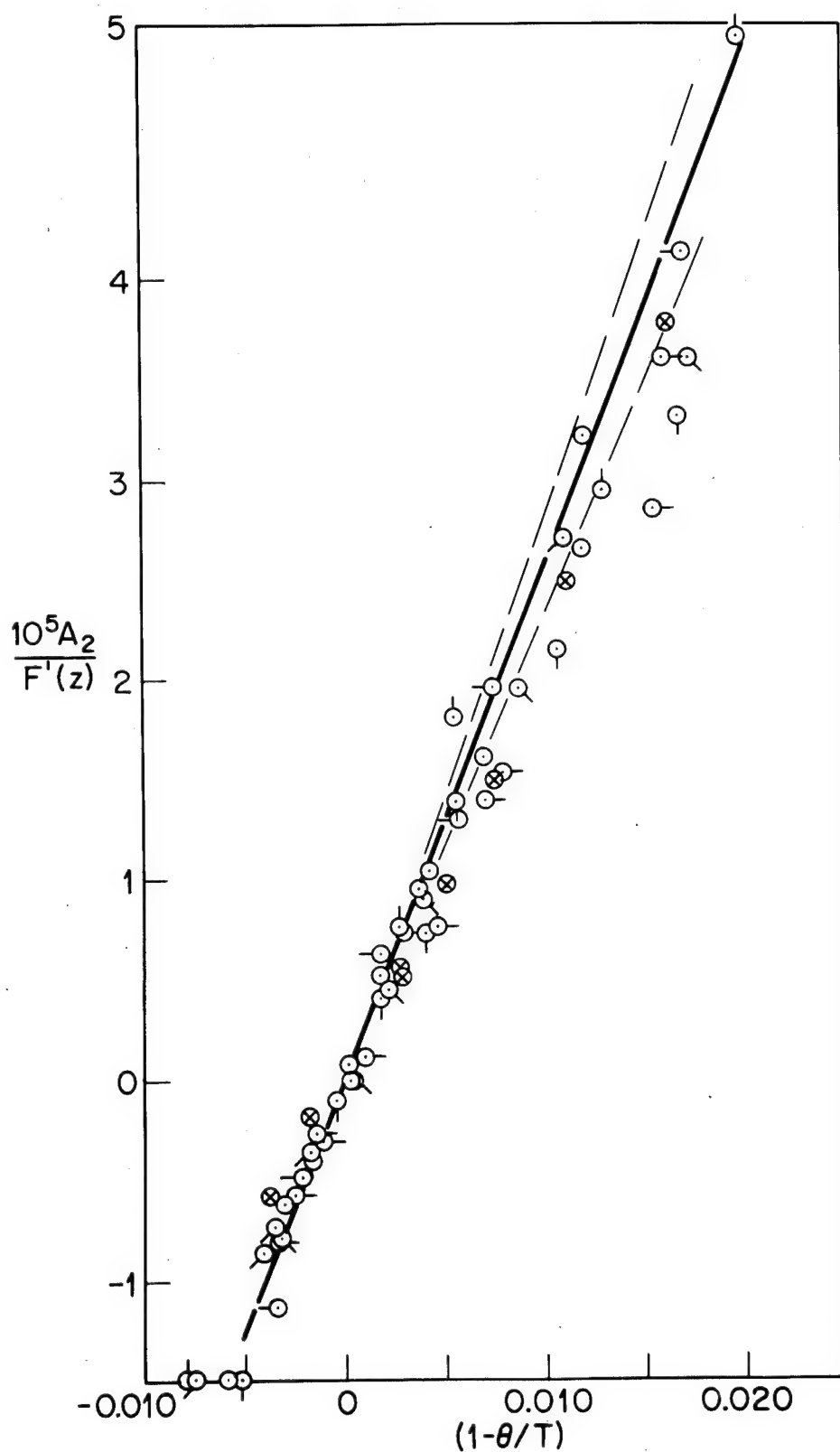


Figure 23 Determination of the parameter  $n^2 \beta_0 / M^2$ . The dashed line indicates slopes of  $\pm 5\%$  from the solid line. The points are identified as in Figure 21.

Fig. 24 shows a plot of  $A_2 M^{1/2}$  versus  $z$  for all of our data. Some data for polystyrene in cyclohexane are also included for comparison. The curve was subjectively drawn to fit the data and does not derive from an analytical expression for  $F'(z)$ . We consider the data to support the basic model in its prediction that the single parameter  $z$  should suffice to correlate data at different molecular weights and temperatures. Moreover, the simple temperature dependence for  $B$  assumed by Eq. (79) for  $z > 0$  appears to be adequate for these data.

2. Approximate theories for  $A_2$  in good solvents. The calculation of  $F'(z)$  with mathematical rigor on the basis of the equivalent chain model has not proved feasible except in the limit of small  $z$ . Approximations yield a function  $F(\xi) = F'(z)$  in Eq. (78), with the exact form for  $F(\xi)$  depending on the assumptions made in its derivation. Here,  $\xi \equiv (z/\alpha^3)$  where  $\alpha^2 \equiv s^2/s_0^2$  is termed the expansion factor. Thus, Eq. (78) may be recast to read

$$\frac{A_2 M^{1/2}}{\alpha^3} = 4 N_0 \pi^{3/2} A^3 \xi F(\xi) \quad (80)$$

The functions for  $F(\xi)$  to be examined here are given, by several theories, as:

$$F(\xi) = 1 - 2.865 \xi + 9.73 \xi^2 + O(\xi^3) \quad (81)^{60}$$

$$F(\xi) = (1/2.30 \xi) \ln [1 + 2.30 \xi] \quad (82)^{61}$$

$$F(\xi) = (1/5.73 \xi) \ln [1 + 5.73 \xi] \quad (83)$$

$$F(\xi) = (1/5.68 \xi) [1 - \exp(-5.68 \xi)] \quad (84)^{48}$$

$$F(\xi) = (1/5.68 \xi_2) [1 - \exp(-5.68 \xi_2)] \quad (85)^{49}$$

where

$$\xi_2 = z/\alpha_2^3; \quad \alpha^5 - \alpha^3 = \frac{a_1}{K} (\alpha_2^5 - \alpha_2^3)$$

and

$$K = 1.9$$

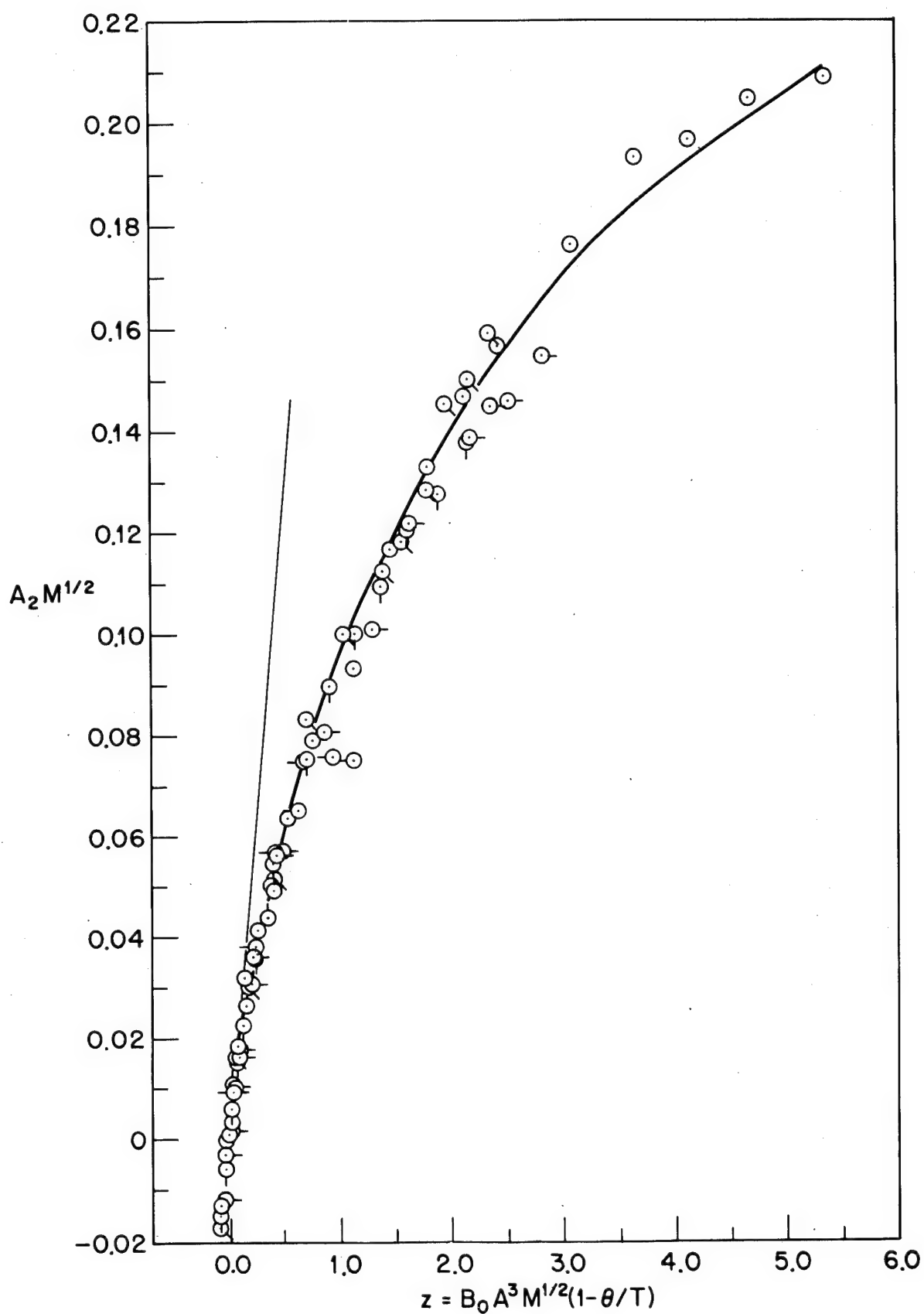


Figure 24  $A_2 M^{1/2}$  as a universal function of the thermodynamic parameter  $z$ . The light line is the theoretical initial slope; the bold line is an empirical fit to these data. The points are identified as in Figure 21.

Eq. (81) results from a rigorous treatment of the equivalent chain model, but is limited to  $\zeta$  near zero. Eqs. (82), (84) and (85) are based on different approximations which are discussed in the references cited. Eqs. (84) and (85) both yield the correct behavior for  $\zeta F(\zeta)$  to the term of order  $\zeta^2$  as a result of the nature of the approximations made in their derivation, whereas Eq. (82) does not. Eq. (83) is obtained from Eq. (82) by arbitrarily adjusting the constant to force agreement with Eqs. (81) to order  $\zeta^2$ . The approximations made in the derivation of Eqs. (84) and (85) may be expected to be most reasonable the smaller is  $\zeta$ , whereas those made in the derivation of Eq. (82) are not so weighted.

Analysis of  $A_2$  in terms of the approximate theories proceeds according to Eq. (80). Hence, in Fig. 25 the product  $A_2 M^{1/2}/\alpha^3$  is plotted against  $\zeta$ . The data are seen to be in good agreement with the theories of Casassa and Markovitz<sup>48</sup> and Casassa<sup>49</sup>, at least for  $\zeta > 0.5$ . For  $\zeta > 0.5$ , the general shape predicted by Eqs. (84) or (85) is observed, but a somewhat higher asymptotic limit is suggested. This behavior is consistent with the nature of the approximations made in the derivation of Eqs. (84) or Eq. (85) since the assumptions ought to become less satisfactory as  $\zeta$  increases. It may be remarked that any possible temperature dependence of  $A^2$  can be properly ignored in this analysis.

It is to be emphasized that no arbitrary parameters have been introduced in this analysis since  $\theta$ ,  $A^2$  and  $n^2 \rho_0 M^2$  were determined directly.

The apparent attainment of a (nearly) constant value for  $A_2 M^{1/2}/\alpha^3$  for  $\zeta > \text{ca. } 0.6$  is interesting and requires further comment. This product is predicted to attain such a limit by some of the approximate forms for  $F(\zeta)$ , Eq. (85) yielding a value of  $3.052 \times 10^{24}$ , for example. The observed value seems somewhat higher, ca.  $4.03 \times 10^{24}$ . A possible procedure for determining  $n^2 \rho / 2M^2$  in good solvents from isothermal  $A_2$ -M data without the assumption of any  $\alpha^2(z)$  relation would be to plot  $A_2 M^{1/2}/\alpha^3 A^3 = A_2 M^2/(\bar{s}^2)^{3/2}$  versus  $B M^{1/2}/\alpha^3 A^3 = B M^2/(\bar{s}^2)^{3/2}$  and adjust the parameter B until the data coincided with a plot of Eq. (80) computed for some choice of  $F(\zeta)$  believed to be correct. Determination of B then yields  $n^2 \rho / M^2$ ; and if B is determined at several temperatures, a plot of B versus  $1/T$  will yield  $n^2 \rho_0 / M^2$  and  $\theta$ . However, if the solvent is so good that  $\zeta > \text{ca. } 1.0$  over the molecular weight range examined, then clearly this procedure cannot be used owing to the asymptotic behavior of  $\zeta F(\zeta)$ . Such appears to be the case for polystyrene in dichloroethane for  $M > 5 \times 10^5$ , for example<sup>62</sup>, where  $A_2 M_2/(\bar{s}^2)^{3/2}$  has a nearly constant value of ca.  $4.2 \times 10^{24}$ . Other data, for example, polyvinyl acetate in butanone or trichlorobenzene<sup>63</sup> exhibits a trend for  $A_2 M^2/(\bar{s}^2)^{3/2}$  from 2.8 to  $4.0 \times 10^{24}$ . The close agreement of the limiting values observed for  $A_2 M^{1/2}/\alpha^3 A^3$  for our data and the data in these good solvents for high molecular weight samples is gratifying.

It may be remarked that our empirical curve for  $A_2 M^{1/2}$  versus  $z$  may be employed to determine  $B_0$  and  $\theta$  instead of  $A_2 M^{1/2}/\alpha^3$  versus  $\zeta$  provided sufficient data exist for  $A_2 M^{1/2} < 0.2$  to accurately determine B. This implies data at low molecular weights in good solvents. For

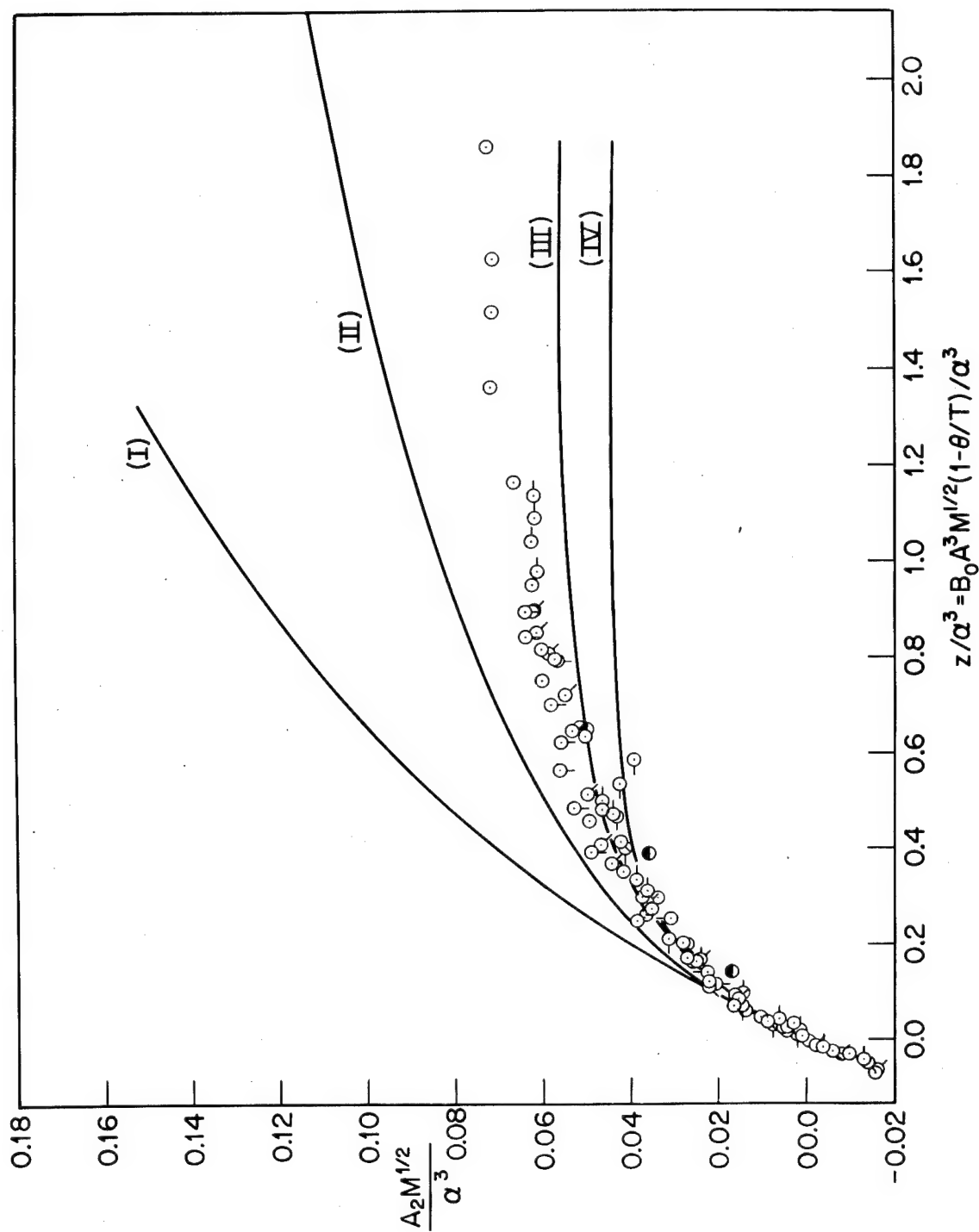


Figure 25  $A_2 M^{1/2} / \alpha^3$  as a function of the thermodynamic parameter  $z / \alpha^3$ . The lines are drawn according to (I) Equation 82; (II) Equation 83; (III) Equation 84; and (IV) Equation 85. The symbols are defined in Figure 21 except for  $\circ$ , which is for data given in Ref. 54.

since  $10^4 A_2 \approx 59.4 M^{-0.230}$  for polyvinyl acetate in trichlorobenzene<sup>63</sup>, this would require data for  $M < 4.5 \times 10^5$  in order to determine B. Incidentally, if such data were available, then determination of  $A_2(M)$  for higher molecular weight polymers would enable more of the function  $A_2 M^{1/2}$  versus  $z$  to be determined. We may, in fact, study our fractions in the good solvent toluene in order to extend the empirical curve given in Fig. 24 to still larger  $z$ .

3.  $A_2$  for branched polymers. The analysis for branched structures follows closely that given for linear chains. One does not, however, expect superposition of these data for a plot of  $A_2 M^{1/2}$  versus  $z$  since  $F'(z)$  is specific for each structure. On the other hand, data for all tetrafunctional star polymers of different molecular weights ought to superpose, etc.

Similarly, Eq. (80) is expected to hold if the proper expression for  $F(\xi)$  is employed. The parameter  $A_2$  retains the definition given above in this discussion and so pertains to dimensions of linear chains. Some expressions for  $F(\xi)$  for tetrafunctional star polymers are given by

$$F(\xi) = 1 - 3.873 \xi + O(\xi^2) \quad (86)$$

$$F(\xi) = (g^{3/2}/2.30 \xi) \ln [1 + 2.30 \xi/g^{3/2}] \quad (87)$$

$$F(\xi) = (1/7.55 \xi) [1 - \exp(-7.55 \xi)] \quad (88)$$

$$F(\xi) = (1/7.55 \xi_2) [1 - \exp(-7.55 \xi_2)] \quad (89)$$

where

$$\xi_2 = z/\alpha_2^3 \quad ; \quad \alpha^5 - \alpha^3 = \frac{a_1}{K} (\alpha_2^5 - \alpha_2^3)$$

and

$$K = 2.127^*; a_1 = 1.342$$

Eq. (86) is the rigorous expression calculated above (in Section III). Eq. (87) follows directly from Eq. (82) since there is nothing in the

\* Here  $K$  is calculated from first order perturbation theory for the expansion of the mean square distance from the branch center for a structure with  $2p$  branches, after a suggestion of Casassa<sup>49</sup>. The general result for star-shaped polymers is

$$k = \frac{2}{\sqrt{p}} \left[ \frac{28}{45} + (2p-1) \left( \frac{202\sqrt{2} - 276}{45} \right) \right]$$

derivation of the latter specific to linear structures and one only need adjust the constant 2.30 by the factor  $g^{-3/2}$ . Here  $g$  is the ratio of the mean square radii of branched and linear chains under theta conditions. Eq. (87) is not limited to star-shaped branched structure, but should apply just as well to any type of branching. Eq. (88) was calculated by Casassa (Section III, above) on the basis of the model used to compute Eq. (84) for linear chains. The result given is specific to star-shaped structures. Eq. (89) is a variant of Eq. (88) introduced here in an attempt to correct for interchain expansion in a way analogous to that used to derive Eq. (85) for linear chains.

The constants  $A^2$ ,  $(n^2\beta_0/M^2)$  and  $\theta$  were determined in a manner analogous to that employed for the linear polymers. Here  $A^2 = [(\overline{s^2}_0)_{br}/M]g^{-1}$ , where  $g$  is 0.625 for tetrastar structures. The parameters  $A^2$ ,  $n^2\beta_0/M^2$  and  $\theta$  are all unaffected by branching for this structure. This is in contrast to the behavior found by Orofino and Wenger<sup>64</sup> for a star-shaped polymer for which  $n^2\beta_0/M^2$ , but not  $\theta$  was altered by branching. The difference may be in the fact that their polymer had a much lower molecular weight, and consequently shorter branches.

Plots of Eqs. (87) to (89) are exhibited in Fig. 26 together with the experimental data. In behavior similar to that observed for linear polymers, Eq. (89) provides a good fit for  $\zeta < 0.5$  and predicts the general shape of the data for  $\zeta > 0.5$ ; but it yields too low an asymptotic value for large  $\zeta$ .

It may be remarked that the ratio  $(A_2)_{br}/(A_2)_l$  at constant  $M$  does not afford a reliable evaluation of the various approximate models since this ratio is predicted to be about the same for any of the models so far introduced.

4. The mean square radius of gyration. The equivalent chain model can also be used to calculate  $\alpha^2$  as a function of  $z$ . Thus,

$$\alpha^2 = \overline{s^2}/\overline{s^2}_0 = \frac{1}{n^2\overline{s^2}_0} \sum_{j>i} \sum \overline{r_{ij}^2} \quad (90)$$

where  $\overline{r_{ij}^2}$  is the average separation of segments  $i$  and  $j$  in an equivalent chain comprised of  $n$  segments:

$$\overline{r_{ij}^2} = \frac{\int \dots \int r_{ij}^2 F(\underline{r}_{ij}) d\underline{r}_i \dots d\underline{r}_j}{\int \dots \int F(\underline{r}_{ij}) d\underline{r}_i \dots d\underline{r}_j} \quad (91)$$

Here the  $F(\underline{r}_{ij})$  are the probability densities for  $\underline{r}_{ij}$  including the effects of segment repulsions. A perturbation theory<sup>2</sup> may be applied to compute



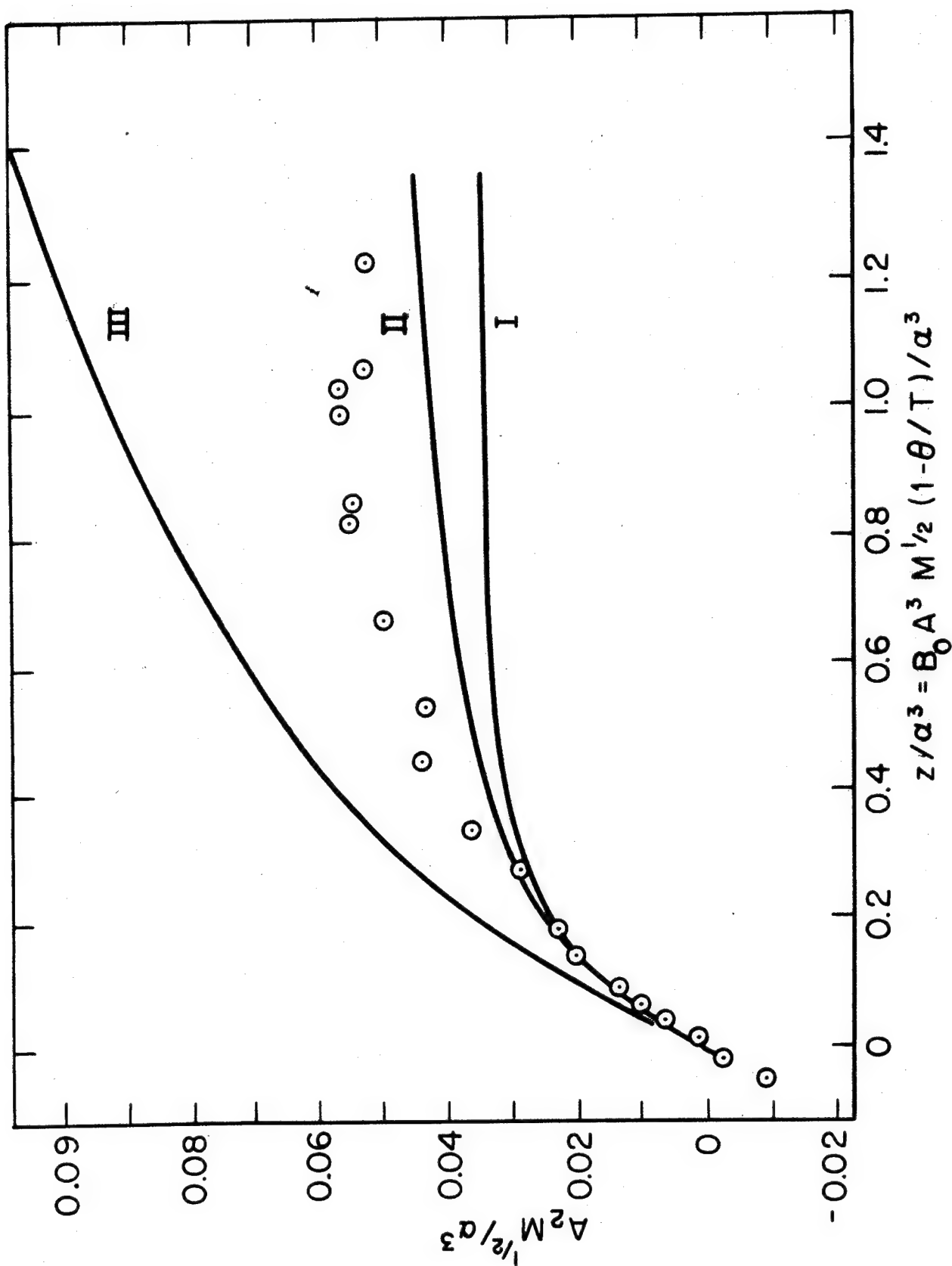


Figure 26  $A_2 M^{1/2} / \alpha^3$  as a function of the thermodynamic parameter  $z / \alpha^3$  for the star branched polymer. The lines are drawn according to (I) Equation (88); (II) Equation (89); (III) Equation (87).

$\alpha^2$  for small  $z$ , by suitable expansion of Eq. (90), with the result

$$\alpha^2 = 1 + a_1 z - a_2 z^2 + O(z^3) \quad (92)$$

Calculations yield  $a_1 = 134/105$  for linear chains<sup>2</sup> and  $a_1$  has been calculated for a variety of branched structures as well (see Section I). Unfortunately, the series is not rapidly convergent, so Eq. (92) is directly applicable only in the limit of small  $z$ . Equation (92) can be rearranged to yield

$$\alpha^2 = 1 + a_1 h(z) \quad (93)$$

where

$$\begin{aligned} h(z) &= \alpha^3 H(z) \\ &= \alpha^3 [1 - (a_2/a_1) z + O(z^2)] \\ &= 1 + g_1 z + O(z^2) \end{aligned}$$

Here  $h(z)$  goes to unity as  $z = 0^*$ , but  $h(z)$  is not identically unity since, for example,  $g_1 \neq 0$ . Unfortunately, little else can be said about the nature of  $h(z)$  without further approximations.

The prediction that data for  $\alpha^2$  as a function of  $T$  and  $M$  should all superpose if plotted as a function of  $z$  can be assessed at once, however. Accordingly,  $\alpha^2$  is plotted against  $z$  in Fig. 27 and it is seen that a single curve does result. Unfortunately, the data exhibit so much curvature that direct analysis to yield the slope  $a_1$  is hazardous.

5. Approximate theories for  $\overline{s^2}$ . Numerous attempts have been to obtain approximate formulations for  $\alpha^2$ . An important result, due to Flory<sup>34</sup>, will be discussed here in language due to Fixman<sup>2</sup> - and somewhat different than that used by Flory since it simplifies later discussion. Without approximation,  $\alpha^2$  can be calculated as

$$\alpha^2 = \frac{\int s^2 \exp(-E(s^2)/kT) F(s^2) ds^2}{\overline{s^2} \int_0^\infty \exp(-E(s^2)/kT) F(s^2) ds^2} \quad (94)$$

Here  $\exp(-E(s^2)/kT)$  is a weight factor for the energies associated with intramolecular interactions of configurations of radius  $s^2$  and  $F(s^2)$  is the random-flight probability distribution for  $s^2$ . Fixman showed that for a spherically symmetric segment mass density  $\rho(\underline{r})$ ,

\* Specifically,  $g_1 = a_1 \left( \frac{3}{2} - \frac{a_2}{a_1^2} \right)$ . Since  $a_2/a_1^2 \simeq 2.075/(4/3)^2$  for linear chains<sup>2</sup>,  $g_1 \simeq +0.425$  for linear chains.

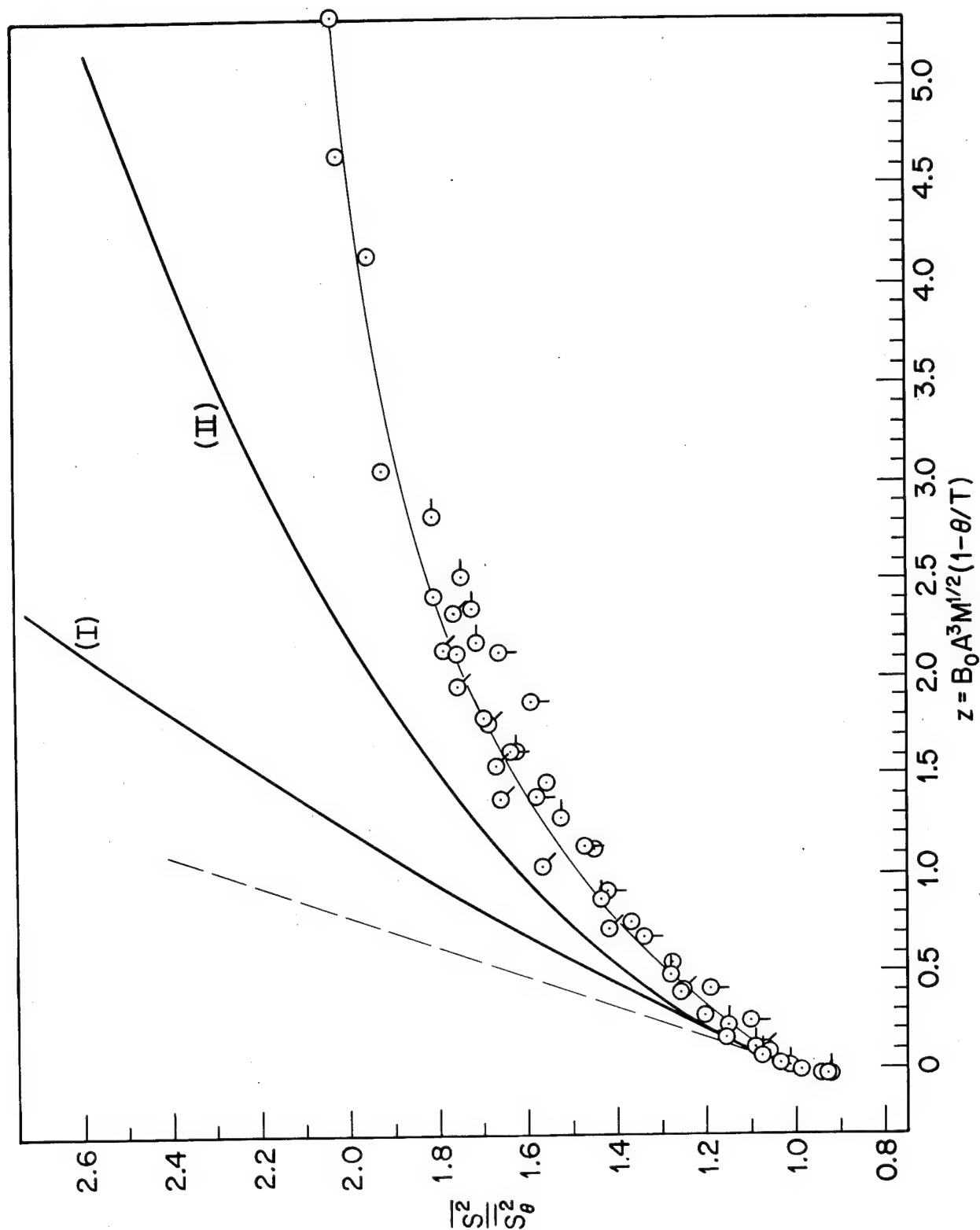


Figure 27 The expansion factor as a function of the thermodynamic parameter  $z$ . The dashed line is the theoretical initial slope. Curves I and II represent Equation 97 with  $k' = 1.914$  and Equation 96 with  $C = 1.276$ , respectively. The light line is an empirical fit to these data. The points are identified as in Figure 21.

$$E(s^2) = \frac{\beta kT}{2} \int r^2 \rho^2(\underline{r}) d\underline{r} \quad (95)$$

where  $\beta$  is the excluded value integral. Unfortunately, the indicated integrations over  $s^2$  cannot be carried out rigorously even after a Gaussian segment density (or a sum of Gaussian segment densities) is<sup>65</sup> assumed for  $\rho(\underline{r})$  and a Gaussian  $F(s^2)$  is assumed. Approximate procedures,<sup>66,67</sup> assuming a Gaussian  $F(s^2)$  and spherically symmetric  $\rho(\underline{r})$ , yield\*

$$\alpha^2 = 1 + C \xi \quad (96)$$

where  $C$  is proportional to  $E(s^2)$ . This result is in accord with Flory's equation based on similar assumptions for  $\rho(\underline{r})$  and  $F(s^2)$ . Eq. (94) follows from assumption of spherical symmetry for  $\rho(\underline{r})$  and is otherwise independent of  $\rho(\underline{r})$  is assumed. It is found that  $C = 3^{3/2}/2 = 2.60$  if  $\rho(\underline{r})$  is taken to be a simple Gaussian, in accord with Flory's result for the same  $\rho(\underline{r})$ , and that  $C = 3.15$  if a sum of Gaussians (correct in the limit  $\alpha^2 = 1$ ) is assumed<sup>67</sup>.

The similarity of Eqs. (93) and (96) is at once evident and suggests that the "constant"  $C$  is to be identified with the function  $a_1 h(z)$ . Accordingly, Stockmayer<sup>68</sup> suggested that  $C$  be arbitrarily set equal to  $a_1$  so that agreement will be obtained between Eq. (96) and the more rigorous Eq. (93) at least for small  $\xi$ . This amounts to the assertion that  $h(z)$  is approximately unity for all  $z$ . Now since  $h(z)$  is not identically unity, this implies that the polynomial  $h(z) - 1$  never takes on values far different from zero for values of  $z \geq 0$  intermediate to the roots of  $h(z) - 1 = 0$  (where  $h(z) = 1$  exactly). It seems at least as likely that  $h(z)$  averaged over any particular interval of  $z$ , may assume different values for different intervals  $\Delta z$ . On this basis, any constant value for  $C$  for all  $z$  seems unlikely.

Calculation of  $C$  for branched structures according to these approximations affords another means of evaluating the assumptions made. Both of the above formulations for  $\rho(\underline{r})$ , i.e., single Gaussian or sum of Gaussians, can be utilized to obtain values for  $C$  for branched polymers<sup>29,63</sup> (see ASD-TR 61-22, Part III). The results yield  $C_{br} = g^{-3/2} C_\ell$  for both star and comb polymers, for example, when a Gaussian function is assumed for  $\rho(\underline{r})$ <sup>29</sup>. Rigorous calculation of  $(a_1)_{br}$  (see Section I, above), however, shows  $(a_1)_{br} \simeq g^{-3/2} (a_1)_\ell$  only for some special structures, namely comb polymers with branches short compared to the backbone length. This is reasonable since these structures might reasonably be assumed to have  $\rho(\underline{r})$  and  $F(s^2)$  similar to that for linear chains. Severe disagreement with this formulation is observed for star-branched and for intermediate comb-shaped structures. Thus, not only does  $C \neq a_1$  by the approximate calculation, but  $(C_{br}/C_\ell)$  is not in general equal to  $(a_1)_{br}/(a_1)_\ell$ . This would seem to imply that regardless of the merits of the functional form  $\alpha^2 - 1 \propto \xi$ , the numerical value obtained for  $C$  is very sensitive to correct choice for either  $F(s^2)$  or  $\rho(\underline{r})$ , or both.

\*This is the familiar  $\alpha^5 - \alpha^3$  relation of Flory rearranged for our purposes.

Fixman<sup>69</sup>, working with a different equation, obtained from a variant of Eq. (91), has derived a different expression for  $\alpha^2$  as a function of  $z$ . An essential approximation is that quantities related to the  $F(r_{ij})$  may be approximated by Gaussian functions with the segment dimension  $b$  increased to  $b\alpha$  where appropriate. The result,

$$\alpha^3 = 1 + k'z \quad (97)$$

is strikingly different from Eq. (96). In particular Eq. (97) predicts that

$$\lim_{z \rightarrow \infty} \zeta = \frac{1}{k'}$$

whereas Eq. (96) allows  $\zeta$  to increase without bound as  $z$  increases. This prediction has immediate effect on the predictions for  $A_2$ , since now  $F'(z) = F(\zeta)$  cannot decrease to zero with indefinite increase in  $z$ , but must assume some asymptotic value at large  $z$ . Fixman sets  $k' = \frac{3}{2} a_1$  to force agreement with Eq. (93) in the limit  $z = 0$ , but an argument similar to that given concerning the assignment  $C = a_1$  applies here as well\*. It should be noted that this value for  $k'$  sets the limiting value for  $\zeta$  at 45/67, a smaller number than some values of  $\zeta$  obtained in our analysis of data.

A third relationship, practically equivalent numerically to Eq. (97), has been obtained by Stockmayer, Kurata and Roig<sup>35</sup> on the basis of a different approximate model. This relation can be cast in the form of Eq. (97) with

$$k' = \left(\frac{4}{3}\right)^{3/2} k'' \lambda(\alpha)$$

where

$$\lambda(\alpha) = \left(1 + \frac{1}{3\alpha^2}\right)^{-3/2} + (\alpha-1)(\alpha^3-1)^{-1}$$

and  $\lambda(\alpha) = 1.01 \pm 0.02$  for all  $\alpha$ . Again,  $k''$  is adjusted to force agreement with Eq. (93) in the limit  $z = 0$ .

Eqs. (96) and (97) in the form  $\alpha^2(\zeta)$  are exhibited in Fig. 28 together with the experimental data. This presentation has been used since Eq. (96) predicts  $\alpha^2$  to be a linear function of  $\zeta$  whereas Eq. (97)

---

\* Specifically:

$$k' = \frac{3}{2} a_1 [1 + p_1 z + O(z^2)]$$

$$p_1 = a_1 \left(\frac{1}{4} - \frac{a_2}{a_1^2}\right)$$

and  $p_1 = 1.17$  for linear chains.

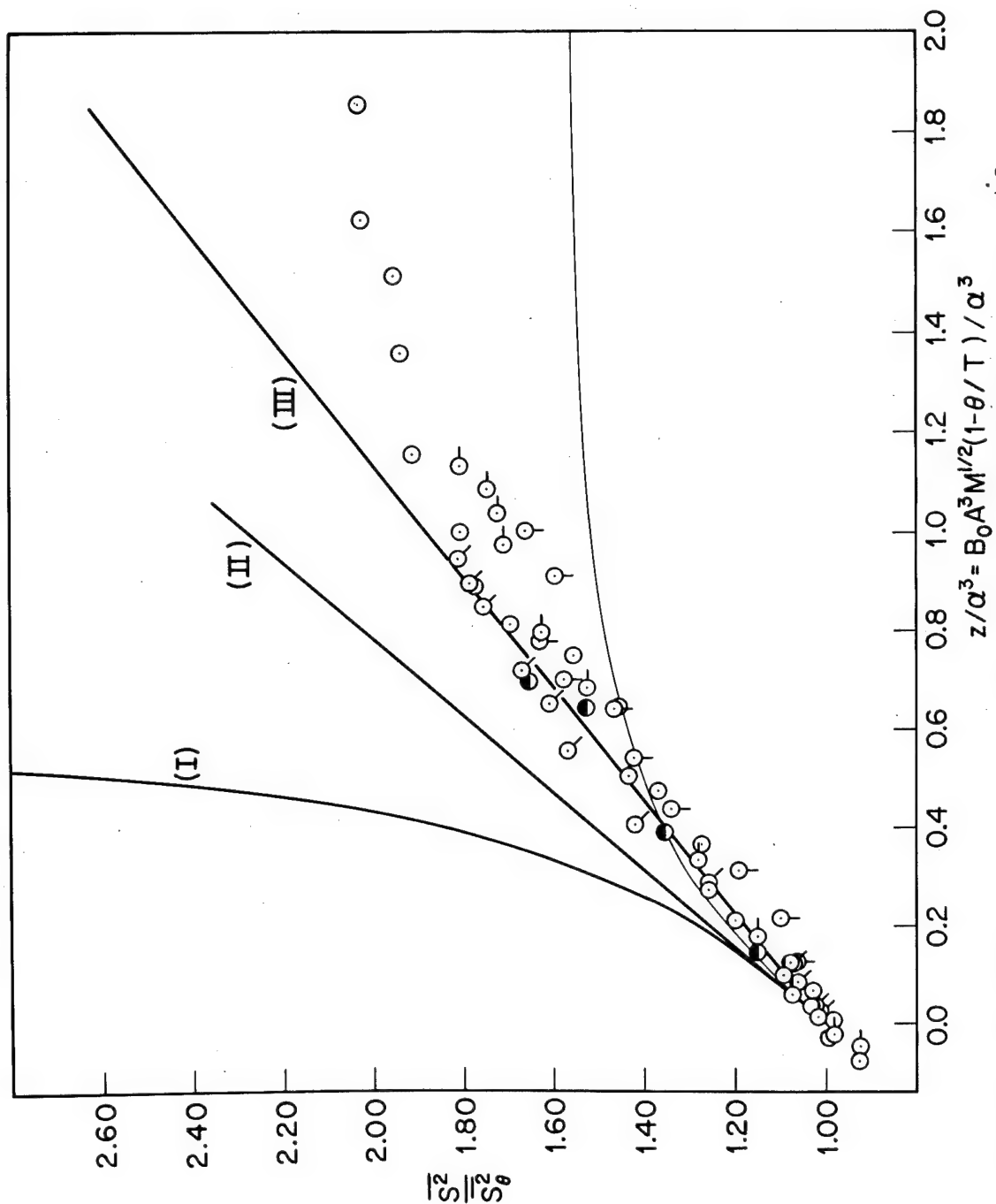


Figure 28 The expansion factor as a function of the thermodynamic variable  $z/\alpha^3$ . Curve I represents Equation 97 with  $K' = 1.914$ ; curves II and III represent Equation 96 with  $C = 1.276$  and with  $C$  arbitrarily adjusted to give a best fit to these data, respectively. The light line represents Equation 99, see text. The symbols are defined in Figures 21 and 25.

predicts an upper bound on  $\xi$ . The data clearly do not exhibit any such limit on  $\xi$ , but they do appear to verify an approximately linear relationship between  $\alpha^2$  and  $\xi$ . The slope  $C$ , however, is equal neither to 2.60 nor to  $a_1$ . Since the slope should equal  $a_1$  at least for small  $z$  (or  $\xi$ ), it is probably indicated that the data are not really linear over the entire span of  $z$  examined, but only approximately so. Thus, we regard the approximate relation

$$\alpha^2 = 1 + C\xi$$

as reasonably accurate (at least over the range of  $\xi$  obtained here), but cannot support the approximate theoretical evaluations of  $C$ . (Indeed,  $C$  may not even be constant.) Eq. (97) greatly overestimates  $\alpha^2$ . The experimental uncertainty in  $\alpha^2$  (ca.  $\pm 8\%$ , depending on the magnitude of  $s^2$ ) is not large enough to account for the large deviations observed from Eq. (97). We hope to extend these measurements to one additional sample of still higher molecular weight as a further check on the basic principle of superposition being employed here.

The data for the branched structures are displayed in Fig. 29 together with curves calculated from Eq. (96) with  $a_1 = 1.342$  and  $C_{br} = C_\ell/g^{3/2} = 5.26$  as calculated for a tetrafunctional star structure. Behavior similar to that of the linear chains is observed.

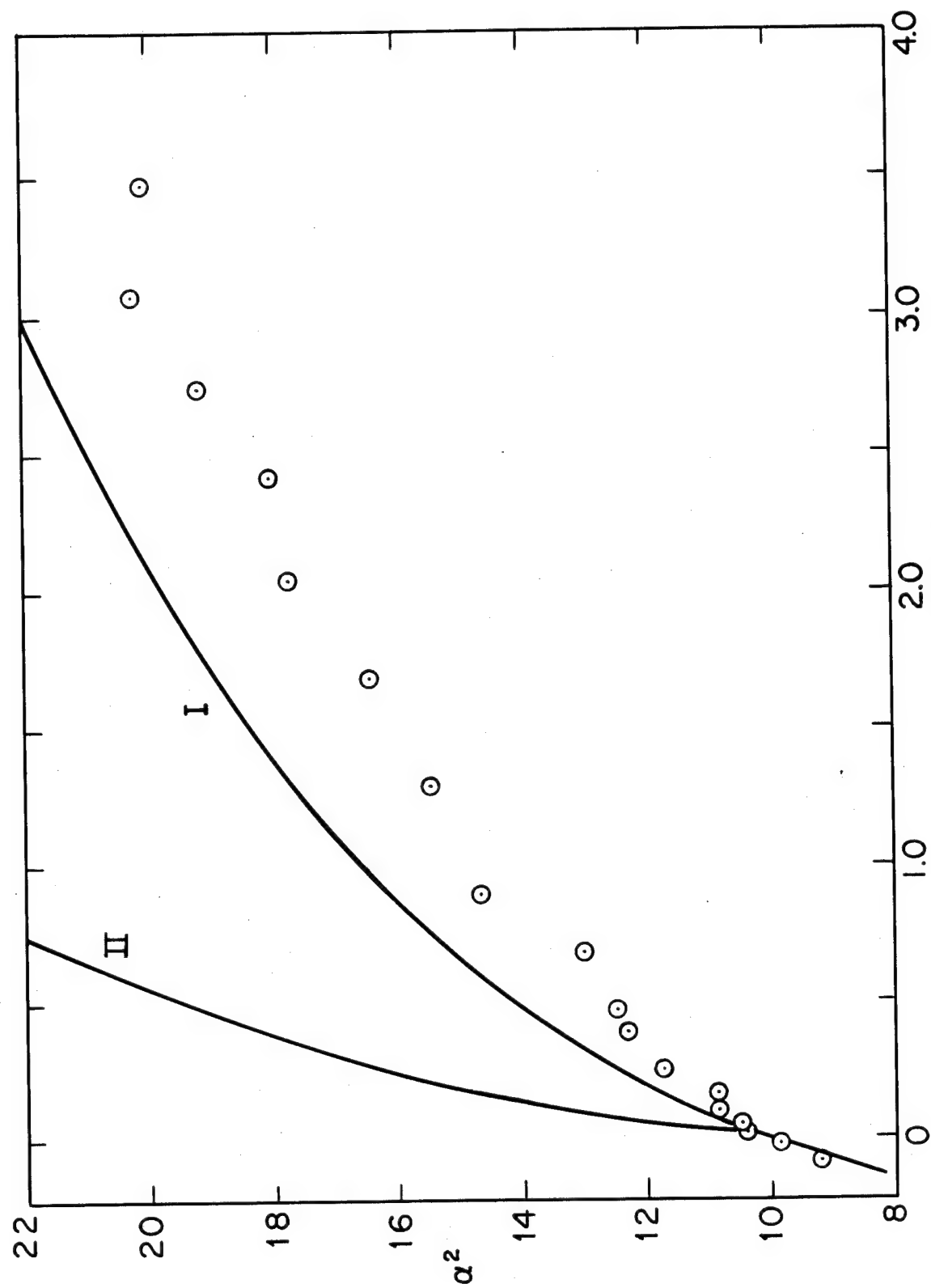
6. A relationship between  $A_2$  and  $\alpha_2$ . It has been suggested<sup>7</sup> that formal elimination of  $z$  from equations for  $A_2$  and  $\alpha_2$  yields a relation between  $A_2$  and  $\alpha^2 - 1$  that seems to be valid to much larger  $A_2$  (or  $\alpha^2$ ) than were the original power series equations in  $z$ . Thus, elimination of  $\xi$  between Eq. (78) and Eq. (93) yields the result

$$A_2 M^{1/2} = \frac{4N_o \pi^{3/2} A^3}{a_1} (\alpha^2 - 1) \frac{F'(z)}{H(z)} \quad (98a)$$

$$= \frac{4N_o \pi^{3/2} A^3}{a_1} (\alpha^2 - 1) + O(\alpha^2 - 1)^2 \quad (98b)$$

where the coefficient of  $(\alpha^2 - 1)^2$  could be evaluated numerically if desired (see ASD-TR 61-22, Part III). Fig. 30 exhibits the data obtained here plotted in this manner. The data are seen to form a good linear relation and the slope yields the value of  $A^2$  obtained by direct measurement within experimental error. Inclusion of the term  $O(\alpha^2 - 1)^2$  makes the correlation less satisfactory.

Some data for polystyrene in three good solvents<sup>62</sup> are shown in Fig. 31 together with the theoretical line ( $10^{18} A^2 = 7.0$ ) for an assumed linear relation between  $\alpha^2 - 1$  and  $A_2 M^{1/2}$ . The data are seen to fit reasonably well to the linear relation, even over this considerably larger range of  $\alpha^2$ .



$$z = B_0 A^3 M^{1/2} (1 - \theta/T)$$

Figure 29 The expansion factor  $\alpha^2$  as a function of the thermodynamic variable  $z$  for a star shaped polymer. Curves I and II are obtained from the modified Flory equation with  $C = 0. = 1.342$  and  $C = 1.276/(g^{3/2})$ , respectively.



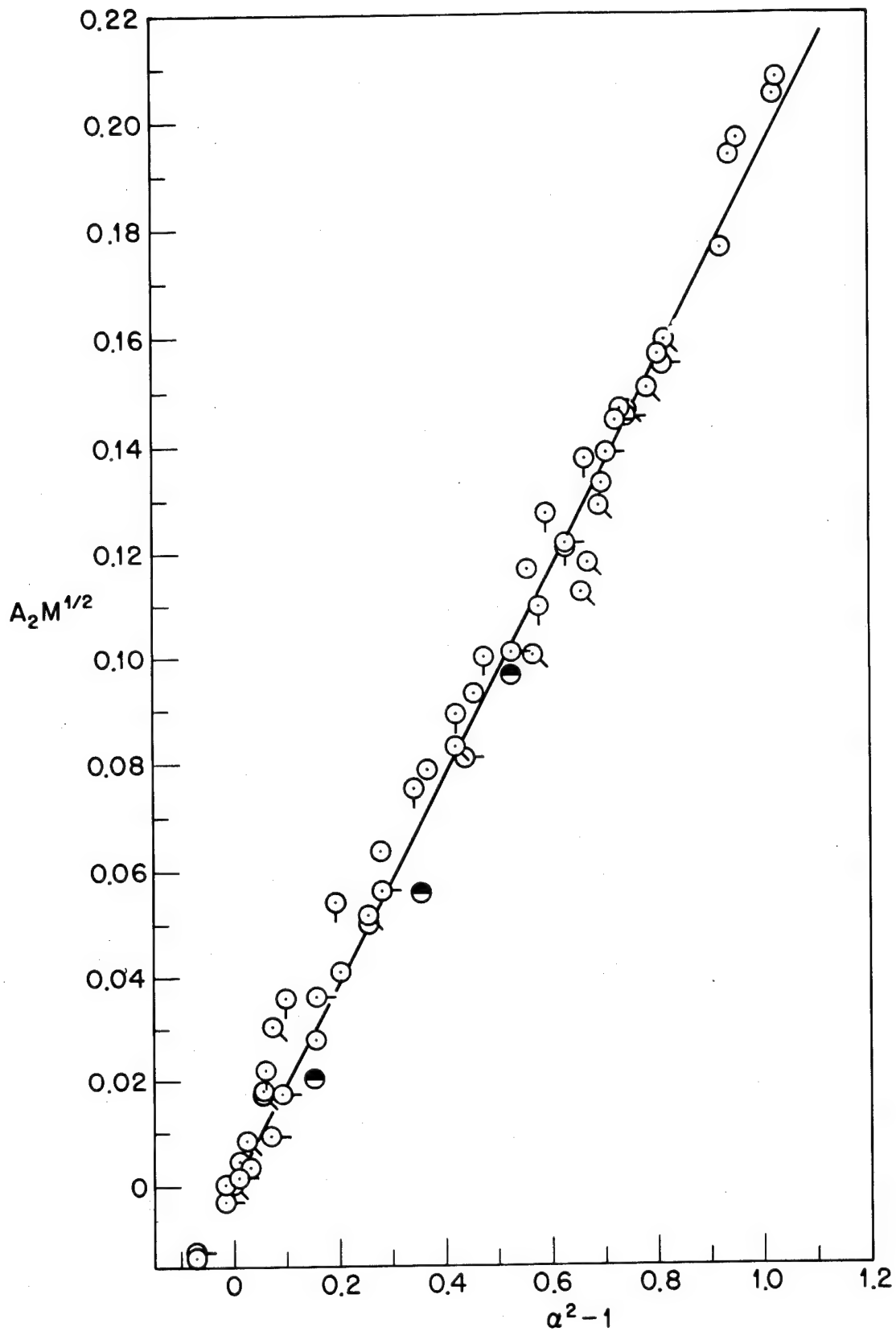


Figure 30 A semi-empirical correlation between  $A_2 M^{1/2}$  and  $\alpha^2 - 1$ .  
The slope is related to the unperturbed dimension  $A^2$ .  
The points are identified as in Figures 21 and 25.

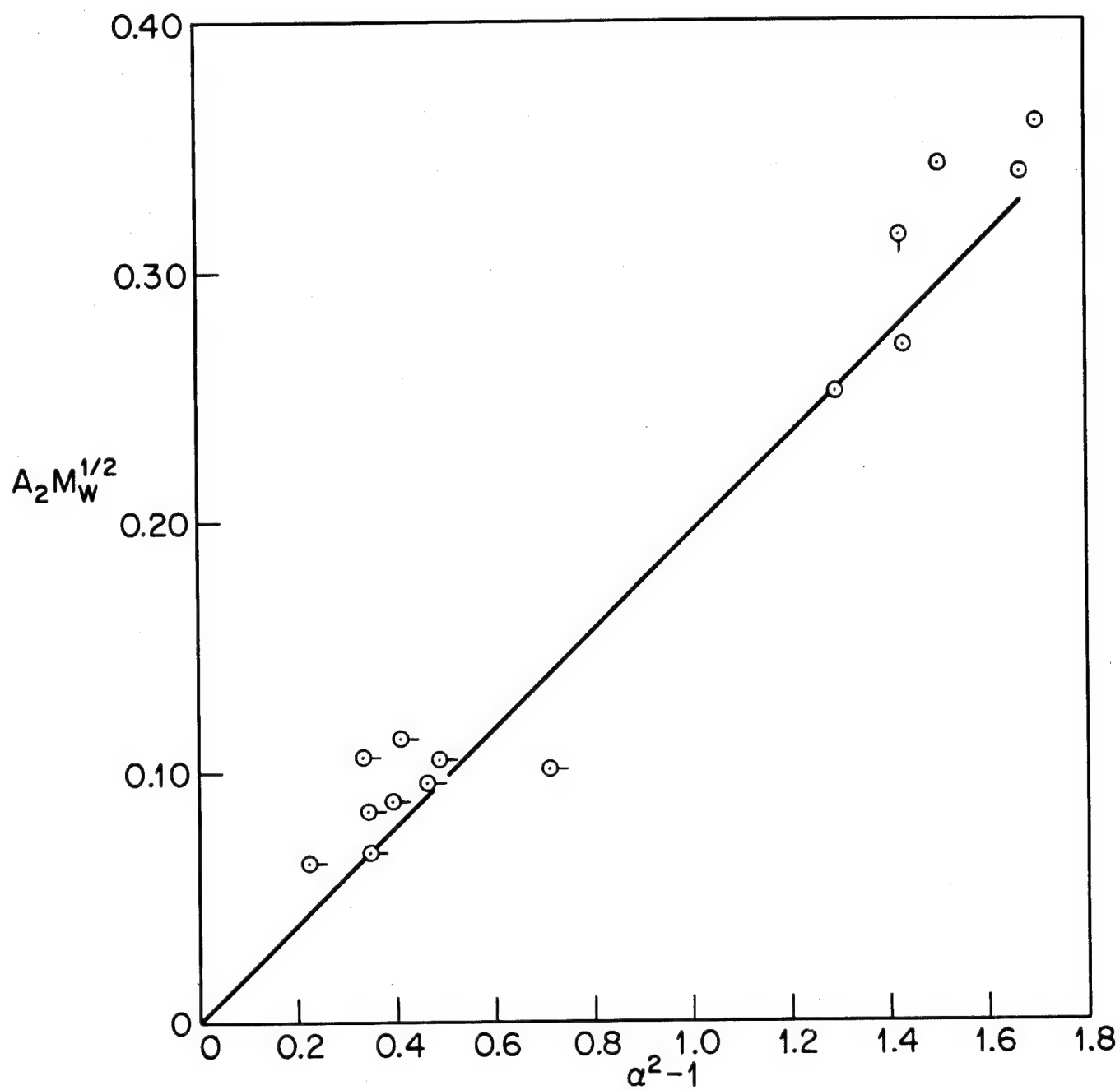


Figure 31 A semi-empirical relation between  $A_2 M_w^{1/2}$  and  $\alpha^2 - 1$  for data from the literature<sup>62</sup> on polystyrene in: methanol,  $\ominus$ -; dichloroethane,  $\ominus$ ; toluene,  $\phi$ .

Thus, one is encouraged to examine in more detail the consequences of the quantity  $A_2 M^{1/2}$  being a linear function of  $\alpha^2 - 1$ . This assumption leads to the result

$$F'(z) \equiv H(z)$$

or, equivalently,

$$\alpha^2 = 1 + a_1 z F'(z) \quad (99)$$

Eq. (99) has been suggested previously by Schulz<sup>70</sup> in a different context. Some immediate consequences of this formulation are at once evident, without assumption of a specific form for  $F'(z)$ . The most interesting concerns the asymptotic limit observed for  $A_2 M^{1/2} / \alpha^3 A^3$ , and hence for  $\xi F'(z)$ , for large  $\xi$ . If this limit is denoted  $Q$ , then Eq. (99) requires a value for  $\alpha$  in the same limit of large  $\xi$  given by

$$\frac{\alpha^2 - 1}{\alpha^3} = a_1 Q$$

The limiting values for  $\alpha^2$  are rather low, ca. 2.5, and probably indicate either the inadequacy of a linear relation between  $A_2 M^{1/2}$  and  $\alpha^2 - 1$  and/or of the asymptotic limit for  $A_2 M^{1/2} / \alpha^3$ .

Even if  $A_2 M^{1/2} / \alpha^3 A^3$  does not attain a true asymptotic limit, the fact that this parameter becomes a very slowly increasing function of  $\xi$  seems indisputable. This means that  $\alpha^2$  would become a very slowly increasing function of  $\xi$  over the same  $\xi$  interval, given the existence of a linear relationship between  $A_2 M^{1/2}$  and  $\alpha^2 - 1$ . That is,  $h(z)$  in Eq. (93) must decrease to nearly zero for large  $z$ .

Data on our high molecular weight samples in very good solvents would serve to further test the linear relationship between  $A_2 M^{1/2}$  and  $\alpha^2 - 1$  and to elucidate the behavior of  $\alpha^2$  at larger  $z$ . A limiting value for  $\alpha^2$  with increasing solvent power  $\beta$  is not physically unacceptable, since the chain length is, after all, finite. The physical reason for a limiting value for  $\alpha^2$  with increasing  $M$  is not as clear, but is implied since both  $\beta$  and  $M$  appear in the parameter  $\xi$ . The necessity for any limit on  $\alpha$  to involve both  $\beta$  and  $M$  has been recognized earlier<sup>7</sup>, but is difficult to demonstrate unequivocally, especially for  $\beta$ . The empirical observation of the proportionality between  $A_2 M^{1/2}$  and  $\alpha^2 - 1$  with the theoretically expected slope  $4N_0 \pi^{3/2} A^3$  may be a consequence of such a physical limitation, however.

Attempts to utilize the approximate functions for  $F'(z) = F(\xi)$  given above in Eqs. (81) to (85) are not entirely satisfactory. For example, the abrupt change in slope for  $F(\xi)$  for  $\xi > \text{ca. } 0.6$  given by Eq. (85), which best correlates our data, makes  $\alpha^2(\xi)$  very sensitive

to the exact choice of  $F(\xi)$ . For example  $\alpha^2(\xi)$  calculated from Eq. (85) is shown in Fig. 28. The curve fits the data well for  $\xi < 0.5$  or  $z < 0.83$ , as expected from the correlation achieved for  $A_2M^{1/2}/\alpha^3$  as a function of  $\xi$ . The failure for  $0.8 < z < 5$  is probably due to inadequacy in the assumed  $F(\xi)$  since the curve  $A_2M^{1/2}$  versus  $\alpha^2 - 1$  seems to be linear to a very good approximation in this range. Failure at still larger  $z$  is probably due both to an inadequate  $F(\xi)$  and nonlinearity in  $A_2M^{1/2}$  versus  $\alpha^2 - 1$ . The fit could doubtless be improved by suitable adjustment of the parameters in Eq. (85), but the predicted behavior for  $z > 5$  would probably not be meaningful.

## E. Conclusions

The experimental data behave in a way consistent with one of the basic assumptions made in the statistical theories for thermodynamic and conformational properties. Thus, both  $A_2M^{1/2}$  and  $\alpha^2$  are single-valued functions of the parameter  $z$  (or  $\xi$ ).

Of the approximate theories for  $A_2$  specifically considered here, that of Casassa<sup>49</sup>, which is a minor adaptation of that due to Casassa and Markovitz<sup>48</sup>, seems to provide the best fit for our data. A very good fit is obtained for  $\xi < \text{ca. } 0.5$ , with the general shape of the data predicted for larger  $\xi$ . The asymptotic limit predicted by this theory seems somewhat low, however.

None of the existing approximate forms for  $\alpha^2(z)$  can be supported without qualifications. The familiar  $\alpha^5 - \alpha^3 \propto z$  relation of Flory<sup>34</sup> probably fits these data as well as any if the constant of proportionality is allowed to be adjustable.

The recent equation for  $\alpha^2(z)$  of Fixman, or that of Kurata, Stockmayer and Roig, does not provide a reasonable fit at all. In particular, prediction of a limiting value for  $z/\alpha^3$  is not substantiated.

A linear relation between  $A_2M^{1/2}$  and  $\alpha^2 - 1$  fits surprisingly well, and gives a line with the expected slope. This correlation extends as well to  $\alpha^2$ -values larger than those obtained here. Assumption that  $A_2M^{1/2}$  is accurately a linear function of  $\alpha^2 - 1$  produces some interesting consequences. First, the constant of proportionality in  $\alpha^5 - \alpha^3 \propto z$  is predicted to depend on  $\alpha$  in a way that can be computed from theories of the second virial coefficient. The results are very sensitive to the exact relation for  $A_2M^{1/2}$  assumed, however. Second,  $\alpha^2$  is predicted to reach some asymptotic limit for large  $\xi$ , that is independent of  $\xi$ , but dependent only on the asymptotic limit for  $A_2M^{1/2}/\alpha^3$ .

Even if a true asymptotic limit is not obtained, the linear relationship between  $A_2M^{1/2}$  and  $\alpha^2 - 1$  implies  $\alpha^2$  will at most increase very slowly with  $\xi$  for large  $\xi$ .

# VIII. Intrinsic Viscosity of Linear Polystyrene in Decalin — G. C. Berry and G. L. Bender

## A. Introduction

The intrinsic viscosity  $[\eta]$  of polystyrene in decalin has been investigated as a function of temperature and molecular weight. These data are for the same samples studied by light scattering, so that the thermodynamic variables required in this analysis are all known. Thus, a direct comparison of data with theory is possible.

Hydrodynamic calculations for  $[\eta]_0$ , the intrinsic viscosity in the absence of thermodynamic interactions, have been available for some time. For various approximate models, these yield the general result<sup>71-74</sup>:

$$[\eta]_0 = \Phi' A^3 M^{1/2} \quad (100)$$

where

$$A^2 = (\overline{s^2})_0 / M$$

$$\Phi' = 6^{3/2} h F(h)$$

The parameter\*  $h F(h)$  increases with molecular weight  $M$  and obtains an asymptotic limit of  $2.89 \times 10^{21}$  ( $[\eta]$  in dl/gm) to within one percent for  $h \geq 3$ , where  $h$  is a monotone increasing function of  $M$ . We will consider  $h \geq 3$  from here on. If it is not, then  $[\eta]_0/M^{1/2}$  will not be constant, but will increase with increasing  $M$ .

Eq. (100) shows that  $[\eta]_0$  is proportional to a reduced volume  $A^3$ . The principle effect of thermodynamic interactions is to augment the coil extension in solution above the temperature  $\Theta$ , and so increase  $[\eta]$ . This effect may be accounted for by inclusion of a factor  $\alpha_\eta^3$  in Eq. (100), thus

$$[\eta] = \Phi' A^3 M^{1/2} \alpha_\eta^3 \quad (101)$$

The factor  $\alpha_\eta$  does not necessarily equal the expansion factor  $\alpha$  for the radius of gyration. Calculation of  $\alpha_\eta^3$  requires simultaneous inclusion of both hydrodynamic and thermodynamic effects and has not been carried out with rigor<sup>28,29</sup>. In fact, calculation of  $[\eta]_0$  has not even been accomplished without the inclusion of some approximations which are difficult to assess<sup>71,74</sup>. An early, and very useful, approximation for  $[\eta]$  given by Flory and Fox<sup>39</sup> simply asserts that  $\alpha_\eta = \alpha$ . This approximation, while admittedly difficult to justify exactly, cannot be too much in error and has served in evaluation of viscosity data for a considerable time.

\* See reference (74) for a definition of  $h$ .

More recent attempts to calculate  $[\eta]$  directly by suitable approximations with one of the more elaborate models used to compute  $[\eta]_0$  lead to the result<sup>28</sup>

$$[\eta] = [\eta]_0 [1 + b_1 z W(z)] \quad (102)$$

where

$$z = BA^{-3} \sqrt{M}$$

Here  $b_1$  is 1.55 and  $W(z)$  is a function of  $z$ , which may be represented by a series expansion. The thermodynamic parameter  $B$  is to be identified with the excluded volume integral  $n^2 \beta / M^2$  discussed above. As with other series expansions in  $z$ , this expression is only slowly convergent, and so is limited to small  $z$ . Eq. (102) is most useful if it can be combined in some way with the relation for  $\alpha^2(z)$  to yield an expression for  $[\eta]$  valid to larger  $z$  than either series is by itself, in a manner similar to that employed for obtaining a relation between  $A_2 M^{1/2}$  and  $\alpha^2 - 1$  in the previous section. This question will be discussed further below.

One other approximate relation is of interest here since it, or a relation almost equivalent to it numerically, has recently received considerable usage. This approximate result gives simply<sup>33</sup>

$$\alpha_\eta^3 = 1 + b_1 z \quad (103)$$

The exclusion of higher order terms in  $z$ , that is, setting  $W(z) \equiv 1$ , was suggested by analogy with an approximate result obtained for  $\alpha^2$  by Fixman discussed elsewhere in this report. Eq. (103) is different in kind than expressions giving  $\alpha_\eta$  as a function of  $\alpha$  since it expresses  $[\eta]$  directly in terms of the thermodynamic variable  $z$ , and so in terms of the molecular weight, without an additional relation between  $\alpha$  and  $M$ .

## B. Experimental

1. Methods. The intrinsic viscosity has been measured over the temperature interval 10° to 100°C with modified Ubbelohde viscometers described elsewhere<sup>63</sup>. Concentrations were adjusted so that  $1.08 < \eta_{rel} < 1.80$ . Kinetic energy corrections could be neglected because of the long flow times (ca. 500 sec) for decalin. The polymers and solvents used are described elsewhere in this report. All measurements were performed under a nitrogen atmosphere to avoid contamination by moisture. Solutions were injected into the viscometer with a syringe fitted with a glass frit to remove dust. The intrinsic viscosity under theta conditions,  $[\eta]_\theta$ , was determined by extrapolation of  $[\eta]/\alpha^3$  versus  $(1 - \theta/T)$  to  $T = \theta$ . Values of  $\alpha^3$  for each temperature were interpolated from the light scattering

data given above. This procedure gives a plot with slope almost zero and so makes extrapolation to obtain  $[\eta]_0$  less hazardous. It is not required that  $\alpha_{\eta}^3 = \alpha^3$  exactly for the procedure to be useful.

The concentrations necessary to compute  $[\eta]$  at each temperature  $t$  (in  $^{\circ}\text{C}$ ) have been computed from the density-temperature relation

$$d(t) = d(25) [1 - 8.13 \times 10^{-4} (t - 25)]$$

determined in a 50 ml pycnometer. This relation agrees satisfactorily with that given by Timmermans<sup>75</sup> over a more restricted temperature interval. The constant  $8.13 \times 10^{-4}$  was found to apply to decalin mixtures independently of isomeric composition.

2. Materials. The polymers and solvents used here are described in the preceding section.

### C. Results

The results obtained thus far are given in Fig. 32 and Table XVII. Additional samples of different molecular weights are now being studied. The ratio  $[\eta]_0/M^{1/2}$  is seen to be  $7.7 \times 10^{-4}$  to within  $\pm 5\%$  for the fractions studied.

### D. Discussion

1. Theta Solvent Correlation. The parameter  $\Phi' = [\eta]_0/A^3M^{1/2}$  is calculated from  $[\eta]_0/\sqrt{M}$  given in Table XVII and  $10^{18}A^2 = 7.0$ . (This value of  $A^2$  is obtained from data given in the preceding section.) The resulting value  $41.6 \times 10^{21}$  for  $\Phi'$  is in good agreement with the theoretical value  $42.5 \times 10^{21}$ . Thus, assumption of constant  $hF(h)$  appears to be satisfactory over this molecular weight interval and Eq. (100) correlates the data within experimental error.

The value obtained for  $[\eta]_0/M^{1/2}$  is slightly lower (ca. 5%) than that usually given for the system polystyrene-cyclohexane. A specific solvent effect may be involved.

It is assumed throughout that, the temperature dependence of  $A^2$  is negligibly small. This is in accord with conclusions discussed by Orofino and Ciferri on the basis of data on bulk polystyrene, on poor-solvent dilute-solution properties, and on our data for sample A-16.

It is also assumed explicitly, as discussed previously that the temperature dependence of  $B$  may be represented by

$$B = B_0(1 - \Theta/T)$$

where both  $B_0$  and  $\Theta$  are obtained from light scattering studies, as is  $A^2$ .

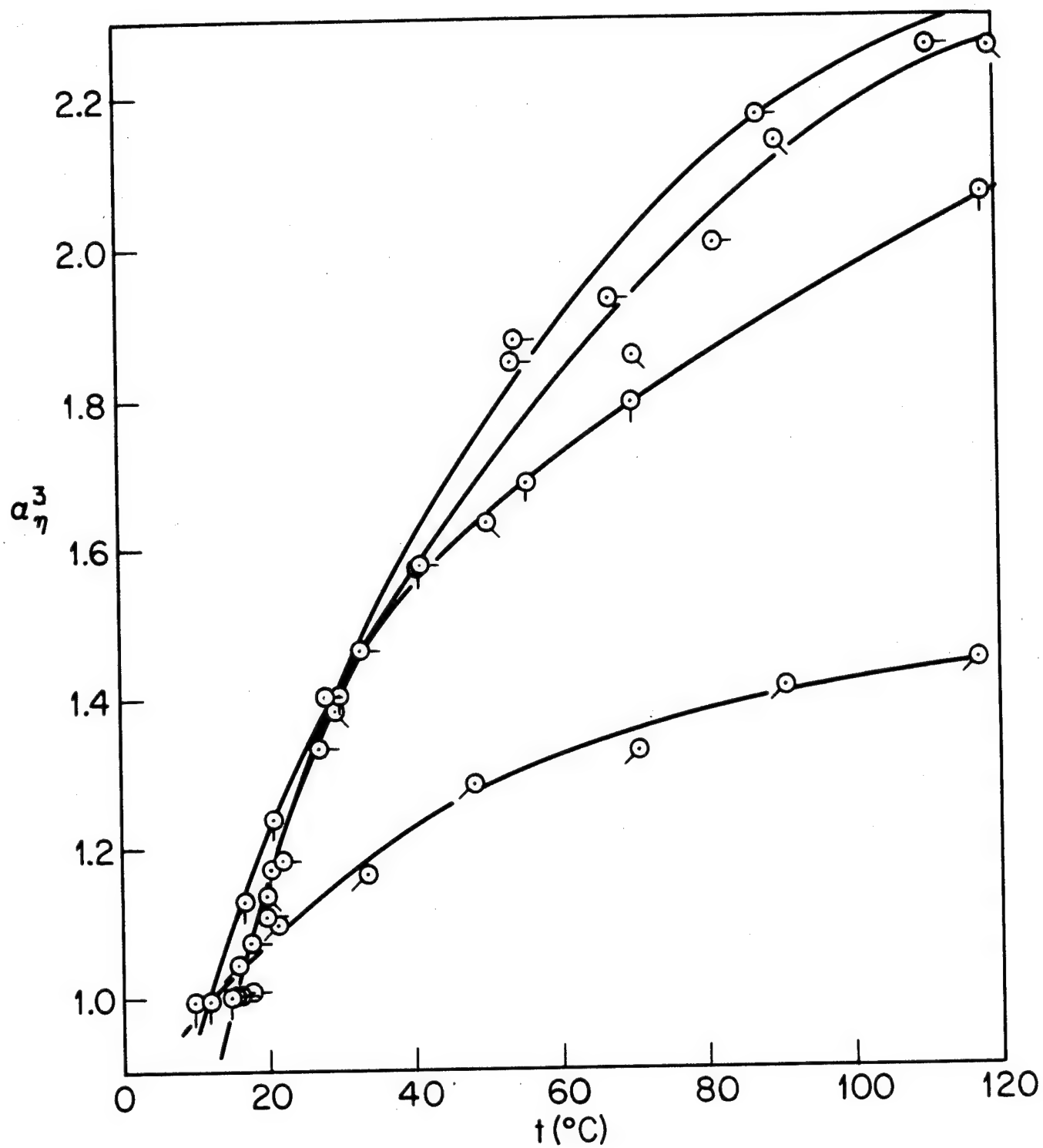


Figure 32 Dependence of  $\alpha_\eta^3 \equiv [\eta]/[\eta]_\theta$  on temperature for various molecular weights. The symbols are defined in Figure 21.



Table XVII

Intrinsic Viscosity of Linear Polystyrene in Decalin

Polymer	Solvent	$\theta, ^\circ\text{C}$	$[\eta]_\theta$	$10^{-6} \bar{M}_w$	$10^4 [\eta]_\theta / \sqrt{\bar{M}_w}$
A-3	4	12.2	0.283	0.135	7.72
A-19	4	12.2	0.608	0.689	7.34
A-16	3	15.2	0.83	1.16	7.73
A-5	2,3	15.2	1.048	1.74	7.95

2. Good Solvent Correlations. The thermodynamic-hydrodynamic theories suggest that  $[\eta]$ , or  $\alpha_\eta^3$ , should be a single valued function of the parameter  $z$ . Accordingly,  $\alpha_\eta^3$  is shown as a function of  $z$  in Fig. 33, where the data are seen to superpose within experimental error. Eq. (103) is the only expression considered here which can be directly evaluated from experimental  $[\eta]$  versus  $z$  data, and it is seen to provide a poor correlation. In particular, it greatly overestimates the increase of  $[\eta]$  with increasing  $z$ .

Correlation of  $\alpha_\eta^3$  with  $z$ , and thus with molecular weight, may be attempted with either of two expressions in current use:

$$\alpha_\eta^5 - \alpha_\eta^3 = K_1 z \quad (104)$$

$$\alpha_\eta^3 - 1 = K_2 z \quad (105)$$

The parameters  $K_1$  and  $K_2$  are calculated from the data and examined for trends with  $z$  or  $\alpha_\eta^3$ , as in Fig. 34. Unfortunately, both 'constants' so evaluated depend on  $z$ , although the dependence of  $K_2$  on  $z$  is considerably stronger than is that of  $K_1$ . A curve calculated for  $K_1 = 0.60$  is included in Fig. 33 and is seen to provide a reasonable fit to the data over the span of  $z$  covered. The significance of the deviation of the data from Eq. (104) for the largest  $z$  obtained here is not clear since deviations are also noted for fractions of other molecular weights at their maximum  $z$  (i.e., at the highest temperature). This could imply that the single parameter  $z$  is insufficient to characterize  $\alpha_\eta^3$ , or that the assumed temperature dependence  $B = B_0(1 - \Theta/T)$  is inadequate. Data at higher  $z$  are required and will be obtained from studies on samples of higher molecular weight.

Evaluation of approximations for  $\alpha_\eta$  in terms of  $\alpha$  may be discussed by eliminating  $z$  from the series expansion Eq. (102) by use of the relation,

$$\alpha^3 = 1 + \frac{3}{2} a_1 z h'(z) \quad (106)$$

There results

$$\alpha_\eta^3 - 1 = \frac{2}{3} \frac{b_1}{a_1} (\alpha^3 - 1) Q(\alpha) \quad (107)$$

where

$$Q(\alpha) = W(z)/h'(z)$$

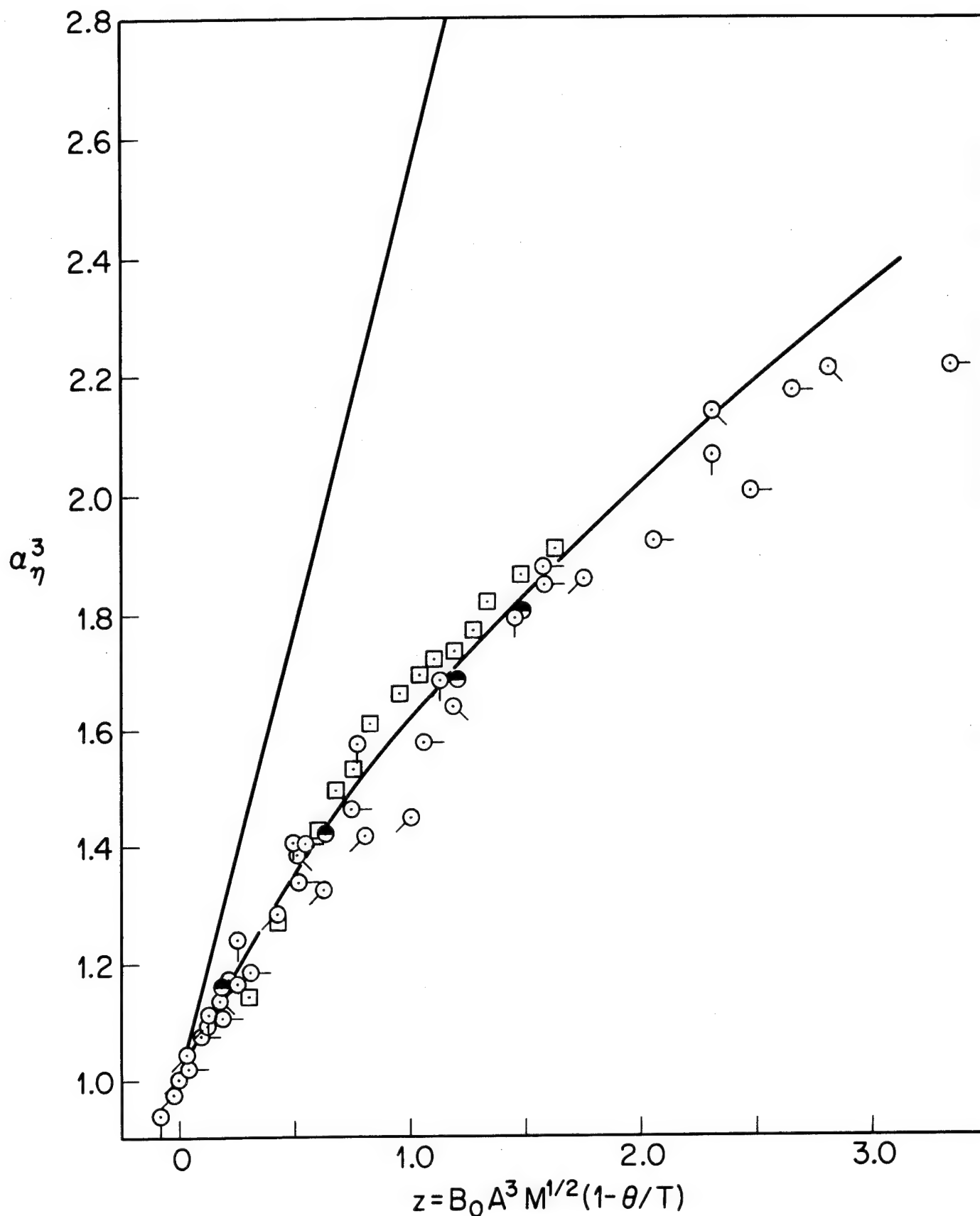


Figure 33 Dependence of  $\alpha_\eta^3$  on the thermodynamic parameter  $z$ . The straight line represents Eq. (103) with  $b_1 = 1.55$ ; the curve represents Eq. (104) with the empirical constant  $k_1 = 0.60$ . The points are as identified in Figures 21 and 25 except for  $\square$ , which represents data from Ref. 43

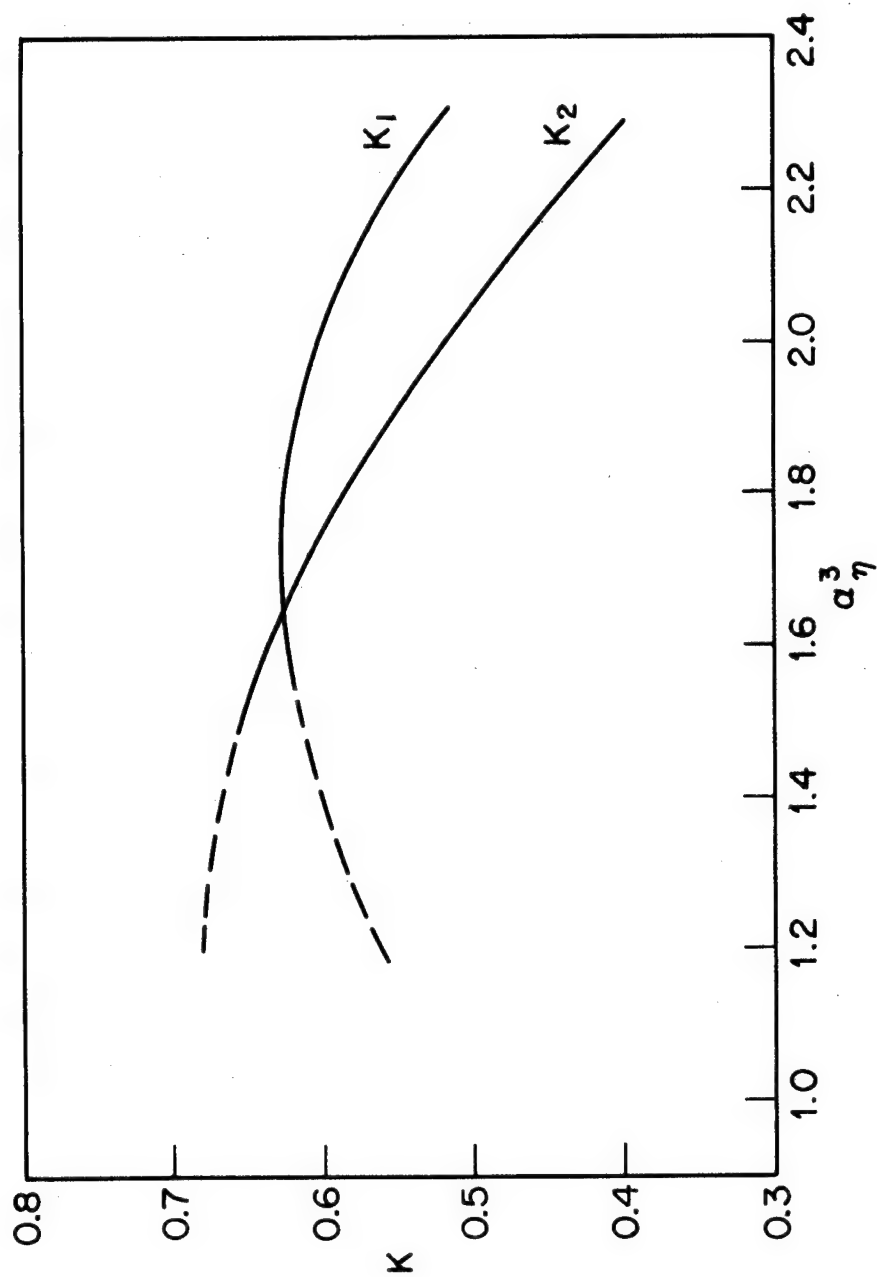


Figure 34 A test of the semi-empirical Equations 104 and 105 labelled  $K_1$  and  $K_2$  respectively.

The Flory-Fox approximation<sup>39</sup> implies that  $b_1 W(z) = \frac{3}{2} a_1 h'(z)$  with the consequence that  $\alpha_\eta^3 = \alpha^3$ . The approximation suggested by Kurata and Yamakawa<sup>28</sup>, on the other hand, uses instead of Eq. (106) the equivalent formulation

$$\alpha^{2b_1/a_1} = 1 + b_1 z h''(z) \quad (108)$$

with the result for  $\alpha_\eta^3$

$$\alpha_\eta^3 - 1 = \left[ \alpha^{2b_1/a_1} - 1 \right] Q'(\alpha) \quad (109)$$

where  $Q'(\alpha) = W(z)/h''(z)$ . Kurata and Yamakawa assume  $Q'(\alpha) \equiv 1$ . The ratio  $2b_1/a_1$  is approximately 5/2 for linear chains.

The data are displayed according to Eq. (107) in Fig. 35. Values of  $\alpha^2$  necessary to construct this plot were interpolated from  $\alpha(T)$  data for each molecular weight as given in the previous section. The dashed line gives the Flory-Fox approximation while the solid line denotes the initial tangent to Eq. (107). The latter is seen to correlate our data very well. The initial tangent for Eq. (109) is also displayed in Fig. 35. As would be expected, this approximate result correlates the data as well as Eq. (107) and proper evaluation of the merits of either would require data over a larger range of  $\alpha^2$ .\*

Insofar as our data are concerned, either of the expressions

$$\alpha_\eta^3 - 1 = 0.81 (\alpha^3 - 1) \quad (110)$$

$$\alpha_\eta^3 = \alpha^{5/2} \quad (111)$$

provide an adequate correlation over the span of  $\alpha^2$  considered. In fact, data for polymethyl methacrylate in good solvents<sup>70</sup> over a larger interval of  $\alpha^2$  also can be correlated nearly as well by either expression, although Eq. (110) seems to provide a better fit at large  $\alpha^2$  (see Fig. 36). Eqs. (110) and (111) are numerically similar, the function  $[1 + 0.81 (\alpha^3 - 1)]/\alpha^{5/2}$  deviating from unity by only 18 percent for  $\alpha^2$  as large as 4.0.

Thus, use of either Eq. (110) or Eq. (111) rests on their respective convenience for a given application since neither seems to be more favored

---

\*It may be remarked that this exercise is not totally futile since a plot of  $\alpha_\eta^3 - 1$  versus  $\alpha^2 - 1$  shows curvature from the initial tangent even for the  $\alpha^2$  interval considered here.

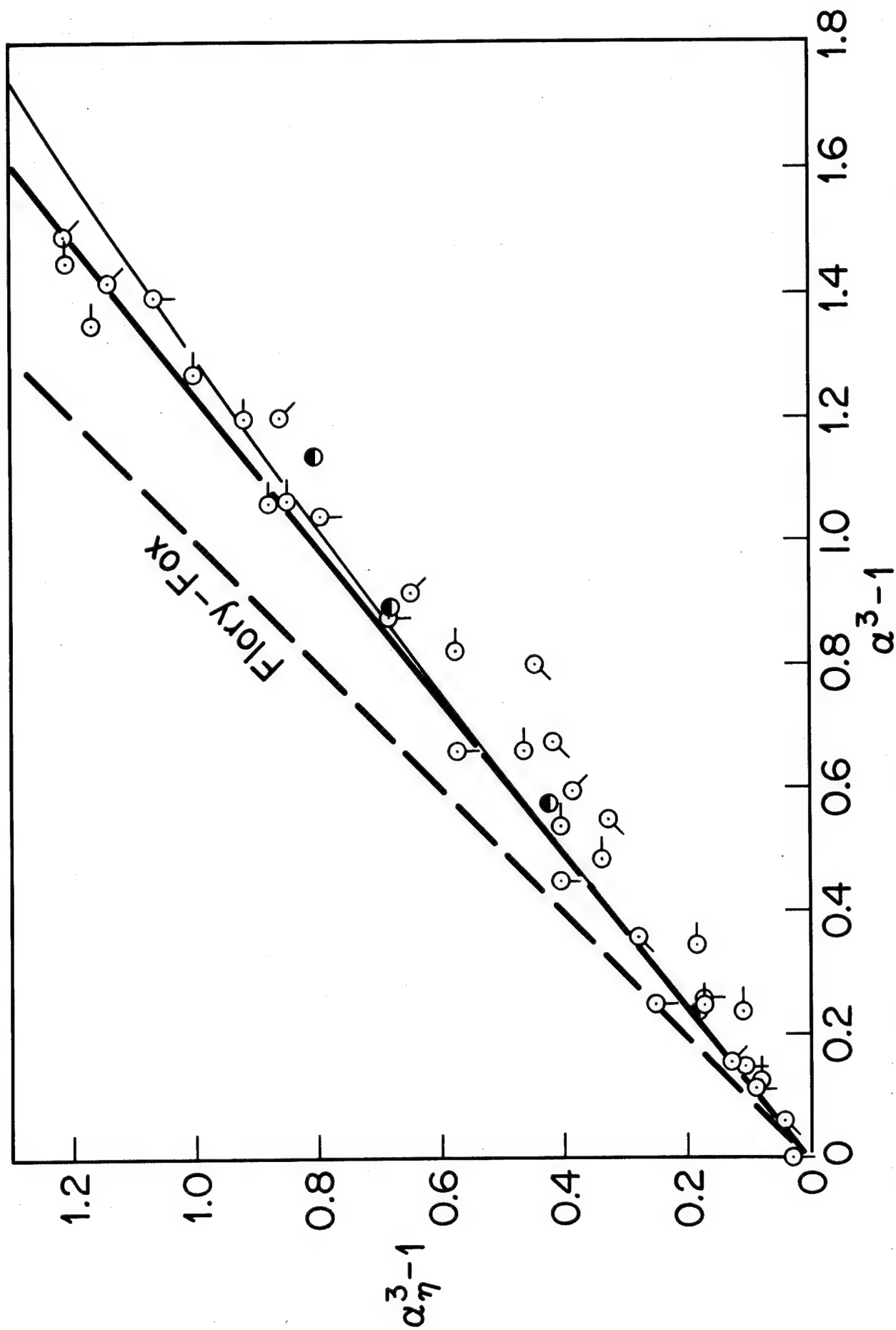


Figure 35 Semi-empirical correlations between  $\alpha_{\eta}^3$  and  $\alpha^3$ . The solid and light curves represent Eqs. (110) and (111) respectively. The symbols are defined in Figures 21 and 25.

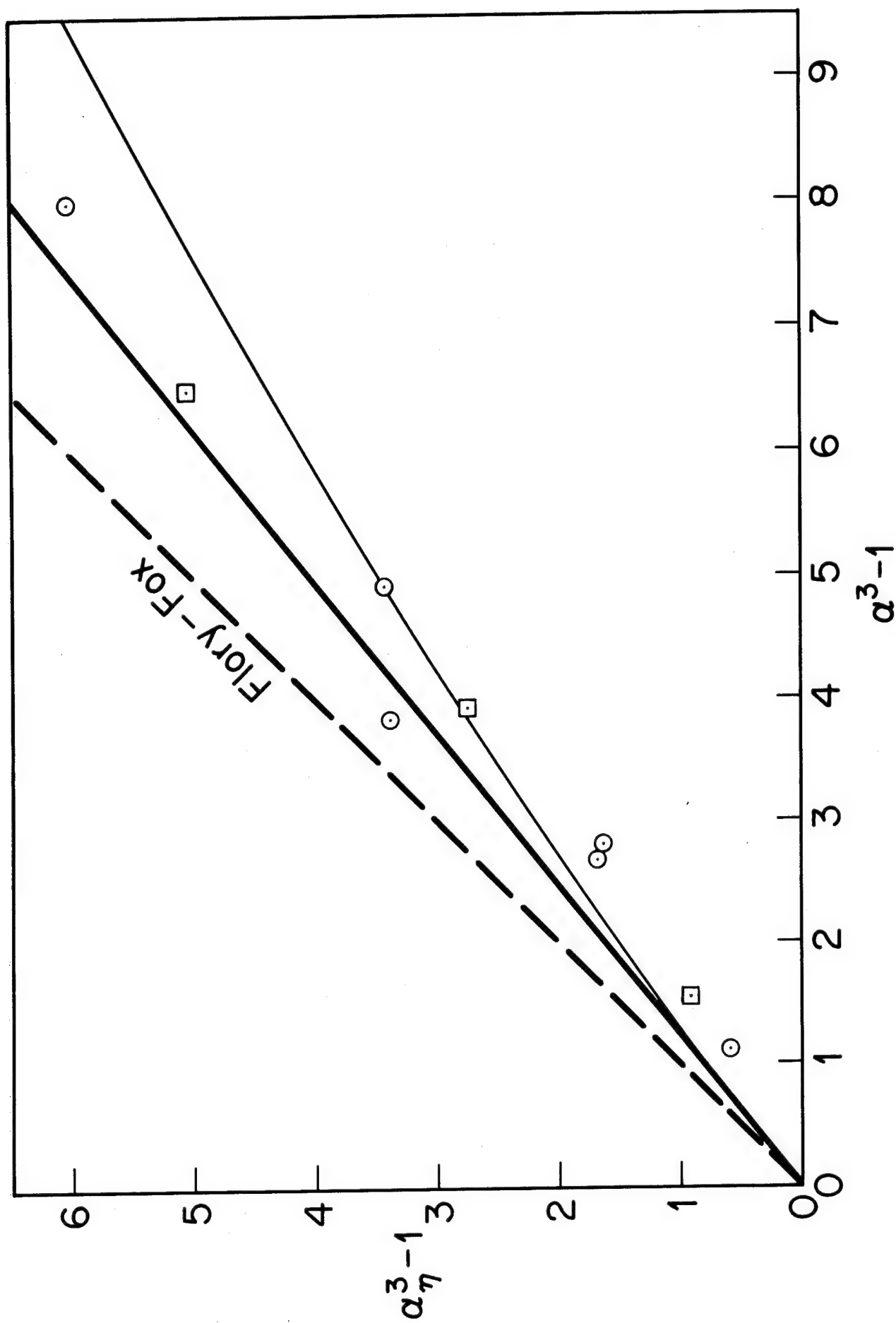


Figure 36 Semi-empirical correlations between  $\alpha^3_{\eta}$  and  $\alpha^3$  for data from the literature on polymethyl methacrylate in several solvents;  $M_w = 4.6 \times 10^6$ ,  $\square$ ;  $M_w = 1.25 \times 10^6$ ,  $\circ$ .

by the available empirical evidence and they both involve the same types of assumptions in their derivations. We are inclined to use Eq. (110) for correlation since the parameters specific to the hydrodynamic calculation appear in the constant 0.81 rather than in the power of  $\alpha$ . Thus, the form of Eq. (110) would be convenient when considering the behavior of branched chains, for example. In addition, this correlation suggests that  $\alpha_{\eta}^3 \propto \alpha^3$  for very large  $\alpha$ , which is physically attractive and seems to be in accord with a considerable body of experimental evidence<sup>43</sup> suggesting that  $\Phi_{app} = [\eta] M / (\bar{s}^2)^{3/2}$  is a constant in good solvents, whereas Eq. (111) implies that  $\Phi_{app}$  will be a continuously decreasing function of  $\alpha$ .

## E. Conclusions

Fig. 33 presents the evidence that  $\alpha_{\eta}^3$  may be represented as a function of the single variable  $z$ . Data for polystyrene-cyclohexane<sup>76</sup> and for polystyrene-decalin<sup>43\*</sup> are included with our data. The principle feature of interest here is whether the data do superpose, and thus provide support for the basic theory and and the assumed temperature dependence  $B_0(1 - \Theta/T)$ . In fact, fair, but not perfect, superposition is obtained. (It may be remarked that one only need know  $z$  to within an arbitrary constant for this part of the analysis.)

The data displayed in Fig. 33 provide the beginnings of an empirical correlation for  $[\eta](T, M)$  that could be used to analyze intrinsic viscosity data to yield such parameters as the unperturbed dimensions, and enthalpies and entropies of mixing. We intend to extend these studies to include data for both higher and lower molecular weight materials as well as for branched polymers.

Fig. 34 shows  $\alpha_{\eta}^3 - 1$  to be nearly a linear function of  $\alpha^3 - 1$ , although there are some marked deviations. Examination of this relation for data over larger intervals in  $\alpha_{\eta}^3$  reveal that the correlation remains valid to larger  $\alpha_{\eta}^3$  as well. Thus, Eq. (110) is advanced as an alternative to the more familiar  $\alpha_{\eta}^3 = \alpha^{5/2}$ . The constant 0.81 is derived from the perturbation theories for  $\alpha_{\eta}^3$  and  $\alpha^2$  in much the same way as is the power  $5/2$ . Although the Flory-Fox approximation as usually stated,  $\alpha_{\eta}^3 = \alpha^3$ , does not represent our data when used with Eq. (101), it may be noted that for large  $\alpha_{\eta}^3$  (> ca. 3.5) Eqs. (101) and (110) yield

$$[\eta] \equiv 6^{3/2} (2.4 \times 10^{21}) \frac{(\bar{s}^2)^{3/2}}{M} \quad (112)$$

which is very close to the Flory-Fox equation as usually applied to data in good solvents. Thus, in this treatment the modified value for  $\Phi'$  associated with the empirical Flory-Fox relation appears naturally as a limit in good solvents.

\* These points are computed using values of  $[\eta](T, M)$  given in reference<sup>43</sup>, but the  $\Theta$  temperature is taken as 13.8°C in correspondence with our light scattering data, and  $[\eta]_{\Theta}$  is computed as  $7.7 \times 10^{-4} \text{ VM}$ . The analysis in reference 43 assumed an erroneous value for  $\Theta$  reported by others<sup>26,56</sup>.



# IX. Investigation of Two Novel Inorganic Polymers — G. C. Berry

Preliminary dilute solution measurements on two inorganic coordination polymers have been completed. These polymers, one derived from zinc methyl phenyl phosphinate(I) and another from hydroxy aquo chromium diphenyl phosphinate(II), were developed in the laboratories of the Pennsalt Corporation.

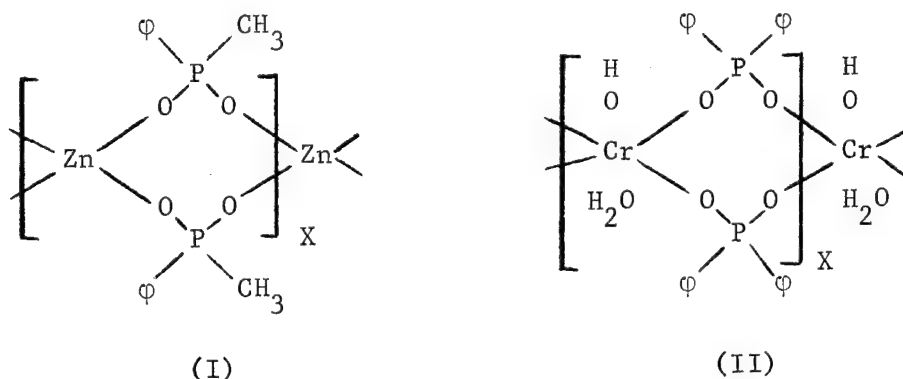


Figure 37 Two coordination polymers.

These investigations showed that the materials were in fact polymers of reasonably high molecular weight, ca. 5000 for I and higher for II; but the molecular weight for both increased substantially during the time required for measurements. The increase in the molecular weight of II was inferred from changes in the intensity of light scattered from a chloroform solution containing 0.00743 g/cc of II: the intensity increased 28 percent in six days and 48 percent in twenty days at 30°C. Similarly, an increase in the molecular weight of I was inferred from the observed change in the inherent viscosity,  $(\ln \eta_{rel})/c$ , of a 0.0289 gm/cc solution in chloroform; the viscosity increased from an initial value of 0.146 dl/g to 0.208 in six days, and to 0.253 in fourteen days at 30°C. In addition, gel-like inhomogeneities were observed to form in solutions of II. These findings were consistent with other studies (at the Pennsalt laboratories). They suggest incomplete reaction in both polymers, and possible network formation in II.

Additional studies at the Pennsalt laboratories have suggested that both I and II may be susceptible to degradation by coordination compounds, such as water and ethanol, which were probably present in the polymers received by us as well as in the reagent grade chloroform used here. Accordingly, additional samples of I have been prepared under anhydrous conditions and we are presently engaged in dilute solution studies on this polymer using purified chloroform as a solvent. Light scattering and intrinsic viscosity measurements will be carried out initially to determine its molecular weight and molecular weight stability under an-

hydrous conditions. If stable, a small quantity of water can be introduced to determine the effect, if any, of moisture on the solution properties. Further studies will depend on the outcome of these experiments, but if the polymer is sufficiently stable, a series of molecular weights will probably be studied by these methods, as well as by sedimentation velocity, to ascertain if possible, the molecular conformation in solution (flexible coil, stiff rod, etc.).

X. Construction of a Couette Viscometer for Steady Flow at Low Shear Rate —  
G. C. Berry and G. L. Bender

A. Introduction

A couette viscometer has been constructed in which a cylindrical rotor, operated by a rotational hysteresis drive, is centered in a fixed cylindrical tube by a combination of gravitational, buoyancy and surface tension forces. The meniscus in the annular gap is such that the contact angle formed by the liquid and the stator does not equal that formed by the liquid and the rotor. This arrangement provides a centering force for the rotor<sup>77,78</sup>. The difference in the contact angles is obtained by the simple expedient of forming the meniscus at the top of the stator so that the normally symmetric meniscus formed between two concentric cylinders cannot be obtained (see Fig. 38). This centering principle and hysteresis drive has been used previously by Zimm and Crothers.

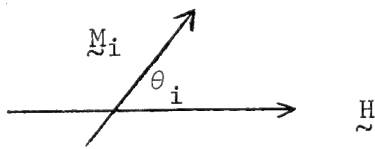
In the following report the viscometer is described in sufficient detail to allow an assessment of its features for dilute solution viscometry, as well as other applications.

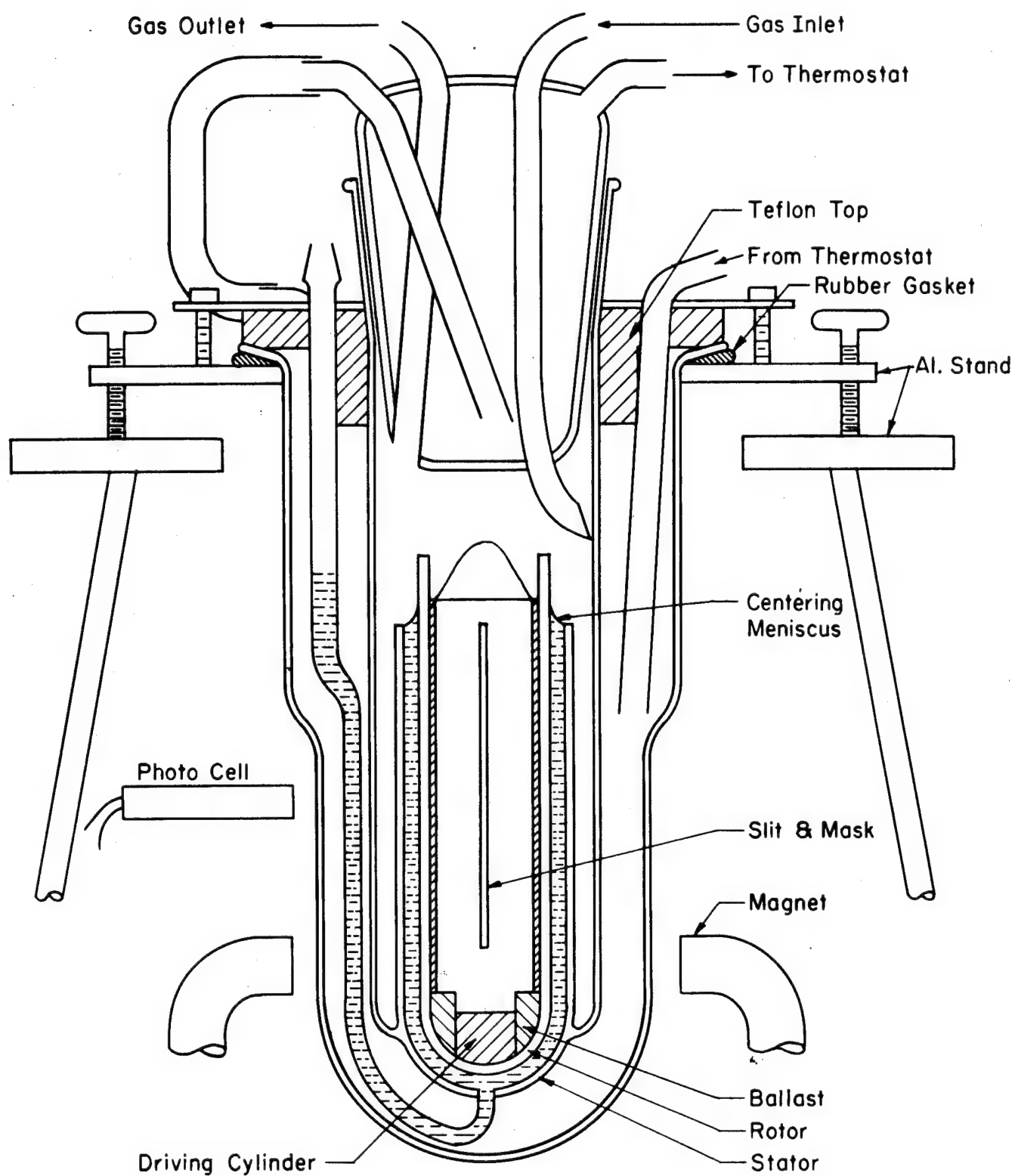
B. General Description

A schematic drawing of the viscometer may be seen in Fig. 38. The fixed stator is entirely enclosed by a thermostated chamber. A tube connected to the bottom of the stator and leading out of the thermostat chamber provides access for liquid level control in the stator. The rotor is a cylindrical tube of ca. 4 mm smaller OD than the stator ID and so provides for an annular gap of about 2 mm filled by the liquid under study. The rotor is turned by a magnetic drive that provides constant torque, independent of the speed of rotation of the rotor. Thus, comparison of the periods of rotation (sec/rev) for two different liquids provides a measure of their (kinematic) viscosities. The following sections will describe these components in more detail.

C. The Magnetic Drive

The rotor is driven by a constant torque derived from rotational hysteresis. The origin of this torque may be understood by considering the interaction of a magnetic domain and the applied field  $\vec{H}$ <sup>79</sup>. Any domain, say the  $i$ -th, can be considered to be equivalent to a dipole of moment  $\vec{M}_i$  whose axis makes an angle  $\theta_i$  with the field  $\vec{H}$ , as in the diagram.





Not to Proportion

Figure 38 Schematic diagram of low shear rate concentric cylinder viscometer.

A couple  $HM_i \sin \theta_i$  exists between the applied field  $H$  and the induced dipole  $\tilde{M}_i$ . If  $\theta_i$  is increased by  $d\theta$ , then the work  $W$  done per unit volume of magnetic material is given by

$$dW = \sum_i M_i H \sin \theta_i d\theta$$

where the sum is to be extended over all domains in a unit volume. Now, the intensity of magnetization  $I$  is simply  $\sum M_i \cos \theta_i$ , that is, the component of  $\tilde{M}_i$  in the direction of  $H$ . Thus,  $I$  is affected when  $\theta$  changes according to

$$dI = d(\sum M_i \cos \theta_i) = -\sum M_i \sin \theta_i d\theta.$$

The work done per unit volume is

$$dW = H dI,$$

or the work done per unit volume per cycle is

$$W = \oint H dI$$

$W$  is in general not zero because of hysteresis loss in the  $H$ - $I$  loop for a magnetic material\*. The more open is the hysteresis loop, the greater will be  $W$ , but in general the characteristics of the material (its permeability, etc.) must be matched to the value of  $H$  associated with the available field<sup>80</sup>. That is, a material with an open loop that requires a large value of  $H$  to be energized is of little value if only weak fields are available. The essential character of this energy loss, as related to a couple acting through an angle, means that  $W$  will be independent of the speed of rotation, that is, the work loss per unit volume per cycle, and hence, the torque developed per unit volume, is independent of the speed of rotation.

Thus the torque  $T$  is dependent on the field  $H$ , the characteristics of the magnetic material and the volume of the magnetic material. In addition to having a large hysteresis loop for the values of  $H$  obtained here, the magnetic material should have low permanent retentivity. A material meeting these specifications is Ferroxcube 4B (manufactured by the Ferroxcube Corporation of America, Saugerties, New York). This material has a Curie temperature of ca. 250°C, and so will provide usable torques over the temperature range of interest here. We have found no evidence of permanent retention of a magnitude such as to disturb our measurements.

Since it is desirable to have an isotropic material for the drive cylinder, the Ferroxcube is ground to a powder, mixed with a ceramic

---

\*The above analysis is given in more detail in ref. 79.

cement (Eccoceram CS, Emerson and Cummings, Inc.) and molded to the desired size and shape. Measurements with these cylinders indicate that the torque developed first increases with increasing volume fraction of metal in the drive cylinder, but then tends to level off with further increase in the metal content. This effect is probably related to distortion of the relatively weak field  $H$  by the presence of the ferromagnetic material in the gap. Accordingly, cylinders used here are fabricated with volume fraction of metal near that for which the maximum torque is obtained since additional metal only serves to provide a horizontal force pulling the rotor off the vertical. This critical volume fraction is ca. 0.1 for our system, but it depends strongly on the field  $H$ .

For volume fractions less than the critical value, the torque increases as the total volume of metal, or as the square of the radius for fixed cylinder height and fixed volume fraction of metal in the drive cylinder. Cylinders containing more than the critical volume fraction, solid disks for example, show a dependence of the torque on the radius. The former dependence is to be expected in light of the discussion presented above. The latter probably arises from distortion of the field  $H$  by the cylinders of high metal content so that no additional magnetic lines are cut when the radius is increased, but the only effect is for the lines to pass through a longer metal path length, proportional to the radius.

As expected, the torque developed is independent of the speed of rotation of the applied field  $H$  over the interval 150 to 1000 RPM examined here. The permanent magnet is normally rotated at ca. 800 RPM by an induction motor with an attached gear train. A synchronous motor could be used in its stead if a constant speed was desired for some other applications (such as an eddy current drive in the rotor).

The magnet used here was obtained from the Indiana General Company (number 20452F). A soft iron spacer was removed and replaced by a longer spacer so that the pole separation was large enough for our apparatus.

#### D. Mechanical Construction of the Rotor

The rotor must float vertically and be balanced so as not to wobble perceptibly about the axis of rotation. The weight  $W$  and the size of the rotor are related to the density  $d$  of the liquid in the annular gap by the well-known relation

$$W = (\text{Volume Immersed})Xd = (L\pi R_2^2 + \frac{4}{6}\pi R_1^3)d$$

where  $R_1$  is the rotor radius and  $L$  is the length of the cylinder wetted\* (to, but not including, the hemispherical bottom). The weight  $W$  is

---

\* Effects of the meniscus on  $L$  are ignored for this qualitative discussion.

comprised of the weight of the glass tube  $W_g$ , of the ceramic ballast-driver assembly  $W_b$ , and of the nylon slit  $W_s$ . The most stable configuration is with  $W_b/W$  as large as possible. Since  $W_g$  increases (approximately) with  $R_1 \times L$  and  $W$  increases (approximately) with  $R_1^2 \times L$ , it is clear that  $R_1$  must be increased until  $W_b/W$  is large enough to insure stability. For ordinary glass tubing and organic liquids ( $d \approx 0.85$ ),  $R_1$  must be about 8 to 10 mm., and  $W$  ca. 17 g. and  $W_b$  ca. 6 g. Introduction of the appropriate weight of ballast material normally does not cause the tube to float in a vertical position, but rather the tube axis assumes some angle of cant  $\alpha$  with the vertical. Introduction of additional ballast will then cause the tube to sink lower, but will not appreciably affect  $\alpha$ . Thus, it is necessary to change the center of mass of the system by affecting the distribution of mass in  $W_b$  until the center of mass and the center of buoyancy both lie on the axis of rotation of the tube. This is conveniently accomplished by drilling small (ca. 1 mm) holes around the periphery of the ballast and filling them with mercury until  $\alpha = 0$ . The mercury may be conveniently added with a 50  $\mu$ l syringe since the amount of mercury required is very small, the tube having been nearly balanced by previous adjustment of  $W_b$ . After each addition of mercury, the rotor is placed in the stator and observed with a cathotometer while being rotated. Any imbalance will appear as a periodic wobble in the rotor motion. Rotors are commonly balanced so that the wobble is less than 0.02 mm by this method.

The materials of construction must be consistent with operation over an extended temperature range (0°C to 180°C) in organic media and with the magnetic drive. The latter excludes the use of aluminum cylinders for either the rotor or the slits, for example, since a torque would then be developed from the eddy currents in the aluminum. The extended temperature interval excludes most organic materials from use as a ballast since their thermal expansion would far from match that of the glass rotor. Thus, we have used a machinable ceramic material, Alsimag, as ballast. This material has a thermal expansion coefficient near glass and may be readily machined to fit into the bottom of the glass tube and drilled to accept the drive cylinder and the mercury drops. The ceramic used here shows little or no weight change due to vapor adsorption of decalin over the temperature interval 10° to 100°C. The slits are machined from black nylon in the form of a cylinder with OD slightly under the ID of the glass tube. They are fitted onto a shoulder on the ceramic ballast and held in place by a nylon pin placed in the ballast. Again, vapor adsorption does not appear significant. The makeup of the drive cylinder is given elsewhere in this report. The entire ballast-driver-nylon slit assembly is cemented into the glass tube with an inorganic ceramic cement (Eccoceram WL-52, Emerson and Cummings, Inc.)

## E. Alignment

There are three independent members to be aligned relative to each other; the rotor, the stator and the rotating magnetic field. The alignment of the rotor is discussed in the preceding paragraphs. The stator is constructed with the upper end cut perpendicular to the wall.

A soft plastic plug was machined to a snug fit in the stator with its upper surface perpendicular to its wall. This surface serves as a platform for a mirror and the plastic plug-stator assembly may be aligned in a vertical position by observing the reflection of a vertically oriented light beam from the mirror. The stator may be aligned to within 8 minutes of angle by this method.

The magnet is mounted on a collar machined so that the poles are equidistant from the axis of rotation of the collar. It remains to orient this axis of rotation with the center line of the stator. This alignment is necessary to prevent the rotor from experiencing a horizontal force from the magnet, which can (in principle at least) cause it to rotate at some constant angle  $\alpha$  with the vertical. This cant of the rotor will be constant as opposed to the periodic wobble caused by an improperly balanced rotor. The magnet and its drive mechanism are mounted on a plate, which in turn may be moved in two (nearly) perpendicular directions by two screws. The axis of rotation of the magnet is first aligned with the center line of the stator by inspection. This initial adjustment is facilitated, through reduction of refraction effects, if the stator is filled to a depth of ca. 10 mm with the same liquid that is in the outside heat exchanger section of the viscometer. The magnet assembly may then be positioned so that a scribe mark on the axis of rotation of the magnet is near the center of the stator as viewed vertically. Further adjustment may, or may not, be required depending on the magnet pole strength and the distance between the rotor and the poles. This may be determined by moving the magnet along an arbitrary direction and noting the change, if any, of the period of rotation  $P$  of the rotor. If  $P$  is unaffected by slight variations of the magnet position in different directions, the alignment may be considered complete. If  $P$  is affected, then a magnet position for minimum  $P$  may be established and taken as the position where the rotor is rotating vertically, otherwise increased shear rate due to the angle of cant  $\alpha$  increases  $P$ . In practice, this adjustment is not too critical since the angle of cant increases the shear rate on one side of the rotor and decreases it on the other, with somewhat compensating results on  $P$ . When required, the adjustment is probably best made with a rotor which leaves only a small gap when rotating vertically so that these effects will be maximized on different sides of the rotor.

Optical inspection of the gap should then be made near the bottom of the rotor to check on the above alignment. Unfortunately, this direct method of alignment may not be relied on because of the effects of refractions in the viscometer assembly when viewed from the side, but it does provide a reasonable check on the alignment.

The positioning of the magnet in the present viscometer is not critical owing to the wide gap (90 mm) between the pole pieces. With narrower gaps (or with stronger pole pieces), more careful alignment of the magnet is required.

#### F. Operating Characteristics

1. The effects of rotor position. As previously described, the rotational hysteresis drive provides a constant torque despite changes



in the angular velocity  $\Omega = 2\pi/P$  of the rotor relative to the rotating magnetic field  $H$ . There remains, however, the possibility that  $H$  is not uniform with respect to the vertical position  $y$  of the rotor drive cylinder relative to the magnet pole pieces ( $y = 0$  may be taken in the horizontal plane bisecting the pole pieces), and hence that the torque  $T$  is a function of  $y$ . In addition, unknown end effects from either the bottom of the rotor or the meniscus can cause the period of rotation  $P$  to vary with  $y$  in a complex manner. The relation for  $P$  may be approximated by

$$P = \frac{2\pi W\eta/d}{T/R_1(R_2 - R_1)} \left( \frac{R_2 + R_1}{R_1} \right)^2 \times p(R_1, R_2) [1 + H_1 + H_2] \quad (113)$$

where 
$$H_1 = \left( \frac{R_2 - R_1}{h} \right) \left( \frac{R_2 + R_1}{16L} \right) \left( \frac{R_1}{R_2} \right)^2$$

and  $H_2$  is a term to account for remaining end effects at the rotor bottom and at the meniscus. Here  $L$  is the vertical length of the rotor wetted by liquid,  $R_1$  the rotor radius,  $R_2$  the stator radius,  $W$  the rotor weight,  $h$  the height of liquid in the end-gap below the base of the rotor,  $\eta$  the liquid viscosity, and  $d$  the liquid density. The function  $p(R_1, R_2)$  is nearly unity for the geometric arrangements used here\*.

The term  $H_1$  in the square brackets approximates the contribution of the viscous loss in the end-gap bounded by the rotor base and the stator base relative to the base in the annular gap. Representative figures for the parameters in  $H_1$  yield  $H_1 \sim 1/800$ ; thus  $H_1$  is not expected to contribute significantly to  $P$ . An estimate for  $H_2$  is not made as easily as it includes several effects not readily analyzed (see, for example, ref. 80).

An estimate for the effect of the meniscus height  $\Delta$  (the maximum height of the meniscus above the stator top) on  $P$  may be obtained experimentally by varying  $\Delta$  over the small range available between the maximum  $\Delta$  obtainable for a given liquid and the minimum  $\Delta$  for which the rotor remains centered. The value for  $\Delta$  may be varied by changing the volume of liquid in the annular gap. As  $\Delta$  is varied, the possible change in the length  $L$  of wetted tube, together with uncertain viscous loss in the region of the meniscus and possible variation of the torque with rotor height due to a non-uniform field  $H$ , causes  $P$  to vary. Actually,  $L$  does not change directly with  $\Delta$  since the rotor height changes as  $\Delta$  is varied. Unfortunately, the change in  $P$  with  $\Delta$  is significant, ca. 1 percent per mm. Typically,  $\Delta$  may be varied over a 3 mm interval. This dependence of  $P$  on  $\Delta$  necessitates the liquid level control tube shown in Fig. 38. This tube enters at the bottom of the rotor and is connected to a syringe so that  $\Delta$  may be maintained constant over prolonged periods of time and/or with temperature changes. It should be

---

\*  $p(R_1, R_2) = R_1 R_2^2 / (R_1 + R_2)^3$

noted that the effects of  $\Delta$  per se on P do not enter in so direct a manner for the viscometer construction used by Zimm and Crothers since in their case, introduction of additional liquid into the viscometer would only have raised the rotor, leaving  $\Delta$  unaffected. The meniscus height  $\Delta$  can be controlled with sufficient precision so that its effects on P are insignificant.

Eq. (113) states that P is proportional to the kinematic viscosity  $\mu = \eta/d$ . This is due to the fact that a rotor of given weight will ride deeper in the liquid the smaller is d. A single rotor may usually be used in liquids over a range of densities differing by ca. 10 percent. A test of this relation was made by comparing the ratio of P determined for Couette flow for two solvents (decalin and tetralin) with two different densities (0.843 and 0.923) respectively with the ratio of the capillary flow times for the two solvents. These ratios agreed to within 5 percent. This result is acceptable since the torque may well depend on the rotor height which varied by 5 mm in this experiment. This variation is not inconsistent with that found by variation of  $\Delta$  and may indicate that the torque depends on the rotor height through non-uniformity of the field H. In any case, this result indicates that P is nearly proportioned to  $\mu$  over a wide range of rotor heights y.

2. The effects of temperature. The variation of P with temperature t for a given liquid is due in part to variation of  $\mu$  with t, and in part to the effect of t on the torque. The first effect may be eliminated by dividing P by the factor  $\exp[A(t - t_r)/(t - B)]$  where A and B are here regarded as empirical constants to be determined from the dependence of capillary flow times on t, and  $t_r$  is a reference temperature. The remaining dependence of  $P \exp[-A(t - t_r)/(t - B)]$  on t may be assigned to dependence of the torque on t. Fig. 39 shows a plot of data for decalin (a cis-trans mixture, for which  $A = 8.03$ ,  $B = 173^\circ\text{C}$ , and  $t = 30^\circ\text{C}$ ) treated in this way over the temperature interval  $12^\circ$  to  $100^\circ\text{C}$ . The graph illustrates the three-fold variation in T found over this temperature range\*. The torque is still large enough to be usable for decalin at  $140^\circ\text{C}$ . The cause of this effect has not been investigated further, but is probably related to changes in the properties of the Ferroxcube 4B with temperature.

It is found that  $\ln[P \exp[-A(t - t_r)/(t - B)]]$  depends almost linearly on t. This means that the percentage change in T with temperature is nearly constant (at about 0.18 percent per degree).

3. The average shear rate. The shear rate in Couette flow does not vary significantly across the gap for gaps narrow compared to the annular radius. The average shear rate  $\langle \kappa \rangle$  may be calculated from

$$\langle \kappa \rangle = \frac{\int_{R_1}^{R_2} R_1 2\pi r \kappa(r) dr}{\int_{R_1}^{R_2} R_2 2\pi r dr}$$

\* The small (ca. 5%) change in P due to the changing rotor height is neglected.

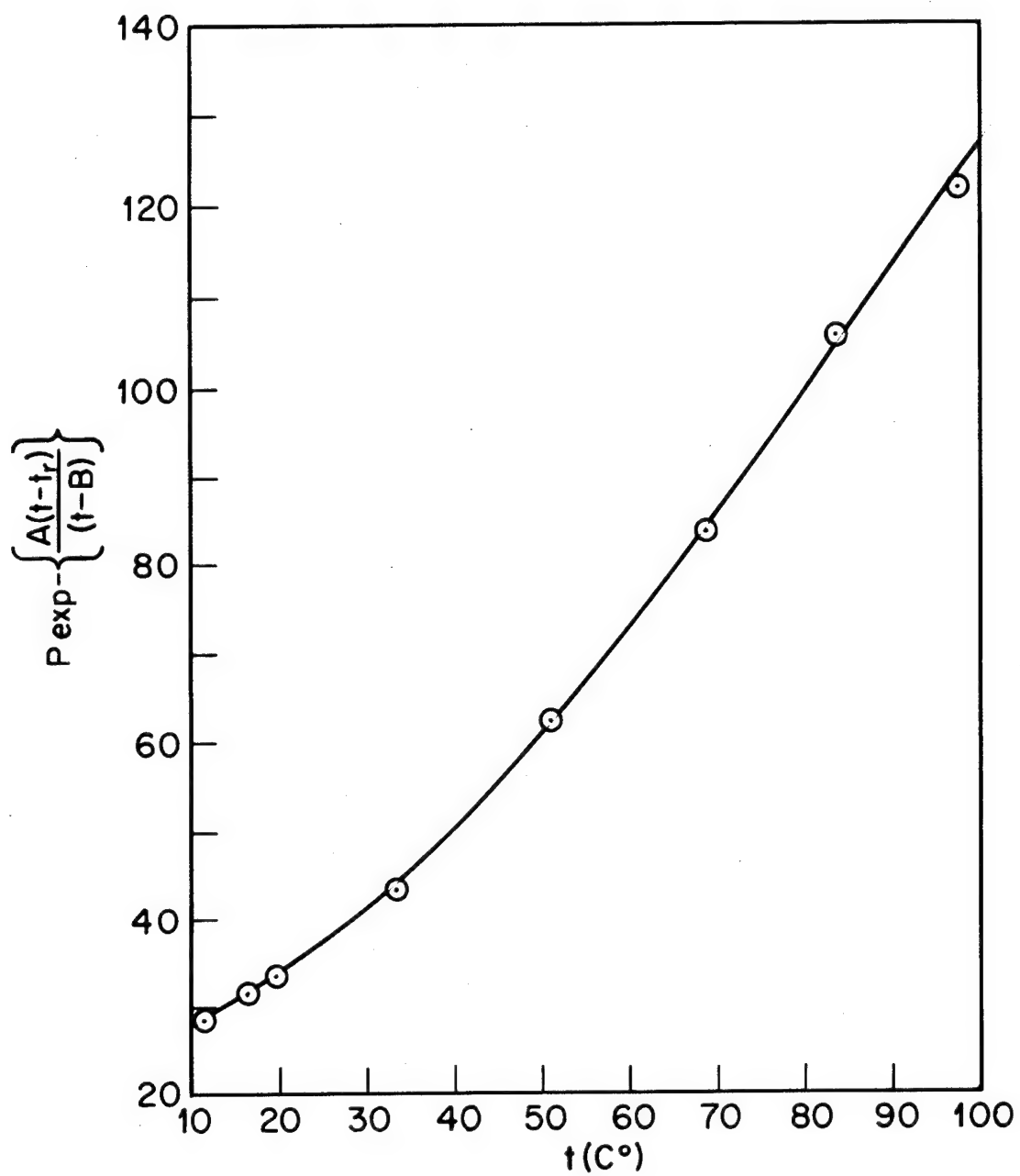


Figure 39 Dependence of the torque derived from a rotational hysteresis motor on temperature.

with  $\kappa(r) = T/2\pi\eta Lr^2$ ,  $T$  denoting the torque. The result gives

$$\langle \kappa \rangle = \frac{\pi}{P} \left( \frac{R_2 + R_1}{R_2 - R_1} \right) f(R_1, R_2)$$

The factor  $f(R_1, R_2)$  differs insignificantly from unity for our viscometer\*. The value for  $\kappa(r)$  varies by only ca. 10% over the entire gap. Typical values of  $R_1$  and  $R_2$  for our viscometer ( $R_1 = 9$  mm,  $R_2 = 11$  mm) yield

$$\langle \kappa \rangle = 10\pi/P$$

Thus, since  $P \propto 30$  sec/rev for decalin at 25°C,  $\langle \kappa \rangle \propto 1$  sec.<sup>-1</sup>. Lower values of  $\langle \kappa \rangle$  can be obtained if desired by reducing the torque  $T$  through reduction of the volume of Ferroxcube in the rotor. Increasing  $R_2 - R_1$  would not decrease  $\langle \kappa \rangle$  since  $P$  would decrease proportionally to the increase in  $R_2 - R_1$ , leaving  $\langle \kappa \rangle$  almost unchanged.

#### G. Photoelectric Timer

The period of rotation  $P$  (sec/rev) is determined by a photoelectric timing device. Two slits (0.25 mm wide) are cut 180° apart in a nylon cylinder attached to the ballast. The slits allow a pulse of light to reach a photo resistor every half revolution. Fig. 40 is a schematic drawing of the circuit used to count and time these pulses. Manipulation of the switch  $S$  causes the pulses to start a timer, count the number of pulses for a desired time interval, and then stop the timer. This device has been used to measure  $P$  to within 0.02 sec. for  $P$  in the range 5 to 60 sec/rev. Since several revolutions may be timed to increase the total time interval to ca. 100 sec., the value of  $P$  may be determined readily to within 0.02%, so far as the timing error per se is concerned.

It is necessary to insert a heat absorbing glass in the optical train to prevent the rotor temperature from being affected by infra-red radiation from the lamp.

#### H. Intrinsic Viscosity Measurements

Measurement of the intrinsic viscosity at low shear rate only requires  $P$  to be proportioned to  $\eta$  (or  $\eta/d$ ) since the values  $P_S$ , for the solution, and  $P_0$ , for solvent, are measured under conditions such that all of the terms on the rhs of Eq. (113) except  $\eta/d$  are constant. Thus, the ratio  $P_S/P_0$  required for computation of  $[\eta]$  does not depend on the details of the operating characteristics of the viscometer. It is necessary to maintain the meniscus height  $\Delta$  at a constant value during measurement of  $P_S$  and  $P_0$  since  $P$  has been demonstrated to vary with  $\Delta$ , but this may be satisfactorily achieved.

\*  $f(R_1, R_2) = 8R_1^2 R_2^2 [\ln(R_2/R_1)] / [(R_2 - R_1)(R_2 + R_1)^3]$



The apparatus requires ca. 15 ml of liquid for operation, about 5 ml of this being required to fill the side-arm.

Measurements are currently in progress to evaluate the long term (order of days) stability of the apparatus prior to beginning extensive viscosity investigations. We must determine how frequently a standard fluid should be checked to provide a stable reference for the torque before undertaking measurements on the system polystyrene-decalin as a function of temperature.

## XI. Differential Refractometer — G. C. Berry

### A. Introduction

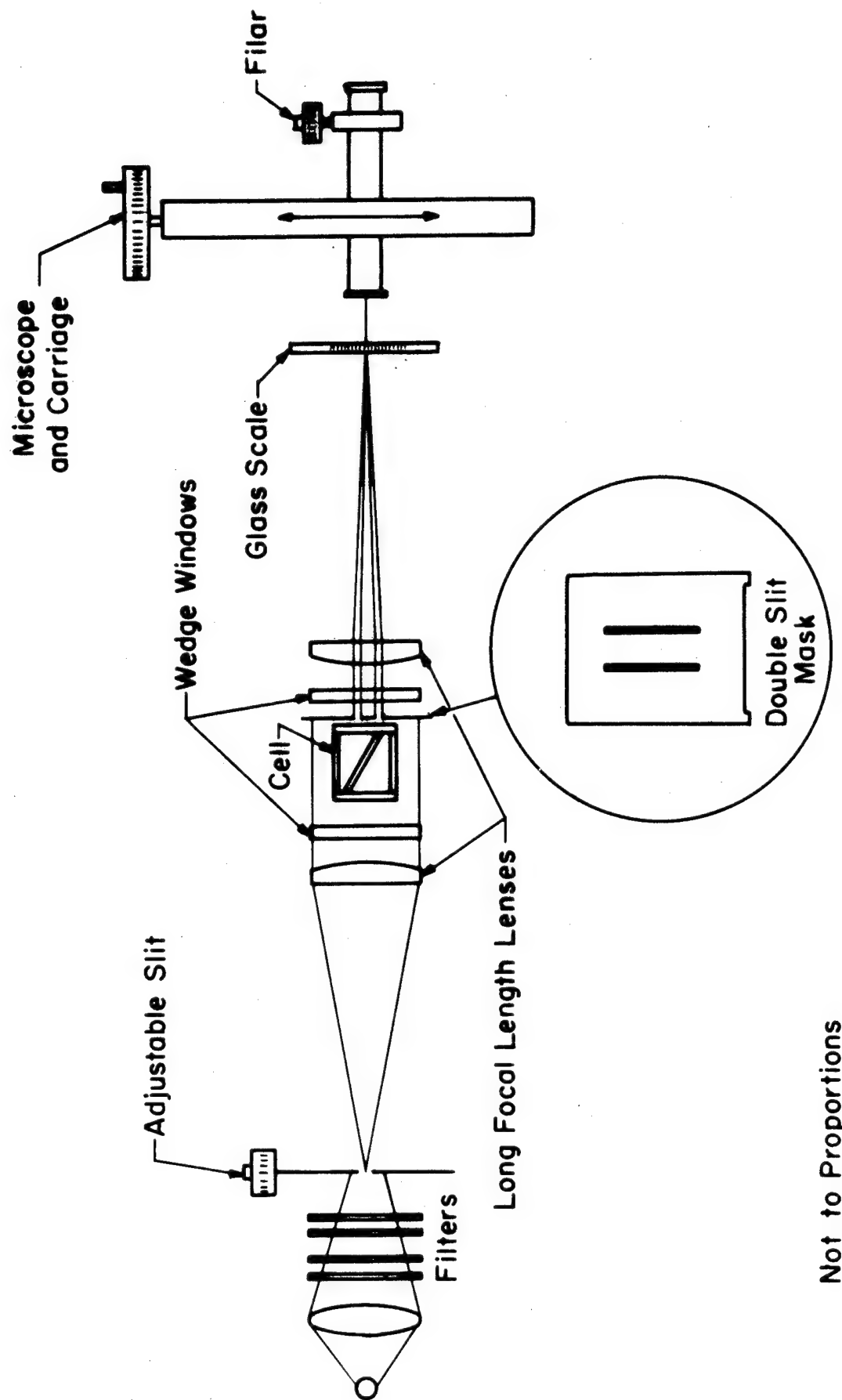
A differential refractometer with a precision of  $\pm 2 \times 10^{-6}$  refractive index units has been designed and constructed. The instrument is of the double prism type, in which the angular deviation of a light beam caused by the prismatic action of a two compartment liquid cell is determined. The particular design employed here closely follows one used by Prof. L. D. Gosting (University of Wisconsin). The principles of construction and operation are discussed below and some experimental results are described.

### B. Instrument Design

The instrument is shown schematically in Fig. 41. The light from a mercury vapor lamp (G.E. AH3) is collected by a lens and focused on an adjustable slit after either the  $4358\lambda$  or  $5461\lambda$  light has been isolated by Corning color filters. The adjustable slit (Gaertner Scientific Corp., Model L161D) provides a secondary source slit of  $\geq 0.03$  mm in width. A normal setting is 0.05 mm. The slit is placed in the focal plane of a long focal length ( $f \approx 520$  mm) lens so that nearly parallel light passes through the cell. Two windows are placed in the light beam as part of a thermostat system. These windows must be wedge-shaped in order to prevent formation of extraneous interference fringes in the final image. A second long focal length lens ( $f \approx 520$  mm) is used to focus the image of the slit on a glass slide with scale divisions engraved precisely every 0.1 mm (by L. Nichols; Fort Collins, Colorado). The position of the image relative to the nearest adjacent scale mark may then be accurately determined with a filar microscope (Gaertner Scientific Corp., Model M113A) reading to 0.0005 mm. The filar microscope is positioned relative to the slit image on the glass scale by a microscope carriage (Gaertner Scientific Corp., Model M-301). It was necessary to enclose the light path from the adjustable slit to the first lens and from the second lens to the glass scale in tubes to minimize image fluctuations due to air disturbances.

The cell housing is thermostated as shown schematically in Fig. 42. The space between the lens and window is filled with a dry atmosphere and supplied with a dessicant breather tube to facilitate measurements near  $0^\circ\text{C}$ . The cell is enclosed by an annular heat exchanger capable of holding the temperature to  $\pm 0.05^\circ\text{C}$  or better over the temperature range of interest. Heat exchange liquid is pumped through the exchanger from an external bath. The cell rests on a holder which may be rotated precisely through  $180^\circ$  to increase the instrument sensitivity by a factor of two if desired.

A top view of the cell is shown schematically in Fig. 41. It is cubical with a glass plane placed at a diagonal to the light beam. Solution and solvent are placed in the two compartments to form the prism and cause an angular displacement of the beam as it passes through the



Not to Proportions

Figure 41 Schematic drawing of optical components of the differential refractometer.



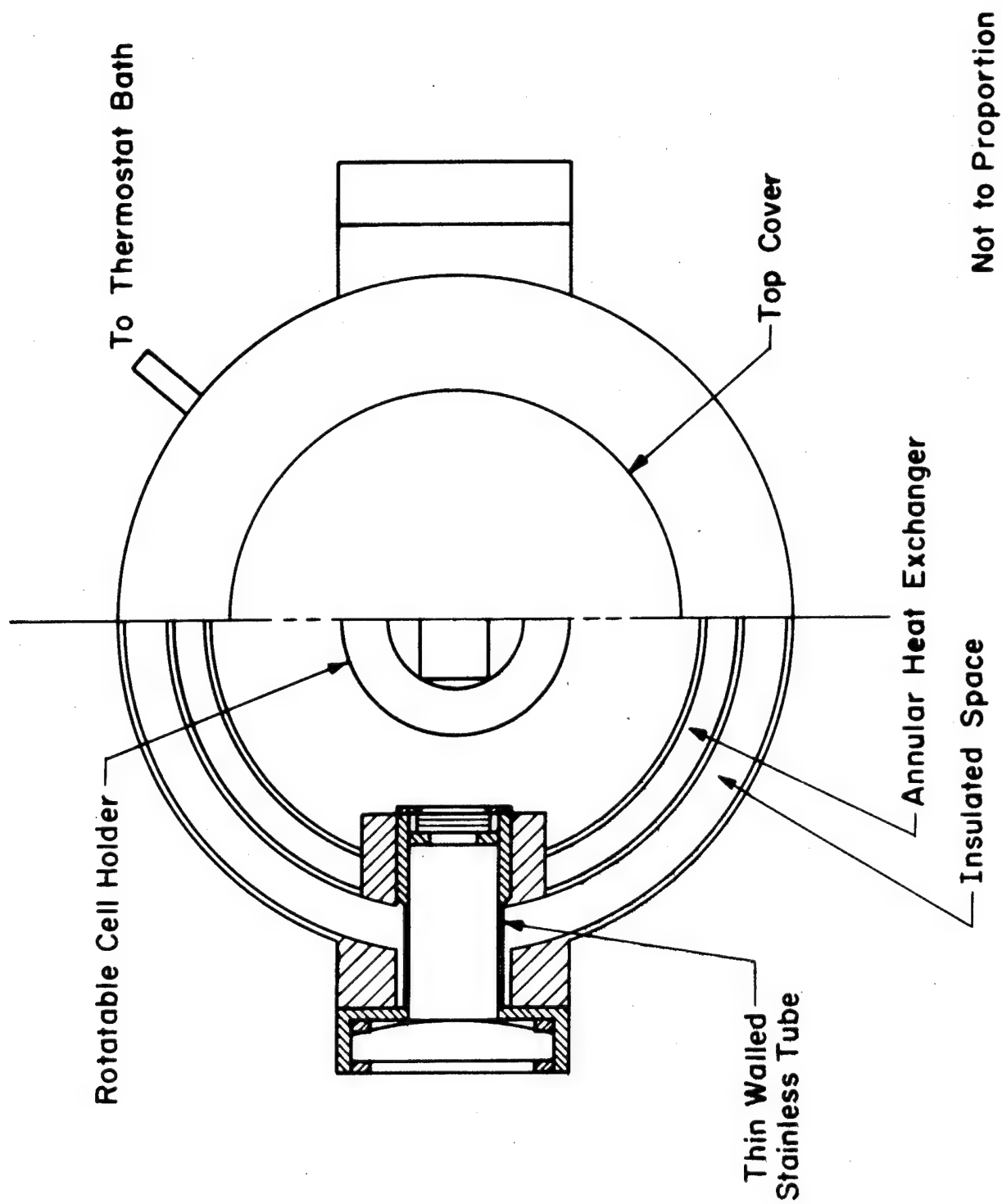


Figure 42 Schematic drawing of differential refractometer thermostat

cell. The two compartments are sealed in such a way that material transfer between them by "creeping" or evaporation of liquids is prevented.

### C. Data Analysis

The angular displacement experienced by the light beam has been analyzed by Brice and Halwer. The resulting relation for the displacement of the image is given by Eq. (114) provided the cell is not rotated.

$$\Delta n = \Delta d \left\{ k \left[ 1 \pm \frac{\Delta d}{2n_0 f^2} + 0 \left( \frac{\Delta d}{f} \right)^2 \right] \right\} \quad (114)$$

The sum of two relations like Eq. (114) with opposite signs for the second term on the rhs holds if the data are for a cell rotated through  $180^\circ$ . Here  $k$  is  $(\cot i)/f$ ,  $\Delta n$  is the refractive index difference between solution and solvent,  $\Delta d$  is the movement of the image caused by  $\Delta n$ ,  $i$  is the angle of the diagonal plate,  $f$  is the focal length of the lens and  $n_0$  is solvent refractive index. The  $\pm$  signs refer to reversal of solvent and solution in the two cell compartments. Eq. (114) predicts a linear dependence of  $\Delta n/\Delta d$  on  $\Delta d$  rather than the constant value for  $\Delta n/\Delta d$  that results when the  $\Delta d$  is measured for a cell rotated through  $180^\circ$ . For the cells being used (Brice-Phoenix Corp.),  $\cot i \approx 0.37$ . Thus,  $\Delta n/\Delta d$  is of the order  $0.37/520 = 0.71 \times 10^{-3}$  as  $\Delta d$  approaches zero. Eq. (114) predicts ca. 2% decrease in  $\Delta n/\Delta d$  by the time  $\Delta d = 10$  mm.

### D. Optical Performance

The image formed on the glass scale in the absence of the cell is a 1:1 magnification of the secondary slit image, and is thus ca. 0.05 mm wide. The introduction of the present cells, however, imposes a 4 mm aperture in the optical train and results in a broadening of the slit image and the separation of weak interference bands at the sides of the primary image. As a result, the image broadens to ca. 0.10 mm and becomes less distinct. This phenomenon can be altered by using cells with a larger aperture, and fabrication of such cells is currently being investigated. In the meantime, insertion of a double slit mark (see Fig. 41) immediately after the cell aids in formation of more distinct and somewhat narrower images, ca. 0.070 mm wide. If the ratio of the width between slits to the slit width is  $k$ , then there will appear  $(2k+1)$  images instead of one. Only the position of the central image is of interest, however, typically,  $k = 2$  or  $3$ . Slits with larger  $k$  result in too large a reduction in the intensity to be generally useful.

### E. Instrument Performance

The instrument has been calibrated with KCl:H<sub>2</sub>O and sucrose:H<sub>2</sub>O solutions. The results are given in Fig. 43.

The estimated error in measurement of  $\Delta d$  is ca.  $\pm 0.003$  mm or less. The largest source of error in the data is believed to be the calculated concentrations necessary for determination of  $\Delta n$ . Even so, the data are good to  $\pm 0.5\%$ , as may be seen in Fig. 43. This is probably typical of the instrument in normal use in that  $\Delta d$  measurement will usually be known to better precision than the corresponding concentrations. The line drawn in Fig. 42 gives a 2.8 percent reduction in  $\Delta n/\Delta d$  for  $\Delta d = 10$  relative to the value for  $\Delta d = 0$ , in fair agreement with the expected value. In addition, the initial value of  $\Delta n/\Delta d = 0.701 \times 10^{-3}$  is in satisfactory agreement with that estimated by  $(\cot i)/f$  since neither of the two parameters  $i$  and  $f$  are known with precision.

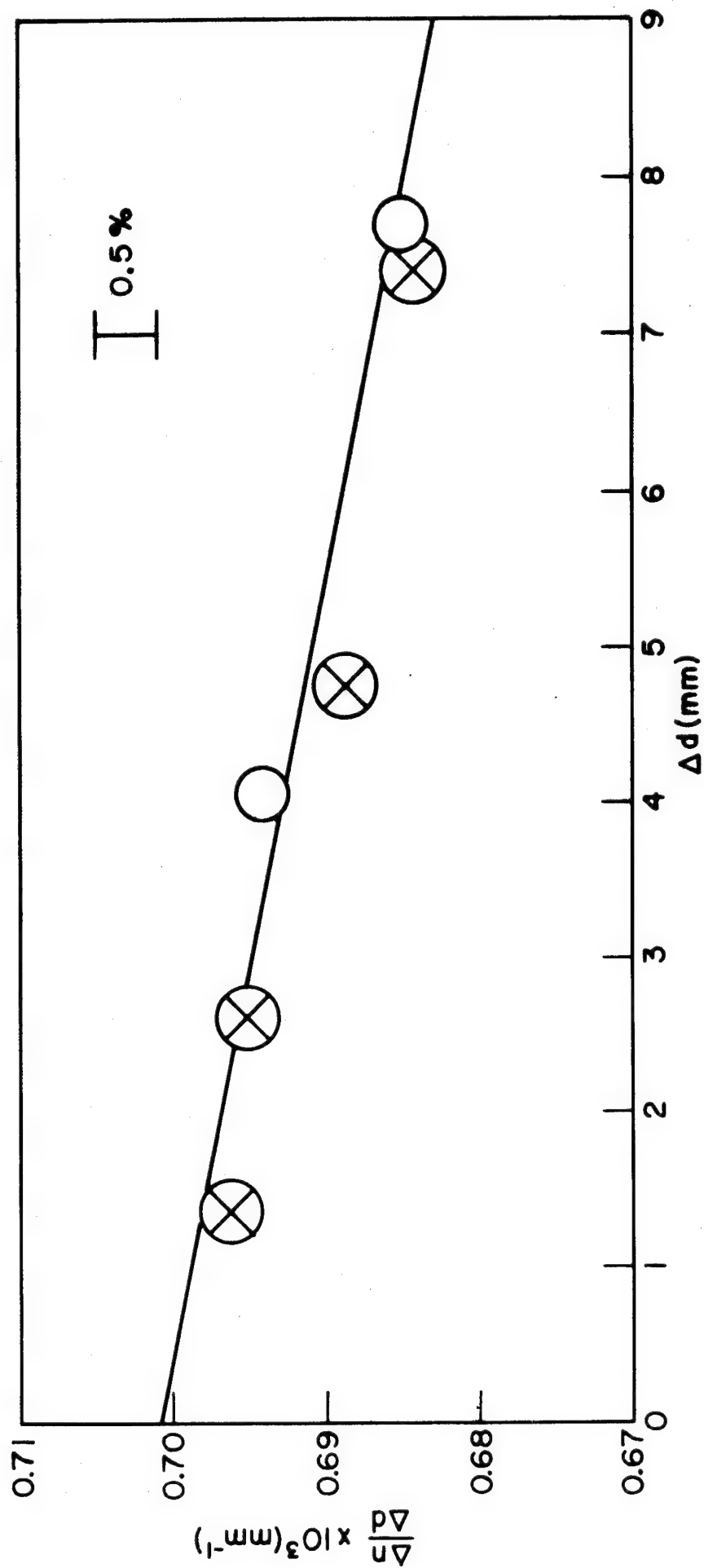


Figure 43 Calibration constant for differential refractometer: ○ KCl:H<sub>2</sub>O at 25°C; ⊗ sucrose:H<sub>2</sub>O at 25°C.

PART I - LIST OF REFERENCES

1. Orofino, T. A., Polymer 2, 305 (1961).
2. Fixman, M., J. Chem. Phys. 23, 1656 (1955).
3. Orofino, T. A., Polymer 2, 295 (1961).
4. Zimm, B. H., J. Chem. Phys. 14, 164 (1946).
5. Berry, G. C., Polymer, in press.
6. Berry, G. C., unpublished results.
7. Zimm, B. H., Stockmayer, W. H. and Fixman, M., J. Chem. Phys. 21, 1716 (1953).
8. Orofino, T. A. and Wenger, F., J. Phys. Chem. 67, 566 (1963).
9. Orofino, T. A. and Mickey, J. W., Jr., J. Chem. Phys. 38, 2512 (1963).
10. Ptitsyn, O. B., Zhur. Fiz. Khim. 29, 396 (1955).
11. Krigbaum, W. R. and Tremontozzi, Q. A., J. Polymer Sci. 28, 295 (1958).
12. Flory, P. J., "Principles of Polymer Chemistry", Cornell University Press, Ithaca, New York (1953).
13. Berry, G. C., Polymer Preprints, American Chemical Society 4, No. 2, 141 (1963).
14. Bianchi, U., J. Polymer Sci., in press.
15. Ciferri, A., J. Polymer Sci., in press.
16. Shultz, A. R. and Flory, P. J., J. Polymer Sci. 15, 231 (1955).
17. Bianchi, U. and Magnasco, V., J. Polymer Sci. 41, 177 (1959).
18. Ivin, K. J., Ende, H. A. and Meyerhoff, G., Polymer 3, 129 (1962).
19. Crescenzi, V. and Flory, P. J., J. Am. Chem. Soc. 86, 141 (1964).
20. Ciferri, A., Trans. Faraday Soc. 57, 846 (1961).
21. Ciferri, A., Hoeve, C. A. J. and Flory, P. J., J. Am. Chem. Soc. 83, 1269 (1961).
22. Williams, M. L., J. Appl. Phys. 29, 1395 (1958).
23. Fox, T. G. and Loshaek, S., J. Polymer Sci. 15, 371 (1955).

24. Tobolsky, A. V., "Properties and Structure of Polymers", John Wiley and Sons, Inc., New York, 1960 (p. 312).
25. Flory, P. J. and Fox, T. G., J. Am. Chem. Soc. 73, 1904 (1951).
26. Schulz, G. V. and Baumann, H., makromol. Chem. 60, 120 (1963).
27. Fox, T. G., and Flory, P. J., J. Am. Chem. Soc. 73, 1915 (1951).
28. Kurata, M. and Yamakawa, H., J. Chem. Phys. 29, 311 (1958).
29. Ptitsyn, O. B. and Eizner, Yu. E., Zhur. Fiz. Khim. 32, 2464 (1958).
30. Flory, P. J., Ciferri, A. and Chiang, R., J. Am. Chem. Soc. 83, 1023 (1961).
31. Ciferri, A., Trans. Faraday Soc. 57, 853 (1961).
32. Mark, J. E. and Flory, P. J., J. Am. Chem. Soc. 86, 138 (1964).
33. Stockmayer, W. H. and Fixman, M., J. Polymer Sci. Part C, 1, 137 (1963).
34. Flory, P. J., J. Chem. Phys. 17, 303 (1949).
35. Kurata, M., Stockmayer, W. H. and Roig, A., J. Chem. Phys. 33, 151 (1960).
36. Cragg, L. H. and Simkins, J. E., Can. J. Research, B27, 961 (1949).
37. Berry, G. C., Private communication.
38. Fox, T. G., Polymer 3, 111 (1962).
39. Fox, T. G., and Flory, P. J., J. Am. Chem. Soc. 73, 1909 (1951).
40. Ciferri, A., Hoeve, C. A. J. and Flory, P. J., J. Am. Chem. Soc. 83, 1015 (1961).
41. Flory, P. J., Crescenzi, V. and Mark, J. E., J. Am. Chem. Soc. 86, 146 (1964).
42. Ptitsyn, O. B., Vysokomol. Soedin. 4, 1445 (1962).
43. Krigbaum, W. R., Mark, F., Hunter, W. L. and Ciferri, A., makromol. Chem., 65, 101 (1963).
44. Benoit, H., private communication.

45. Casassa, E. F., J. Chem. Phys., 37, 2176 (1962).
46. Wyman, D. P., Altares, T., Allen, V. R. and Meyersen, K., to be published.
47. McMillan, W. G. and Mayer, J. E., J. Chem. Phys. 13, 276 (1945).
48. Casassa, E. F. and Markovitz, H., J. Chem. Phys. 29, 493 (1958).
49. Casassa, E. F., J. Chem. Phys. 31, 800 (1959).
50. Flory, P. J., J. Chem. Phys. 17, 1347 (1949).
51. Flory, P. J. and Krigbaum, W. R., J. Chem. Phys. 18, 1086 (1950).
52. Flory, P. J., J. Chem. Phys. 13, 453 (1945).
53. Isihara, A. and Koyama, R., J. Chem. Phys. 25, 712 (1956).
54. Carpenter, D. K. and Krigbaum, W. R., J. Chem. Phys. 28, 513 (1958).
55. Stockmayer, W. H., J. Chem. Phys. 18, 58 (1950).
56. Reiss, C. and Benoit, H., Compt. rend. 253, 268 (1962).
57. Okada, R., Toyoshima, Y. and Fujita, H., kromol. Chem. 59, 137 (1963).
58. Benoit, H., J. Polymer Sci. 11, 507 (1953).
59. Kuhn, W., Kolloid Z. 68, 2 (1934).
60. Albrecht, A. C., J. Chem. Phys. 33, 151 (1960).
61. Orofino, T. A. and Flory, P. J., J. Chem. Phys. 26, 1067 (1957).
62. Outer, P., Carr, C. I. and Zimm, B. H., J. Chem. Phys. 18, 830 (1950).
63. Berry, G. C., Long, V. C., and Hobbs, L. M., Polymer 5, 31 (1964).
64. Orofino, T. A. and Wenger, F., J. Chem. Phys. 35, 532 (1961).
65. Stockmayer, W. H. and Fixman, M., Ann. N. Y. Acad. Sci. 57, 334 (1953).
66. Grimley, T. B., Trans. Farad. Soc. 55, 681 (1954).
67. Casassa, E. F. and Orofino, T. A., J. Polymer Sci. 35, 553 (1959).
68. Stockmayer, W. H., J. Polymer Sci. 15, 595 (1955).

69. Fixman, M., J. Chem. Phys. 36, 3123 (1962).
70. Schulz, G. V. and Kirste, R., Z. physik. Chem. (Frankfurt), 30, 171 (1961).
71. Kirkwood, J. G. and Riseman, J., J. Chem. Phys. 16, 565 (1948).
72. Debye, P. and Bueche, A. M., J. Chem. Phys. 16, 573 (1948).
73. Brinkman, H. C., Physica, 13, 447 (1947).
74. Zimm, B. H., J. Chem. Phys. 24, 269 (1956).
75. Timmermans, J., Physico-Chemical Constants of Pure Organic Compounds, Elsevier Publishing Co., Inc., New York (1950).
76. Krigbaum, W. R. and Carpenter, D. K., J. Phys. Chem. 59, 1166 (1955).
77. Partington, J. R., An Advanced Treatise on Physical Chemistry, Longmans, Green & Co., London, Vol. 2, pp. 173-174, (1951).
78. Zimm, B. H. and Crothers, D. M., Proc. Nat. Acad. Sci., U.S. 48, 905 (1962).
79. Trevena, D. H., Static Fields in Electricity and Magnetism, Butterworths, London (1961).
80. Oka, S., in Rheology, Vol. 3 (F. R. Eirich, ed.), Academic Press, New York (1960).



## PART II - FLOW IN CONCENTRATED POLYMER SYSTEMS

### I. The Dependence of the Zero Shear Melt Viscosity and the Related Friction Coefficient and Critical Chain Length on Measurable Characteristics of Chain Polymers\* — T. G Fox and V. R. Allen

#### A. Introduction

Strong confirmation of the equation of F. Bueche for the zero shear viscosity of short polymer chains<sup>1,2</sup>

$$\eta = \left[ \left( \frac{N_0}{6} \right) \left( \frac{\overline{s_0^2}}{M} \right) \frac{Z_w}{v} \right] \zeta \quad (115)$$

was provided in an earlier discussion (ASD-TR 61-22, Part III) by the successful computation of this coefficient for short chain polystyrenes ( $Z \leq Z_c$ ) from the independently measured values of the pertinent molecular parameters. (Here,  $Z_w$  denotes the weight average number of chain atoms per polymer molecule;  $v$  is the specific volume of polymer; and  $\zeta$  is the frictional coefficient per chain atom.) Conversely, the theoretical equation facilitates precise determination of  $\zeta$  from viscosity data and of the critical chain length  $Z_c$  above which the Bueche equation for short chains fails.

A general equation for  $\eta$  (obtained by simultaneous solution of Eq. (115) and the empirical flow law,  $\eta = K_T Z_w^{3.4}$ , for long chains) applicable to polymer homologs of any length was also proposed

$$\eta = \frac{N_0}{6} \left[ \left( \frac{\overline{s_0^2}}{M} \right) \frac{Z_c}{v} \right] \left( \frac{Z_w}{Z_c} \right)^\alpha \cdot \zeta \quad (116)$$

$$\alpha = 3.4 \text{ for } Z_w \geq Z_c$$

$$\alpha = 1.0 \text{ for } Z_w \leq Z_c$$

Alternatively, but defining  $X = \left( \frac{\overline{s_0^2}}{M} \right) \frac{Z_w}{v}$  and  $X_c = \left( \frac{\overline{s_0^2}}{M} \right) \frac{Z_c}{v}$ , we may write Eq. (116) in the form

$$\eta = \frac{N_0}{6} X_c \left( \frac{X}{X_c} \right)^\alpha \cdot \zeta \quad (117)$$

$$\alpha = 3.4 \text{ for } X \geq X_c$$

$$\alpha = 1.0 \text{ for } X \leq X_c$$

---

\* This work was additionally supported in part by the Office of Naval Research under Contract No. Nonr 2693(00).

The values of  $Z_c$  and  $X_c$  (and of  $Z_e$  below) and, for sufficiently long chains, of  $(s_0^2/M)$ ,  $v$ , and  $\zeta$  are, at a given temperature, expected to be constants characteristic of the polymer type but independent of  $Z$ . The dependence, if any, of  $Z_c$ ,  $X_c$  and  $Z_e$  on chain structure and on the reduced chain dimensions is unknown.

Expressions virtually identical with Eqs. (116) and (117) may also be deduced by simultaneous solution of Eq. (115) and Bueche's theoretical equation for the zero shear viscosity of long chains

$$\eta = \frac{1}{8} \frac{N_0^2}{\sqrt{6}} \left[ \left( \frac{s_0^2}{M} \right)^{2.5} \frac{Z^{3.5}}{\sqrt{m_a} v^2 Z_e^2 f(\lambda)} \right] \zeta, \quad Z \gg Z_e \quad (118)$$

Here

$$Z_e \sqrt{f(\lambda)} = \left[ \frac{6 N_0^2 m_a (s_0^2/M)^3 Z_c^5}{64 v^2} \right]^{1/4} \quad (119)$$

Evidence was presented in the preceding report suggesting the applicability of Eq. (119) for polystyrene.

The  $\eta$ - $T$ - $Z$  data for polystyrene fractions and blends are represented by Eq. (116). The friction coefficient is given approximately by a W-L-F type equation<sup>3,4</sup>  $\log \zeta = \log \zeta_g - \frac{c_1(T-T_g)}{c_2 + T - T_g}$  with<sup>5</sup>

$$\frac{1}{T_g} = \frac{1}{T_{g,\infty}} + \frac{K_g}{M_n} \quad (120)$$

where  $T_{g,\infty}$  and  $K_g$  are constants characteristic of the given homologous polymer series.

To provide additional tests of Bueche's theories, and to obtain values of  $Z_c$  (also  $X_c$  and  $Z_e$ ) and of  $\zeta$  for many different polymers, we now fit to the above equation available  $\eta$ - $Z$ - $T$  data for various well defined polymeric systems. Simple equations of broad applicability, relating  $Z_c$ ,  $\zeta$ , and  $\eta$  to experimentally assessable parameters, for long and short chain linear polymers, for branched polymers, and for polymer-diluent mixtures are thereby established.

## B. The General Plan

Here we propose to fit Eq. (116) to available viscosity data for different polymeric systems, and to evaluate  $Z_c$  and  $\zeta$  from data on

the measurable molecular characteristics  $Z_w$ ,  $v$ , and  $\left(\frac{s_0^2}{M}\right)$ . Tests of the applicability of Eq. (116) will be the ability to reproduce the  $\eta$ - $Z$ - $T$  data satisfactorily, and agreement between the values of  $\zeta$  derived here and the corresponding literature values obtained from viscoelastic relaxation spectra. Finally we seek expressions of general applicability relating  $\zeta$  and  $Z_c$  (hence  $X_c$  and  $Z_e$ ) to other readily measured characteristics of the structure and composition of the macromolecular system.

The computation of  $\zeta$  by means of Eq. (115) from viscosity data for  $Z < Z_c$  is straightforward. In this range, generally,  $\zeta$  increases with  $Z_n$  towards an asymptotic limit which in some instances (coincidentally) may be approached only in the vicinity of  $Z_c$ . Unfortunately, positive deviations from Eq. (116) are generally found in this transition region, rendering difficult the precise determination of the limiting value of  $\zeta$  for long chains. Of course, it can be determined readily by Eq. (116) from  $\eta$  at  $Z > Z_c$  provided the value of  $Z_c$  is known. Hence, we undertake first, in the following section, to evaluate  $Z_c$  for different polymeric materials of interest.

### C. The Critical Parameters $Z_c$ and $X_c$

Two methods (illustrated by Figs. 44 and 45) are used to evaluate  $Z_c$  for the four homopolymers in Table XVIII for which most extensive  $\eta$ - $M$  data are available.

The first method of determining  $Z_c$  from viscosity data is based on Eq. (116). Writing Eq. (116) for a reference polymer of  $Z^* > Z_c$  and of viscosity  $\eta^*$ , and for a polymer of  $Z < Z_c$  of viscosity  $\eta$  and rearranging, we have:

$$3.4 \log Z^* - \log \eta^* + \log \eta/Z = 2.4 \log Z_c - \log (\zeta^*/\zeta) \quad (121)$$

A plot of the left side of Eq. (121) vs.  $\log Z$ , for a series of polymers of  $Z < Z^*$ , will be a horizontal line with ordinate equal to  $2.4 \log Z_c$ , if  $Z < Z_c$  and  $\zeta = \zeta^*$ . For  $Z > Z_c$ , higher values of the ordinate, increasing with increasing  $Z$  will obtain; below a certain range,  $\zeta^*/\zeta$  will be  $> 1$ , and lower values of the ordinate will result with decreasing  $Z$ . The value of  $Z_c$  can be computed from the magnitude ( $2.4 \log Z_c$ ) of the intermediate horizontal line; as a further check, the line representing the ordinate for  $Z > Z_c$ , of slope 2.4, should intersect the horizontal line at  $Z = Z_c$ .

Plots conforming to Eq. (121) are shown in Fig. 44 for several polymers for which the appropriate data are available. Generally, a value of  $Z_c$  (Table XVIII) can be determined within  $\pm 10$  percent from the height of the horizontal region of the plot, or, with less precision, from the point of intersection of this line with the line of positive slope obtained for higher molecular weights.

A second method is based on the use of empirical expressions<sup>30</sup> for the dependence of the viscosity-temperature coefficient on  $T$  and  $Z_n$

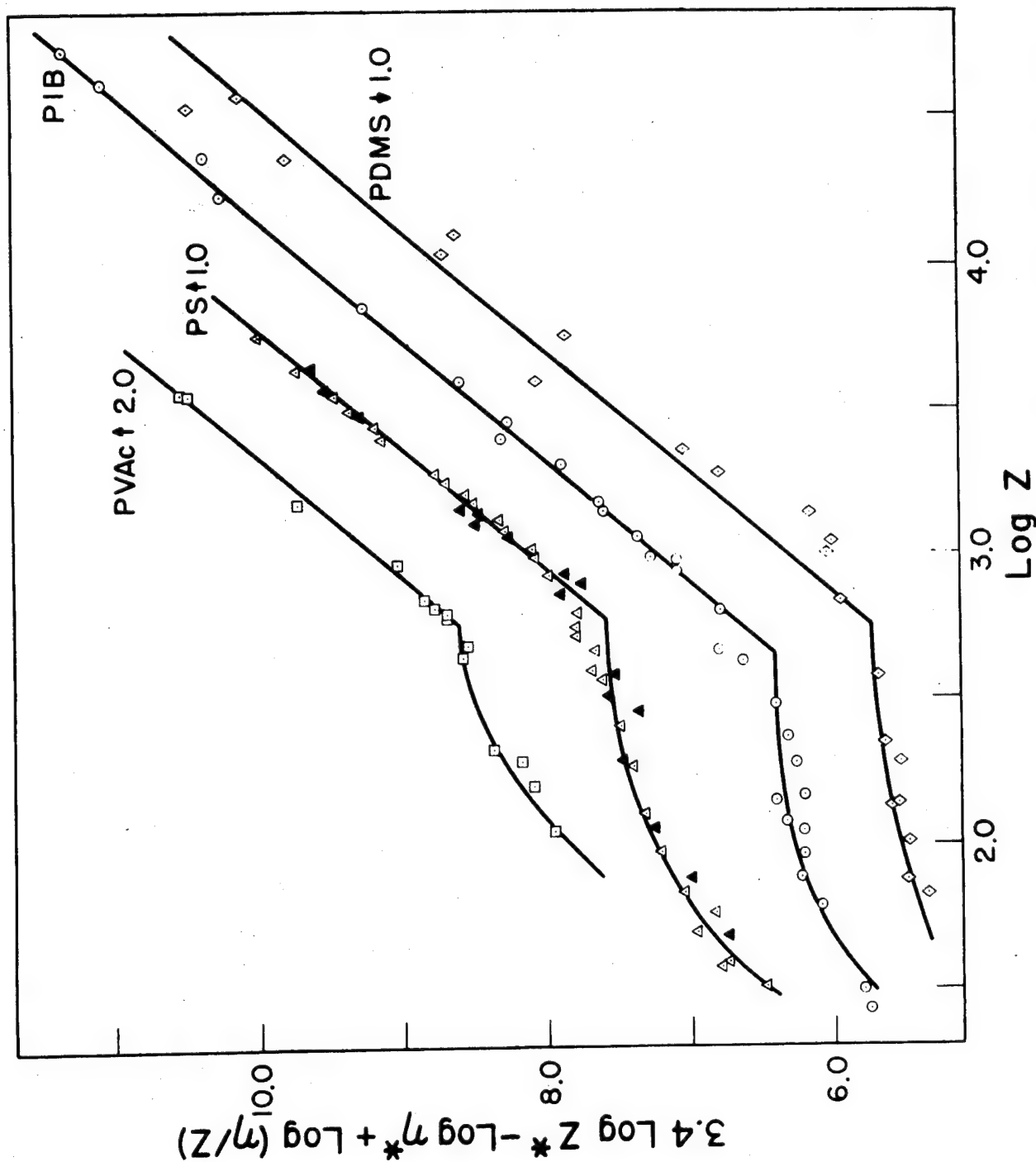


Figure 44 Reduced viscosity function  $3.4 \log Z^* - \log \eta^* + \log (\eta/Z)$  versus  $\log Z$  for anionic polystyrene  $\blacktriangle$  (see ASD-TR 61-22, Part III), free-radical polystyrene<sup>6,7</sup>  $\triangle$ , polyvinyl acetate<sup>8</sup>  $\square$ , polyisobutylene<sup>9</sup>  $\circ$ , and polydimethyl siloxane<sup>10-12</sup>  $\diamond$ . (The arrows designate shifts in the ordinate scale, of the indicated magnitude.)

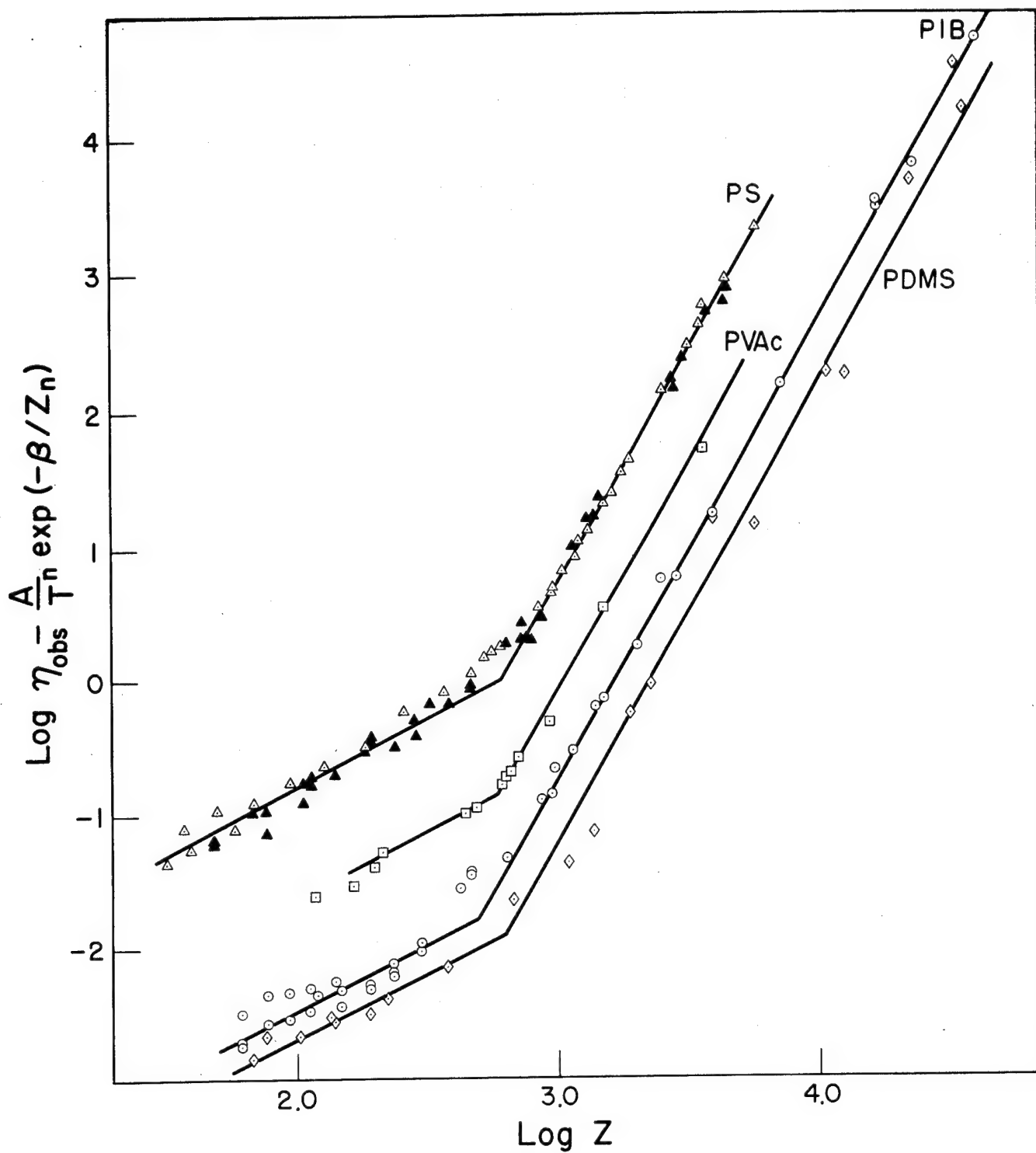


Figure 45 Reduced viscosity function  $\log \eta - A/T_n \exp(-\beta/Z_n)$  versus  $\log Z$  for polyisobutylene<sup>9</sup>  $\circ$ , polydimethyl siloxane<sup>10-12</sup>  $\diamond$ , polyvinyl acetate<sup>8</sup>  $\square$ , anionic  $\blacktriangle$  and free-radical  $\triangle$  polystyrene<sup>6,7</sup>.

Table XVIII

Values of  $Z_c$  and of  $X_c$  for Various Polymers

Polymer	$Z_c^a$	$T^\circ C$	$-100 \left[ \frac{d \ln \left( \frac{\overline{s_0^2}}{M_v} \right)}{dT} \right] \% / 100^\circ b$	Computation of $X_c$	
				$\left( \frac{\overline{s_0^2}}{M} \right) \times 10^{-18} c$	$X_c \cdot 10^{-15} d$
			<u><math>Z_c</math> Values from Fig. 44</u>		
Polyisobutylene	460	25-217°	5 <sup>19,20</sup>	10.5	4.3/20° <sup>5</sup>
Polydimethyl siloxane	630	25°	7 <sup>21</sup>	8.9	5.4/20° <sup>5</sup>
Polystyrene	600	160-217°	16 <sup>22</sup>	7.8	4.7/160° <sup>6,7</sup>
Polyvinyl acetate	570	120-160°	30 <sup>23-26</sup>	6.8	4.4/120° <sup>28</sup>
			<u><math>Z_c</math> Values from log <math>\eta</math> vs. log <math>Z</math></u>		
Polyethylene	275	140°	17 <sup>20</sup>	18.8	4.1/140° <sup>5</sup>
Polydecamethylene sebacate	290	109°	--	17 <sup>27</sup>	4.9/25° <sup>28</sup>
Poly- $\epsilon$ -caproamide	324	253°	--	15.5 <sup>27</sup>	5.0/25°
Polyoxypropylene glycol	400	25°	--	8-11 <sup>14,27</sup>	(3.2-4.4)/ 25°
Polydecamethylene adipate	280	109°	--	10 <sup>27</sup>	2.7/25° <sup>29</sup>
Polymethyl methacrylate	210	140°	6 <sup>19</sup>	6.2	1.5/140° <sup>5</sup>

<sup>a</sup>The first four values are from Fig. 44. The remainder are from ref. 13, except for polyoxypropylene glycol<sup>12</sup> and polyethylene (estimated).<sup>15-18</sup>

<sup>b</sup>Values of the temperature dependence of  $(\bar{s}_0^2/M)$  for polyisobutylene, polyethylene, polydimethyl siloxane are based on relatively precise modulus-temperature measurements;<sup>20,21</sup> for the others "best" values were computed from  $(K/\Phi)^{2/3}/6$  using  $\Phi = 2.1 \times 10^{21}$  and values of  $K$  at different temperatures taken, or estimated from the indicated literature. The estimate for polyoxypropylene glycol is based, in part, on values<sup>27</sup> for polyethylene oxide and polypropylene oxide. The v-T data were taken from the indicated sources in column 6 (see d below).

<sup>c</sup>Computed at temperature noted in column 6; source references given here or in column 4.

<sup>d</sup>Computed from  $(\bar{s}_0^2/M) \cdot Z_c/v$ , with values of  $v$  from the indicated literature. For poly- $\epsilon$ -caproamide and polyoxypropylene glycol  $v$  was taken as unity.

to "correct" the observed viscosities for the effects of change in density with changes in these variables. Plots of the "corrected"  $\log \eta$  vs.  $\log Z$  should then yield two straight lines of slope 1.0 and 3.4, intersecting at  $Z = Z_c$ . For this purpose we employ an empirical expression of the form

$$\log \eta_{\text{corrected}} = \log \eta_{\text{obs}} - \frac{A}{T^n} e^{-\beta/Z_n} \quad (122)$$

Here,  $A$ ,  $n$ , and  $\beta$  are characteristic of the homologous series. Data for various polymers treated in this way are plotted in Fig. 45; in each case, the data could be represented by straight lines of slope 1 and 3.4, with the point of intersection defining  $Z_c$ . The numbers thus obtained agree, within the estimated experimental uncertainty ( $\pm 10$  percent), with the corresponding values obtained in Fig. 44.

The values of  $Z_c$  obtained in Fig. 44 are lower than the corresponding numbers determined earlier from the same data<sup>8,13</sup>. Previously, lines of slope greater than one were employed to fit the data for  $\log \eta$  vs.  $\log Z$  in the low molecular weight range; i.e., the point of intersection with the line for the high molecular weight range was influenced by the rate of decrease of  $\zeta$  with decreasing  $Z_n$ . We believe the present method, wherein compensation is made for this change of  $\zeta$  with  $Z$ , yields values of  $Z_c$  of more theoretical significance.

Values of  $Z_c$  for six other polymers are also listed in Table XVIII. Those numbers, determined from log-log plots of  $\eta$  vs.  $Z$ , would be little changed (except, perhaps, for poly- $\epsilon$ -caproamide) if the data were plotted by the methods of Figs. 44 or 45, since the coefficient ( $d \ln \eta / dT$ ) is relatively small and insensitive to  $Z$ , and the slope of  $\log \eta$  vs.  $\log Z$  for  $Z < Z_c$  is not markedly different from unity. The data, however, are not sufficiently extensive to define  $Z_c$  within the precision ( $\pm 10$  percent) cited above. For poly-(methyl methacrylate) the value of  $Z_c$  is extrapolated from that found for 25% solutions in diethyl phthalate<sup>31</sup>.

Differences in excess of the above uncertainties exist between values of  $Z_c$  for different polymers in Table XVIII. For example,  $Z_c$  values for polydimethyl siloxane, polystyrene, and polyvinyl acetate (ca. 600) are more than twice that (ca. 280) found for polyethylene and for the two paraffin-like polyesters.

Conceivably, differences in the values of  $Z_c$  for different polymers are related to differences in some measurable characteristics of their chain structures. In seeking such a relation, we compute values of  $X_c = (\bar{s}_0^2/M)Z_c/v$  for different polymers. For the first seven polymers in Table XVIII the values of  $X_c$  agree, within the estimated experimental uncertainty ( $\pm 15$  percent for the first four and  $\pm 20$  percent for the next

three)\* and average  $(4.7 \pm 0.4) \times 10^{-15}$ ; furthermore, there is no discernible trend in the values of  $X_c$  with decreasing  $(\overline{s_0^2}/M)$ , though values of the latter vary by nearly a factor of three. Lower values of  $X_c$  are computed for the last three polymers; these values are, however, less certain. Although more precise studies may establish variations of  $X_c$  with structure, for the present we hypothesize that  $X_c$  is, approximately at least, a universal constant for flexible chain macromolecular systems: i.e., that

$$X_c = \left( \frac{\overline{s_0^2}}{M} \right) \frac{Z_c}{v} = 4.7 \times 10^{-15} \quad (123)$$

We can now rewrite Eq. (117) as follows:

$$\eta = 4.8 \times 10^8 \left( \frac{X}{4.7 \times 10^{-15}} \right)^\alpha \zeta \quad (124)$$

$$\alpha = 3.4 \text{ for } X \geq 4.7 \times 10^{-15}$$

$$\alpha = 1.0 \text{ for } X \leq 4.7 \times 10^{-15}$$

It appears that for a homologous series,  $\eta$  is proportional to  $X$  till  $X$  attains the critical value  $X_c$ , the same for all polymer systems, and thereafter, abruptly, for longer chains,  $\eta$  is proportional to  $X^{3.4}$ .

Eq. (123) is useful for estimating  $Z_c$  from molecular parameters when the necessary  $\eta$ - $Z$  data for its direct evaluation are not available. This also makes possible, in such instances, the computation of  $\zeta$  by (124) from a measurement of  $\eta$  for a single long chain sample.

Assuming constancy of  $X_c$ , we obtain by differentiation of Eq. (123) an equation for the temperature dependence of  $Z_c$

\* On the assumption of a precision of  $\pm 10$  percent for  $Z_c$  and for  $(\overline{s_0^2}/M)$ , the precision for  $X_c$  is estimated as ca.  $\pm 15$  percent for the first four polymers in Table XVIII. Appreciable additional error may exist in the estimate of  $Z_c$  for polyethylene and poly-(methyl methacrylate), of  $v$  for poly( $\epsilon$ -caproamide) and for poly-(oxypropylene glycol), and of  $\overline{s_0^2}/M$  for the latter polymer and for poly-(decamethylene adipate). Errors may be introduced in three instances by the computation of  $X_c$  using values of  $\overline{s_0^2}/M$  determined at  $25^\circ$  and of  $Z_c$  determined at higher temperatures; on the other hand, values of  $Z_c$  insensitive to temperature were found for other polymers for which extensive  $\eta$ - $Z$ - $T$  data exist.



$$\frac{d \ln Z_c}{dT} = \frac{d \ln v}{dT} - \frac{d \ln(\overline{s_0^2}/M)}{dT} \quad (125)$$

For most polymers the increase in  $v$  with temperature is about 5 to 10 percent per 100°C, and  $d \ln(\overline{s_0^2}/M)/dT$  is negative. The latter coefficient, however, may be zero or even positive. Values of  $-d \ln(\overline{s_0^2}/Mv)/dT$  (in Table XVIII) correspond to an increase in  $Z_c$  of about 5 to 30 percent per 100°, i.e., to an "apparent heat of association" of  $10^2$  to  $10^3$  cal/mole. Precise determination (within  $\pm 10$  percent) of  $Z_c$  from  $\eta$ - $Z$  plots at two temperatures have been made in only a few cases and then, except for polyisobutylene, only for a 50° interval. In no case do such data indicate a temperature coefficient for  $Z_c$  in excess of the corresponding value indicated in the table.

In the next section we consider the relation between values of  $\zeta$  deduced by application of Eq. (116) to data for various polymers with corresponding values determined from the observed relaxation spectra. We shall then return to further consideration of the influence of chain-coil dimensions and density on the values of  $\eta$ ,  $X_c$ , and  $Z_e$ .

#### D. The Frictional Coefficient Per Chain Atom, $\zeta$

We now compute by Eq. (116) values of  $\zeta$  for various polymers from available  $\eta$ - $T$ - $Z$  data and values of  $\overline{s_0^2}/Mv$  (from the numbers in Table XVIII). The results, represented as the open symbols in the plot of  $\log \zeta$  vs.  $T - T_g$  in Fig. 46, are in good agreement with the corresponding measures of  $\zeta$  (solid symbols in Fig. 46) determined independently<sup>32</sup> from the observed viscoelastic relaxation spectra and application of the Rouse theory<sup>34</sup>. This agreement is again strong evidence for the validity of Bueche's theoretical Eq. (116) for the zero shear viscosity of short chains, and of the empirical extension Eq. (116), for long chains.

In a later section we shall seek an empirical relationship for predicting  $\zeta$  for different polymer systems from other measurable structurally dependent characteristics of the system. We now return to the influence of chain dimensions and density on  $\eta$ ,  $Z_c$ ,  $X_c$ , and  $Z_e$ .

#### E. Effect of Branching and of Diluent

The quantity  $(\overline{s_0^2}/M)(Z/v)$  designated here as  $X$  arises in the derivation<sup>1,2</sup> of Eq. (115) in the computation of the product of the moment of inertia of the average polymer coil with the number of chains per unit volume. This suggests that for branched polymers, where the mean square radius of gyration is smaller by a factor  $g$  than that,  $(\overline{s_0^2}/M)_\ell$ , of the corresponding linear polymer, and in the presence of a diluent, where the volume fraction of polymer is  $\phi_1$  and the partial specific volume is  $\overline{v}_1$ , we should expect

$$X = \left[ \left( \frac{\overline{s_0^2}}{M} \right)_\ell \frac{Zg\phi_1}{\overline{v}_1} \right].$$

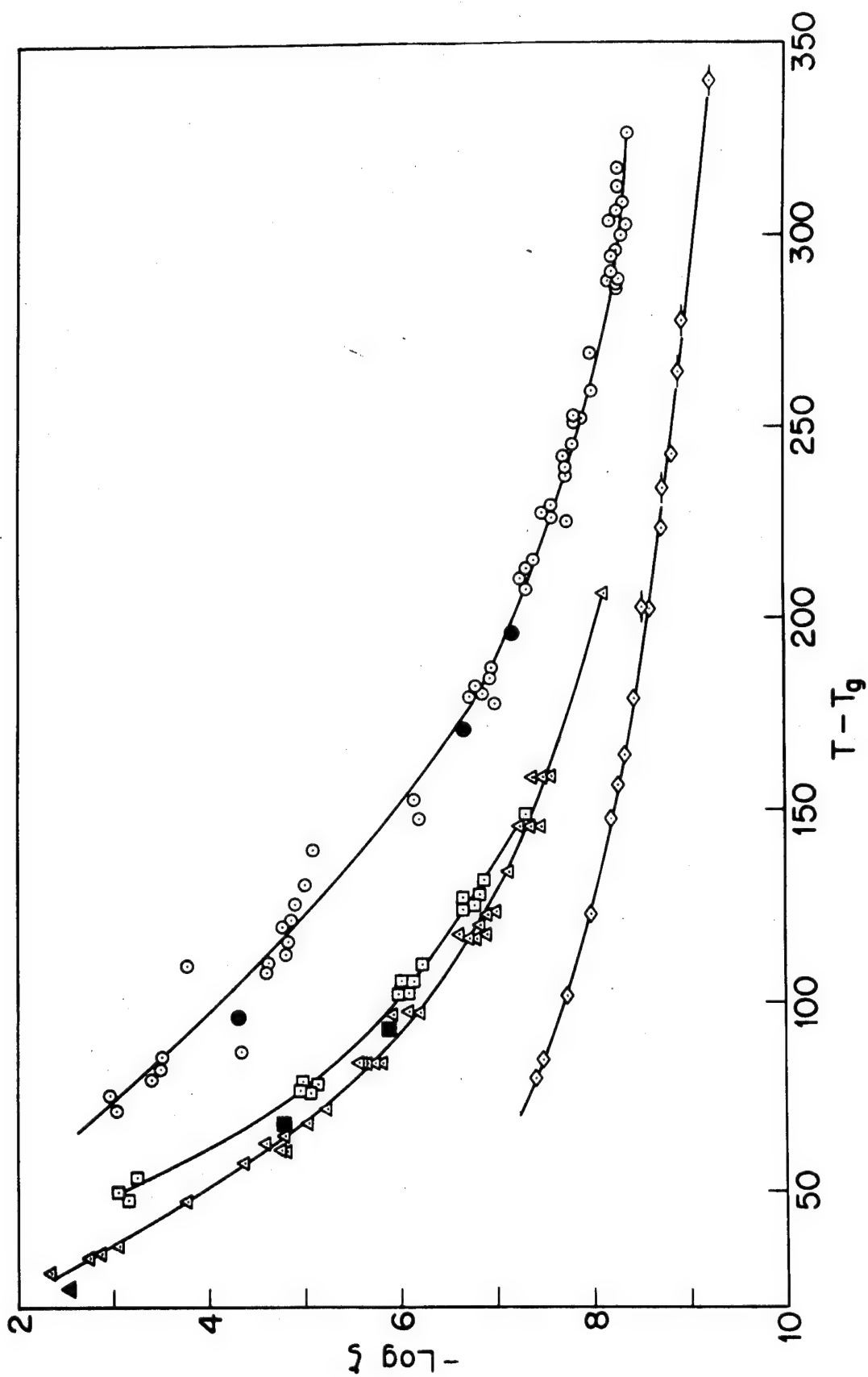


Figure 46  $-\log \zeta$  versus  $(T - T_g)$  for polyisobutylene<sup>9</sup> ○, polyvinyl acetate<sup>8</sup> □, polystyrene<sup>6,7</sup> △, and polydimethyl siloxane<sup>10-12</sup> ◇. Corresponding values of  $\log \zeta$  from relaxation spectra<sup>22,33</sup> are plotted as filled symbols.

Inserting this in Eq. (116), we get

$$\eta = \frac{N_0}{6} \left( \frac{\overline{s_0^2}}{M} \right)_\ell \frac{(g\phi_1 Z)}{\overline{v}_1} \zeta; X \leq 4.7 \times 10^{-15} \quad (125)$$

$$\eta = \frac{N_0}{6X_c^{2.4}} \left[ \left( \frac{\overline{s_0^2}}{M} \right)_\ell \frac{1}{\overline{v}_1} \right]^{3.4} (g\phi_1 Z)^{3.4} \cdot \zeta; X \geq 4.7 \times 10^{-15} \quad (126)$$

$$g\phi_1 Z_c = \frac{4.7 \times 10^{-15} \overline{v}_1}{\left( \frac{\overline{s_0^2}}{M} \right)_\ell}$$

Of course,  $\zeta$  may also be affected by branching or the addition of diluent but the effect should be separable from that on  $X$ .

Data for linear and branched poly- $\epsilon$ -caprolactam<sup>35</sup> plotted in Fig. 47 as  $\log \eta$  vs.  $\log (gZ)$ , where  $g = (3\overline{y}_w/p\overline{y}_n) - (2\overline{y}_z/p^2\overline{y}_n^2)$  for these star-type branched polymers<sup>36</sup> of functionality  $p$ , coincide (except at the lowest chain lengths), in accord with the above suggestion. Here  $\overline{y}_z$ ,  $\overline{y}_w$ , and  $\overline{y}_n$  are the "z", weight-, and number-average degrees of polymerization, respectively.

Data for polystyrene-dibenzyl ether mixtures<sup>37</sup> are plotted in Fig. 48 as  $\log \eta$  vs.  $\log \phi_1 Z$ . At each fixed value of  $\phi_1$ , the values of long  $\eta$  are represented by two intersecting lines with the family of lines at different  $\phi_1$ , displaced vertically from one another, also in accord with the above equations. The shift to lower  $\eta$  with decreasing  $\phi_1$  reflects the decrease in  $\zeta$  on the addition of diluent. More comprehensive evidence on the effect of branching and of diluent on  $\eta$  will be presented elsewhere<sup>23,37</sup>.

#### F. The Critical Chain Entanglement Length, $Z_e$

The observed dependence of  $\eta$  on  $gZ$  for short chains and on  $(gZ)^{3.4}$  for long chains, for linear ( $g=1$ ) and branched ( $g<1$ ) homologs is in accord with Bueche's theoretical Eqs. (115) and (118), and with his recent extension of these to branched chains<sup>38</sup>. A more critical test of Eq. (118) requires an independent measure of  $f(\lambda)$ , the "interchain slippage" parameter, and of  $Z_e$ , the "average number of chain atoms between coupling entanglements". Values of the latter (designated as  $\Lambda$ ) computed by rubber elasticity theory from the pseudo-equilibrium modulus of compliance, or from the maximum  $J_m''$  of the loss compliance, have been tabulated for a number of polymers<sup>39</sup>. Comparison of these values with

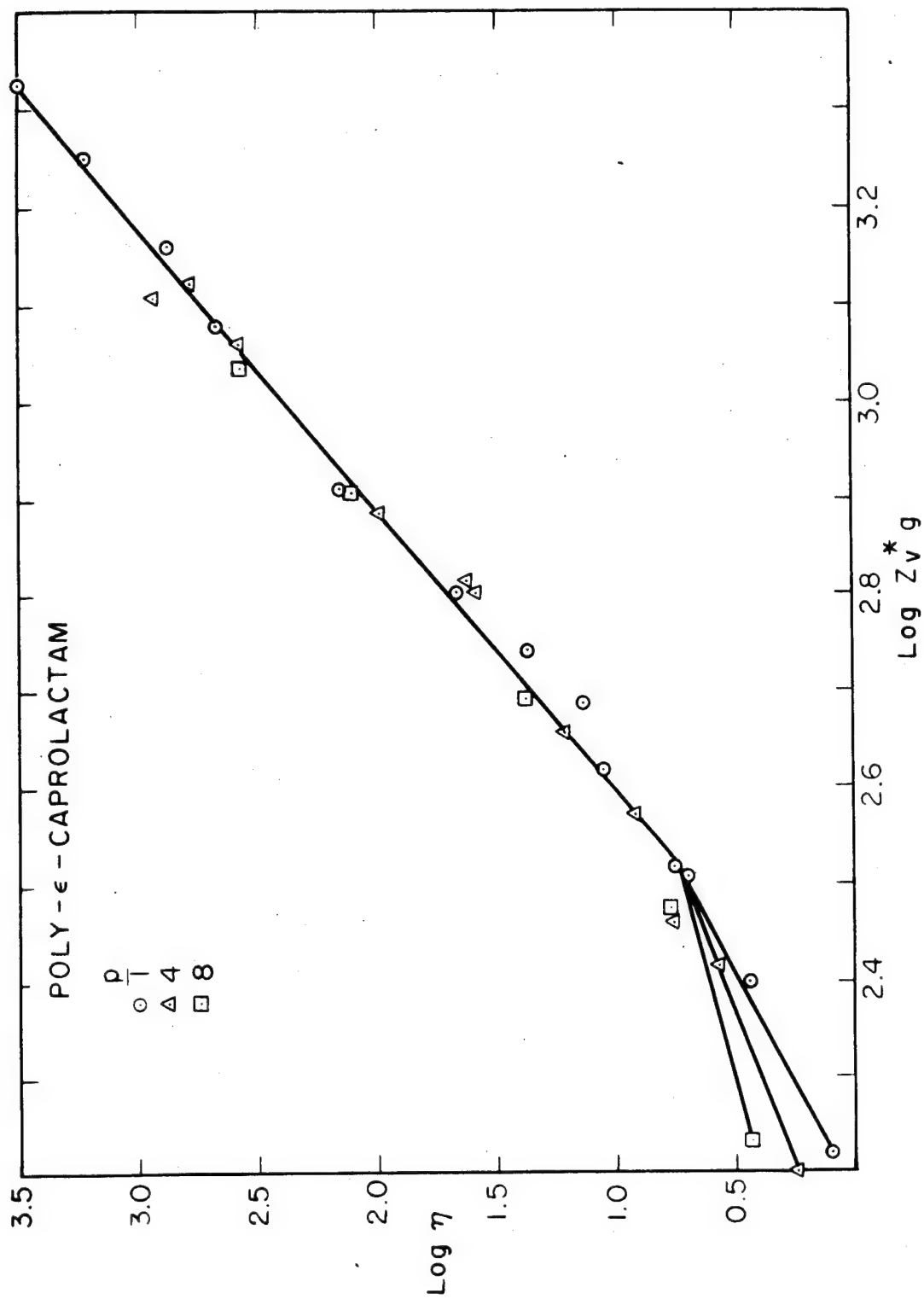


Figure 47  $\log \eta$  140° versus the parameter  $\log Z_v^*$  for linear and branched polycaprolactamides.  
(Data of Schaeffgen and Flory<sup>35</sup>).

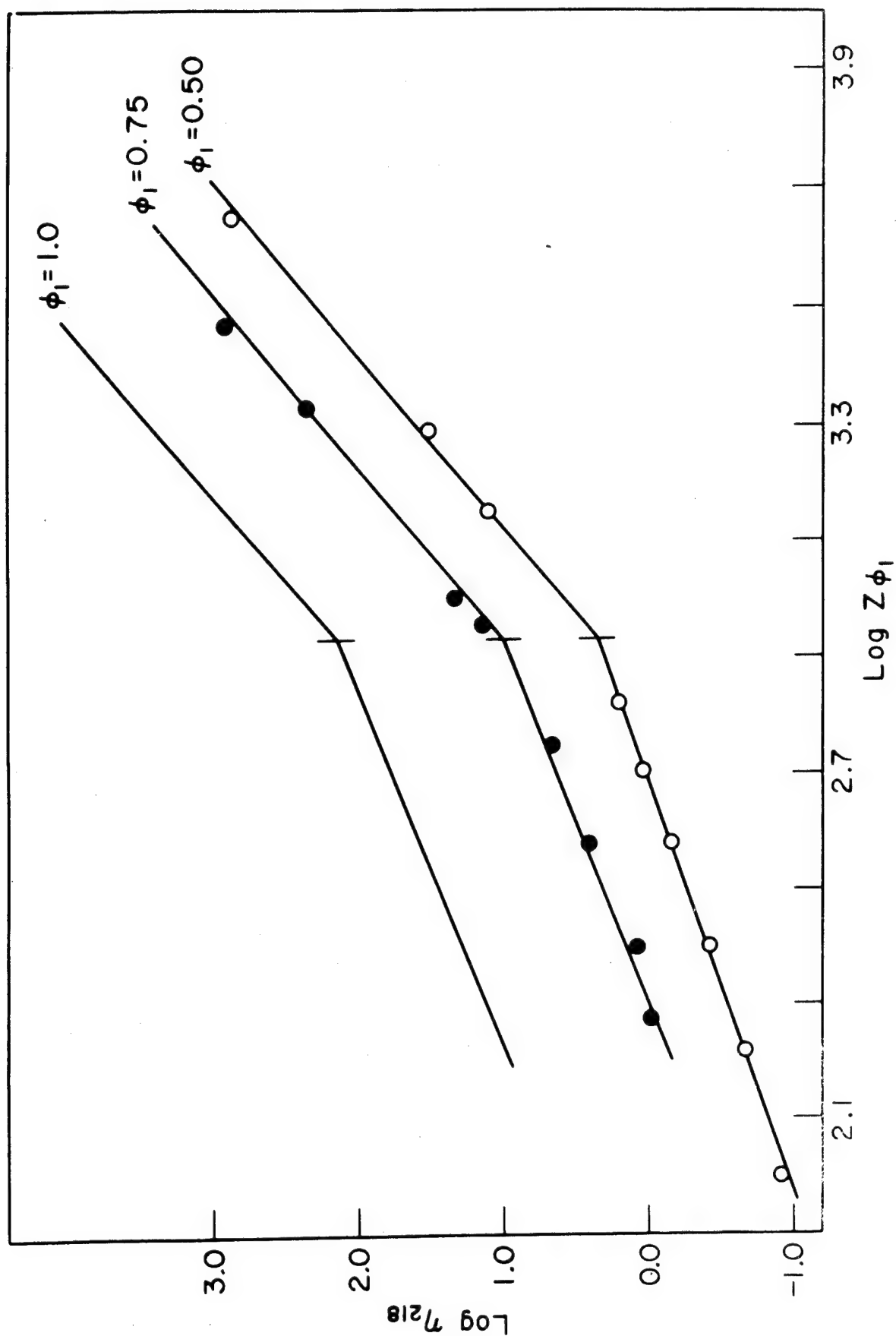


Figure 48 Viscosity - concentration - molecular weight relations for fractions of polystyrene in benzyl ether<sup>37</sup>.

those calculated by Eq. (119) for corresponding polymers (taking a "universal" value of  $f(\lambda) = 1.7$  as estimated by Bueche)<sup>1,2</sup> is afforded by the data in Table XIX. In four of five cases where observed values of  $Z_c$  are available, they agree well with those predicted by Eq. (123). In these instances and for most of the other polymers where values of  $Z_c$  had not been measured but were predicted by Eq. (123), values of  $Z_e$  computed by Eq. (119) agree with these from viscoelasticity measurements within the uncertainty of the latter evaluation.

More critical evaluation of Eq. (118) and of the relation between these measures of interchain interactions in elastic and in viscous deformations awaits more extensive and more precise measurements of  $Z_c$  and of for different polymers.

#### G. An Approximate (Modified W-L-F) Equation Relating $\zeta$ to Measurable Structure-Dependent Parameters

We seek next an empirical relationship of general applicability for predicting  $\zeta$ , over a broad temperature range, for different polymer systems from other measurable structure-dependent characteristics of the system. We are guided in this quest by experience with the successful W-L-F equation<sup>32,33</sup>; we shall explore modifications of it which extend its applicability to a broader temperature range, and which enable us to compute, from measurable material constants, required specific values of its parameters<sup>32,33</sup> (especially  $c_2$ ) for specific materials.

Values of the frictional coefficient, plotted as  $\log \zeta$  vs.  $T - T_g$  in Fig. 46, define characteristic curves for different polymers, which lie relatively close to each other, but are neither coincident nor "parallel". An attempt to fit the data to the W-L-F expression would require the assignment of a set of different values for each polymer for the four parameters-- $T_g$ ,  $\zeta_g$ ,  $c_1$  and  $c_2$ --in that equation.

A much simpler result would obtain, of course, if the data had fallen on a single curve. It is, therefore, useful to ask whether by suitable accounting of some additional factors they may be brought into coincidence. Modifications of the W-L-F equation for this purpose have been suggested previously, based on the observations first, that the expansion coefficient for the fractional free volume may be different for different liquids<sup>30,32,33</sup>, and second, that the temperature coefficient

\*Uncertainties in the values of  $\log \zeta$  presented at a given value of  $T - T_g$  in Fig. 46 arise from experimental errors in the determination of  $\eta$  and of  $Z$  ( $\pm 0.02$  in  $\log \zeta$ ), from uncertainties in the values used for  $s_0^2/Mv$  ( $\pm 0.15$ ) and in its temperature coefficient ( $\pm 0.10/100^\circ$ ), from possible individual variations in  $X_c$  from system to system ( $\pm 0.1$ ) or with temperature ( $0.15/100^\circ$ ), and from errors in the assignment of  $T_g$ , especially for short chain polymers and for polyethylene. We estimate the uncertainty in  $\log \zeta$  at  $T - T_g = 160^\circ$  to be  $\pm 0.2$  with a maximum uncertainty in  $d \log \zeta / dT$  to be  $\pm 0.3/100^\circ$ . For most of the polymer pairs the difference in Fig. 46 in the heights and slopes of the curves, for  $T - T_g < 250^\circ$  at least, exceed these limits.

Table XIX

Comparison of Calculated and Observed  $Z_c$  and  $Z_e$ 

Repeating Unit	$Z_c$		$Z_e$		
	Calcd <sup>a</sup> from $X_c = 4.7 \times 10^{-15}$	Observed (Table XVIII)	Calcd <sup>b</sup> from $Z_c$	Observed	
				Max. in $J''$	Inflection of Viscoelastic Properties
n-octyl methacrylate	1300/110°	---	630	1320/90°	
n-hexyl methacrylate	800/110°	---	550	720/105°	
n-butyl methacrylate	1000/110°	---	570	368/125°	
methyl acrylate	500/60°	---	350	400/80°	
ethylene oxide	430/25°	---	250		200/70°
natural rubber (Hevea)	450/25°	---	270	272/-50°	120 296 480/-30°
styrene	600/110°	600/160°	340		320, 610/100°
vinyl acetate	520/50°	570/120°	340	480/90°	338/50°
isobutylene	500/25°	460/25°	260	500/50°	240/-30° 320/90°
dimethyl siloxane	550/25°	630/25°	390		320/25°
methyl methacrylate	640/140°	210/140°	88		74 88/140°

(a) Calc'd as  $Z_c = 4.7 \times 10^{-15} / (\overline{s_0^2}/Mv)$  with values of  $(\overline{s_0^2}/Mv)$  estimated as in Table XVIII.

(b) Calc'd by Eqs. (118) to (126) with  $f(\lambda) = 1.7$ , and the observed  $Z_c$  (column 3) or its computed values (column 2) in the other instances.

of the viscosity of liquids at temperatures far above the glass temperature  $T_g$  (where the temperature dependence of the W-L-F term is small) generally approaches adherence to an Arrhenius-type equation with a non-zero activation energy  $E$ <sup>30,32,33</sup>.

In accord with this hypothesis, we were led to attempt to fit the data to a modified W-L-F equation of the form

$$\log \zeta = \log \zeta_0 + \frac{E}{2.3 RT} - \frac{B}{2.3 f_g} \left[ \frac{\Delta\alpha_f(T-T_g)}{f_g + \Delta\alpha_f(T-T_g)} \right] \quad (128)$$

where  $E$  and  $\zeta_0$  are parameters to be evaluated,  $B$  is a constant of order of magnitude unity,  $f_g$  may be thought of as the familiar "fractional free volume at the glass temperature", and  $\Delta\alpha_f$  as the expansion coefficient of this fractional free volume<sup>3,32,33</sup>. We have found it expedient to take<sup>5,6,32,33,40</sup>  $\Delta\alpha_f = \alpha_l - \alpha_g$ , where  $\alpha_l$  and  $\alpha_g$  are the experimentally measured thermal expansion coefficients for the polymer system above and below the glass temperature, respectively. The insertion of a term  $E/RT$  was explored previously<sup>30</sup>.

The results of attempts to reduce the data of Fig. 46 to a single curve corresponding to Eq. (128) are shown graphically in Fig. 49, and may be expressed in analytical form as follows

$$\log \zeta = -1.2 + \frac{E}{2.3RT} - 11.4 \left( \frac{\Delta\alpha_f(T-T_g)}{0.024 + \Delta\alpha_f(T-T_g)} \right) \quad (129)$$

In Fig. 49a a plot of  $\log \zeta$  vs.  $\Delta\alpha_f(T-T_g)$  (open symbols) brings the data more nearly in coincidence than the plot of  $\log \zeta$  vs.  $(T-T_g)$  in Fig. 46. The further reduction in Fig. 49a by the subtraction of  $E/RT$  from the ordinate, using the values of  $E$  in Table XX brings the data (filled symbols) for several polymers into approximate coincidence with the solid straight line of that figure, corresponding to Eq. (129). Here, values of  $E$  to achieve the optimum coincidence for all four polymers were arrived at by trial and error.

Thus the seemingly justifiable modification of the W-L-F relationship attempted here is partially successful. We are able, with the introduction of one arbitrary parameter  $E$ , to reduce the  $\zeta$ - $T$  data for several polymers to a single curve. However, we found no way to reduce the data for polydimethyl siloxane (Fig. 49) or (not shown) polyphenylene siloxane, polyethylene, or various polymer-diluent mixtures, to coincidence with the line representative for most of the polymers in Fig. 49b. In all these unsuccessful instances, viscosity data were available only at temperatures relatively far above  $T_g$ . It is thus undetermined whether such failure places an upper limit on  $\Delta\alpha_f(T-T_g)$  for the universal application of Eq. (129), or whether a different form of the relation is required for different "families" of liquids each with its characteristic structure.





Table XX

Tentative Values of  $\bar{E}$  for Various Polymers

Polymer	<u>E, kcal/mol, computed by Eq. (129)</u>		<u>Internal Energy</u>	
	Computed From a	Computed From	Barriers, kcal/mol.	Molecule
	$\zeta(T^\circ\text{C})$ in ref. <sup>33</sup>	$\eta$ -Z data <sup>b,c</sup>		
polymethyl methacrylate	7 (125)	3 (140°); 5 (140°); 8 (217°)	CH <sub>3</sub> -CH <sub>2</sub> CN	3.3, 5.2 <sup>44</sup>
polyethyl methacrylate	6 (100, 125)			
polyisobutylene	5.5 (100, 125)	5.5 (Table XIX)	CH <sub>3</sub> -C(CH <sub>3</sub> ) <sub>3</sub>	4.3 <sup>43</sup>
			CH <sub>3</sub> -CH(CH <sub>3</sub> ) <sub>2</sub>	3.6 <sup>43</sup>
polyethylene		5 (Table XIX)	CH <sub>3</sub> CH <sub>2</sub> -CH <sub>2</sub> CH <sub>3</sub>	3.3 <sup>43</sup>
polyvinyl acetate	3.5 (100, 125)	4.4 (Table XIX)		
polybutyl methacrylate	4 (100, 125)	4 (25°) <sup>13</sup>		
polyoxypropylene glycol				
polystyrene	2 (125)	3.6 (Table XIX)	CH <sub>3</sub> -CH <sub>2</sub> CH=CH <sub>2</sub>	3.6 <sup>43</sup>
Hevea rubber	3.2 (25)		CH <sub>3</sub> -Si(CH <sub>3</sub> ) <sub>3</sub>	1.3 <sup>43</sup>
polydimethyl siloxane		3 (Table XIX)		
polyvinyl chloride	1.8 (125)		CH <sub>3</sub> -CH <sub>2</sub> Cl	2.7, 3.6, 4.7
polymethylacrylate	1.7 (100, 125)			

(a) Values for  $\log \zeta$  at  $T^\circ\text{C}$  and of  $T_g$  for each polymer taken from ref. 33, p. 258. Values of  $\Delta\alpha_f$  were taken from Table XIX or from the data of refs. 5, 40, and 41.

(b) Computed by Eqs. (120) and (129) from the observed value of  $\eta$  at  $T$  for a given  $Z$ , using  $X_c = 4.7 \times 10^{-15}$  and  $(\bar{s}_0^2/Mv)$  from Table XVIII and data of refs. 5, 19, 27, 40, 41 and 42.

(c) The first two values of  $\bar{E}$  for polymethyl methacrylate were computed from the published  $\eta$ - $Z$  data taking  $T_g = 378^\circ\text{K}$  and  $10^{15}X_c$  alternatively as 1.5 (Table XVIII) or 4.7. The third value was computed from viscosity data<sup>40</sup> at  $217^\circ$  on a polymethyl methacrylate of lower syndiotactic content, with  $X_c = 4.7 \times 10^{-15}$ ,  $T_g = 350^\circ\text{K}$ , and the values of  $(\bar{s}_0^2/M)$  for the conventional polymer.

Tentatively then, we advance Eq. (129) for further trial as an empirical representation of observed  $\zeta$ -T data for polymer systems generally, over a wide temperature range above  $T_g$ , requiring the assignment of three parameters-- $T_g$ ,  $\Delta\alpha_f$ , and  $E$ --to each system. Two of these,  $T_g$  and  $\Delta\alpha_f = \alpha_l - \alpha_g$ , are assessable by independent measurements. For the present,  $E$  remains a parameter which must be determined from the  $\zeta$ -T data themselves. If it is taken as ca. 4.4 kcal, the absolute magnitude of  $\zeta$  for all curves in Fig. 47 would be given within a factor of 4. A closer estimate, or even an independent measurement, may be possible, perhaps, since differences in values of  $E$  obtained (Table XX) may be related to differences in the internal barriers to rotation about the chain valence bonds. Thus, high values of  $E$  for  $\zeta$  are observed for chains containing two bulky side groups on alternate carbon chain atoms (polymethacrylate and polyisobutylene), intermediate values of  $\zeta$  are found for chains containing only one bulky side group on alternate chain atoms (polystyrene and polyvinyl acetate), and the lowest values of  $\zeta$  obtain for the unsubstituted polyethylene and for the polysiloxane with the relatively long Si-O-Si bond.

Comparison of Eqs. (128) and (129) illustrates the useful result that the values of  $\log \zeta_0$  and of  $f_g$  may be taken, respectively, as -1.2 and 0.24 (a familiar result)<sup>32,33</sup>, for the different polymeric systems. The corresponding value obtained for  $B$ , 0.69, is somewhat lower than the expected value of unity<sup>32,33</sup>.

Eqs. (116), (120), (128), and (129) represent the complete expression of the  $\eta$ -T-Z relations for linear flexible chain molecules. From them  $\zeta$ ,  $Z_c$  and  $\eta$  can be computed if values of the characteristic parameters  $v$ ,  $s_0^2/M$ ,  $E$ ,  $\Delta\alpha_f$ , and  $T_g$  are known or can be estimated.

## H. Discussion

We regard the demonstration of the validity of the theoretical Eq. (115) and of the empirical Eq. (116), expressing the dependence of the zero shear viscosity for short and long chain polymers on pertinent molecular characteristics, as the most significant aspect of the preceding paragraphs. It is now possible with these equations to compute the viscosity from the independently measured chain dimensions and friction coefficient; but at present, it is more likely that measurements of the viscosity and of chain dimensions will be used to compute  $\zeta$ .

A significant feature of Eq. (116) for the viscosity of long chains is the dependence of  $\eta$  on  $(s_0^2)^{3.4}$ . A similar result was suggested by Tobolsky<sup>45</sup>, who observed proportionality between the maximum relaxation time  $\tau_m$  and  $(s_0^2)^{3.4}$  for long chain polymers, with the same value of the proportionality constant applicable to the four different polymers for which data are available, where  $\tau_m$  for different polymers are measured in corresponding states, i.e., at corresponding values of  $T - T_g$ .

In both the theoretical relation Eq. (115) and the empirical form Eq. (117), the parameter  $X$  plays a central role. Thus, with increasing  $X$ ,  $\eta$  is proportional to  $X$  until  $X = 4.7 \times 10^{-15}$  and then  $\eta$  varies as

$X^{3.4}$ . As mentioned, the parameter  $X = (\overline{s_0^2}/M)(Z/v)$  arises in the derivation of Eq. (115) as the moment of inertia of the average polymer coil multiplied by the number of such coils per unit volume. Presumably,  $X$  represents a measure of the hydrodynamic interaction or "entanglement" between different coils; and both the viscosity and the applicable interaction law are dependent on its magnitude.

More precise data on  $\eta$ ,  $Z$ ,  $\overline{s_0^2}/M$ , and  $v$ , at the same temperature are required, of course, to determine whether  $X_c$  is actually the same constant for all polymer systems. The only serious existing discrepancy is that for conventional polymethyl methacrylate. Further studies on both the conventional and the ideal atactic polymer are in progress; more precise determinations of the parameters for other linear and model branched polymers are planned as well.

The observed dependence of  $\eta$  on  $Z^{3.4}$  and on  $(Zg)^{3.4}$  for long chain linear and branched homologs, respectively, and the agreement between values of  $Z_e$  computed by Eq. (119) and those from elasticity data lend support to Bueche's approximate theoretical treatment for the viscosity of long chains. More extensive and careful theoretical and experimental examination of his concepts of "interchain coupling entanglements" and their role in determining the viscosity and time-dependent elasticity of macromolecular substances appear, more than ever, to be of critical importance in further developments of molecular interpretation of the viscoelastic behavior of such materials.

The theories of Eyring, Rhee, and Hirai<sup>46</sup> yield for short chains, a result different from the linear  $\eta$ - $Z$  relation established here, and give no means for predicting the dependence of  $\eta$  for long chains on their chain dimensions.

The present attempt to modify the W-L-F equation with the purpose of establishing a "universal" equation for predicting  $\zeta$  for various polymers over a wide temperature range from a few measurable parameters, while not completely successful, may be useful. It suggests that the dependence of the frictional coefficient on intermolecular and on intramolecular factors may be separable, at least partially. For example, Eq. (129) may represent in primitive form, an expression of the influence of both intramolecular and intermolecular barriers to motion (through  $E/RT$ ) and of the requirement that thermal fluctuations (against intramolecular and intermolecular potentials) produce locally the "free volume" needed for motions of chain segments from one equilibrium position to another. Precise determination of the temperature dependence of  $\eta$ , or of other viscoelastic deformations, over wider temperature ranges and for different types of polymers should yield further insight into the questions raised here.

More detailed and precise study of the  $\eta$ - $Z$ - $T$  relationships for the initial members of a homologous series would be also of interest. Here we would expect  $\overline{s_0^2}/M$  to vary with  $Z$ , and both the values of  $\zeta$  and of  $T_g$  may depart from those computed by Eqs. (120) and (129).

## PART II - LIST OF REFERENCES

1. Bueche, F., J. Chem. Phys. 20, 1959 (1952).
2. Bueche, F., "Physical Properties of Polymers", Interscience Publishers, New York, 1962.
3. Williams, M. L., J. Phys. Chem. 59, 95 (1955).
4. Williams, M. L., Landel, R. F. and Ferry, J. D., J. Am. Chem. Soc. 77, 3701 (1955).
5. Fox, T. G and Loshaek, S., J. Polymer Sci. 15, 371 (1955).
6. Fox, T. G and Flory, P. J., J. Am. Chem. Soc. 70, 2384 (1948).
7. Fox, T. G and Flory, P. J., J. Appl. Phys. 21, 581 (1950); J. Polymer Sci. 14, 315 (1954).
8. Nakayasu, H. and Fox, T. G, Colloid Chemistry Division Abstracts, 137th Meeting of the American Chemical Society, Cleveland, Ohio, April 1960.
9. Fox, T. G and Flory, P. J., J. Phys. Chem. 55, 221 (1951).
10. Barry, A., J. Appl. Phys. 17, 1020 (1946).
11. Warrick, E. L., Piccoli, W. A. and Stark, F. O., J. Am. Chem. Soc. 77, 5017 (1955).
12. Plazek, D. J., Dannhauser, W. and Ferry, J. D., J. Colloid Sci. 16, 101 (1961).
13. Fox, T. G and Loshaek, S., J. Appl. Phys. 26, 1080 (1955).
14. Havlik, A. J. and Moacanin, J., Research Summary No. 36-10, Vol. I, p. 92, Jet Propulsion Laboratory, Pasadena, California, Sept. 1, 1961.
15. Doolittle, A. K., J. Appl. Phys. 22, 1031 (1951).
16. Doolittle, A. K. and Peterson, R. H., J. Am. Chem. Soc. 73, 2145 (1951).
17. Tung, H. L., J. Polymer Sci. 46, 409 (1960).
18. Peticolas, W. L. and Watkins, J. M., J. Am. Chem. Soc. 79, 5083 (1957).
19. Fox, T. G, Polymer 3, 111 (1962).
20. Ciferri, A., Hoeve, C. A. J. and Flory, P. J., J. Am. Chem. Soc. 83, 1015 (1961).

21. Flory, P. J., private communication.
22. Fox, T. G and Flory, P. J., J. Am. Chem. Soc. 73, 1915 (1951).
23. Nakayasu, H. and Fox, T. G, to be published.
24. Shultz, A., J. Am. Chem. Soc. 76, 3422 (1954).
25. Matsumoto, M. and Ohyanagi, Y., J. Polymer Sci. 46, 441 (1960).
26. Matsumoto, M. and Ohyanagi, Y., J. Polymer Sci. 50, S1 (1960).
27. Kurata, M. and Stockmayer, W. H., Adv. Polymer Sci. 3, 196 (1963).
28. Meares, P., Trans. Faraday Soc. 53, 31 (1957).
29. Flory, P. J., J. Am. Chem. Soc. 62, 1057 (1960).
30. Fox, T. G, Gratch, S. and Loshaek, S., in "Rheology", Vol. I, (F. R. Eirich, ed.), Academic Press, N. Y. (1956) Chapter 12.
31. Bueche, F., J. Appl. Physics 26, 738 (1955).
32. Ferry, J. D. and Landel, R. F., Kolloid Z. 148, 1 (1956).
33. Ferry, J. D., "Viscoelastic Properties of Polymers", John Wiley and Sons, N. Y., (1961).
34. Rouse, P. E., Jr., J. Chem. Phys. 21, 1272 (1953).
35. Schaefgen, J. R. and Flory, P. J., J. Am. Chem. Soc. 70, 2709 (1948).
36. Orofino, T. A., Polymer 2, 305 (1961).
37. Allen, V. R. and Fox, T. G, to be published.
38. Bueche, F., J. Chem. Phys. 40, 484 (1964).
39. Markovitz, H., Ferry, J. D. and Fox, T. G, J. Phys. Chem. 66, 1567 (1962).
40. Simha, R. and Boyer, R. F., J. Chem. Phys. 37, 1003 (1962).
41. Wood, L. A., J. Polymer Sci. 28, 319 (1958).
42. Beevers, R. B. and White, E. F. T., Trans. Faraday Soc. 56, 744 (1960).
43. Janz, Estimation of Thermodynamic Properties of Organic Compounds, Academic Press, Inc., N. Y. (1958), p. 161.
44. Wilson, E. B., in Advances in Chemical Physics, II. (I. Prigogine, ed.) Interscience Publishers, Inc., (1959), p. 370.

45. Tobolsky, A. V., "Properties and Structures of Polymers", John Wiley and Sons, N. Y., (1960), p. 318.
46. Eyring, H., Rhee, T. and Hirai, N., Proc. Nat. Acad. Sci. U.S., 44, 1213 (1958).

### PART III - ANIONIC POLYMERIZATION

#### I. On the Two-State Mechanism for Homogeneous Ionic Polymerization\* — Bernard D. Coleman and T. G Fox

##### A. Introduction

To explain the occasional occurrence of "stereoblock" structures in homogeneous<sup>1</sup> anionic polymerization of  $\alpha$ -olefins we recently proposed that in these polymerizations the reactive end of a growing polymer can have several, say  $N$ , states  $\{1\}$ ,  $\{2\}$ , ...,  $\{N\}$  which are in dynamic equilibrium and that each such state is capable of adding monomer with its own rate and stereospecificity. In the absence of quantitative experimental evidence to the contrary, it appears that for the present it is expedient to take advantage of the reduction in the number of free parameters which results when  $N = 2$ , and to consider in detail the consequences of a two-state mechanism. Indeed, most of the interesting qualitative features of the multistate mechanism are already present in the two-state case. Here we summarize those theoretical results on the two-state model which appear to us to be accessible to experimentation. The emphasis here is on the diastereosequence and molecular weight distributions. Of course, to illustrate the effect on these distributions of the presence of two polymerizing species in dynamic equilibrium, it is not necessary to specify the detailed chemical structures of the species.

##### B. Chemical Hypotheses

We use here the notation of Fox and Coleman<sup>2,3</sup>. Consider a poly- $\alpha$ -olefin molecule and number the asymmetric carbon atoms of its principal chain in the order in which they were added during polymerization. If the  $m$ th and  $(m + 1)$ th asymmetric chain atoms have the same stereoconfiguration, then we say that the  $m$ th placement is isotactic; if these two asymmetric atoms have opposite stereoconfigurations, then we say that the  $m$ th placement is syndiotactic. Note that one placement involves two monomer units. A diastereosequence of length  $k$  is an ordered set of  $k$  adjacent placements, say, the  $m$ th,  $(m + 1)$ th, ...,  $(m + n - 1)$ th placements which express, respectively, the stereorelationship between the  $m$ th and  $(m + 1)$ th, the  $(m + 1)$ th and  $(m + 2)$ th, ..., the  $(m + n - 1)$ th and the  $(m + n)$ th asymmetric chain atoms.

The polymerizations which we consider here are idealized in that we assume instantaneous initiation, no irreversible termination, and no chain transfer or depolymerization. We assume that the diastereosequences generated in the states  $\{1\}$  and  $\{2\}$  are free from penultimate

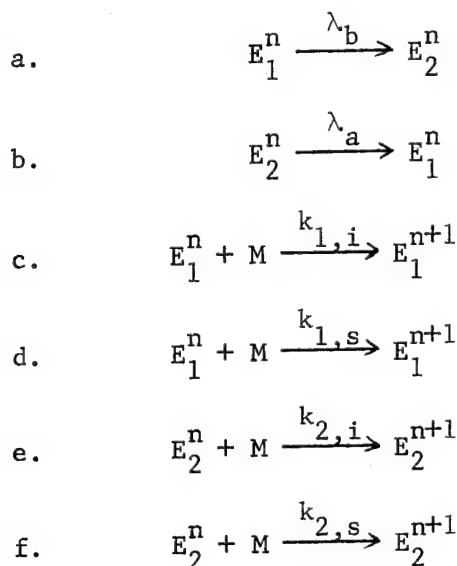
---

\* The following is the text of a paper presented at the I.U.P.A.C. International Symposium on Macromolecular Chemistry, Paris, July 1-6, 1963. In addition to support under Contract No. AF 33(616)-6968, the work was aided in part by Contract No. AF 49(638)-541 with the Air Force Office of Scientific Research.



effects, i.e. are Bernoullian in the sense in which the term is used in references 2 and 3. Of course, when reactions  $\{1\} \rightleftharpoons \{2\}$  are not instantaneously fast when compared with the addition reactions, the diastereosequence distribution of the resulting polymer will be non-Bernoullian; in fact, it will be non-Markoffian<sup>3,4</sup>.

We indicate the condition of a polymer molecule by the symbol  $E_x^n$ . The superscript  $n$  represents the degree of polymerization, and  $x = 1$  if the reactive end is in state  $\{1\}$  while  $x = 2$  for the state  $\{2\}$ . Denoting the monomer by  $M$  we can write the six basic chemical reactions of the two-state mechanism as follows:



Here  $\lambda_b$  is a rate coefficient for that reaction which takes a growing chain from state  $\{1\}$  to state  $\{2\}$ . In other words, the probability that a polymer molecule, known to be in the state  $\{1\}$  at the time  $t$ , goes to the state  $\{2\}$ , i.e., makes a transition of type a, in a time interval  $dt$  at  $t$  is given by  $\lambda_b dt + o(dt)$  where

$$\lim_{dt \rightarrow 0} o(dt)/(dt) = 0$$

Similarly,  $\lambda_a dt + o(dt)$  represents the probability that  $E_2^n \rightarrow E_1^n$  occurs in  $dt$  at  $t$ , given  $E_2^n$  at time  $t$ . The parameters  $k_{1,i}$  and  $k_{2,i}$  represent ordinary rate constants for the addition of monomer to polymer chains in states  $\{1\}$  and  $\{2\}$ , respectively, to form isotactic placements;  $k_{1,s}$  and  $k_{2,s}$  represent the corresponding rate constants for the addition to form syndiotactic placements. For example, the probability that a given polymer molecule, known to be in the state  $E_1^n$  at time  $t$ , makes the transition  $E_1^n \rightarrow E_1^{n+1}$  in  $dt$  at  $t$  and that this transition results in an isotactic placement is  $[M]k_{1,i} dt + o(dt)$ , where  $[M]$  denotes the monomer concentration in molecules per unit volume.

The numbers  $\lambda_a$ ,  $\lambda_b$ ,  $k_{1,i}$ ,  $k_{1,s}$ ,  $k_{2,i}$ ,  $k_{2,s}$  will depend on the temperature and solvent used; we assume here that they are independent of the degree of polymerization  $n$ . We also assume that the reactions  $\{1\} \rightleftharpoons \{2\}$  are in equilibrium when the monomer is added at  $t = 0$  and that  $[M]$  does not change appreciably as the polymerization proceeds for  $t > 0$ . It then follows<sup>4</sup> that the probability  $\psi$  that a polymer molecule selected at random is in the state  $\{1\}$  at a given moment  $t$  is given by

$$\psi = \frac{\lambda_a}{\lambda_a + \lambda_b} \quad (130)$$

and is independent of  $t$ .

The numbers  $k_1$  and  $k_2$ , defined by

$$k_1 = k_{1,i} + k_{1,s} \quad (131)$$

$$k_2 = k_{2,i} + k_{2,s} \quad (132)$$

are the rate constants for addition of monomer to polymer molecules in the states  $\{1\}$  and  $\{2\}$ , respectively, without regard to tacticity.

### C. Diastereosequences

Let  $\phi_x$  ( $x = 1, 2$ ) be the probability that a monomer unit, known to have been added to its chain before time  $t$  but otherwise selected at random, was added while its chain was in the state  $\{x\}$ . It is easy to show that  $\phi_x$  is independent of  $t$  and is given by<sup>4</sup>

$$\phi_1 = \frac{k_1 \lambda_a}{k_1 \lambda_a + k_2 \lambda_b} \quad (133)$$

$$\phi_2 = \frac{k_2 \lambda_b}{k_1 \lambda_a + k_2 \lambda_b}$$

The quantity  $\alpha_x$  defined by

$$\alpha_x = k_{x,i} / k_x \quad x = 1, 2 \quad (134)$$

gives the probability that a placement, known to have been formed in the state  $\{x\}$ , is isotactic. (In other words,  $\alpha_x$  is the probability that a

monomer unit is in isotactic placement to its predecessor, given that the unit was added while the polymer molecule was in the state {x}.)

We denote by  $p\{I\}$  the probability that a placement is isotactic, given no information about the tacticity of other placements or its position along its chain. Clearly

$$p\{I\} = \phi_1 \alpha_1 + \phi_2 \alpha_2 \quad (135)$$

Eqs. (133)-(135) yield

$$p\{I\} = \frac{\lambda_a k_{1,i} + \lambda_b k_{2,i}}{\lambda_a k_1 + \lambda_b k_2} \quad (136)$$

Letting  $p\{S\}$  be the probability that a placement, selected at random, is syndiotactic, we have

$$p\{I\} + p\{S\} = 1 \quad (137)$$

Let  $p\{II\}$  and  $p\{SS\}$  be the probabilities that a randomly selected pair of adjacent placements consists, respectively, of two isotactic placements and two syndiotactic placements. Let  $p\{IS_V SI\}$  be the probability that a pair of adjacent placements is a "heterotactic pair," i.e., either an isotactic placement followed by a syndiotactic placement or a syndiotactic placement followed by an isotactic placement. Note that the diastereosequences here characterized by II, SS, and  $IS_V SI$  are diastereosequences of length two. They each involve two placements or three monomer units. It follows from our definitions that

$$p\{II\} + p\{SS\} + p\{IS_V SI\} = 1 \quad (138)$$

We assume now the mean molecular weight is high enough so that every placement has both a successor and predecessor. Then the following formulae must hold, regardless of the mechanism of polymerization<sup>3</sup>.

$$p\{I\} = p\{II\} + \frac{1}{2} p\{IS_V SI\} \quad (139a)$$

$$p\{I\} = 1/2 [1 + p\{II\} - p\{SS\}] \quad (139b)$$

$$p\{I\} = 1 - \frac{1}{2} p\{IS_V SI\} - p\{SS\} \quad (139c)$$

The equations obtained from these through interchange of the symbols I and S must also hold.

For our present mechanism it can be shown that<sup>4</sup>

$$p\{II\} = \alpha_1^2 \phi_1 + \alpha_2^2 \phi_2 - \frac{\lambda_b \phi_1 (\alpha_1 - \alpha_2)^2}{k_1 \{(\lambda_b/k_1 \phi_2) + [M]\}} \quad (140a)$$

$$p\{SS\} = (1 - \alpha_1)^2 \phi_1 + (1 - \alpha_2)^2 \phi_2 - \frac{\lambda_b \phi_1 (\alpha_1 - \alpha_2)^2}{k_1 \{(\lambda_b/k_1 \phi_2) + [M]\}} \quad (140b)$$

$$\frac{1}{2} p\{SI_V SI\} = \alpha_1 (1 - \alpha_1) \phi_1 + \alpha_2 (1 - \alpha_2) \phi_2 + \frac{\lambda_b \phi_1 (\alpha_1 - \alpha_2)^2}{k_1 \{(\lambda_b/k_1 \phi_2) + [M]\}} \quad (140c)$$

The probabilities considered in Eqs. (136)-(140) are, for practical purposes equivalent to concentrations in a large sample. For certain polymers, such as poly(methyl methacrylate), the quantities  $p\{I\}$ ,  $p\{S\}$ ,  $p\{II\}$ ,  $p\{SS\}$ ,  $p\{IS_V SI\}$  can all be determined by high resolution NMR spectroscopy<sup>5</sup>. Of these five quantities only three can be regarded as independently measured, for the relations (137) and (183) are always used by the experimenter to normalize his data. An example of independently measured data would be any set containing one placement probability (i.e.,  $p\{I\}$  or  $p\{S\}$ ) and two pair probabilities (i.e., any two of the three numbers  $p\{II\}$ ,  $p\{SS\}$ ,  $p\{IS_V SI\}$ ). Each set of independently measured probabilities should obey one of the consistency relations, Eqs. (139), which must hold in general, and which serve, not to check a particular mechanism, but rather to convince the experimenter that he has properly identified his spectroscopic peaks. It is Eqs. (136) and (140) which serve to check the applicability of the present mechanism, and we shall discuss their use below.

General results are known<sup>4</sup> which give for our mechanism the probability of occurrence of diastereosequences of length greater than two. We do not discuss these results here, for the concentrations of diastereosequences of length three or greater (i.e., involving four or more asymmetric chain atoms) are not yet accessible to measurement. The mean length of certain types of diastereosequences are measurable, however,

We define a closed sequence of isotactic placements to be a sequence of  $m + 2$  consecutive placements,  $m \geq 1$ , all of which are isotactic, except for the two at the ends, which are both syndiotactic. Let  $\mu\{I\}$  be the mean (number-average) length of the closed sequences of isotactic placements. When the mean molecular weight is high, the following formula should hold for all mechanisms of polymerization:

$$\mu\{I\} = \frac{p\{I\}}{p\{S\} - p\{SS\}} = \frac{2p\{I\}}{p\{IS_VSI\}} \quad (141)$$

We say that a diastereosequence distribution is Bernoullian if formulae of the following type hold:  $p\{II\} = p\{I\}p\{I\}$ ,  $p\{IS_VSI\} = 2p\{I\}p\{S\}$ , etc. (A more formal definition is given in Section 1 of reference 3.) For a Bernoullian distribution Eq. (141) reduces to  $\mu\{I\} = 1/p\{S\}$ . For a general (i.e., non-Bernoullian) diastereosequence distribution, the quantity

$$\rho = \mu\{I\}p\{S\} \quad (142)$$

is called the persistence ratio, for it gives the ratio of the actual mean length of closed sequences of isotactic placements to the mean length which one would calculate assuming that the distribution be Bernoullian with the same values of  $p\{I\}$  and  $p\{S\}$ . It follows from Eqs. (141) and (142) that

$$\rho = 2p\{I\}p\{S\}/p\{IS_VSI\} \quad (143)$$

We note that  $\rho$  can be calculated from NMR data and gives a convenient measure of "statistical after-effects."

For our present mechanism Eqs. (136) and (140) yield

$$\rho = \frac{\{(1 - \alpha_1)\phi_1 + (1 - \alpha_2)\phi_2\}(\alpha_1\phi_1 + \alpha_2\phi_2)}{\alpha_1(1 - \alpha_1)\phi_1 + \alpha_2(1 - \alpha_2)\phi_2 + \frac{\lambda_b\phi_1(\alpha_1 - \alpha_2)^2}{\{\lambda_b/k_1\phi_2\} + [M]k_1}} \quad (144)$$

#### D. Molecular Weights

Let  $\bar{n}(t)$  and  $\bar{n}_w(t)$  be, respectively, the number-average and weight-average degrees of polymerization, and let  $r(t)$  be their ratio:

$$r(t) = \bar{n}_w(t)/\bar{n}(t) \quad (145)$$

Assuming that (instantaneous) initiation occurs at  $t = 0$ , we take as initial conditions

$$\bar{n}(0) = \bar{n}_w(0) = r(0) = 1 \quad (146)$$

A lengthy calculation then yields the following results for our mechanism<sup>6</sup>:

$$\bar{n}(t) = 1 + [M]\bar{k}t \quad (147)$$

$$\bar{n}_w(t) = 1 + \frac{\{1 + [M]b/(\bar{k}a)\}([M]\bar{k}t) - [M]^2b(1 - e^{-at})/a^2}{1 + [M]\bar{k}t} + \bar{k}[M]t \quad (148)$$

$$r(t) = 1 + \frac{1 + [M]b/(\bar{k}a)}{\bar{n}(t)} - \frac{1 + [M]b/(\bar{k}a) + [M]^2a^{-2}b(1 - e^{-at})}{\bar{n}(t)^2} \quad (149)$$

where

$$\bar{k} = \psi k_1 + (1 - \psi)k_2 \quad (150a)$$

$$a = \lambda_a + \lambda_b \quad (150b)$$

$$b = 2(k_1 - k_2)^2\psi(1 - \psi) \quad (150c)$$

The results in Eqs. (147)-(149) are mathematically exact and follow from our chemical hypotheses without approximation. It should be emphasized, however, that these results on the molecular weight distribution are far more sensitive than our results on diastereosequence distribution to our idealized assumptions of instantaneous initiation, no irreversible termination, and no chain transfer or depolymerization. For example, a violation of any one of these assumptions renders invalid the following conclusion which follows immediately from Eqs. (149) and (147):

$$\text{If } a\bar{k} > 0, \text{ then } \lim_{t \rightarrow \infty} r(t) = 1 \quad (151)$$

In reference 6 we give a detailed discussion of the limiting circumstances for which our present molecular weight distribution becomes identical to the Poisson distribution obtained by Flory<sup>7</sup> for the more familiar one-state polymerization.

It should not be concluded from Eq. (151) that  $r$  is close to 1 for all degrees of polymerization. When  $[M]_b \gg \bar{k}a$ , our present distribution differs markedly from the Poisson distribution in that Eq. (149) yields  $r \gg 1$  even for large  $\bar{n}$ . When  $\lambda_a + \lambda_b = 0$ , Eq. (151) is replaced by the assertion:

$$\text{If } a = 0 \text{ and } \bar{k} \neq 0, \text{ then } \lim_{t \rightarrow \infty} r(t) = 1 + \frac{b}{2(\bar{k})^2} \quad (152)$$

This last result can also be derived by considering a mixture of non-interacting one-state polymerizations, each yielding a Poisson distribution.

#### E. Comparison with Experiment

We have discussed earlier<sup>4,6</sup> experimental methods for testing the applicability of the two-state mechanism when certain special restrictive assumptions apply. If all of the six rate coefficients in the reactions a - f are independent of the monomer concentration, a quantitative test is provided by NMR spectroscopy on a series of polymers prepared at different monomer concentrations but under otherwise identical conditions. According to Eqs. (136) and (140), under the present assumptions  $p\{I\}$  should be a constant independent of  $[M]$ , while  $p\{II\}$  should increase with increasing  $[M]$  as

$$p\{II\} = \delta - \frac{\epsilon}{\gamma + [M]} \quad (153)$$

where expressions for  $\delta$ ,  $\epsilon$ , and  $\gamma$  may be obtained by comparison with Eq. (140a). Evidence that  $p\{I\}$  is independent of  $[M]$  while  $p\{II\}$  varies with  $[M]$  in the manner required by Eq. (153) would indicate strongly the applicability of the two-state mechanism and would provide a method for determining  $\delta$ ,  $\epsilon$ , and  $\gamma$  from NMR data.

If it should also happen, under limited conditions at least, for anionic polymerizations carried out in a mixture of a Lewis base and a hydrocarbon, that the rate constants for addition of monomer ( $k_{1,i}$ ,  $k_{1,s}$ ,  $k_{2,i}$ , and  $k_{2,s}$ ) are independent of the concentration  $[L]$  of the Lewis base, but that  $\lambda_a$  and  $\lambda_b$  do depend on  $[L]$ , it is possible, from NMR data and measurements of the overall rate coefficient  $\bar{k}$  of Eq. (147) to determine all of the six rate coefficients in the reactions a-f. It can be shown<sup>4</sup> that

$$\delta = p\{I\}(\alpha_1 + \alpha_2) - \alpha_1\alpha_2 \quad (154)$$

$$\phi_1 = (p\{I\} - \alpha_2)/(\alpha_1 - \alpha_2) \quad (155)$$

$$\lambda_b/k_1 = \gamma\phi_2 \quad (156)$$

$$\lambda_a/k_2 = \gamma\phi_1$$

and

$$\phi_2/\phi_1 = (k_2/\bar{k}\phi_1) - (k_2/k_1) \quad (157)$$

Here the values of  $\delta$ ,  $p\{I\}$ , and  $\gamma$ , which will vary within a series of polymers prepared at different  $[L]$ , can be determined by application of Eq. (153) to NMR data on polymers prepared at different values of  $[M]$  for each value of  $[L]$ . By plotting  $\delta$  versus  $p\{I\}$  (varying  $[L]$ ) one should, according to Eq. (154), get a straight line whose slope and intercept yield the constants  $\alpha_1$  and  $\alpha_2$ . Eq. (155) then yields  $\phi_1$  (and, of course,  $\phi_2 = 1 - \phi_1$ ), as a function of  $p\{I\}$ , which is, in turn, now a known function of  $[L]$ . According to Eq. (156) the product of  $\gamma$  and  $\phi_1$  (or  $\phi_2$ ), then yields  $\lambda_a/k_2$  (or  $\lambda_b/k_1$ ) as a function of  $[L]$ . From Eq. (157) we see that a plot of  $\phi_2/\phi_1$  versus  $(\bar{k}\phi_1)^{-1}$  should be linear and should yield  $k_1$  and  $k_2$ ; and on combining these two numbers with the now known values of  $\alpha_1$ ,  $\alpha_2$ ,  $\lambda_a/k_1$ ,  $\lambda_b/k_2$ , one computes the constants  $k_{1,i}$ ,  $k_{1,s}$ ,  $k_{2,i}$ , and  $k_{2,s}$ , and also  $\lambda_a$  and  $\lambda_b$  as functions of  $[L]$ . We consider it to be particularly interesting that, at least in principle, the absolute rates  $\lambda_a$ ,  $\lambda_b$  of the reactions  $E_1 \rightleftharpoons E_2$  are determinable from NMR and rate of polymerization data alone.

We cannot expect all six rate coefficients to be always independent of monomer concentration, since the monomer may form a complex with the reactive polymer chain, thereby affecting  $\lambda_a$ ,  $\lambda_b$  and possibly other rate coefficients as well. In fact, 1:1 complexes of methyl methacrylate with metal salts have been isolated and identified<sup>8</sup>. The observed<sup>9</sup> complicated dependence on  $[M]$  of the rate of polymerization of methyl methacrylate with fluorenyl-Li in toluene-tetrahydrofuran mixtures and the finding<sup>10</sup> that polymerizations in toluene at 30°C initiated by metallic sodium yield highly crystalline polystyrene or poly(methyl methacrylate) only in the range of dilute monomer concentration are evidence for the strong influence of the monomer concentration on the character of the anionic polymerization. The present mechanism can be made compatible with these observations by the postulate that the monomer at high  $[M]$  complexes with, and alters the concentration of, that reactive state that produces highly isotactic polymer. Thus, only in very special circumstances should we expect the assumption of nondependence of rate coefficients on  $[M]$  to be approximately valid. The search for such circumstances is an important goal, however, since they would render possible a quantitative demonstration of the mechanism's applicability.

In Tables XXI-XXV we have compiled the NMR data known to us on poly(methyl methacrylate) and poly- $\alpha$ -methylstyrene prepared by ionic polymerizations. These data illustrate the effect of varying the monomer, the initiator, the solvent medium, and the polymerization temperature. Although the results do not provide a definitive test of the applicability of the mechanism, we can speculate on their significance using the framework of the two-state mechanism.

The data of Wiles and Bywater<sup>18</sup> on the products of the polymerization of methyl methacrylate in toluene, at -30°C with butyllithium (Table XXIV), show a decrease in both  $\rho$  and  $\{I\}$  with an increase in the initial  $[M]$ , and an increase in  $\rho$  and  $p\{I\}$  as the monomer is consumed in the polymerization. Here, as the evidence cited above suggested, the monomer unfortunately participates in the reactions that control the nature and concentration of the reactive states, and we cannot assume that all of the rate constants are independent of  $[M]$ .



Table XXI

NMR Data on Poly(methyl Methacrylate) Polymerized Anionically in Hydrocarbon Media

Solvent and reference	Initiator	T, °C	$\rho$	p{I}	$\mu\{I\}$	$\mu\{S\}$	p{II}	p{IS <sub>v</sub> SI}	p{SS}
Toluene <sup>5</sup>	C <sub>6</sub> H <sub>5</sub> MgBr	0	---	1.0	$\infty$	0	1.0	0	0
Octane <sup>11</sup>	C <sub>6</sub> H <sub>5</sub> MgBr	0	---	1.0	$\infty$	0	1.0	0	0
Octane <sup>11</sup>	Butyl MgCl	-60	2.8	0.615	7.2	4.5	0.53	0.17	0.30
Toluene <sup>12</sup>	Butyl Li	-80	2.5	0.835	15	3.0	0.78	0.11	0.11
Toluene <sup>5</sup>	Butyl Li	-62	2.1	0.725	7.6	2.9	0.63	0.19	0.18
Toluene <sup>13</sup>	Butyl Li	0	1.8	0.81	9.6	2.3	0.72	0.173	0.107
Toluene <sup>5</sup>	Butyl Li	25	1.7	0.78	7.8	2.2	0.68	0.20	0.12
Toluene <sup>13</sup>	Butyl Li	-70	1.7	0.77	7.5	2.2	0.67	0.205	0.125
Toluene <sup>14</sup>	Butyl Li	-70	1.6	0.80	8	2.0	0.70	0.20	0.10
Ether <sup>13</sup>	Amyl Na	-70	1.4	0.71	4.7	1.9	0.55	0.30	0.14
Petroleum ether <sup>13</sup>	Amyl Na	-70	1.4	0.70	4.7	2.0	0.55	0.30	0.15
Hexane <sup>13</sup>	Amyl Na	-70	1.4	0.61	3.5	2.2	0.43	0.354	0.215
Toluene <sup>13</sup>	Amyl Na	-70	1.3	0.79	6.3	1.7	0.67	0.24	0.09
Toluene <sup>13</sup>	Amyl Na	0	1.3	0.72	4.6	1.8	0.57	0.31	0.12
Toluene <sup>13</sup>	Octyl K	-70	1.2	0.57	2.8	2.1	0.37	0.40	0.23
Toluene <sup>13</sup>	Octyl K	0	1.2	0.56	2.7	2.1	0.35	0.42	0.23

Table XXII

NMR Data on Poly(methyl Methacrylate) Polymerized Anionically in Lewis Bases

Solvent and reference	Initiator	T, °C	$\rho$	p{S}	$\mu\{I\}$	$\mu\{I\}$	p{II}	p{IS <sub>v</sub> SI}	p{SS}
Dimethoxyethane <sup>13</sup>	Butyl Li	0	1.6	0.70	2.3	5.3	0.17	0.26	0.57
Dimethoxyethane <sup>13</sup>	Butyl Li	-70	1.3	0.81	1.6	6.7	0.07	0.24	0.69
Pyridine <sup>13</sup>	Butyl Li	0	1.2	0.76	1.5	4.8	0.08	0.32	0.60
Pyridine <sup>13</sup>	Butyl Li	-60	1.15	0.76	1.4	4.6	0.07	0.33	0.59
Tetrahydrofuran <sup>15</sup>	Na Naphthalene	-78	1.2	0.72	1.5	3.8	0.12	0.33	0.55
Dimethoxyethane <sup>13</sup>	Amyl Na	0	1.18	0.79	1.5	5.6	0.06	0.28	0.65
Dimethoxyethane <sup>13</sup>	Amyl Na	-70	1.11	0.85	1.3	7.4	0.04	0.23	0.73
Pyridine <sup>13</sup>	Amyl Na	-60	1.08	0.71	1.5	3.6	0.10	0.39	0.51
Pyridine <sup>13</sup>	Amyl Na	0	0.98	0.65	1.5	2.8	0.12	0.46	0.42
NH <sub>3</sub> (l) <sup>13</sup>	Amyl Na	-70	1.06	0.72	1.5	3.2	0.09	0.38	0.53
Tetrahydrofuran <sup>16</sup>	K Naphthalene	30	1.06	0.535	2.0	2.3	0.23	0.47	0.30
Dimethoxyethane <sup>13</sup>	Octyl K	0	1.00	0.63	1.6	2.7	0.14	0.46	0.40
Dimethoxyethane <sup>13</sup>	Octyl K	-70	0.95	0.63	1.5	2.5	0.12	0.49	0.39
Pyridine <sup>13</sup>	Octyl K	0	0.92	0.60	1.5	2.3	0.14	0.53	0.33
Pyridine <sup>13</sup>	Octyl K	-60	0.90	0.66	1.4	2.7	0.09	0.49	0.42

Table XXIII

Data on Poly(methyl Methacrylate) Polymerized Anionically in Mixtures of Toluene with Lewis Bases

Lewis base initiator, and reference	T, °C	Base, %	$\rho$	p{I}	$\mu\{I\}$	$\mu\{S\}$	p{II}	p{SI <sub>v</sub> SI}	p{SS}	r
Dimethoxyethane <sup>13</sup> (butyllithium)	-30	0	1.8	0.70	6.1	2.6	0.59	0.28	0.18	
	-30	36	1.8	0.51	3.7	3.6	0.38	0.27	0.35	
	-30	62	1.5	0.40	2.5	3.7	0.24	0.32	0.44	
	-30	98	1.5	0.30	2.1	4.9	0.16	0.29	0.55	
	-30	100	1.5	0.25	2	6	(0.12)	(0.25)	(0.63)	
Dimethoxyethane <sup>5</sup> (butyl- lithium) Pyridine <sup>13</sup> (butyl- lithium)	-62	50	1.6	0.495	2.7	2.7	0.31	0.32	0.32	
	-30	0	1.8	0.70	6.1	2.6	0.59	0.23	0.18	
	-30	10	1.1	0.26	1.5	4.4	0.0	0.35	0.56	
	-30	20	1.03	0.22	1.3	4.7	0.05	0.33	0.62	
	-30	30	1.11	0.21	1.4	5.3	0.06	0.30	0.64	
	-30	40	1.15	0.23	1.5	5.0	0.08	0.31	0.61	
	-30	50	1.13	0.23	1.5	5.9	0.08	0.31	0.61	
	-30	100	1.18	0.24	1.45	4.7	0.08	0.33	0.59	
	-62	0.1	1.9	0.82	11	2.4	0.75	0.15	0.10	12
		1	3.9	0.73	15	5.4	0.68	0.10	0.22	4.6
Tetrahydrofuran <sup>17</sup> (9-fluorenyllithium)		1	3.0	0.75	13	4.3	0.69	0.11	0.20	4.0
		2.5	3.3	0.53	7	6.2	0.46	0.15	0.39	3.8
		5	3.3	0.27	8	21	0.24	0.07	0.69	9.8
		5								3.2
		7.5	2.2	0.26	3	9	0.17	0.17	0.66	1.6
		7.5								1.6
		10	2.4	0.12	2.7	20	0.07	0.09	0.83	2.1
		10								3.0
		15	1.7	0.13	2	14	0.07	0.13	0.80	2.4
	-62	40	1.9	0.675	5.9	2.7	0.56	0.23	0.21	
Dioxane <sup>5</sup> (Butyllithium) Ether <sup>17</sup> (9-fluorenyl- lithium)	-62	5	4	0.90	40	4.4	0.88	0.04	0.07	14.6

Table XXIV

NMR Data on Poly(methyl Methacrylate) Polymerized in Toluene at  
-30°C with Butyllithium at Two Different Monomer Concentrations<sup>18</sup>

[M], mole/l.	Conver- sion, %	$\rho$	p{I}	$\mu\{I\}$	$\mu\{S\}$	p{II}	p{IS <sub>v</sub> SI}	p{SS}
0.125	52	1.84	0.82	10	2.2	0.74	0.16	0.10
0.125	94	2.26	0.87	17	2.6	0.82	0.10	0.08
0.125	100 <sup>a</sup>	2.25	0.90	23	2.8	0.86	0.08	0.06
0.500	32	1.4	0.67	4.2	2.1	0.52	0.29	0.19
0.500	34	1.4	0.68	4.3	2.1	0.52	0.31	0.17
0.500	73	1.7	0.81	8.5	2.1	0.72	0.18	0.10
0.500	73 <sup>b</sup>	2.0	0.86	14	2.3	0.80	0.12	0.08

<sup>a</sup> Polymerized completely, then the same amount of monomer was added and polymerized completely.

<sup>b</sup> Approximately a quarter of the same polymerized to 73% conversion, removed by extraction with 4-heptanone.

Table XXV

NMR Data on Poly- $\alpha$ -methylstyrene<sup>19</sup>

Catalyst	Solvent	T, °C	p{S}	$\rho$	$\mu\{S\}$	$\mu\{I\}$	$\mu\{SS\}$	$p\{IS_v SI\}$	p{II}
BF <sub>3</sub>	Toluene	-78	0.95	0.9	17	0.9	0.89	0.11	--
AlCl <sub>3</sub>	Toluene	-78	0.925	1	12	1	0.85	0.15	--
SnCl <sub>4</sub>	Toluene	-78	0.925	1	12	1	0.85	0.15	--
SnCl <sub>4</sub>	Nitromethane	-30	0.91	0.9	10	1	0.82	0.18	--
TiCl <sub>4</sub>	Toluene	-78	0.91	0.9	9.6	1	0.81	0.14	--
SnCl <sub>4</sub>	Ethylene chloride	-35	0.87	0.9	6.7	1	0.74	0.26	--
Butyl Li	Cyclohexane	4	0.85	0.8	5.5	1	0.69	0.31	--
AlEt <sub>3</sub> /TiCl <sub>4</sub>	Benzene	25	0.80	0.9	4.6	1.1	0.62	0.35	0.03
x-ray		30	0.79	1	5	1.3	0.63	0.32	0.05
AIBN at 600 atm (free radical)		100	0.75	1	3.8	1.3	0.55	0.40	0.06
Na	Tetrahydrofuran	0	0.67	1	1.5	3	0.44	0.45	0.11
Na-Naphthenide	Tetrahydrofuran	-78	0.63	1	1.5	2.6	0.39	0.48	0.13

In the anionic polymerization of methyl methacrylate in hydrocarbons (Table XXI), predominantly isotactic polymers are formed with values of  $\rho$  and  $p\{I\}$  decreasing in the order  $Li^+ > Na^+ > K^+$ , i.e., decreasing on going from strongly to weakly complexing cations<sup>8,13</sup>. Predominantly syndiotactic polymers are formed in polymerizations in Lewis bases (Table XXII), with  $\rho$ , and now not  $p\{I\}$ , but rather  $p\{S\}$ , decreasing in the order  $Li^+ > Na^+ > K^+$ <sup>13,16</sup>; the parameters here are also sensitive to the temperature and to the nature of the Lewis base. In mixed solvents (Table XXIII),  $p\{I\}$  decreases with increasing  $[L]$  in toluene<sup>9,13,17,20</sup>; although  $\rho$  may increase with increasing  $[L]$  at low  $[L]$ , it invariably decreases at higher  $[L]$ .

It appears that in the polymerization of methyl methacrylate the use of a strongly complexing cation tends to yield values of  $\rho$  appreciably greater than one. The scanty available data on molecular weights indicates that conditions which produce large  $\rho$  also produce larger  $r$ . Under the two-state mechanism, assuming of course that  $\alpha_1 \neq \alpha_2$ ,  $k_1 \neq k_2$ , we interpret this as meaning that the reactions  $\{1\} \rightleftharpoons \{2\}$  are slow relative to the addition reactions, (c-f). Glusker and Galluccio<sup>17</sup> found that they could separate the product of polymerization of methylmethacrylate by fluorenyl-Li in a toluene-tetrahydrofuran mixture into high molecular weight fractions which were highly isotactic and lower molecular weight fractions which were less isotactic; Wiles and Bywater<sup>18</sup> have extracted with 4-heptanone (Table XXIV) a poly(methyl methacrylate) fraction more isotactic than the whole polymer prepared in toluene with butyllithium. Further, binodal molecular weight distributions in the products of polymerizations of methyl methacrylate in such systems were observed by a number of workers<sup>8,9,18,20,21</sup>. These observations suggest that the reactions  $\{I\} \rightleftharpoons \{2\}$  can be very much slower than the addition reactions. The fact that the reported values of  $r$  for these polymers are large and do not seem to approach 1 at large  $\bar{n}$ , even though initiation has been shown to be instantaneous and no irreversible termination occurs, is in accord with this hypothesis.

We are led, therefore, to explore the consequences of the assumption that in the anionic polymerization of methyl methacrylate in the presence of strongly complexing cations we have, as a rough approximation,  $a = \lambda_a + \lambda_b = 0$ , but  $\psi = \lambda_a/(\lambda_a/(\lambda_a + \lambda_b)) \neq 0$  and  $1 - \psi \neq 0$ . We now assume  $\psi$ , and hence  $\phi_1$  and  $\phi_2$ , to be dependent on  $[L]$ , but take  $\alpha_1$  and  $\alpha_2$  to be (approximately) independent of  $[M]$  and  $[L]$ . From Eqs. (135) and (140a) we then obtain

$$p\{II\} = (\alpha_1 + \alpha_2)p\{I\} - \alpha_1\alpha_2 \quad (158)$$

It follows that, for each initiator and solvent pair, if one varies  $[L]$ , plots of  $p\{II\}$  versus  $p\{I\}$  should yield (approximately) straight lines. Using the data of Table XXIII, we have found this to be the case with values of  $\alpha_1$  approximately equal to 0.9 and of  $\alpha_2$  in the range 0.05-0.15, with the actual values depending on the solvent pair and initiator. If such a representation of data is valid, it is suggested that the polymerizations in the different mixtures are similar in that in each case there are

two reactive species, changing only very slowly from one to the other: one, {1}, producing quite isotactic chains (very high values of  $\alpha_1$ ), and the other, {2}, producing moderately syndiotactic chains (low values of  $\alpha_2$ ).

Glusker and co-workers<sup>9</sup> have proposed from kinetic evidence that more than two states are involved in the polymerization of methyl methacrylate by fluorenyllithium in mixtures of toluene with tetrahydrofuran or ether. Bywater<sup>22</sup> has come to similar conclusions. In the cases where the reactions  $\{x\} \rightleftharpoons \{y\}$  are slow, a multistate mechanism becomes equivalent to a two-state mechanism, as far as NMR spectra are concerned, if the  $\alpha_x$ 's fall into only two separated sets, one with  $\alpha_x$  close to 0 and the other with  $\alpha_x$  close to one.

If, in the highly stereospecific anionic polymerization of methyl methacrylate it is really true that  $\lambda_a$  and  $\lambda_b$  are practically zero, then we have the case of two reactive states polymerizing independently, with only rare conversion of one to the other form. Such a polymerization is, in a sense, heterogeneous, and we see that we have here, at best, a limiting case of the dynamic equilibrium between two states which we have treated theoretically. Experimentally, this means that one would have to reduce the monomer concentration by a very large factor in order to obtain a measurable reduction of  $\rho$ . It is intriguing to note that if the reactions  $\{1\} \rightleftharpoons \{2\}$  are slow, once the species {1} and {2} are formed, their relative concentrations should change only slowly upon subsequent changes in the medium. Since the nature of the polymerization is sensitive to the polymerization medium, however, it appears that the initial reactions  $E_1^n \rightarrow E_2^n$ , say,  $n < 10$  are sensitive to the medium; i.e., it appears that the relative concentrations of {1} and {2} are affected by events occurring early in the polymerization, but become "frozen" at fixed values when  $n$  is large. This picture requires that we modify our original mathematical assumption that the rate coefficients  $\lambda_a$  and  $\lambda_b$  be independent of  $n$ . This picture is in accord with the conclusion of Glusker and co-workers<sup>9</sup> that the kinetics of anionic polymerizations of methyl methacrylate are strongly affected by events occurring during the first few seconds of the reaction, and by their observation that the rate of polymerization depends in a complicated way on the initial monomer concentration but decreases simply in proportion to  $[M]$  as the monomer is converted to polymer during the polymerization. On the other hand, the observation of Wiles and Bywater<sup>18</sup> that  $\rho$  and  $p\{I\}$  increase as the monomer is consumed in the polymerization of methyl methacrylate in toluene with butyllithium (Table XXIV) suggests that here, even when  $n$  is large,  $\lambda_a + \lambda_b$  is not negligible, and may be affected by  $[M]$ .

In the anionic polymerization of methyl methacrylate in the presence of less strongly complexing cations, e.g.  $K^+$ , values of  $\rho$  of 1, or only slightly greater than 1, are observed. Evidently here either  $\alpha_1 \approx \alpha_2$ , or the approximation  $\lambda_a + \lambda_b = 0$  is not even roughly applicable, or both. Systematic studies of the dependence of the NMR spectrum and of the molecular weight distribution on the monomer concentration and other variables in the polymerization of methyl methacrylate with less strongly complexing cations are now being started in this laboratory.

The NMR data on poly- $\alpha$ -methylstyrene prepared in ionic polymerizations<sup>19</sup> (Table XXV) correspond to Bernoulli trial statistics ( $\rho = 1$ ). It is known that polymers of narrow molecular weight distribution ( $r < 1.05$ ) are obtainable in the anionic polymerization of  $\alpha$ -methylstyrene and of styrene as well. If the two-state mechanism is applicable for these monomers, it appears that for them the rates of the reactions  $\{1\} \rightleftharpoons \{2\}$  are much greater than the rates of the addition reactions. Actually, the precise kinetic studies of Bywater and Worsfold<sup>23</sup> on the polymerization of styrene initiated by butyllithium in mixtures of toluene with tetrahydrofuran indicate that at least three reactive states participate in the polymerization and that the equilibrium between the various states is very rapid indeed. It follows that in attempts to demonstrate the two-state mechanism for these monomers, one would have to increase  $[M]$  many fold to obtain a measurable increase in  $\rho$ .



## II. Anionic Polymerization of Methyl Methacrylate — W. H. Janes

The recent theoretical treatment of homogeneous ionic polymerization by Coleman and Fox<sup>3,4,6</sup>, (see also the preceding section) has explained some of the features of such reactions. Published data on the anionic polymerization of  $\alpha$ -methyl styrene and, more particularly, methyl methacrylate, do not, however, provide a completely definitive test for their theory. The present work has, in part, been directed towards obtaining supporting evidence, of a more specific nature, for the two-state mechanism proposed. In conjunction with this, it was considered that it would be useful if poly(methyl methacrylate) of narrow molecular weight distribution and controlled stereostructure could be produced. Such a polymer would be particularly useful for studies of physical chemistry in solution and in bulk media. In melt viscosity studies, poly(methyl methacrylate) produced by free radical reactions has given unexpected results; and polymers of well-characterized molecular weight and stereoregular structure would assist in finding the source of the anomaly.

Several examinations of the anionic polymerization of methyl methacrylate have been reported in the literature. Braun et al.<sup>13</sup> examined the effect of counter-ions on the stereoregularity when polymerizations were carried out in solutions of hydrocarbons, Lewis bases, and mixtures of these. Their data have been summarized in the preceding section. Bywater and Wiles<sup>18,24,25</sup> and Glusker et al.<sup>9,20,26,27</sup> have made detailed kinetic investigations of polymerization systems initiated by butyllithium and fluorenyllithium respectively. Both groups found evidence that more than one reactive state existed in the reaction systems. The former authors found evidence that reactions, other than initiation, can take place between the initiator and the monomer. Products from these side reactions may influence the rate, stereoregularity and molecular weight distributions in several ways. In both investigations, bimodal molecular weight distributions were observed with some initiators but not with others. One important feature of the reactions is the formation of considerable quantities of products of molecular weight below 1000.

Clearly, compared to the anionic polymerization of styrene or  $\alpha$ -methyl styrene, the system to be examined is considerably more complex, both in theory and experiment. To achieve reliable results it is necessary to ensure extreme purity of materials and cleanliness of reaction vessels. Wherever possible, solvents were purified by stirring with active anions and vessels were washed with anionically pure solutions prior to the introduction of the reaction mixtures. The purification of the monomer was a difficult task, as it forms colorless ions; hence the generation of a colored species to indicate the removal of impurities, as with styrene, was not possible. Rigorous drying under vacuum, with type 5A molecular sieves and stirring with several portions of calcium hydride, also in *vacuo*, were carried out. The results of polymerizations indicate a high level of purity. All reactions were carried out under high vacuum. In the polymerization reactions, monomer was added either batchwise, or by slow vacuum distillation, to the initiator dissolved in the solvent.

The system chosen for investigation, after some preliminary experiments, comprised tetrahydrofuran as solvent and triphenylmethyl sodium as the initiator. The latter was prepared, with slight modifications to suit vacuum techniques, by the method described in ref. 28, but with tetrahydrofuran as solvent. This compound was used in an attempt to eliminate the side reactions, which Bywater and Wiles<sup>25</sup> suggested, of the initiator with the ester group of the methacrylate. The stability of the triphenylmethyl anion and its sterically bulky nature should assist in a reduction of these side effects. A further reason for the use of a sodium compound as initiator is that there is no reported information, on molecular weight distributions or stereoregularity effects in reaction mixtures of toluene and tetrahydrofuran, comparable to that on lithium compounds as described by Glusker et al.<sup>9,27</sup>.

Tables XXVI and XXVII show some details of molecular weight distributions obtained and tacticity parameters deduced from NMR spectra. The nomenclature for the latter quantities follows that of the preceding section. The experiments at -78°C listed in Table XXVI show from the yield of polymer, insoluble in petroleum ether, a marked absence of the low molecular weight products found by Bywater and Wiles<sup>18</sup>. At -40°C, with comparable reaction times, the yield of polymer is reduced; and the high value of 3.3 for  $M_w/M_n$  may indicate that complexities may be introduced as the temperature is raised. The low values of  $M_w/M_n$  for experiments A8, A9, and A10 are of interest, A8 and A10 giving among the lowest values reported for methyl methacrylate. It may be significant that the slightly higher figure of 1.57 in A9, as against 1.3 for A8 and A10, reflects the difference in the technique of monomer addition in the latter experiments. Although the value of 1.3 is still some way removed from values obtained for "monodisperse" polystyrene, it shows a trend in the right direction and is encouraging as compared to the usual values of  $M_w/M_n$  for anionic poly(methyl methacrylate). The ultracentrifuge sedimentation patterns of A8 and A9 are shown in Fig. 50. That of A8, in particular, appears quite sharp.

The NMR data are in keeping with the findings of Braun et al.<sup>13</sup> for polymers initiated by sodium compounds in Lewis base solvents. In mixtures of toluene and tetrahydrofuran, however, there are some considerable differences between the tacticity parameters for polymers formed with organolithium initiators and those from the sodium compounds. This is illustrated by Table XXVII. In the present work the stereoblock nature of the polymers vanishes and the change from highly isotactic polymers ( $p\{I\} = 0.81$ ) to more random structures with increasing concentrations of THF is much more gradual. Thus, at about 10 percent THF,  $p\{I\}$  is 0.65 for the sodium initiator, but only 0.12 for the lithium compound. It is also worth noting that the  $\rho$  values are much lower in the present experiments and are apparently unaffected by the change in the amount of base.

In summary, it would seem that a system has been found, which is less complex than those previously reported, in that it yields narrower molecular weight distributions. At present, experiments are being conducted with triphenyl methyl potassium to obtain polymers of a more random stereoregular structure for melt viscosity studies. Some of the polymers obtained in the experiments described here are also being used to assess the effect of stereoregularity and structural randomness on the glass transition temperature.

Table XXVI

## Anionic Polymerization of Methyl Methacrylate with Triphenylmethylsodium Initiator

Expt. No.	Percent Conversion (a)	Poly-merization Temperature °C	$M_v$	$M_n$	$M_n$ (Pre-dicted) (b)	$M_w/M_n$	p{I}	p{SS}	p{SI-IS}	$\mu\{I\}$	$\mu\{S\}$	$\rho$
A8 (e,c)	99	-78°C	$2.6 \times 10^5$ ( $2.41 \times 10^5$ ) (g)	$1.85 \times 10^5$	--	1.41	0.27	0.54	0.39	1.35	3.7	1.0
A9 (f,c)	95	-78°C	$1.77 \times 10^5$	$1.13 \times 10^5$	--	1.57	0.32	0.47	0.42	1.5	3.2	1.04
A10 (e,c)	95	-78°C	$2.10 \times 10^5$	$1.61 \times 10^5$	$1.72 \times 10^5$	1.30	0.26	0.55	0.39	1.3	3.7	1.0
A12 (e,c)	40	-40°C	$5.98 \times 10^4$	--	--	--	0.29	0.50	0.43	1.4	3.2	1.0
A14 (f,c)	91	-40°C	$1.03 \times 10^5$	$3.1 \times 10^4$	$1.8 \times 10^4$	3.3	0.33	0.45	0.44	1.5	3.0	1.0
A15 (f,d)	99	-72°C	$5.0 \times 10^4$	$2.6 \times 10^4$	$2.3 \times 10^4$	1.91	0.15	0.71	0.21	1.2	6.5	0.98

(a) Percent conversion was calculated from the yield of polymers insoluble in petroleum ether.

(b)  $M_n$  (predicted) was calculated from  $\frac{\text{gms monomer}}{\text{moles catalyst}}$ .

(c) Solvent tetrahydrofuran

(d) Solvent 1,2-dimethoxymethane

(e) Monomer addition by vacuum distillation

(f) Batchwise addition of monomer

(g)  $M_w$  from light scattering measurements.

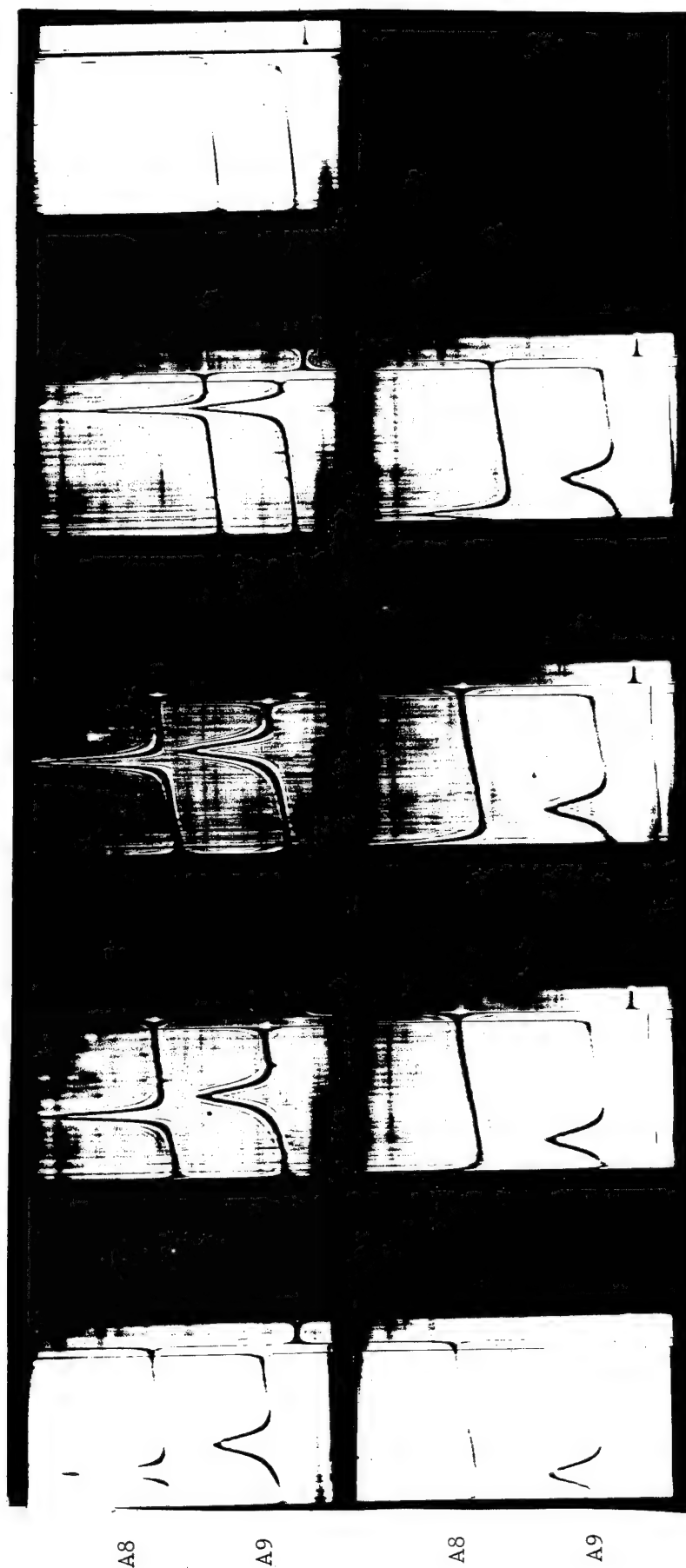
0

1

2

3

4



5

6

7

8

Figure 50 Ultracentrifuge schlieren patterns for poly(methyl methacrylate) Samples A8 and A9. Spinco Model E centrifuge; speed, 59,780 rpm; polymer concentration ca. 1%; solvent, 3-heptanone; temperature 34°C; 16 minute intervals between photographs.

Table XXVII

Anionic Polymers of Methyl Methacrylate  
(Prepared in Toluene-Tetrahydrofuran Mixtures)

Expt. No.	Solvent % THF	Initiation	p{I}	p{SS}	p{IS <sub>v</sub> SI}	μ{I}	μ{S}	ρ
A11	3	Φ <sub>3</sub> CNa	0.81	0.07	0.24	6.8	1.6	1.3
--- <sup>a</sup>	2.5	F1Li	0.53	0.39	0.15	7.0	6.2	3.3
A.3	12	Φ <sub>3</sub> CNa	0.65	0.18	0.34	3.8	2.0	1.3
--- <sup>a</sup>	10	F1Li	0.12	0.83	0.09	2.7	2.0	2.4

<sup>a</sup>From Glusker et al.<sup>27</sup>

Φ<sub>3</sub>CNa - triphenylmethyl sodium

F1Li - fluorenyllithium

### III. NMR Spectroscopy of Poly(vinyl Alcohol) — W. H. Janes

It has recently been found possible to obtain spectra from poly(vinyl alcohol) at 90°C with the Varian A60 spectrometer. The samples were prepared by hydrolysis of vinyl formate polymers<sup>29</sup> that had been formed at temperatures between +30°C and -20°C with initiation by free radicals. The spectra were taken from solutions of the polymer in D<sub>2</sub>O with the HDO resonance as an internal reference at 3.78 ppm. This reference peak interferes with the OH peak from the polymer so only the methylene resonances were suitable for examination to determine tacticity. Only one NMR spectrum of poly(vinyl alcohol) has been previously published<sup>30</sup>.

Two examples of the spectra obtained in the current work are shown in Fig. 51 below with a reproduction of those given by Danno and Hayakawa<sup>30</sup>. If their assignment of resonances is correct, then the samples used in the current work are evidently syndiotactic. Comparison of (a) and (b) indicate that there is no change in the tacticity of the two samples prepared by extreme temperatures. This is in contradiction to published information on these samples<sup>29</sup> which shows gradual changes in water solubility and Huggins constant. Two explanations are possible: either the tacticity changes are too small to be detected by NMR (which seems unlikely as this is probably the most sensitive test we have) or the previous data have shown changes in branching and not, as first supposed, of tacticity. This work is continuing, to establish the reason for the contradictory evidence.

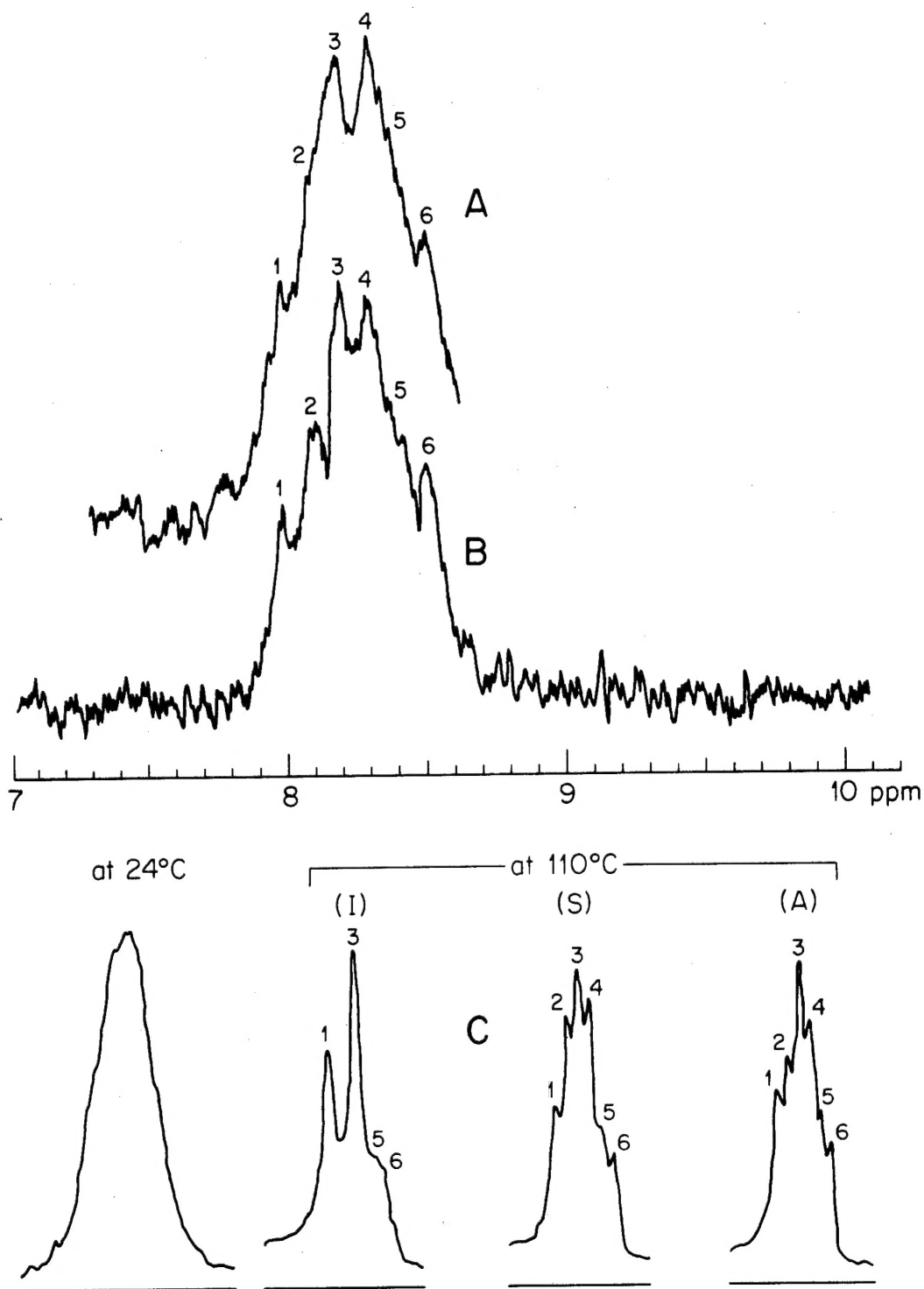


Figure 51 NMR spectra (methylene resonances) from poly(vinyl alcohol). Varian A60 spectrometer probe temperature 90°C: (A) polymer prepared from poly(vinyl formate) polymerized at -20°C; (B) polymer from poly(vinyl formate) polymerized at +30°C. The traces in (C)<sup>30</sup> are for isotactic, syndiotactic, and atactic polymers.

### PART III - LIST OF REFERENCES

1. Fox, T. G, Garrett, B. S., Goode, W. E., Gratch, S., Kincaid, J. F., Spell, A. and Stroupe, J. D., J. Am. Chem. Soc. 80, 1768 (1958).
2. Coleman, B. D., J. Polymer Sci. 31, 155 (1958).
3. Coleman, B. D. and Fox, T. G, J. Polymer Sci. A1, 3183 (1963).
4. Coleman, B. D. and Fox, T. G, J. Chem. Phys. 38, 1065 (1963).
5. Bovey, F. A. and Tiers, G. V. D., J. Polymer Sci. 44, 173 (1960).
6. Coleman, B. D. and Fox, T. G, J. Am. Chem. Soc. 85, 1241 (1963).
7. Flory, P. J., J. Am. Chem. Soc. 62, 1561 (1940).
8. Goode, W. E., Owens, F. H., Fellmann, R. P., Synder, W. H. and Moore, J. E., J. Polymer Sci. 46, 317 (1960).
9. Glusker, D. L., Galluccio, R. A. and Evans, R. A., Polymer Division Preprints 142nd Meeting of the American Chemical Society, Atlantic City N. J., September, 1962, p. 336.
10. Okamura, S. and Higashimura, T., J. Polymer Sci. 46, 539 (1960).
11. Schnecko, H. and Fox, T. G, Polymer 3, 575 (1962).
12. Miller, W. L., Brey, W. S., Jr. and Butler, G. B., J. Polymer Sci. 54, 329 (1961).
13. Braun, U., Herner, M., Johnsen, U. and Kern, W., Makromol. Chem. 51, 15 (1962).
14. Johnsen, U., Kolloid-Z. 178, 161 (1961).
15. Graham, R. K., private communication.
16. Graham, R. K., Dunkelberger, D. L. and Panchak, J. R., J. Polymer Sci. 59, S43 (1962).
17. Glusker, D. L. and Galluccio, R. A., Polymer Division Preprints, 142nd Meeting of the American Chemical Society, Atlantic City, N. J., September, 1962, p. 331.
18. Wiles, D. M. and Bywater, S., Polymer 3, 175 (1962).
19. Brownstern, S., Bywater, S. and Worsfold, D. J., Makromol. Chem. 48, 127 (1961).



20. Glusker, D. L., Stiles, E. and Yoncoskie, B., J. Polymer Sci. 49, 297 (1961).
21. Weakley, T. J. R., Williams, R. J. P. and Wilson, J. D., J. Chem. Soc. 1960, 3963.
22. Bywater, S., Pure Appl. Chem. 4, 319 (1962).
23. Bywater, S. and Worsfold, D. J., Can. J. Chem. 40, 1564 (1962).
24. Cottam, J., Bywater, S. and Wiles, D. M., Can. J. Chem. 41, 1905 (1963).
25. Bywater, S. and Wiles, D. M., Preprints, Division of Polymer Chemistry, ACS, Vol. 4, No. 2, 317 (1963).
26. Glusker, D. L., Lysloff, I. and Stileo, E., J. Polymer Sci. 49, 315 (1961).
27. Glusker, D. L., Galluccio, R. A. and Evans, R. A., J. Am. Chem. Soc. 86, 187 (1964).
28. Moyer, W. W. and Marvel, C. S., in "Organic Syntheses", Collective Vol. II (A. H. Blatt, ed) John Wiley & Sons, New York, (1943), p. 602.
29. Rosen, I., McCain, G. H., Hendry, A. L. and Storm, C. L., J. Polymer Sci. A1, 951 (1963).
30. Danno, A. and Hayakawa, N., Bull. Chem. Soc. Japan, 35, 1749 (1962).